The application of a continuous nourishment on wave and tide-dominated systems

H.R.H. Rutteman

The application of a continuous nourishment on wave and tide-dominated systems

by

H.R.H. Rutteman

to obtain the degree of Master of Science in Civil Engineering
at the Delft University of Technology,
to be defended publicly on Monday October 25, 2021 at 14:45.

An electronic version of this thesis is available at `http://repository.tudelft.nl/`.

Cover: *The Sandwindmill system in action.* Drawing by Michiel Nelissen.

TUDelft **SWECO**

Acknowledgements

Summary

Land subsidence and sea-level rise form a threat to coastal safety in the Netherlands. Regular sand nourishments are used to protect the hinterland from flooding. In the Dutch coastal management, a paradigm shift towards building with nature is taking place. The Sand Engine is an excellent example of this new approach. Natural forces distribute this mega nourishment along and across the coast. Trailing suction hopper dredgers generally carry out both regular and mega nourishments. These dredgers sail on and off between the shore and the assigned sand mining location, typically a distance of 12 kilometres. During these trips, the vessels emit large amounts of carbon dioxide: they help in fighting the impact of climate change whilst aggravating the problem. As the decarbonization of dredging vessels is a difficult task, new solutions for sustainable coastal management should be sought.

The Sandwindmill system could decarbonize the coastal protection whilst harmonizing with the building with nature approach. The system consists of a pipeline connecting an offshore borrow location to a nearshore area, where the mined sediment is discharged. The equipment is powered by wind turbines. As long as the wind blows sufficiently, sediment is pumped through the system, leading to a near-continuous nourishment. After the sediment has left the pipes, natural forces should distribute the material. Despite the considerable environmental benefit, one substantial challenge is the financial competitiveness with the traditional hoppers. This research aims to provide insights that can enable the system to be also financially competitive to the hoppers. In the first part, an integral analysis of the Sandwindmill is carried out. The second part of this thesis focuses on the optimization of the dispersion of the nourished sediment.

In the first part, all sub-systems of the Sandwindmill concept are treated separately. Wind data, theoretical formulations, and an exploration of the mining options are used to identify optimization opportunities. From the assessment, it becomes apparent that the interdependency of these sub-systems complicates the cost-optimization. Hence, a competitive system design requires an accurate harmonization of these sub-systems. Three main conclusions are drawn. First of all, the costs per cubic meter decrease with an increasing nourishment volume. Finding the marginal costs is essential in determining the feasibility of the system for certain volumes. Secondly, it is concluded that - given an annual nourishment volume - the pump capacity and windmill size should be attuned. Their cost-optimum is found at a set-up that leads to a yearly operational time of approximately 70%. Lastly, the analysis shows that the application of batteries to support the system in case of lower wind velocities can contribute to a more economical system. This is mainly the case if the system has wave-induced limited operational times.

Due to the costs of the displacement of the pipe outlet and the financial benefits of nourishing large volumes, the second part of the research aims at generating guidelines to designing a dispersive nourishment. Both wave- and tide-dominated systems are a potential field of application for the Sandwindmill. North-Holland is selected as an appropriate case study, containing the Marsdiep tidal inlet and a wave-dominated closed coastal section. A process-based coastal area model is set up to determine the sensitivity of different nourishment strategies on the dispersion at a one-year timescale. A tidal channel wall nourishment at the Marsdiep and a shoreface nourishment at Callantsoog are assessed.

One of the key findings of the second part is that the strong tidal velocities at the Marsdiep inlet are more capable of transporting the nourishment than the conditions at the wave-dominated coast. After one year, the distance travelled by a significant part of the nourished sediment is a factor four higher for the Marsdiep nourishment. Secondly, the research shows that the grain size plays a vital role in the local and regional dispersion. Therefore, the borrowed grain size should be part of the system design. Under the evaluated scenarios, the nourishment application under forcing conditions with a higher transporting potential has a smaller effect in the longer term. This implies that the optimal operational time could be determined solely based on the cost-optimization and should hence be around 70%.

The outcomes of this report contribute to the development of the Sandwindmill system in two ways. First of all, the system analysis provides a framework that can be used in the integral design of the Sandwindmill system. Some design aspects, such as battery usage and the principle of an optimal operational time, are worked out. The main goal herein is to show system dependencies and optimization opportunities. Secondly, this research shows the sensitivities of a nourishment to some design variants. In its current form, the Sandwindmill appears to be best applicable at the wall of a tidal channel ('geulwand'), using smaller grain sizes.

Contents

List of Figures

List of Tables

<div align="right">

1

</div>

Introduction

1.1. Background

On August 7th 2021, the Intergovernmental Panel on Climate Change (IPCC) launched its sixth assessment report, making clear how humanity is responsible for unprecedented changes in the climate (IPCC, 2021). It is virtually certain that the current sea-level rise is the result of human behaviour and that its effect will be irreversible for centuries. There is also proof of the intensification of storms due to human behaviour. A large part of The Netherlands lies below the sea, making the country vulnerable to extreme events such as storm surge (Van Koningsveld et al., 2008). The shallow, funnel-shaped character of the North Sea and the predominant western winds make this sea very susceptible to storm surge (Bosboom & Stive, 2015). The 1953 flood disaster confirms this vulnerability, flooding 165,000 hectares of land and taking 1,835 lives (Gerritsen, 2005). Dunes and beaches provide significant protection against coastal inundation (Verhagen, 1990). Approximately 72% of the 353 km Dutch coastline is protected by dunes (Noortwijk & Peerbolte, 2000). The rising sea level leads to a retreat of the coastline, reducing the protectiveness offered by these beaches and dunes (Cooper & Pilkey, 2004). Next to the rising sea level, the land has been subsiding over the past centuries, increasing the severeness of possible inundations (NHV, 1998). The coincidental sea-level rise and land subsidence are schematised in Figure 1.1.
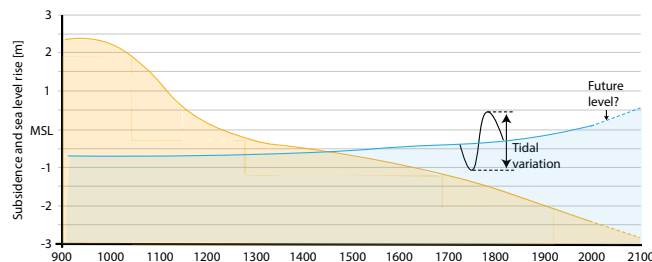
Figure 1.1: Illustration of the simultaneous land subsidence and sea-level rise over the past centuries. Adapted from NHV (1998)

In line with the aim of the government to use natural solutions as coastal protection, it adopted a new policy called 'Dynamic Preservation' in 1990 (Min.V&W, 1991; Smits et al., 2006). The strategic aim of the policy was to attain a certain safety level while preserving the values and functions of the dune areas. The government decided that this goal could be effectuated by maintaining the coastline at its position of 1990. This reference coastline is referred to as the Basal Coastline (BCL), or Basiskustlijn in Dutch. Figure 1.2 shows how sand nourishments can counteract the landward shift of the coastline due to sea-level rise.
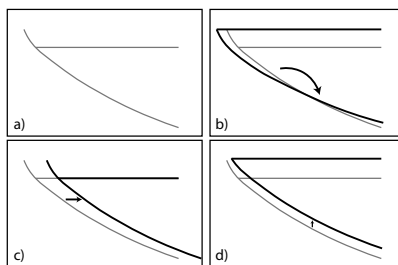
Figure 1.2: Response of the equilibrium profile: a) indicates the equilibrium profile, b) the retreat of the shoreline due to sea-level rise, c) progradation of the coast due to nourishing, d) the combined effect of sea-level rise and sediment supply. After Bosboom & Stive (2015).

The BCL is maintained by the governmental nourishment program (Roelse, 2002). As sand losses at larger depths were not taken into account in the BCL policy, the Dutch government decided to take a larger-scale area into consideration (Mulder et al., 2011). The government defined the 'coastal foundation' as the area between the dunes and the -20 m depth contour. The government's policy of measuring and maintaining the amount of sediment in the coastal foundation led to an increase of the yearly nourishment volume from 6 million m^3 to 12 million m^3. This increase compensates for the sediment loss due to the sea-level rise of 1.8 mm/year.

The government strives towards working according to the Building with Nature (BwN) approach in her effort to prevent the Netherlands from flooding (Rijkswaterstaat, 2015; De Vriend et al., 2015). The BwN concept attempts to meet the infrastructural requirements (e.g. flood safety), using natural resources and processes. Even more in accordance with the BwN principle would be the use of natural processes like wind and currents to help distribute the sediment, allowing for a graduate adaptation of the system. Recently carried out mega nourishments are an example of this shift towards BwN. Currently, these nourishments are executed by dredging vessels. Because of the high emissions of these vessels, Rijkswaterstaat launched a program called 'Innovaties in de Kustlijnzorg' (IKZ) (also called the 'Dutch Coastline Challenge' (DCC)) (Management Ministry of Infrastructure and Water, n.d.). The program aims to enhance the sustainability of the Dutch nourishment program in a cost-effective way. Hereto, Rijkswaterstaat engages in innovation partnerships with third parties. Rijkswaterstaat has reserved €18 million for the development of sustainable alternatives to the current nourishing methods.

1.2. Problem formulation

The Netherlands has been dealing with water-related challenges for centuries. These challenges have led to the building and the invention of many types of water-retaining structures and methods; hard structures such as dykes and barriers and 'soft' structures such as nourishments. After the 1953 flooding, the Delta Works program was initiated in 1959 (Louters et al., 1998). This multi-billion program established state of the art constructions that still protect the Netherlands from the sea. Also, the transition from beach nourishments towards mega nourishments can be seen as an innovative development of our continuous battle against the sea. However, these mega nourishments still affect the ecology. Another disadvantage of all contemporary nourishment methods is that these nourishments are executed with fossil fuel driven dredging vessels.

Morselt et al. (2010) have calculated the expected CO_2 emissions by dredging vessels that are used for sand nourishments at the Dutch coast. These emissions are dependent on the type of nourishment (through bottom valves, pipes or by rainbowing) and the sailed distance. The locations that may be used for sand winning must be at least beyond the -20m NAP line (C. F. Van Duin et al., 2017). Typical winning locations lie 12 km from the coast. For these winning locations, the average CO_2 emissions are estimated at 3 kg per m^3 of nourished sand. The current annual nourishment volume is 12 million m^3, leading to the emission of $3 \cdot 12 \cdot 10^6 = 36 \cdot 10^6$ kg CO_2/year. To put this number in perspective: this equals the yearly direct emission (e.g. residential heating and car emissions) of 5,000 EU residents (Eurostat, 2020). If the coast from Zeeland to the Wadden Sea is to grow with the sea level, every millimetre of sea-level rise would require 7 million cubic metres of sand. The Royal Netherlands Meteorological Institute (KNMI) estimated that the sea level would have risen 15 to 35 centimetres in 2050 compared to the sea level of 1990 (Veerman et al., 2008). This calculation

is made with the 'moderate' temperature increase of 2°C in 2100, which is very likely to occur (IPCC, 2021). When this sea-level rise should be compensated with the current nourishment methods, this would lead to a required nourishment volume of 1,050-2,450 *million* cubic metres over these 60 years, or 53 - 122 million kilograms of CO_2 *each year*. This equal the annual direct carbon emission of 8,000-17,000 EU residents. Next to CO_2, dredging vessels emit other greenhouse gasses, such as sulfur oxides (SO_x) and nitrogen oxides (NO_x) (Olmer et al., 2017).

The reduction of the greenhouse gas emissions by dredging vessels would cut back the environmental impact of the current nourishment methods. The transition towards carbon-neutral vessels is one of the main challenges of the maritime sector. For dredging vessels, this forms an even larger challenge, since they need to operate under heavy conditions and around the entire world (Gonçalves Castro et al., 2019). Whereas a full tank of diesel can power a hopper for weeks, the same weight in batteries (approximately 2,000 tons) would be just enough to provide energy for 10 hours. The costs of the batteries will be in the order of €100,000,000 (Van Rhee, personal communication, September 6th, 2021). The disadvantage of fuel cells, required for using hydrogen power, is that they cannot handle the large and quick power fluctuations inherent to dredging. The numbers described above show the urgency to develop alternative methods to the current nourishing. Next to the apparent decarbonization of the traditional dredging vessels, alternatives should be given the opportunity to be researched and developed. These alternatives could not only contribute to the emission reduction. They could also allow for the application of novel nourishment approaches. The Sand Engine is a successful manifestation of the paradigm shift towards working with nature. Looking further than the marginal adaptation of traditional methods might be needed to guarantee safety against the rising sea.

One of the IKZ partnerships focuses on the development of the Sandwindmill (SWM). The Sandwindmill is a concept that uses pumps driven by wind energy that transport sediment from an offshore borrow area towards the coast. As long as the wind blows sufficiently, sediment will be discharged at the pipe outlets. The first designs aim to an annual operational time of 50% (Grontmij, 2013). As traditional nourishments may take place in days, the SWM nourishments are addressed here as being continuous. Dredging vessels can displace themselves and therewith the positioning of a nourishment easily. Financially, the displacement of the outlet pipes of the SWM over a considerable distance (O(km)) is deemed impracticable. As the location of the outlet pipes is rather fixed to a particular location, natural processes are responsible for the distribution of this sediment. The capabilities of nature to spread this sediment is therefore crucial to the success of the Sandwindmill.

Through the IKZ, Rijkswaterstaat is looking for a sustainable and cost-effective alternative to the current nourishment methods. With sediment dispersion as one of the key potential bottlenecks, this thesis aims to identify how the Sandwindmill can be a solid competitor to these traditional methods. As the development of the Sandwindmill is still in the design phase, many configurations can still be considered. Both the costs and the influence on the sediment dispersion of the configurations should herein be taken into regard. The knowledge obtained by an integral system analysis, which treats different possible configurations, could demonstrate the system's interdependencies.

1.3. Research questions
This research aims to identify the potential of the Sandwindmill as an alternative to the current nourishment methods. The main research question is:

> *What type of nourishment strategy enables the Sandwindmill to be competitive with traditional nourishment methods?*

The sub-questions that will help to answer the main research question are:

1. How does the Sandwindmill relate to the current nourishment methods?
2. What are the interdependencies of the Sandwindmill subsystems, and how do these relate to sediment dispersion?
3. How well is the Dutch coast capable of dispersing a continuous nourishment?
4. How can the continuous nourishments be designed to improve sediment dispersion?

1.4. Methodology and outline

The answering of the first two sub-questions (SQ1 & SQ2) will be done based on a comprehensive analysis of the integral Sandwindmill system in Chapter 3. After this general review of the system, the second part of this thesis goes more into detail on the nourishment design. Finally, after answering SQ3 and SQ4, the main research question (MQ) will be answered in the final two chapters.
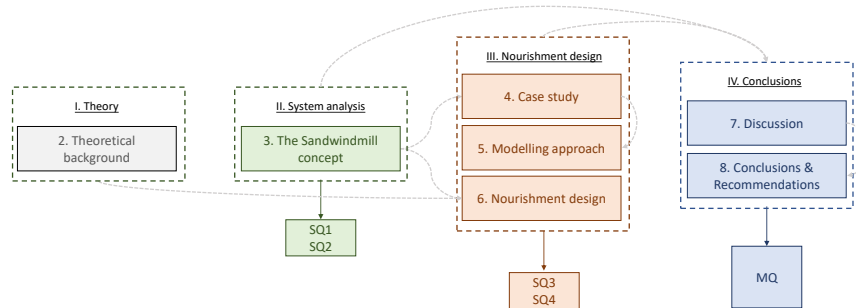
Figure 1.3: Overview of the methodology of this thesis. The grey dotted lines indicate the coherence between the different sections as discussed in the methodology.

- **Chapter 2** provides a theoretical foundation for the design of a nourishment. The principles that force sediment transport are discussed. The chapter furthermore treats the behaviour of nourishments in coastal regions. Gaining an understanding of these principles is key to the design of a nourishment.

- **Chapter 3** gives an exploration of the current nourishment methods. The advantages and drawbacks are described, forming a benchmark against which the Sandwindmill system can be compared. This answers the first sub-question. Furthermore, all separate subsystems of the Sandwindmill are treated. In the conclusion, the interdependency of these subsystems is described, as well as the implications of these dependencies on the nourishment strategy. The costs of the system are a common thread in this exploration, as these are a determining factor in the success potential of the Sandwindmill. The aim is not to define the exact costs of the different Sandwindmill configurations. The goal is rather to show how the costs relate to the interaction of the subsystems, and how these costs could be reduced. This answers the second and third research questions and provides boundary conditions for the nourishment design, which is assessed in the following chapters.

- In **Chapter 4**, two locations are selected that match well with the requirements for the Sandwindmill. The information gathered in Chapter 2 provides boundary conditions for this choice. Subsequently, a geographical and morphological description of the areas in given.

- In **Chapter 5** a numerical model is selected that can assess the application of a continuous nourishment at the chosen locations. The model set-up, calibration and validation are discussed, such that a good understanding of the possibilities and limitations of the model application is obtained. The representativity of the selected hydrodynamic conditions is also tested. This is done by the comparison of these conditions with a larger data set, and by using transport formulations that are discussed in Chapter 2.

- In **Chapter 6** the findings of the previous chapters on the system requirements, costs, sediment transport mechanisms and location are aggregated in multiple nourishment scenarios. These scenarios are simulated using the numerical model presented in Chapter 5. The results of each scenario are analysed, providing implications of the nourishment designs on the success of the Sandwindmill. Using these results, the third and fourth sub-questions are answered.

- The conclusions that are drawn in the preceding chapters are debated in **Chapter 7**. The conclusions are reflected against the limitations of the executed approach. Also, the practical implications of the analysed scenarios are discussed in this chapter.

- **Chapter 8** answers the main research question using the results of Chapters 2 to 6 and the reflection on these from Chapter 7. Lastly, recommendations are given on improving the performed study and on further research to the identified knowledge gaps.

Part I

Theory

Chapter 2: Theoretical background

2

Theoretical background

The durability of a nourishment is dependent on many conditions. One of those conditions is the transport capacity of the nourished area. Therefore, understanding the mechanisms that drive this transport is essential. As the Sandwindmill nourishments are of the 'feeder' type, understanding the natural processes can contribute to designing a nourishment that spreads out efficiently. The main focus will be on the alongshore sediment transport, which is mainly driven by alongshore currents (Bosboom & Stive, 2015). Therefore, first, the driving mechanisms of these currents are assessed. Secondly, the processes that lead to sediment transport by these currents are treated. In each part, some formulations are treated that were derived during the past decades. It is important to note that these formulas are mainly empirical and that their applicability to specific cases should be treated with care. The purpose is to give insight into how some key parameters may influence the behaviour of the described phenomena. Figure 2.1 indicates the coastal sections as they are used in this research. In the shoaling zone (lower shoreface), waves start to feel the bottom. In the littoral/surf/breaker zone, waves start breaking. The active profile is the part where noticeable morphological changes occur. When assessing a longer timescale, the domain of interest grows as the slower processes that occur on larger depths become relevant.
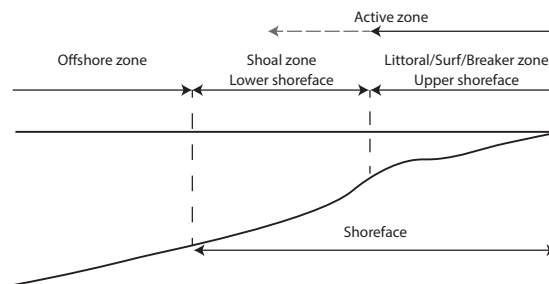
Figure 2.1: The shore sections as used in this thesis. The domain of the active profile grows with the considered timescale.

2.1. Alongshore currents

Three processes that can induce alongshore currents are distinguished here: waves, winds and tides. The influence of these forcings on the alongshore current will be treated first.

Wave induced

Waves can alter the momentum of a fluid element with its particle velocities and wave-induced pressure forces (Bosboom & Stive, 2015). The wave-averaged and depth-integrated flow of momentum due to waves is called radiation stress. According to Newton's second law, if there is a variation in radiation stress, it must be counteracted by some force. In the cross-shore direction, a change in the normal radiation stresses is counteracted by a water level difference: a lowering in the shoaling zone and a rise in the surf zone. The water level set-up provides a seaward directed pressure to balance the decrease in normal radiation stress due to

breaking waves. When waves approach the coastline obliquely, they induce shear radiation stress. When these obliquely incident waves break, the shear radiation stress changes. For a long shoreline, a change in the shear radiation stress cannot be counteracted by a change in the water level. The counteracting force is delivered by the bed shear stresses that are developed by alongshore currents (Elfrink et al., 1996). The larger the change in radiation stress, the larger the counteracting force and thus the currents must be. As the largest stress change occurs at the seaward boundary of the surf zone, the largest alongshore currents would occur here. Bosboom & Stive (2015) propose formula 2.1 for the alongshore current driven by waves at a constant beach slope. The formula implies that a doubling of the wave height at breaking leads to a discharge increase in the surf zone of a factor 8.

$$V(x) = \frac{5}{16}\pi \frac{H_b}{c_f} g \frac{\sin\phi_0}{c_0} \frac{h}{h_b} \tan\alpha \tag{2.1}$$

where:

V(x)	depth averaged alongshore current at location x	[m/s]
H_b	wave height at breaking	[m]
c_f	dimensionless friction factor	[-]
g	gravitational acceleration	[m/s^2]
ϕ_0	offshore wave direction	[°]
c_0	deep water phase velocity	[m/s]
h	water depth	[m]
h_b	water depth at breaking	[m]
α	beach slope	[°]

Turbulent forces lead to a smoothing of this profile. This leads to a landward shift of the maximum velocity, see Figure 2.2a. Also, the irregularity of waves smoothens out the velocity profile. Furthermore, the alongshore current is dependent on the breaking of waves and thus on the wave height and the bottom profile. This is illustrated in Figure 2.2b.

(a) Turbulence (based on Bosboom & Stive (2015))

(b) Wave height and bottom profile (based on (Fredsøe & Deigaard, 1992))
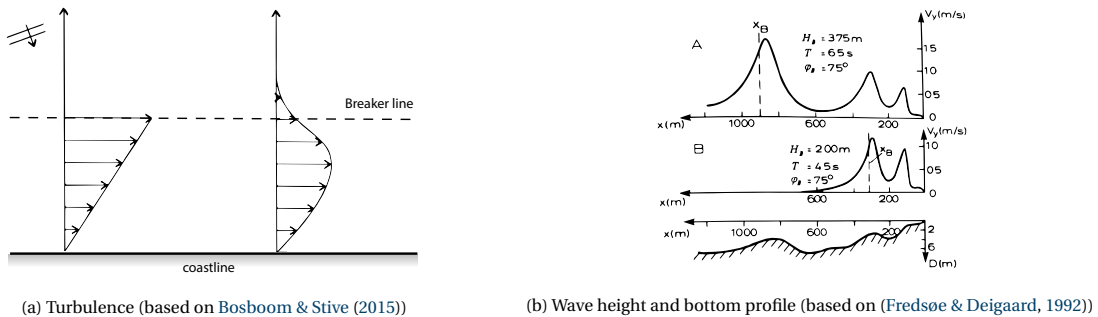
Figure 2.2: Influence of turbulence, bottom profile and wave height on the velocity profile of wave-induced alongshore currents.

Wind-induced

Wind induces a shear stress on the water surface. When the wind acts parallel to the coastline for some time, an alongshore current can be generated. As this force only acts on the surface of the water, the velocity of the wind-induced current decreases sharply with an increasing depth (Davies, 1985).

Tide-induced

The gravitational pull of the moon and the sun on the earth and its oceans leads to the daily rise and fall of the ocean water level, called the tide (Bosboom & Stive, 2015). In the Netherlands, the tidal wave propagates to the north. In contrast to wind waves, which have a stochastic character, the tide's motion is deterministic. This implies that the tide is not dependent on the weather or the climate.

For all tidal waves on the Dutch coast, the rising period of the water is shorter than the falling period, which is called flood-dominance. This can be explained as follows. The crest of a tidal wave, which can be seen as

high water, propagates faster than the trough of the tidal wave, which can be seen as low water (Nidzieko & Ralston, 2012). In IJmuiden, for example, the rising period is 4.22 hours, whereas the falling period is 8.03 hours (Bosboom & Stive, 2015). These tidal waves induce an alongshore current. The velocity of this current is dependent on the alongshore water level gradient and the water depth. The smaller the depth, the larger the influence of friction. This relationship is given in Equation 2.2 and illustrated in part a of Figure 2.3.

$$u \propto \sqrt{h\frac{\partial h}{\partial y}} \tag{2.2}$$

As opposed to for example the Mediterranean, is the tidal influence on the alongshore current in the Netherlands significant and could thus best be accounted for when assessing alongshore sediment transport (Van Rijn, 1995). If the maximum velocity of the flood is larger than the maximum velocity of the ebb, a net sediment transport in flood direction is likely to occur. This can be deducted from the relation between sediment transport and the current velocity given in Equation 2.12, which depicts the stirring and transporting capacities of a current.

Overall current
The combined effect of wave and tide induced currents is depicted in Figure 2.3. In the Netherlands, the direction of the tidal velocity changes approximately twice per day.
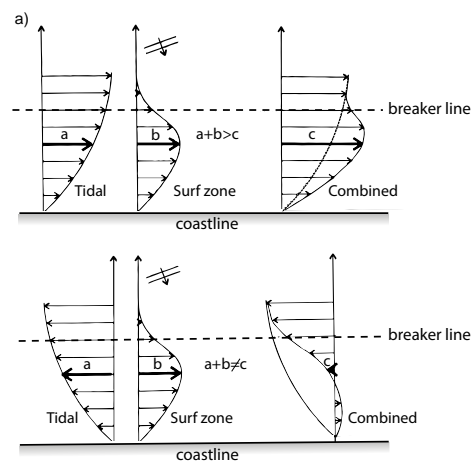
Figure 2.3: Combined effect of the tide- and wave-induced velocity for a given incoming wave angle, and ebb and flood tides. After Bosboom & Stive (2015).

2.2. Sediment transport

Section 2.1 explains the phenomena that induce currents. In this section it is described how these currents can lead to the transport of sediment.

2.2.1. Forces on sediment grains

Two forces acting on a sediment grain are distinguished: a downward directed gravity force (Equation 2.3) and an upward directed drag force (Equation 2.4) (Bosboom & Stive, 2015). If these forces are in equilibrium, the sediment particle falls with a constant velocity (Equation 2.6). These equations assume that the grain size is a perfect sphere. This fall velocity is dependent on the grain size, relative density of the sediment and the drag force, which is mainly influenced by the grain Reynolds number. The relationship between the drag force and grain Reynolds number is dependent on the sediment characteristics. For sand sediment the proportionality between the fall velocity and the grain size lies between $w_s \propto \sqrt{D}$ and $w_s \propto D^2$. Multiple empirical formulations have been derived that relate these two. See Figure 2.4 for the relationship derived by Van Rijn (1993). If a grain moves downward, an equal volume of fluid must move upward. When the sediment concentration becomes high, this upward moving fluid contains more sediment, reducing the effective fall velocity. This principle is called hindered settling and may be significant for high-concentration mixtures.

$$F_G = (\rho_s - \rho_w)g(\frac{\pi}{6}D^3) \tag{2.3}$$

$$G_D = \frac{1}{2}C_D\rho_w w_s^2(\frac{\pi}{4}D^2) \tag{2.4}$$

$$w_s = \sqrt{\frac{4(s-1)gD}{3C_D}} \tag{2.5}$$

$$Re_g = \frac{w_s d}{\nu} \tag{2.6}$$

with:

F_G	gravity force	[N]
ρ_s	sediment density	[kg/m^3]
ρ_w	water density	[kg/m^3]
D	grain size diameter	[m]
G_D	drag force	[N]
C_D	drag coefficient	[-]
w_s	fall velocity	[m/s]
s	relative density (ρ_s / ρ_w)	[-]
Re_g	grain Reynolds number	[-]
ν	kinematic viscosity	[m^2/s]
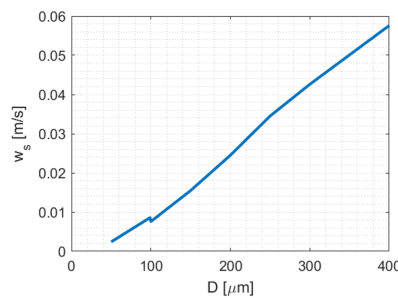
Figure 2.4: Empirically derived relationship between fall velocity and grain size according to Van Rijn (1993). Adapted from Sistermans (2002).

Grains can only move if the shear stress (τ_b) exerted on them is large enough. This shear stress is dependent on the density of the water and the velocity, which is driven by near-bed wave orbital velocities and current velocities. Shields (1936) introduced a dimensionless bed shear stress, of which the critical value is dependent on the grain Reynolds number. Equations 2.8 to 2.9 show how this Shields parameter can be determined.

$$\theta = \frac{\tau_b}{(\rho_s - \rho_w)gD} \tag{2.7}$$

$$\tau_b = \rho_w \frac{u^2}{C_*^2} \tag{2.8}$$

$$C_* = \frac{h^{1/6}}{n\sqrt{g}} \tag{2.9}$$

with:

θ	Shields parameter	[-]
τ_b	bed shear stress	[N/m^2]
u	depth averaged water velocity	[m/s]
C_*	dimensionless Chézy coefficient	[-]
n	Manning's roughness coefficient	[s/m$^{1/3}$]
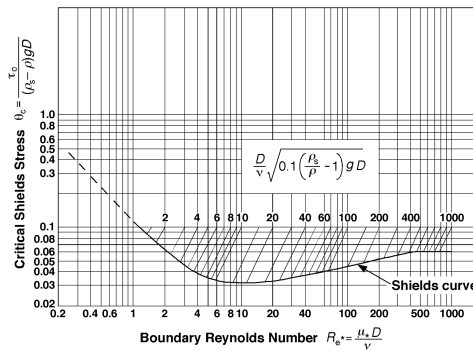
Figure 2.5: Shields curve relating the particle Reynolds number to a critical dimensionless shear stress value, adopted from Schwimmer (2007).

Based on experiments, Shields deducted a relationship between the critical value of θ and the grain Reynolds value, which he visualized in a curve (Figure 2.5). Van Rijn (1993) established a formulation for the critical value that is dependent on the dimensionless grain size, see equations 2.10 and 2.11. Equation 2.11 holds for grain sizes between 160 and 400 μm. This allows to calculate the critical shear stress value without any iteration. Limitations of the critical values used is that they do not account well for sloping beds, non-uniform flows, armouring of sediment fractions and cohesive forces (Bosboom & Stive, 2015).

$$D_* = D_{50} \left(\frac{g(s-1)}{v^2} \right)^{1/3} \tag{2.10}$$

$$\theta_c = 0.14(D_*)^{-0.64} \text{ for } 4 \leq D_* < 10 \tag{2.11}$$

where:

D_{50}	median grain size	[m]

2.2.2. Bed-load and suspended load
Sediment transport can be separated in bed-load transport and suspended load transport. When bed-load transport occurs, the sediment particles are (close to) in contact with the bed during the transport. When the particles do not have any contact with the bed, it is called suspended load.

Bed-load transport
If the critical shear stress is slightly exceeded, the grains start to roll and slide over the bed. This transport method is called bed-load transport. The bed-load transport is almost entirely controlled by bed-shear stress. Therefore, it is often formulated as a function of current and wave induced bed-shear stresses. For higher velocities (>0.8 m/s), the effect of grain size on the bed-load is limited Van Rijn (2007). This is the result of the balance between increased drag due to a higher particle area, and a higher gravitational force due to a higher particle weight (equations 2.3 and 2.4). An example of the time-averaged bed-load transport is given by Bijker

(1967), see Equation 2.12. This is a formulation that represents the transport rates of the Dutch coastline quite well (Huisman, 2014).

$$S_b = B D_{50} \frac{U_0}{C} \sqrt{g} \exp \frac{-0.27(s-1)D_{50}\rho g}{\mu \langle |\tau_{cw}| \rangle} \qquad (2.12)$$

where:

S_b	time-averaged bed-load transport	[m³/m/s]
B	Bijker coefficient (=5)	[-]
C	Chézy coefficient	[m$^{1/2}$/s]
μ	ripple coefficient	[-]
$\langle |\tau_{cw}| \rangle$	time-averaged shear stress magnitude of wave-current motion	[N/m]

The exponential term indicates the stirred-up sediment due to wave and current induced shear stress, whereas $\frac{U_0}{C}\sqrt{g}$ demonstrates that the average transport is due to currents only. Regarding the grain size, one would expect more sediment transport if the grain size decreases, as the gravitational force would decrease. If Equation 2.12 is plotted with the D_{50} as unknown on the horizontal axis, it follows a Weibull distribution shape. This indicates that below a certain grain size diameter (the maximum in the graph), the transport decreases with a decreasing D_{50}. This is not in line with the above-mentioned hypothesis but can be explained by the fact that the transport will become suspended below a specific grain size. The calculated bed-load transport thus decreases.

Suspended load transport
The turbulence of the water can keep these particles in suspension. The total suspended load transport is often calculated as a function of the horizontal water velocity and the sediment concentration, integrated over the depth. For time-averaged suspended sediment transport, one could use the relation of Equation 2.13, described by Soulsby (1997). The wave related part is given in the second term on the right-hand side of the equation. As this part of suspended sediment transport is assumed to be smaller than the current-related part, it is often left out (Bosboom & Stive, 2015).

$$S_s = \int_a^h U(z)C(z) \; dz + \int_a^h \overline{\bar{u}(z)\bar{c}(z)} \; dz \qquad (2.13)$$

where:

S_s	time-averaged suspended transport	[m³/m/s]
U(z)	time-averaged fluid velocity at height z	[m/s]
C(z)	time-averaged sediment concentration at height z	[m³/m³]
$\overline{\bar{u}(z)}$	time-averaged oscillating fluid component at height z	[m/s]
$\overline{\bar{c}(z)}$	time-averaged oscillating concentration component at height z	[m³/m³]
a	thickness of bed-load layer	[m]

The concentration at a certain height depends amongst others on the bed-load transport, as the latter influences the concentration at the lower boundary of the suspended load transport region. Figure 2.6 illustrates the relations of Equation 2.13.
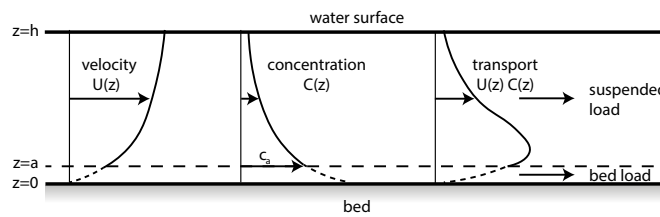
Figure 2.6: The relationship between the concentration, the current velocity and sediment transport as expressed by Soulsby (1997). Image from Bosboom & Stive (2015).

The concentration profile of Figure 2.6 is dependent on the sediment characteristics and fluid velocity. When neglecting the horizontal advective components, averaging the turbulent motion (called Reynolds averag-

ing) and assuming a concentration-independent fall velocity, the advection-diffusion equation becomes as presented in Equation 2.14. The second term denotes the downward going sediment and the last term the upward going sediment due to turbulence.

$$\frac{\partial c}{\partial t} - w_s \frac{\partial c}{\partial z} + \frac{\partial \langle c' w' \rangle}{\partial z} = 0 \tag{2.14}$$

$$\langle c' w' \rangle = -v_{t,s} \frac{\partial c}{\partial z} \tag{2.15}$$

where:

c	turbulence averaged concentration	[-]
z	distance from bed	[m]
$\langle c' w' \rangle$	sediment flux due to turbulence	[m/s]
$v_{t,s}$	turbulence diffusivity of sediment mass	[m^2/s]

When taking the boundary between bed-load and suspended load at a certain height a, the concentration of the fluid at height a can be related by the bed-load transport (see Equation 2.16).

$$C(a) = \frac{S_b}{ua} \tag{2.16}$$

with:

C(a)	concentration at reference point	[-]

By integrating the advection-diffusion equation presented in Equation 2.14 over the depth and assuming a parabolic distribution of the diffusion coefficient ($v_{t,s}$) as suggested by Rouse (Equation 2.17), the concentration profile can be calculated by Equation 2.18.

$$v_{t,s} = \kappa u_* \frac{z}{h}(h - z) \tag{2.17}$$

$$C(z) = C_a \left[\frac{h - z}{z} \frac{a}{h - a} \right]^{z_*} \tag{2.18}$$

with:

κ	Von Kármán constant (0.41)	[-]
z_*	Rouse number ($\frac{w_s}{\kappa u_*}$)	[-]
u_*	shear velocity ($\sqrt{\frac{\tau_b}{\rho_w}}$)	[m/s]

The dependence of the concentration profile on the rouse number shows that the profile is steeper for particles with higher fall velocities, hence for larger grain sizes (as can be read from Figure 2.4). For three grain sizes and two shear velocities the distribution is given in Figure 2.7.
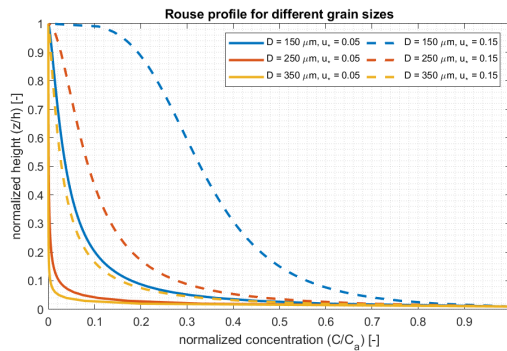
Figure 2.7: Concentration profile for different grain sizes under two different shear velocities, according to Equation 2.18. The typical value for the Von Kármán constant of 0.41 is used. The fall velocities as proposed by van Rijn (Figure 2.4) are used.

2.2.3. Cross-shore transport

Bosboom & Stive (2015) state that cross-shore transport induces mainly short-term variations and that long-term cross-shore variation is often hard to observe. A few assumptions can form the basis of modelling the shoreline changes on a year to decade time scale. First, it is assumed that only the upper shoreface is morphologically active on these timescales. This upper shoreface extends from the first dune face to just a little seaward of the surf zone. Secondly, the shape of the active profile remains at equilibrium when averaged over time (years to decades). Lastly, the amount of sediment in this active zone remains constant in the absence of alongshore transport gradients.

The active equilibrium profile, as stated before, was described by Bruun (1954). The profile could be specified by Equation 2.19.

$$h = A(x')^{2.5} \tag{2.19}$$

where:
  A   shape factor   [$m^{1/3}$]
  x'   distance from mean waterline, positive in offshore direction   [m]

Bruun, who determined the shape factor empirically for different coastlines, stated that this factor is dependent on the characteristics of the bed material. Dean (1991) tried to define the shape factor as a function of the median grain size, and found that a coarser grain size would lead to a steeper coastal profile.

Roelvink & Stive (1989) distinguish multiple drivers of cross-shore sediment transport. Longuet-Higgins streaming outside the surf zone, wave asymmetry and free long waves inside the surf zone are responsible for transport onshore. Undertow in the surf zone and (bound) long waves outside the surf zone can transport sediment offshore. Gravity can move sediment downward when the bed is sloping.

2.2.4. Alongshore transport

As waves refract towards the coast, the short wave motions act mainly in the cross-shore direction. The oscillatory component of the alongshore current is therefore mostly neglected. Furthermore, the oscillatory part of the sediment transport does not lead to a net sediment transport as $V(z) \cdot \tilde{c}(z, t)$ has a time-mean of 0 (Bosboom & Stive, 2015). This leaves only the first term of the right hand side of Equation 2.13, leading to Equation 2.20.

$$\langle S_y \rangle = \int_a^h U(z)C(z) \ dz \tag{2.20}$$

where:

  S_y net alongshore sediment transport (pores excluded)   [$m^3/m/s$]
  U(z)   alongshore current velocity at height z   [m/s]

The role of the waves is twofold. Oblique incoming waves are responsible for driving the alongshore current. Furthermore, the orbital motion and breaking of waves stir up sediment, leading to an increased suspended sediment concentration. There are many sediment transport formulas in the form of Equation 2.20. Bayram et al. (2001) have analysed and compared a few of these. They found a significant difference in predicted transport capacity, sometimes differing over a factor of 10. Also, the formulas had difficulty in determining the location of the maximum transport. These findings stress the importance of calibration and validation when using a numerical model.

The models that Bayram et al. (2001) compared tried to solve the cross-shore distribution of alongshore sediment transport. Bosboom & Stive (2015) state that often, these models do not predict the total alongshore sediment transport better than bulk formulas, which predict the total sediment transport over the surf zone. The latter is often more easy to calibrate, faster and more robust. One of these formulas is the CERC formula (CERC, 1984). A reformulation assuming that waves break only in shallow water is given in Equation 2.21.

$$S = \frac{K}{16(s-1)(1-p)} \sqrt{\frac{g}{\gamma}} \sin 2\phi_b H_b^{2.5} \tag{2.21}$$

where:

S	deposited volume of sediment transported	[m^3/s]
K	empirical coefficient	[-]
p	porosity	[-]
γ	breaker index	[-]
ϕ_b	wave angle of incidence at outer edge of breaker zone	[-]

The value of the coefficient K is dependent on which wave height has been used for H$_b$; the significant wave height or the root mean square wave height. From this formula, we can see that an increase in incoming wave angle has a positive effect on the sediment transport, with a maximum angle of 45°. Furthermore, the influence of waves on both the sediment load and the alongshore current is reflected in the power of 2.5. An important characteristic is associated with this power: the sensitivity to errors. When the wave height at breaking point is misjudged by 10%, the CERC formula yields a transport rate error of 25%. The CERC formula has a few weak spots. First of all, it does not take into account the tide and wind-driven currents. Other formulas could be used to include those. Secondly, it ignores the grain size diameter and beach slope. Lastly, it is a bulk formula, meaning that it does not calculate the cross-shore distribution of the alongshore transport.

Kamphuis (1991) introduced a formula that does include the effect of grain size, beach slope and wave steepness, see equations 2.22 and 2.23. However, the influence of the tide induced currents is still not accounted for.

$$I_m = 2.27 H_{s,b}^2 T_p^{1.5} (\tan \alpha_b)^{0.75} D_n^{-0.25} (\sin 2\phi_b)^{0.6} \tag{2.22}$$

$$I_m = \rho(s-1)(1-p)S \tag{2.23}$$

where:

I$_m$	immersed mass of transported sediment	[kg/s]
H$_{s,b}$	significant breaking wave height	[m]
T$_p$	peak period of the spectrum	[s]
α_b	beach slope at breaker point	[°]
D$_n$	nominal grain size	[m]

It must be noted that both Kamphuis and CERC formulas have an empirical foundation. As equilibrium profile slope and grain size are interrelated, their absence in the CERC formula does not directly make the CERC formula less accurate than the Kamphuis formula: the CERC formula just does not separate them. The same holds for the interdependent wave height, wave period and angle of incidence. The relation between sediment transport and the angle of wave incidence can be visualized in a (S, ϕ)-curve. The angle of incidence around the breaker line usually has a maximum of around 20°-30° due to the refraction of waves. Figure 2.8 shows the response of a curved coastline for two different incoming wave angles. The curvature of a coastline will almost always lead to longshore sediment transport, as the orientation of the coastline changes with respect to the incoming waves. Also, refraction can lead to the divergence and convergence of wave energy.
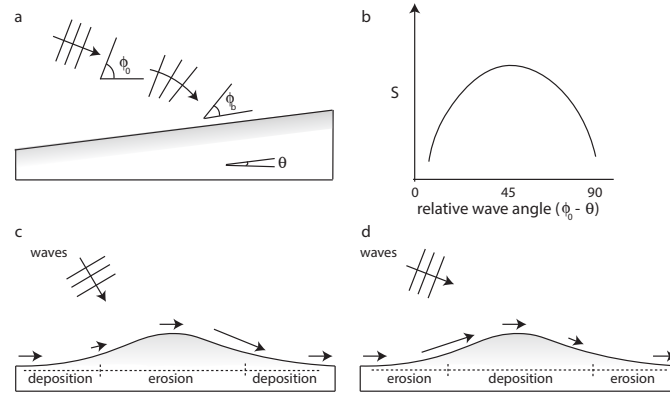
Figure 2.8: Figure (a) shows the relative deep water wave angle and the wave angle at the breaker point. Figure (b) depicts the relative S-ϕ-curve. Figure (c) shows the shoreline response to obliquely (<45°) incoming waves. Figure (d) shows the shoreline response to very obliquely (>45°) incoming waves. After Ashton & Murray (2006).

2.2.5. Aeolian transport

Next to the hydraulic erosion, also the direct influence of wind on sediment transport is of importance for understanding the behaviour of a nourishment. Above the waterline, wind can exert a surface shear stress on the sandy bed, leading to a sediment exchange between the dunes, beach and intertidal areas. When this stress exceeds a threshold, which depends on the sediment grain size, an initial movement will occur. This threshold was first described by Bagnold (1937) in an aeolian sediment transport model, see the parenthesized part of Equation 2.24.

$$q = \alpha_c C_{gsd} \frac{\rho_a}{g} \sqrt{\frac{D_n}{D_{n,r}}} (u_z - u_{th})^3 \tag{2.24}$$

where:

q	equilibrium sediment transport	[kg/m/s]
α_c	constant for conversion of wind velocity to near-bed shear velocity	[-]
C_{gsd}	constant indicating the grain size distribution width	[-]
ρ_a	density of air	[kg/m^3]
$D_{n,r}$	reference grain size	[m]
u_z	wind velocity at height z	[m/s]
u_{th}	wind velocity threshold	[m/s]

The non-parenthesized part of the right-hand side of Equation 2.24 depicts the characteristics of the sediment. The C_{gsd} indicates the uniformity of the grains, with 1.5 for a nearly uniform grading and 2.8 for a wide range of grain size. A wider grading would thus lead to an increase in aeolian transport. At first sight, an increase in the nominal grain size suggests a transport increase too. However, an increase in grain size increases the threshold value of particle movement. Though many studies have followed and proposed new parametrizations of the sediment properties, the application and characteristics have remained principally the same as the Bagnold formula (Hoonhout & Vries, 2016). According to S. De Vries et al. (2012), the moisture and beach geometry can be of even more considerable importance to transport than the wind velocity.

2.3. Morphodynamics

Beach morphodynamics concern the dynamic interactions between wave, tide and wind processes and the response of the bed (Short & Jackson, 2013). Through feedbacks, the beach system tries to maintain an equilibrium profile. This section aims to explain the behaviour of a system on disturbances like nourishments. First, the equilibrium profile is explained, addressing the difference in a winter and summer profile. Secondly, the behaviour of the natural system on different kinds of nourishments is treated.

2.3.1. Equilibrium profile

For the longer time scale, the equilibrium was already described by Bruun (1962). Sea-level rise will increase the depth at a certain distance from the coastline. This "Bruun Rule" describes that this equilibrium can only be restored by a decrease in depth which, in absence of external sediment, must be provided by a sediment volume eroded from the coastline. Figure 1.2b illustrates this. On the shorter term, rapid changes in the position of the coastline occur during storms. Storm surge can have a similar disturbing effect as sea-level rise, with storm waves providing the energy to adjust the profile (Dean, 2019). Generally, the offshore transported sediment by storms is deposited as an offshore bar. The breaking of large storm waves induces an undertow, transporting sand in offshore direction (Roberts et al., 2013). During milder conditions, swell waves recover the original beach profile, leading to a nourishment of the beach and eventually dunes through aeolian transport (Butt et al., 2004; Aagaard et al., 2004; Roberts et al., 2013). This recovery could take many months, which is a long timescale relative to the duration and eroding capacity of a storm. Due to the higher storminess in the Dutch winter than in the summer, one can distinguish a summer profile and a winter profile, see Figure 2.9 (Winant et al., 1975).
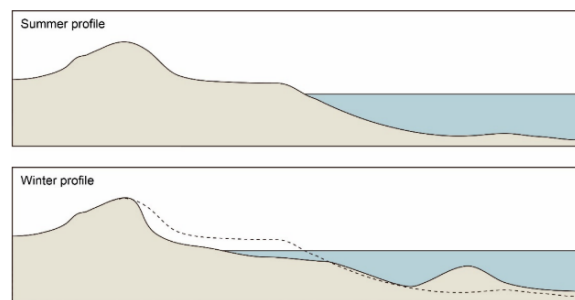
Figure 2.9: The summer and winter profile of the shore have a distinct shape. Image based on Hallin (2019).

Next to a storm event, human-induced changes can also bring the system out of its equilibrium. An example of such a change is the appliance of nourishments. Although slow processes could restore the equilibrium, Elko & Wang (2007) have shown that profile equilibration can also be an event-driven process: storm events not only quickly bring a system out of equilibrium, they can also contribute significantly to the shift towards an equilibrium. The timing of a nourishment with regards to stormy conditions could become an aspect in the design process of a nourishment (Van der Spek et al., 2007).

2.3.2. Nourishment placement and shape

The placement and shape of a nourishment could be altered to increase the erosion rate of the nourishment. As the Sandwindmill nourishment acts as a feeder for the adjacent coast, such erosion is considered a positive effect. The most basic form of a nourishment with the Sandwindmill is the placement of sediment through one outlet above the seabed. The deposited sediment would probably adopt a conic shape. When multiple outlets are placed next to each other, other shapes such as a bar could be created. The shape of the nourishment is expected to have an effect on the erosion rate, as waves and currents will interact differently with different shapes (Huisman et al., 2019).

Berm nourishment

Most of the nourishments nowadays are applied at the shoreface. In the Netherlands, these nourishments are mostly placed seaward of the outer bank (Van der Spek et al., 2007). The main reason is that this is economically more favourable. Morphologically this has an advantage too, as it prevents the existing bars from migrating offshore. M. J. P. Van Duin et al. (2004) showed that the existing bars do not only move shoreward but also increase in height. This has two positive effects. As waves break at the shoreface nourishment, the wave climate shoreward of the nourishment becomes calmer. This leads to a reduced wave-driven longshore current and thus to a settlement of alongshore driven sediment in this lee-side. Downdrift of the nourishment, this could lead to erosion as alongshore sediment transport is blocked. Secondly, the shoaling of waves over the nourishment leads to onshore sediment transport. For the case in Egmond aan Zee, the direct feed of the sediment to the coast due to cross-shore processes is estimated to take 5-10 years (the nourishment was placed 600-800 m offshore). If there are no bars present, Van der Spek et al. (2007) suggest placing the shoreface nourishment as shoreward as possible. Furthermore, it is advised not to place the heads of a bar near critical (recreational) spots, as eddies and rip currents can lead to beach erosion and dangerous swimming conditions.

Huisman et al. (2019) analysed the behavior of multiple shoreface nourishments along the Dutch coastline. The influence of the alongshore length, cross shore width and depth of the nourishment crest were assessed. A significant correlation between the inverse of the nourishment length and the erosion rate per metre length was found. The shorter the nourishment in the alongshore direction, the larger the observed erosion rates. For the cross-shore width and depth of the crest, no significant correlation was found. It must be noted that the nourishments were placed at a depth between -6 m NAP and -4.5 m NAP. When the nourishments would have been placed in a shallower area, it could be expected that the nourishments would induce more wave breaking. As waves have a significant role in sediment transport, these shallower nourishments could be subject to higher erosion rates. Furthermore, the placement in the cross-shore profile where the alongshore currents are the highest could also increase the alongshore transport. Another observation is that the bars move onshore in the first five years after the nourishment. After those five years, the bars again migrate offshore, which is the 'natural' behaviour (M. J. P. Van Duin et al., 2004).

Mega feeder nourishment

A similar relationship regarding the length and width of the nourishment was derived by the numerical modelling of the Sand Engine by Tonnon et al. (2018). A larger cross-shore width over the alongshore length ratio of the mega nourishment led to a significant reduction in nourishment lifetime. This research differs considerably from the one of Huisman et al. (2019), as the Sand Engine can be seen as a shore extension rather than a sub-aqueous berm nourishment. However, these two pieces of research stipulate how altering the shape can influence the (erosive) behaviour of a nourishment.

Point source nourishment

Little research is executed on nourishments that are placed by one outlet in a fixed location. Therefore, it is difficult to predict its behaviour based on historical measurements. Van Hugten (2019) has modelled the behaviour of a continuous nourishment (also supplied by the Sandwindmill) at the Delfland coastal stretch. The research found that the placement of the nourishment at -3m NAP led to the largest alongshore distribution, which was 500 m after one year.

The closest existing system to such a nourishment is the outlet of a sand-bypassing system, such as applied at the Australian Gold Coast (Boswood et al., 2005). A sand-bypassing system intercepts the littoral drift using a trapping jetty, before it reaches a channel in which sedimentation is undesirable, such as a navigation channel. The sediment is pumped through pipelines towards a deposition zone downdrift of the channel. There, an outlet releases the sediment. In this particular bypassing system, the increased sediment supply led to the formation of a continuous bar. This bar had a very welcome side effect as it created perfect surfing waves, a good reason for its nickname "superbank". Most of the conditions that lead to the formation of such a spit are present at that location: an abrupt change in the coastline, extremely oblique incoming waves and the feed of sediment. As the Holland coastline is relatively straight and the incoming wave angles are not very oblique, the fast evolution of such a surfer bar is unfortunately rather unlikely. Around the Wadden islands, such a formation might be more probable.

Smith et al. (2017) did research to point source nourishment in the surf zone, using a Large-scale Sediment Transport Facility (LSTF) physical model. The sediment was transported in alongshore direction rather well, as also predicted by the modelling study of Van Hugten (2019). The growth of the coastal profile in the lee side of the nourishment as described by M. J. P. Van Duin et al. (2004) was also observed by Smith et al. (2017). Furthermore, three bulk-longshore sediment transport formulas were compared with the measurements. The CERC (1984) formula performed rather weakly, overestimating the transport by a factor of 10. The Kamphuis (1991) and the more recent general longshore transport (GLT) model of Tomasicchio et al. (2013) performed much better. This research confirms the required careful interpretation of modelling results using extensively attested empirical relationships.

2.4. Tidal inlets

The Dutch coast exists of multiple tidal inlets. As these inlets have different characteristics than the closed coastal systems described in the previous sections, the inlets are discussed here. A tidal inlet is a gap in the shoreline through which water is exchanged between the sea and a basin (Elias, 2006). These inlets are often sustained by tidal influences. The presence of barrier islands, such as Texel, can be often attributed to the influence of waves (Bosboom & Stive, 2015). Correspondingly, barrier tidal inlet systems are often under the influence of both tides and waves. Figure 2.2 shows the classification of tidal inlet systems as proposed by Davis & Hayes (1984).
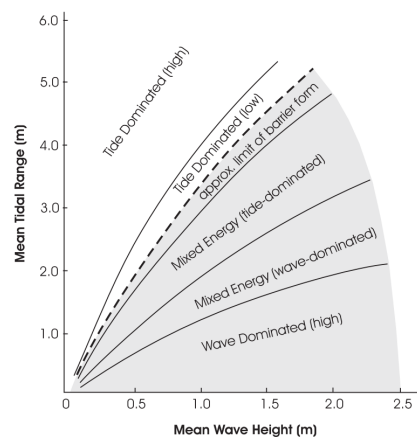
Figure 2.10: The classification of tidal systems as proposed by Davis & Hayes (1984), adopted from Elias (2006).

The large flow velocities through channels bring about a significant sediment exchange between the basin and the area outside. Ebb-tidal deltas are sand deposits that result from decreasing flow velocities due to the diverging ebb-tidal flow. These ebb-tidal deltas are located at the seaward side of the system. Furthermore, a tidal basin system consists of flats and deeper channels. The tidal range and geometry of the back-barrier system determine how much water can flow in and out during one tidal cycle, which is called the tidal prism. The tidal prism has an influence on the size of the inlet and the volume of the ebb-tidal delta. These influences follow from the attempt of the system to get into a (dynamic) equilibrium, like the equilibrium of a cross-shore profile as discussed in Section 2.3 (Elias & Van der Spek, 2017). Sea-level rise can also affect the system. If the water level rises, this will result in a relatively large change of depth of the flats. The intertidal flats will try to maintain their equilibrium depth, which can be accomplished by the import of sediment (Bosboom & Stive, 2015).

2.5. Climate change

Globally, climate change can drive changes in the wind direction, wave heights and, of course, the sea level (Morim et al., 2019). Furthermore, the increasing sea surface temperature may lead to increased tropical storm intensities (Emanuel, 2005; IPCC, 2021). In this section, the effects of climate change are briefly explained. The possible implications for the Dutch coastline are also touched upon.

Sea-level rise

As already discussed, a sea-level rise leads to an upward and landward shift of the coastline when no sediment

is added to the active profile (Figure 1.2) (Bruun, 1962; Wolinsky & Brad Murray, 2009). The Intergovernmental Panel on Climate Change has formulated four Representative Concentration Pathways (RCPs), which can be used for decision making (IPCC, 2014). In the most optimal scenario, RCP2.6, a stringent GHG emission reduction is effectuated. The most pessimistic scenario, RCP8.5, describes the situation with very high GHG emissions. IPCC has calculated the expected sea-level rise according to those scenarios; see Figure 2.11.
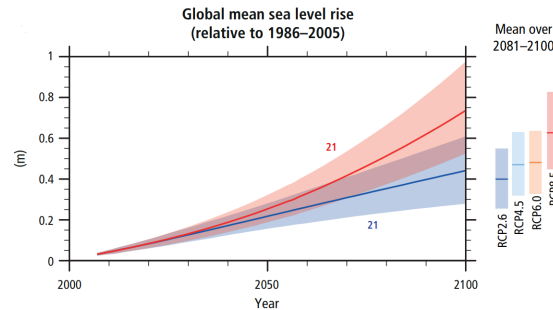
Figure 2.11: The expected sea-level rise for different emission scenarios as formulated by the IPCC (2014).

The dark blue line for the RCP2.6 scenario indicates an average increase of 0.4 mm/year. The mean line for the RCP8.5 scenario indicates an increase of 0.8 mm/year. Next to the retreating of a coastline, the rising sea level is also expected to influence the sediment import by the Wadden Sea, as it will try to compensate for SLR by increasing the height of the flats. Elias & Wang (2020) have calculated the expected change in sediment import of the western Wadden Sea for four sea-level rise scenarios (0.2, 0.4, 0.6 and 0.8 mm/year), see Figure 2.12. The effect of sea-level rise on the sediment import shows to be retarded, as changes become apparent only after 2040. The decrease during the first decades (and in the mildest scenario during the entire modelling period) is due to the reach of an equilibrium with regards to the closure of the Zuiderzee. A change in sediment import may have an effect on the sediment transport rates along the Dutch coastline, especially in the northern part of North Holland (Stive, 1989).
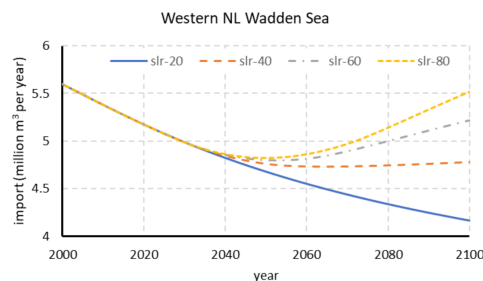
Figure 2.12: The modelled sediment import by the western part of the Wadden Sea under four SLR scenarios, as calculated by Elias & Wang (2020) with the ASMITA model. The import as calculated by ASMITA is expected to be overestimated by a factor of 2, based on measurements.

Wind and wave climate

As discussed in Section 2.2, sediment transport is sensitive to changes in the wave height. As climate change is expected to impact the global wind and wave climate, taking a variability in the wave climate into regard is essential. Morim et al. (2019) predict a 5-15% change in wave height and period under the RCP8.5 scenario. Next to wave height, also the mean wave direction can shift due to climate change. A 5-15° change of mean wave direction can be the result of the highest emission scenario. As can be seen in e.g. the Kamphuis (1991) formula (Equation 2.22), the alongshore sediment transport is dependent on this wave angle too. It must be noted that these are global numbers. The expected changes in wave climate along the Dutch coast may be of a less extreme extent. According to Van Rijn (1997), some stretches along the Dutch coast are very sensitive to changes in incoming wave angle. For Egmond, which has a coastline orientation of just 8°, a 5° change of the wave direction can lead to an alteration of the sediment transport rate of 50%. This example shows the possible sensitivity of a coastal system to minor adaptations in forcing conditions that are due to climate change.

Part II

System analysis

Chapter 3: The Sandwindmill concept

3

The Sandwindmill concept

In this chapter a comprehensive view on the Sandwindmill is given. In Section 3.1 the existing nourishment methods are briefly treated. The advantages and disadvantages of the execution of these methods show the need for an alternative approach. Section 3.2 provides an introduction to the Sandwindmill system. The subsystems of the Sandwindmill are independently treated in sections 3.3 to 3.6. The goal herein is to provide an insight on the implications of design choices of the subsystems on both the costs and the sediment nourishment itself. Section 3.7 shows the interdependency of the different subsystems and the relationship with the costs of the system, providing insight in effective methods to reduce the system costs.

3.1. Current nourishment techniques

In the following section, an overview of the existing nourishing methods is given. A distinction is made between traditional methods like beach and shoreface nourishments, and the most recent mega nourishments.

3.1.1. Traditional methods

Until the year 2000, the most common way of nourishing in the Netherlands was the application of beach nourishments (De Sonneville & Van der Spek, 2012). With beach nourishments, sand is placed between the low water line and the dune foot, mostly using dredging vessels. In the Netherlands, mostly trailing suction hopper dredgers (TSHDs) are used for the nourishments. These vessels can load while sailing, and deposit the sediment through bottom valves or pipelines (Roelse, 2002). An advantage of a beach nourishment is the direct increase of the beach width, which is beneficial from a recreational aspect. Also, the dunes can grow relatively fast due to aeolian transport. However, this method has some drawbacks. Vessels should sometimes operate in the breaker zone, which is the cross-shore region where harsh wave conditions prevail (Bosboom & Stive, 2015). According to Bakker et al. (2012), the beach nourishments mostly take place in the summer, which means that beach recreation is hindered by these nourishments. Also, a too wide beach is considered unattractive from a recreational perspective (Parkinson & Ogurcak, 2018). Lastly, infrastructure and establishments near the beach can be covered by the sand blown away.

A more economical and recreation-friendly nourishing method is the shoreface nourishment. With shoreface nourishments, sediment is supplied at the seaward side of the breaker zone, which is easier for dredging vessels to operate in. Sediment transport processes redistribute the sediment over the coastal profile. Furthermore, shoreface nourishments seem to last longer than beach nourishments (De Sonneville & Van der Spek, 2012; Baptist et al., 2009). However, the nourishment of the upper part of the shoreface leads to over-steepening of the profile and consequently to more erosion and offshore-directed transport of sediment (De Vriend et al., 2015; Stive et al., 1991). De Schipper et al. (2015) confirm this hypothesis based on the morphological data from a nourishment in Vlugtenburg, The Netherlands. The accelerated erosion in the short period following a nourishment makes these high-frequency nourishments rather inefficient. Another downside of the shoreface nourishments is the burial of marine species (Defeo et al., 2009; Jones et al., 2008). Although systems can recover after some time, the necessity of regular shoreface nourishments due to this over-steepening and coastline retreat lead to a continuously disturbed ecosystem (Herman et al., 2016).

The last type of nourishment is the channel slope (or wall) nourishment, in Dutch named a 'geulwandsuppletie' (Van der Spek et al., 2007). Such a nourishment can be applied if a channel, which is often the result of high tidal velocities, approximates the coast. Sediment is placed at the wall of a tidal channel, with the aim of keeping these channels away from the shallow and dry part of the coast.

3.1.2. Mega nourishments

The described disadvantages of regular nourishments led to an innovative solution: a mega nourishment. In 2011, Rijkswaterstaat and the Province of South Holland started an experiment to see if nourishing a large amount at once could be an adequate alternative to the traditional two to five-year nourishments. The nourishment, called the Sand Engine, is located at the Delfland coast in the Southern part of the province and consists of 19 million m^3 of sand (Mulder & Stive, 2011; Tonnon et al., 2018). The idea is that this excess of sand can be redistributed by natural processes, allowing the coast to grow naturally. One of the mechanisms that governs this redistribution is the residual current velocity of 0.1 m/s that is directed northward along the Holland coastline (Van Rijn, 1997; Luijendijk et al., 2017). This concept complies very well with the strategic aim of the 'Dynamic Preservation' policy, as the natural processes reinforce the dune areas. Such mega-nourishments are expected to be re-executed every 20 years, which is much less frequent than the typical 2-5 year interval between regular nourishments (Stive et al., 2013; De Vriend et al., 2014).

The Sand Engine is a good example of the feeder type of mega nourishments, as it feeds adjacent coasts with its sediment. Another type of mega nourishment is the permanent mega nourishment, which is designed to maintain safety levels at the location of deposition for a long time (Tonnon et al., 2018). Such a nourishment has been executed near Petten and consisted of 35 million m^3 of sand (Wenneker et al., 2016). This newly created landscape is called the Hondsbossche Dunes.

One of the main assets of these mega nourishments is that they don't bring the ecosystem in a continuously perturbated state. Moreover, they provide a space that allows for ecological and recreational development (Mulder & Stive, 2011). However, this space diminishes over time, as the nourishments erode away. Furthermore, these nourishments need to be repeated every 20 years, and thus they still burden the ecosystem from time to time.
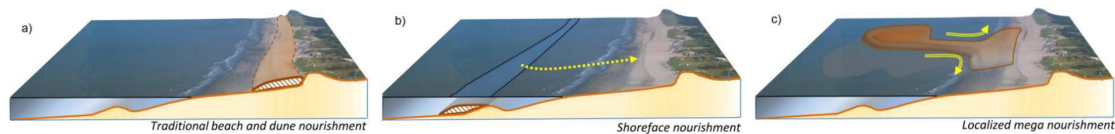
Figure 3.1: Visualisation of the current nourishment methods, from Stive et al. (2013).

3.2. Introduction to the Sandwindmill

As explained in Section 1.2, the Sandwindmill is a concept that can overcome both ecological and emission-related challenges that are associated with the current nourishment methods. Figure 3.2 illustrates the concept. In the Netherlands, the borrowing must take place seaward of the -20 m NAP depth contour (Mulder, 2000).
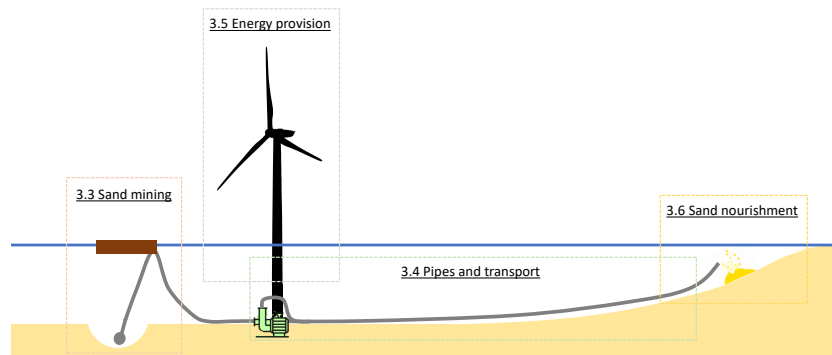
Figure 3.2: A visualisation of the entire Sandwindmill system. Subsystems and the section in which they are treated are indicated with the dotted boxes.

The Sandwindmill has two main advantages over the current methods. Ecologically, the system might have a smaller footprint as the sediment is not dumped all at once at the entire coastline that must be reinforced. Only a local placement is executed, where the currents are expected to distribute the sediment slowly along the coastline. The species in the sea could potentially keep up with the bottom elevation and prevent themselves from being buried, as the pace is more governed by natural processes than for regular nourishments. Secondly, and mostly, does the sustainable character of the concept make it a sound alternative over the current methods. The displacement of the sediment towards the nearshore can now occur using solely green energy instead of fossil fuels.

The Sandwindmill has some challenges and uncertainties with regards to the financial and technological feasibility. Internal research from Sweco shows that the Sandwindmill is expected to become financially more feasible at larger discharges (Grontmij, 2013). This implies that applying the system at a location with high sediment needs can be a requirement. The expected ecological advantage relative to the current methods has not been proved yet. One complication could be the continuous existence of turbidity plumes that can harm the ocean flora and fauna (Manzanera et al., 2014). However, as the Sandwindmill can potentially overcome most of the current challenges of nourishing, examining those knowledge gaps contributes to the development of an innovation that can supply many coasts around the world. The worldwide demand can be roughly derived from research by Luijendijk et al. (2018). With satellite imagery, the research has shown that 24% of the world's sandy beaches are eroding. Part of this erosion can be explained by the reduction of fluvial sediment discharge due to the built of river dams, as is the case for the Yangste river in China (Luijendijk et al., 2018; Yang et al., 2006).

In the coming sections, the different subsystems of the Sandwindmill are treated separately. The aim is to provide a better understanding of the system and to show the dependencies between the subsystems. The identification of bottlenecks can provide relevant information for further research. One of these bottlenecks is selected and treated in-depth in this report. Section 3.7 shows how the subsystems are interrelated and provides a framework for the optimization of the Sandwindmill design. A primary thread is the cost of the system. One of the demands of Rijkswaterstaat is that newly developed nourishment methods may not cost a lot more than the current methods. Rijkswaterstaat uses the costs per nourished cubic metre as a criterion. In the exploration below, no exact prices are mentioned. The reasoning behind this is that some prices are not to be publicly shared. Additionally, there is rather large uncertainty in the prices.

3.3. Sand mining

A large design challenge is the choice of equipment that should be used for the borrowing of the sediment. The design of the equipment has implications for the execution of the nourishments. In this section, three different techniques for the winning of sediment are treated and judged on their proof of concept, operability and an estimate of the costs. A more elaborate review of the mining methods is presented in Appendix A. The ideas and some of the data originate from brainstorm sessions with the Sandwindmill consortium (consisting of Royal IHC, De Vries & van de Wiel, and Sweco) and from research by the author. It must be noted that this exploration is meant as an indication of the potential consequences of certain design choices on the entire system. Many more winning methods can and must be considered.

3.3.1. Sandcrawler

The first mining option that is assessed is the sandcrawler. The sandcrawler works like a vacuum cleaner on the ocean floor. Remote-controlled vehicles that operate in the deep sea exist since the 1970s (Knodt et al., 2016). The aim of these vehicles is the mining of nodules that are present at large depths up to 5,000 m. The application of a sand crawler should be much more straightforward, as it would operate at depths of approximately 20 metres and would only need to dredge sediment instead of heavy 30 cm nodules. Under the more severe offshore wave conditions with a wave height of 5 metres, the wave-induced orbital velocities at 20 m depth are expected to have a magnitude of 1.5 m/s (using Equation A.1 for orbital velocities). When the crawler is assembled with the appropriate weight, it can probably resist these values. This would make the theoretical operability of the crawler 100%. The costs of the deep-sea mining crawlers are almost as high as many types of standard dredging equipment . Although the sediment crawler can be simplified, R&D costs of adapting the deep-sea mining crawler could be high.

3.3.2. Operated winning vessel

Another option for sediment borrowing would be the use of a standard winning vessel, such as a trailing suction hopper dredger (TSHD), cutter suction dredger (CSD) or a plain suction dredger (PSD) (Vlasblom, 2003). The advantage of such equipment is that it has been used for decades with the purpose of dredging. In that sense, its use comes with little risk. The use of the equipment at sea level comes with the risk of limited operability due to higher waves. A typical smaller TSHD can operate at conditions up to H_s = 2.5 m (Boskalis, 2010). When looking at the probability density function in Figure 3.3, it can be observed that waves exceed this height approximately 10% of the time.
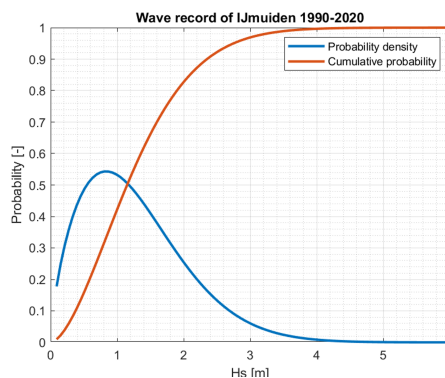
Figure 3.3: Probability and cumulative density functions of waves measured at IJmuiden between 1990-2020.

As waves and wind correlate well, this implies that the system would be unable to operate under the conditions that enough energy can be delivered (wind), and that is more energy available to disperse the sediment (waves). The costs of an operated winning vessel are estimated to be high: the sailing ability of TSHDs will be used marginally, whereas a PSD is built for operation in calmer conditions. The latter would thus need fortifications. Furthermore, the on-site operation leads to high operational costs. In Appendix A.2 the costs are elaborated on more extensively.

3.3.3. Dredging raft

The last type of equipment that is discussed, is the (autonomous) dredging raft. The raft can be a small and simple piece of equipment that is connected to four buoys. Winches on board of the raft can manoeuvre the raft between these buoys, allowing the raft to dredge the sediment in the area between these buoys. Such systems are already used for dredging calm waters, such as rivers. The idea of such a raft is to keep it limited in size in order to reduce costs. Although the operability can be increased with the use of active compensation systems, the system is expected to become inoperable at waves larger than 2 m (Adriaan Ruiter, personal communication, June 20th, 2021). This would induce an operational limit of 20% according to Figure 3.3. Next to the low capital costs, the operational costs could be kept at a very reasonable level due to the simple navigation mechanism. This system would allow for autonomous or remote control, not requiring on-site personnel, hence reducing operational costs.

Conclusion

From the analysis of the three options, it becomes apparent that the choice of a mining option is inherent to trade-offs. The choice for existing types of equipment comes with less risk but means that not all features of this equipment might be needed or appropriate for the application of the Sandwindmill system. High research and development costs might be required for newer systems. When looking at the global scale of erosion, the development of an inexpensive system is a valid objective. The development costs could be earned back with the worldwide sale of a robust (autonomous) offshore dredging system. Furthermore, the more expensive systems can have a smaller limit on the operational time. The coming sections will show how this limit on the operational time can lead to the overall system cost.

3.4. Pipes and transport

After the sediment has been removed from the seabed, the dredged material will be transported through flexible pipelines to a steel pipeline. The steel pipeline can transport the sediment from the hub towards the coastline. Based on information from CIRIA (2009), the power required for the dredging is estimated a few factors smaller than the power for transport. The former is thus left out from this analysis. This section aims to assess some requirements of the steel transport pipeline. In order to determine the power that the entire Sandwindmill system will cost, the power required for different nourishment volumes is determined. The subscript s stands for sediment, the subscript w for water and the subscript m for mixture.

$$V_{s,situ,design} = \frac{V_{s,situ,year}}{T_{operational}} \tag{3.1}$$

$$V_{s,real,design} = V_{s,situ,design} \cdot (1 - p) \tag{3.2}$$

$$M_{s,real,design} = \rho_s \cdot V_{s,real,design} \tag{3.3}$$

If a certain amount of sediment must be placed in one year ($V_{s,situ,year}$), system downtime should be taken into account. The operational time is denoted by $T_{operational}$ and expressed in [%]. In-situ refers to the dry bed volume of sediment, including pores. If the system is operational for 50% of the time, this means that the pumping capacity should be twice the yearly demand ($V_{s,situ,design}$). In Equation 3.2, the effect of pores is removed, which are included in the in-situ design quantities. A porosity of p = 0.4 is used here, as is common for medium sized sand (e.g. (Van Rijn, 1997; Roelvink et al., 2015)). The used densities of water and sand are 1,025 and 2,650 kg/m^3, respectively.

$$v_{critical} = 1.7 \cdot (5 - \frac{1}{\sqrt{D_{50}}}) \sqrt{D_{pipe}} \ (\frac{C_{vd}}{C_{vd} + 0.1})^{1/6} \sqrt{\frac{(\rho_s/\rho_w) - 1}{1.65}} \tag{3.4}$$

$$v_{design} = v_{critical} \cdot f_{safety} \tag{3.5}$$

$$Q_{m,real} = v_{design} \cdot \pi \cdot (0.5D_{pipe})^2 \tag{3.6}$$

In order to avoid sediment particles from settling and clogging the pipeline, a certain minimal velocity should be maintained. Matousek (2004) proposes the empirically derived Equation 3.4. C_{vd} denotes the concentration of sediment in the mixture (where $\rho_{mixture} = C_{vd}\rho_s + (1 - C_{vd})\rho_w$). A safety factor should be applied to be above this critical velocity (Equation 3.5). For this analysis, a value of $f_{safety} = 1.3$ is used. The particle diameter D_{50} is in mm, the pipe diameter D_{pipe} is in m and the critical velocity $v_{critical}$ is in m/s. Figure 3.4 visualises this relationship. The required velocity increases with an increasing grain size, as the fall velocity of larger grains is higher and it costs more energy to keep larger particles in suspension.
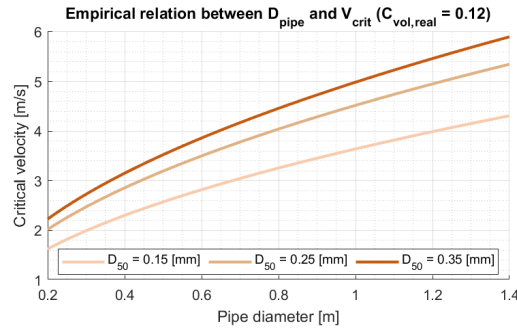
Figure 3.4: Relationship between the pipe diameter and critical velocity for multiple grain sizes and a constant C_{vd} of 12%.

Now that the velocity is known with a given concentration and pipe diameter (assuming the D_{50} not to be a design variable), the corresponding sediment discharge can be calculated. By varying C_{vd} and D_{pipe}, a desired volume of in-situ sediment can be determined. There are multiple combinations of these variables that can lead to a desired nourishment volume. The required power for pumping the sediment can now be determined.

$$Re = v_{design} \cdot D_{pipe} / v \tag{3.7}$$

$$\lambda = \frac{1.325}{(\ln[\frac{\epsilon}{D_{pipe} \cdot 3.7} + \frac{5.74}{Re^{0.9}}])^2} \tag{3.8}$$

$$\Delta p = \lambda \cdot \frac{L}{D_{pipe}} \cdot \frac{1}{2} \rho_m \cdot v_{design}^2 \tag{3.9}$$

$$P = \frac{\Delta p \cdot Q_{m,real}}{\eta} \tag{3.10}$$

First, the friction (λ) must be determined. To do this in a non-iterative manner, the equation of Swamee & Jain (1996) is used, which is an adaptation to the Haaland equation (see Equation 3.8). For the determination of the Reynolds number, a kinematic viscosity (v) of 0.0013 Pa · s for water at 10°C has been used. A wall roughness (ϵ) of 0.03 mm has been used, which is typical for steel pipes (Langelandsvik et al., 2008). When the friction is known, the head loss (Δp) due to friction can be determined. This drop is dependent on the length of the pipeline (L). As the 20 m depth line in the Netherlands is approximately 12 km away from the nourishment location, this value is used for L. The quadratic relation of flow velocity and head loss shows the importance to pump as slow as possible, hence as close to the critical velocity as possible. When the pressure drop over the pipeline is know, one can determine the required power to pump the sediment mixture over a distance of L metres, with a discharge of $Q_{m,real}$. A pump efficiency (η) of 60% has been used. The result for multiple volume concentrations, nourishment quantities ans grain sizes is given in Figure 3.5. The optimal pipe diameter yielding the right sediment volume at the critical velocity has been calculated in an iterative manner. As a first analysis by Sweco estimates a yearly operability of 50%, this has been used (Grontmij, 2013). This implies that a required annual volume of 100,000 m^3 would require a pumping capacity of 200,000 m^3 per year (resulting in 100,000 m^3 as the operability is 50%). In Sections 3.5 and 3.7, this operability value will be reassessed. As concluded in Section 3.3, this value depends amongst others on the choice of winning method and the installed windmill capacity.
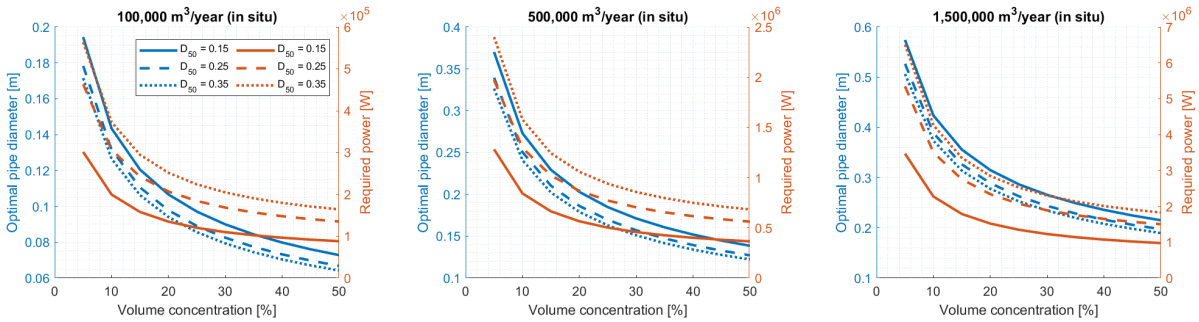
Figure 3.5: Overview of the ideal pipe diameter and required power for different nourishment volumes and grain sizes at an operability of 50%. At an operability of 100%, the values for the required power would be half the values presented here. The other values would remain equal. D$_{50}$ values are in millimetre. The left axis indicates the calculated pipe diameter and the right axis indicates the required pump power.

The increase of concentration comes with the higher risk of clogging the pipeline. For a long pipeline, this clogging can be disastrous as it is difficult to flush a pipeline that has much stagnant sand in it (Edwin de Hoog, personal communication, August 5, 2021). A few things can be read from the figure. First of all, there is a non-linear decrease of required power with the increase of concentration. As higher concentrations give a smaller drop in energy demand, at a certain point the gain in required power does not weigh up to the increase in concentration. For long pipelines, concentrations of 15% are therefore often used (Edwin de Hoog, personal communication, August 5, 2021). Furthermore, it becomes apparent that a decreasing grain size results in lower energy requirements. The required pipe diameter does grow with a decreasing grain size. With regards to the nourishment volumes, a logical increase of required power and pipe diameter with the required nourishment volume can be observed. The amount of power per nourished m^3 decreases with the increasing volumes; nourishing larger volumes is more energy-efficient. For the larger grain sizes, the nourishments at 1,500,000 m^3/year are approximately 50% more efficient than the nourishments of 100,000 m^3/year.
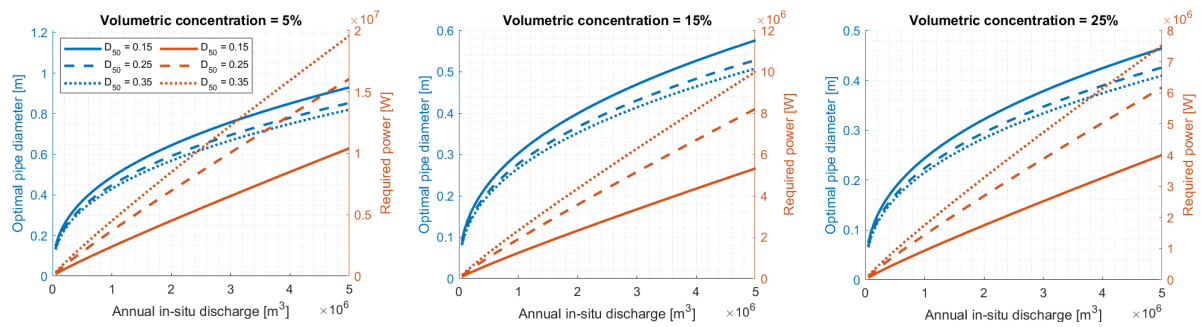
Figure 3.6: Required power for different discharges and different concentrations at an operability of 50%. At an operability of 100%, the values for the required power would be halve the values presented here (all other values remaining equal). D_{50} values are in millimetre. The left axis indicates the calculated pipe diameter and the right axis indicates the required pump power.

This approach gives an indication of the required power for different volumes, grain sizes and concentrations. The value used for efficiency is dependent on many characteristics, such as the discharge and the amount and grain size of the sediment that is being pumped (Matoušek, 2004). Furthermore, friction losses due to bends and the flexible pipeline were not taken into account.

The costs

From Figure 3.6 it can be read that nourishing 2 Mm^3 costs 2.32 MW (= 1.159 W/m^3), whereas pumping 0.5 Mm^3 costs 0.664 MW (= 1.328 W/m^3). The required power per m^3 is thus lower for the larger nourishment quantities. A higher required power means higher capital costs for both the windmills and the pumping system. The increase of pipe diameter is a factor 6 smaller than the increase in nourishment volume; unless the price of a pipe grows spectacularly with the diameter, it can be assumed that also the transport pipes are cheaper (per m^3) for larger nourishment quantities. With regards to the grain size it can be concluded that smaller grain sizes are more cost-effective despite the slightly larger pipe diameter required. Another benefit of smaller grain sizes is that they lead to a smaller wearing of the pipe walls (Lian et al., 2018). This elongates the design lifetime of the pipelines.

Conclusion

From the executed assessment of the sediment transports, it can be concluded that an increase in nourishment volumes makes the transport process relatively cheaper. Furthermore it has been observed that smaller grain sizes are to be preferred from the perspective of energy requirements and abrasion, hence costs.

3.5. Energy provision

In the previous sections it was assumed that the wind would blow sufficiently 50% of the time during a year. This number is highly dependent on the system requirements and the installed power delivery capacity. It this analysis, a pumping system is assumed that is on or off. Now that it is known how much power the system would require, the different options for power delivery are assessed. From this delivery side, the main variable is the windmill size. The diameter of the rotor is the design characteristic with the largest influence on the delivered power. In Equation 3.11 this relationship is displayed (Tong, 2010). Windmills have a wind-dependent power efficiency, with a maximum value of $C_{p,max}$ = 59%, referred to as the Betz limit (De Lellis et al., 2018).

$$P_{wind} = 1/2 \cdot \rho_a \cdot \pi \cdot r^2 \cdot v_{wind}^3 \cdot C_p \tag{3.11}$$

where:

P_{wind}	power delivered by the wind	[W]
ρ_a	air density	[kg/m^3]
r	radius of windmill blade	[m]
v_{wind}	velocity of air	[m/s]
C_p	power coefficient	[-]

Windmills have a threshold wind velocity that should be exceeded before the windmill will deliver any power. For most windmills, this value lies around 3 m/s. Thereafter, the delivered power increases with the third power of the wind velocity, corrected by the power coefficient. At a certain point, the power coefficient slows down the power growth to such an extent that the delivered power does not grow anymore with the wind velocity, see Figure 3.7a. If a wind turbine would be installed with an installed power of 2 MW and the system would require 1.5 MW, this would mean that the system would only operate under wind speeds higher than 10 m/s, as can be seen from Figure 3.7a. Figure 3.7 shows that this velocity is exceeded approximately 50% of the time.

(a) Power curve for a 2MW windmill

(b) Weibull distribution for wind velocities at North Sea at 10m height.
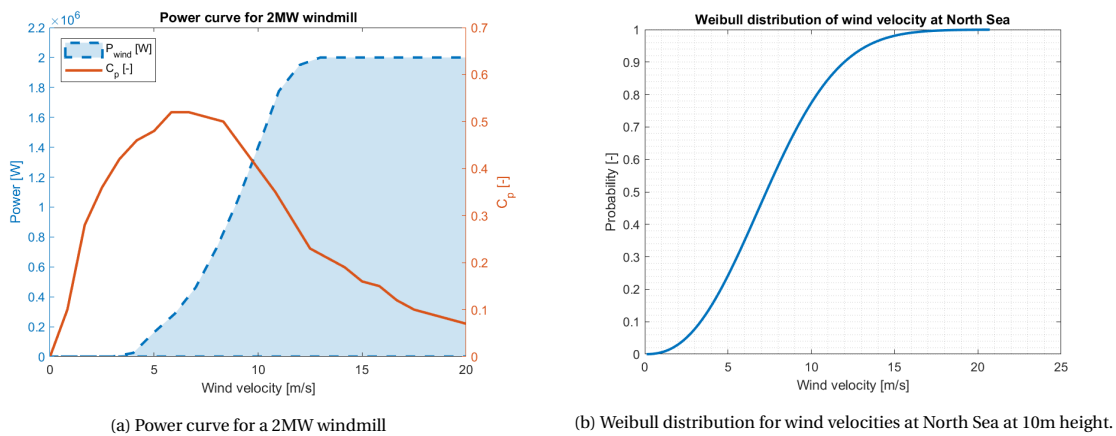
Figure 3.7: Curves that can be used for the determination of the power that can be delivered through wind at the North Sea. The wind data is based on the ERA5 reanalysis data of 2017 (Hersbach et al., 2020).

When the wind would fall below this velocity, the system would become inoperable. However, when battery capacity is added to the system, the pumps can also be powered at smaller wind velocities. This would allow for a system with a windmill capacity lower than the pumping system requirement. As wind turbines increase in price almost linearly with their capacity, there might be a more cost-effective combination of windmill power and battery capacity (Wiser & Bolinger, 2008).

Figure 3.8 and Table 3.1 show how such a system would work. The installed windmill power is just above the required system power (P_{system}), which are 4.1 and 4 MW, respectively. This would correspond to a system that can pump approximately 2,000,000 m^3 in-situ per year, following the calculations for the pipe transport in the previous section (for $C_{vol,real,\%}$ = 15%; D_{50} = 250 μm; $T_{operational}$ = 50%). The installed windmill power of 4.1 MW is enough to both charge the battery and power the system at the same time. From calculating the system activity using one year of wind data, it follows that the system runs for 2816 hours on wind-only, and uses the battery capacity for 1424 hours. The 3 MWh battery hence increases the operability with 50%. This same operability would have been achieved on wind-only with a windmill of 5MW. When the cost of a windmill is €1.5M per MW and the cost of a battery €150k per MWh, the system with the battery would be 12% cheaper compared to the 5MW wind-only alternative. The prices mentioned are based on Wiser & Bolinger (2008) and Cole & Frazier (2019), but are just given to exemplify how battery usage could reduce costs.
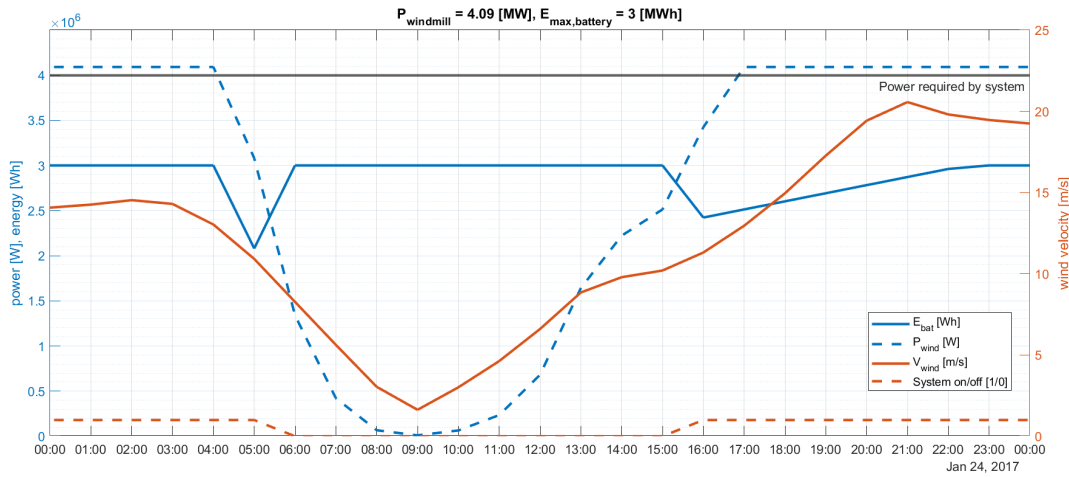
Figure 3.8: Exemplification of the modelled interaction between the battery storage and the windmill for a duration of 24 hours. An explanation is given in Table 3.1.

Time	Wind and power	Energy source	Battery state
00:00 - 04:00	Wind blowing sufficiently to generate 4.1 MW (= P_{wind})	Systems runs entirely on wind energy	Battery is fuly charged
04:00 - 05:00	P_{wind} drops below system requirement to 3.08 MW	Battery (at previous t) is charged with 3 MWh: together enough for 4MW requirement	Battery is being drained with 4MWh - 3.08MWh = 0.92MWh
05:00 - 06:00	P_{wind} drops further to 1.3MW	Battery (at previous t) is charged with 2 MWh: together not enough for 4MW requirement	Battery charged with all available energy up to its capacity (3MWh)
06:00 - 12:00	P_{wind} drops below 1MW	Full battery cannot let system run for 1 hr. System does not run	Battery is fully charged
14:00 - 15:00	Power exceeds 1MW: enough to run together with battery	At current wind speed, only battery for 3MWh/(4MW - 1.6MW) = 1.25 hours System does not run[1]	Battery is fully charged
15:00 - 16:00	Enough wind to have reliable support from the battery	System runs on both the battery and wind	Battery is being drained with P_{system} - P_{wind} = 0.6MW
17:00 - 23:00	Wind power exceeds P_{system}	System runs on wind only	Battery is being charged with P_{wind} - P_{system}
23:00 - 00:00	Wind power exceeds P_{system}	System runs on wind only	Battery is fully charged

Table 3.1: Step-by-step explanation of the curves in Figure 3.8.

---

[1] In order to prevent the system from just running for one hour, there has been set a threshold that the required energy from the battery must be at least enough to operate the system for three consecutive hours, based on the current wind condition. If wind falls, the system will operate for shorter than this three hour threshold. Meteorological models could forecast the short-term future wind velocities to ensure this minimum working period.

For this analysis, a few assumptions have been made. The wind velocities used are coming from the ERA5 reanalysis of 2017, which gives wind velocities and directions at 10 metres height (Hersbach et al., 2020). As the hub height of wind turbines is much higher, these velocities are increased with 30%. This 30% results from the internationally used formulation given in Equation 3.12, with a vegetation height of 3 centimetres and a hub height of 100 m (Van den Berg, 2004).

$$v_{wind,h} = v_{wind,ref} \cdot \frac{\log(h/z)}{\log(h_{ref}/z_v)} \tag{3.12}$$

where:

$v_{wind,h}$	wind speed at height h [m/s]
$v_{wind,ref}$	wind speed at height h_{ref} [m/s]
h	height of interest [m]
h_{ref}	reference height [m]
z_v	height of vegetation [m]

Van den Berg (2004) shows that this the relationship between wind speed and height is highly dependent on the stability of the atmosphere, where the increase of wind speed at 100 m compared to 10 m can be between a factor 1.2 - 2.6. The 30% should therefore be seen as a safe choice, with actual wind speeds and hence operational times being probably higher than calculated. The costs that are being used are mostly indicative, with the main goal of showing that the batteries can have a financially beneficial effect. Lastly, the power curves that have been used are a generalization of multiple wind turbines. Each brand and type of wind turbine has its own power curve.

3.6. Sand nourishment

The last subsystem of the Sandwindmill is the nourishment system. As discussed in Section 3.1, three different nourishing methods can be distinguished: beach nourishments, shoreface nourishments and tidal channel slope nourishments.

Beach nourishment

With a beach nourishment, the sediment slurry is deposited on the beach, above MLW (Rijkswaterstaat, 1988). With machinery, the sediment can be distributed along the beach. After the sediment has been distributed initially, natural processes like waves, tides and wind will take over the distribution. For the case of the Sandwindmill, the initial distribution of the sediment or the sediment outlet would cost additional manpower (see Section 3.3 for an estimation of the amount of manpower per dredging alternative).

Shoreface nourishment

For the execution of a shoreface nourishment, the outlet pipe can be placed above or just below the sea level. Due to the placement at a certain height above the bed, there is room for the initial distribution of the sediment. In this case however, as opposed to a beach nourishment, the natural processes are entirely responsible for the distribution of the sediment once it has left the system. This is in the case that the pipe outlet is fixed. If this transporting capacity is not sufficient, the sediment will pile up. Therefore, applying a winch system comparable to the dredging raft of Section 3.3 can be a good way to make the initial sediment distribution less labour-intensive. It should be assessed whether such a system can be robust enough to withstand the power of breaking waves in the nearshore.

Tidal channel nourishment

Channel nourishments take place at the sides of tidal channels, which can be tens of metres deep. The aim of such nourishments is mostly the stabilization of a tidal channel or adjacent stretches and structures. Due to the high flow velocities in tidal channels, they can also serve as a feeder for nearby coastal sections. The execution of a tidal channel nourishment with the Sandwindmill can look like the shoreface nourishment, although the large steepness of the channels and large depths might make the displacement of the outlet unnecessary. This nourishment method could thus be autonomous for a relatively long period of time.

Conclusion

The ideal situation for the Sandwindmill would be that a single system could feed a large coastal stretch. As the displacement of the outlet can be expensive and a technical challenge, nourishing at a location where no or the least displacement is needed, is preferred (Van der Spek et al., 2007). The beach nourishments would require a continuous effort to distribute the sediment when it leaves the outlet. After time, the outlet itself should be displaced as well. The initial sediment dispersion for the first two types is done by nature. After some time, the outlet itself should be probably displaced. This could be at a lower frequency for locations with a larger depth and with a stronger natural forcing. In Section 3.3, the high personnel costs were already briefly touched upon. In order to be competitive with traditional forms of nourishing, these costs must be kept as low as possible. This insinuates that the choice for an autonomous nourishment system is to be preferred.

3.7. System interdependencies

The review on potential mining methods shows that there seems not to be a dominant 'winner' based on the limited set of criteria used. More extensive research on these and other options should be conducted. The operability of each system has consequences for the energy requirements discussed in Section 3.4. The difference in the winning systems' energy requirements is small compared to the required power for pumping the sediment mixture to the coast. From the analyses of the required power and the energy provision, an interesting optimization issue arises. When the system is active during a larger period of the year, the discharge $[m^3/s]$ of the system when it is turned on can be lower, given a fixed yearly nourishment volume. This lower discharge allows the use of a lower pumping capacity [MW]. This pumping capacity sets a lower limit for the installed windmill power. The lower the installed windmill power, the lower the costs of the system. These relationships are (almost) linear. However, the lower the installed power, the less the operational time can be. For the high operational times required for a low Q, the windmill should also generate enough power during lower wind velocities, which requires an over-dimensioned windmill. The costs must be optimized by finding the right balance between operational time and installed capacity. Figure 3.9 shows a causal relationship diagram for this problem. The possibility of the use of battery capacity makes this problem even more interesting. Another interacting factor is the winning method used. This sets an upper limit on the wind velocities that can be used, assuming that high wind velocities coincide with the high waves that limit the operational times. Lastly, an increase in Q for the same annual nourishment volume leads to larger pipe diameters and higher pressures, hence more expensive pipes.
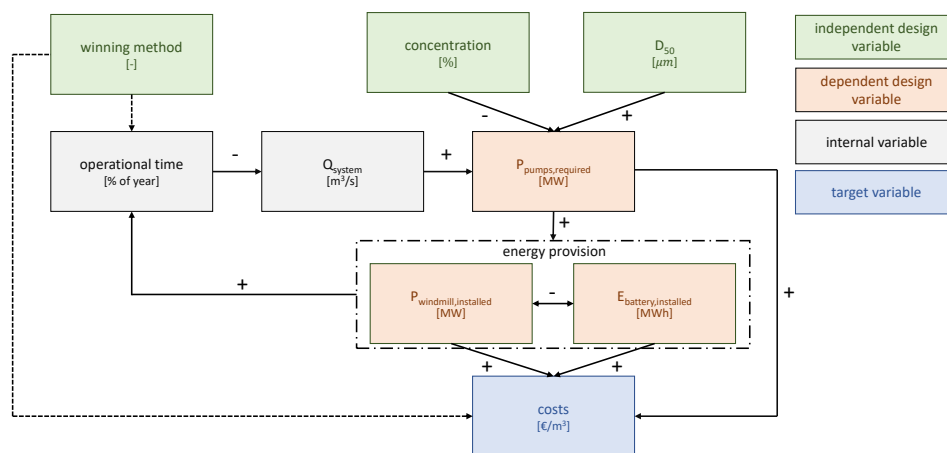
Figure 3.9: Causal relationship diagram of energy optimization problem for a determined annual nourishment volume. For the external variables, it holds that there are no trade-offs included for the scheme as they only directly influence one parameter. A '+' indicates that an increase of the source parameter leads to an increase in the target parameter, or that a decrease leads to a decrease. The '-' sign indicates that a value change in the first parameter leads to a change of opposite sign of the second parameter. A dashed line indicates a relationship that can not be expressed by a '+' or '-'.

3.7.1. Operational times

The above optimization problem is illustrated with an example. As concluded, an increase in nourishment quantity suppresses the nourishment costs per m^3 since some costs are not sensitive to system size changes. A location is found where $500,000 \, m^3$ must be supplied annually with a D_{50} of $250 \, \mu$m. A design concentration of 15% is chosen as the optimum trade-off between safety and costs. The question is what the minimum costs would be per m^3 if a dredging raft is used.

1. From the maximum operational wave height of the raft and the CDF of the offshore wave height, it can be concluded that the raft cannot be operational under approximately 20% of the highest waves (see Figure 3.3).
2. When assuming that the waves and wind correlate well, this means that the system cannot operate under the winds that occur in the upper 20% of the CDF, which are winds >15 m/s (Figure 3.7). These winds *can* be used to charge the battery while the pumps are off. This condition is set in the script of the energy storage calculations (Figure 3.8).
3. The energy storage calculations are executed for many different windmill capacities, battery capacities and $P_{required}$. This results in a table with operational times for each configuration. The configurations

      are selected for which the combination of P_{system} and $T_{operational}$ lead to the required 500,000 m^3 volume, for the given concentration and grain size.

4. From these different configurations yielding the same annual volume, the one with the lowest cost should be selected.

5. It becomes apparent that the most cost-effective is the combination of a smaller windmill (1 MW), an intermediate pump capacity (1 MW) and some battery storage (3 MWh), leading to an operational time of 42%. The results also show that without the weather limitation, a system with the same windmill, a pump of 0.5 MW and a battery of 1 MWh would have resulted in the same discharge with an operational time of 75%. The cost reduction would be 22% under the currently assumed costs of the different parts.

For the computations mentioned in item 3 of the above list, calculations with 11 battery capacities (0 - 25 MWh), 14 pump sizes (0.1 - 8 MW), 8 windmill sizes (1 - 8 MW) and 3 wind limits (no limit, upper 10%, upper 20%) have been executed. For all of these 3,600 scenarios, the hour-to-hour calculations as shown in Figure 3.8 have been made for the wind velocities in the Netherlands in 2017. A pump price of 1.5 €/W has been set, based on the price of a booster station according to CIRIA (2009). No pipe prices have been taken into account, nor maintenance and building costs. The results are shown in Figure 3.10. The vertical point clouds at 80%, 90% and 100% are induced by the operational limits of the winning options.
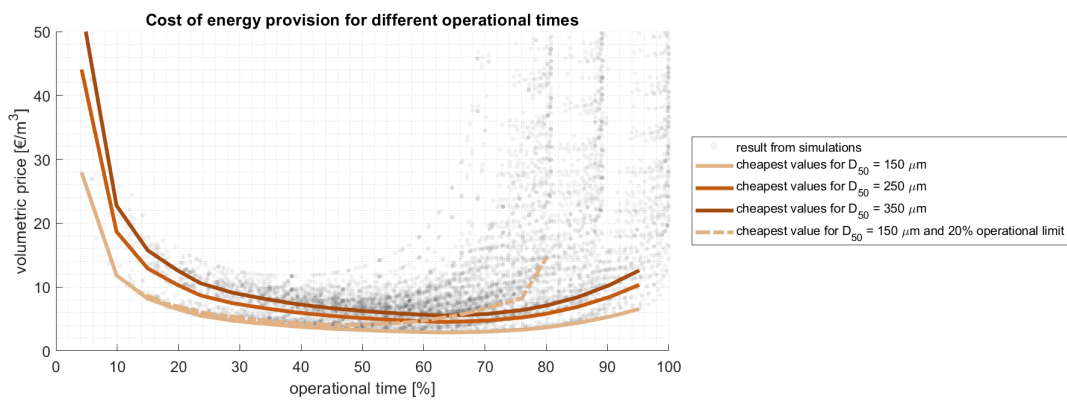
Figure 3.10: Result of approximately 3,600 simulations with different variations of installed windmill power, pump power, battery capacity and maximum operational time due to weather circumstances. The indicated prices consist of the pump, windmill and battery price. To get the annual cost, the values should be divided by the design lifetime of the equipment.

Higher operational times would be cheap from the energy-requirement perspective. However, a high operational time would require large installed windmill power and battery capacity. The relationship between those two, as schematized in Figure 3.9, appears to have the optimum value around 60-70% operational time as appears from 3.10.

3.7.2. Nourishment volume and costs

Nourishing larger volumes is required to keep the price per m^3 at a reasonable level. Section 3.4 explains how the required energy per m^3 decreases with an increasing volume. This suggests a relatively lower price for the energy provision for higher nourishment volumes. Next to the energy system, which grows in absolute costs with the nourishment volume, there are other elements that contribute to the cost of the Sandwindmill system. Many costs, such as the installation of a 12 km pipeline or the mining equipment, will depend to a smaller extent on the nourishment volume. These elements that are less sensitive to a change in nourishment volume, make a high design production an attractive way of reducing the costs per m^3.

3.8. Conclusion

The applied approach shows some sensitivities that should be taken into account in the design of the system. The proof-of-concept and therewith the risks of the winning methods are not expressed financially herein. Installation and maintenance costs are assumed to be moderately dependent on the chosen configuration and nourishment quantity. The more sediment is being nourished with the system, the smaller these costs are per cubic metre. It seems furthermore financially attractive to have as least human intervention as possible on the nourishment side. Areas where natural processes are capable of distributing the sediment along the coastline are therefore more desired. It does - next to the technological and financial benefits - also fit in more with the building with nature philosophy aimed at by Rijkswaterstaat (De Vriend et al., 2015; Rijkswaterstaat, 2015). An assessment of areas with a large erosive behaviour and the local transporting mechanisms can help gain insight into the feasibility and applicability of the Sandwindmill. In the coming chapters, these mechanisms are assessed, and such areas are selected for the Netherlands. Afterwards, the application of a continuous nourishment in the selected regions is assessed. The conclusions from these assessments and this chapter can provide in designing a nourishment strategy that makes the Sandwindmill the better alternative to traditional nourishment methods.

Part III

Nourishment design

4

Case study

In Chapter 3 it is explained that the Netherlands is a good starting point for the Sandwindmill. In Section 4.1, an area in the Netherlands is selected that suits with the requirements of the Sandwindmill. Within this area, two locations are selected for the application of the Sandwindmill. In Sections 4.2 and 4.3, these locations are assessed.

4.1. Area of interest

As the sediment provided by one Sandwindmill outlet is not able to cover the entire Dutch coastline, a more specific location must be chosen for a case study. In this section, an area of interest is selected based on two criteria: the sediment demand and the abundance of nearby windmill parks. Secondly, the most important components of the selected area are touched upon.

4.1.1. Selection of area
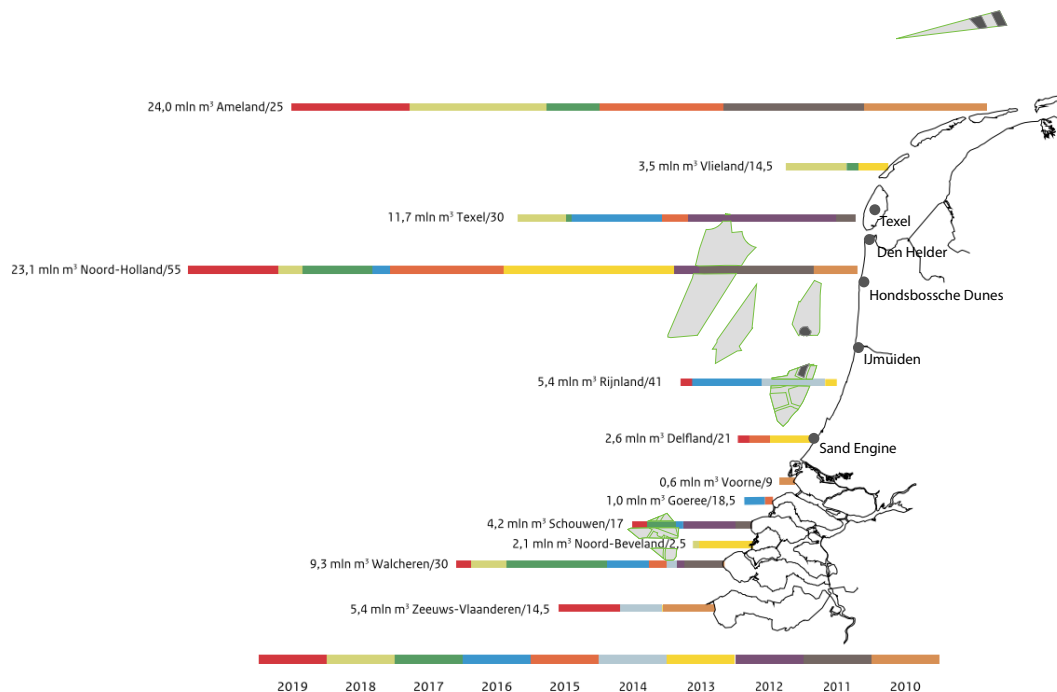
Figure 4.1: The nourishment volumes in the Dutch coastal sections between 2010-2019 are shown in the horizontal bars. The planned (light grey) and current (dark grey) windmill parks in the Dutch North Sea are also depicted. Based on Rijkswaterstaat (2019b) and RVO (2020).

Figure 4.1 shows the total nourishment volumes for different stretches of the Dutch coastline between 2010 and 2019. It can be seen that the nourishment volumes at the North Holland coast, Texel, Ameland and Walcheren are the largest. This makes assessing these regions interesting. Firstly, as those regions receive the largest volumes of sand, they are likely to erode seriously and form a critical coastal stretch. As the Sandwindmill system is only financially viable at larger nourishment volumes, it is preferred to apply it at a location with high demand. One of the processes that underlie the high sediment need of these areas is the prominent role of tidal velocities in these regions (Van Rijn, 1997; Van Weerdenburg & Van der Werf, 2021). A physical explanation of these processes around the Wadden Sea is elaborated in Section 2.4.

Figure 4.1 gives a view on the maintenance intensity of certain coastal regions and the vicinity of windmill parks. The Sandwindmill profits the most from areas with a very local sediment demand (on an even smaller physical scale than presented in Figure 4.1). In Figure 4.2 the nourishment volumes per 100 m for each coastal stretch have been determined. A database with information on the executed nourishments between 1990-2019 provided by Rijkswaterstaat has been used. Locations with high peaks in the blue lines indicate nourishment-intensive areas.
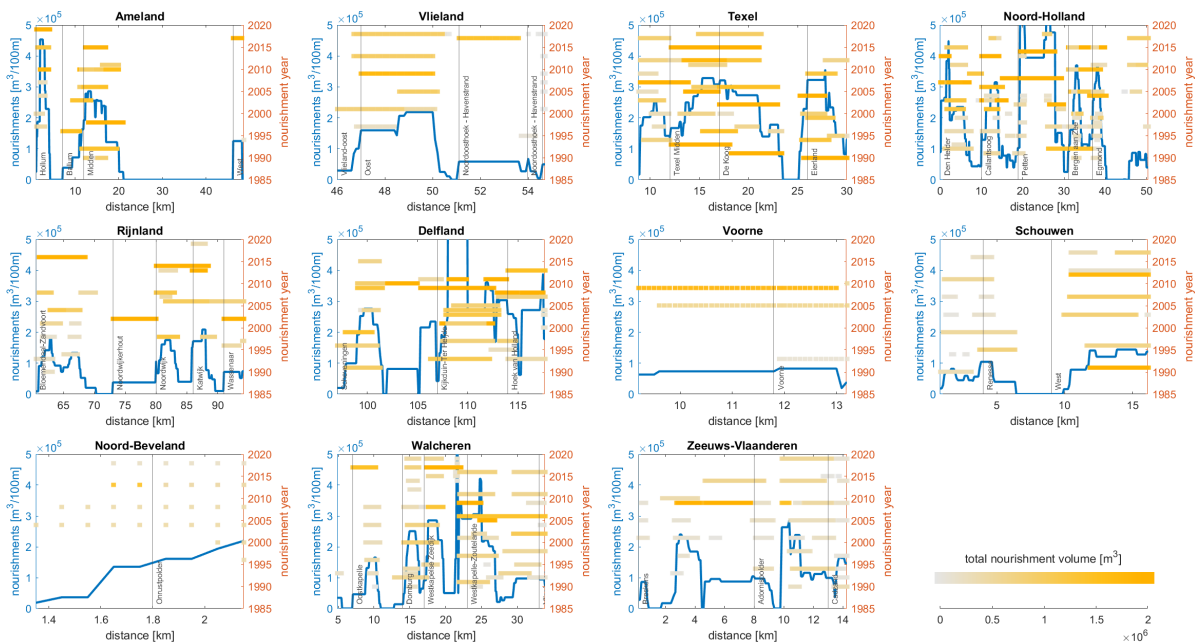
Figure 4.2: Detailed overview of the nourishments executed in coastal sections of the Netherlands. The blue line indicates the total amount of sediment nourished between 1990 and 2019 per 100 m of coast for the different coastal regions shown in Figure 4.1. The vertical position of the yellow bars indicates the nourishment years, whereas the colour gradient of the bar indicates the total volume of the executed nourishment. The horizontal scales of the figures are not equal. The figure is created with raw data from Rijkswaterstaat, which has has not been fully validated by the author.

From Figure 4.2 the nourishments of the Hondsbossche Dunes (20-30 km in North Holland) and the Sand Engine (107-110 km in Delfland) can be distinguished. When ignoring these mega nourishments, the nourishment-intensive areas that can be distinguished are the tip of North Holland (between 0-20 km), Texel, Ameland and Walcheren. From these locations, Walcheren and North Holland are the closest to the planned windmill parks. The heterogeneity of both locations offers the possibility to assess a tidal channel wall nourishment and a shoreface nourishment, which appeared to be the most appealing from Section 3.6. For this research, the North Holland section is assessed. An assessment of the applicability of a Sandwindmill at Walcheren is recommended.

4.1.2. Assessment of area

In this section, the selected area is explored on three components. First: the georgraphical characteristics, the local hydrodynamics and lastly the prevailing sediment transports.

Geographic

The area to be studied, encompassing the region between IJmuiden and Texel, is morphologically and hydro-dynamically dynamic. The following section provides a brief overview of the history and characteristics of this area, which entirely falls within the region of the water board Hollands Noorderkwartier.

For hundreds of years, the coastal stretch north of IJmuiden has suffered structural erosion. The erosion rate between the years 1600 and 1800 was approximately 3-5 metres per year. From 1800 onward, artificial structures were built to fight this erosion. These structures have led to a reduction of the erosion rates to 0.5-1.5 metres per year (Van Rijn, 1997).

IJmuiden forms the southern boundary of the focal area. There, the mouth of the North Sea Canal is protected by large breakwaters. The entire coastal stretch north of Bergen aan Zee, from -20 m NAP up to the dunes, is classified as a Natura2000 area (Verbrug, 2008). This implies that the area is of significant importance to breeding and resting species. This makes the preference for a Building with Nature approach in the area even larger (Vikolainen, 2012). However, the classification could also induce limitations on the design.
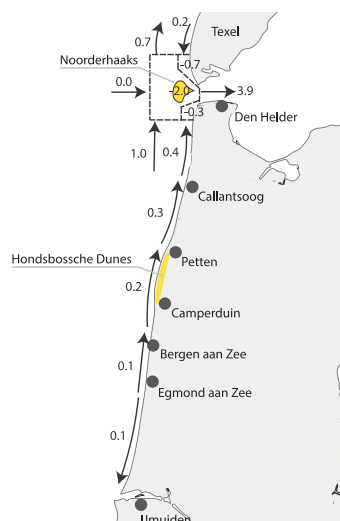
Figure 4.3: The Hollands Noorderkwartier area including the names of some discussed locations. The numerical values indicate an estimation of the yearly net sediment transports along the area of interest between +3m NAP and -8m NAP [$\cdot 10^6$ m^3/year].

It is important to include the Texel inlet (or Marsdiep) in this study, as the Wadden Sea is importing sediment through this tidal inlet. The major source of the sediment are the ebb-tidal deltas (Elias, 2006). The Noorder-haaks forms a large supratidal ebb-tidal delta, meaning that tides never inundate it. Other sediment sources are the North Sea shorelines of the barrier islands Texel and the North Holland coast. The nourishment of these coasts following the dynamic preservation policy thus forms a sediment source for the Wadden Sea too (Wang et al., 2018). Studying the mechanisms that drive these interactions will contribute to a better understanding and ability to model the sediment flows provided by the Sandwindmill. Section 2.4 therefore treats the relevant processes at tidal inlets.

Hydrodynamics

The North Holland coastline can be characterized as a micro-tidal and wave-dominated (Cooper, 2005). There are two dominant wave directions: SW and NNW waves (Stronkhorst et al., 2018). Section 5.3 goes into further detail on the wave climate. The tidal wave is dominated by the M_2 constituent. Towards the north, the M_4 constituent becomes more apparent, increasing the tidal asymmetry. This leads to a faster rise than the fall of the tide. The mean tidal range is 1.38 m at Den Helder, with extremes of 1.0 m and 2.0 m and neap and spring tide, respectively (Elias, 2006). The interaction between the M_2 and S_2 component results in

a spring-neap tide cycle of approximately 15 days (Van de Rest, 2004). Winds, waves and atmospheric pressure can alter the water levels by another two metres. The morphological features near the Marsdiep show that the influence of the tide is fairly large, despite the relatively small tidal range. This is due to the large tidal prism and low wave energy at the Marsdiep area (Davis & Hayes, 1984).

Sediment transport

The exact sediment transports along the Holland coast and around the Texel inlet are not known. In previous research, many measurements and models have been used to estimate these figures. Figure 4.3 gives a rough overview of the sediment fluxes. The fluxes around the Marsdiep have been mainly based on Van Rijn (2015). The numbers along the Holland coastline are based on Van de Rest (2004), who used results from Van Rijn (1995), Stive (1989), Steetzel & De Vroeg (1999) and Roelvink & Stive (1989). Those numbers are roughly in congruence with more recent findings by Tonnon et al. (2018) and Elias & Wang (2020).

There are a few factors that could explain the behaviour of the net alongshore sediment transport, as shown in Figure 4.3. The average transport in the Netherlands is northward due to the northernly propagating tidal wave and as a result of the more dominant SW wave direction (Van de Rest, 2004). The breakwaters that protect the harbour channel at IJmuiden block the southwest waves, reducing the northward component of the sediment transport. This leads to an expected southward net transport, possibly amplified by a sand-attracting effect of the shipping channel (Van Rijn, 1995). This effect leads to visible accretion at the breakwaters. North of Egmond aan Zee, the northward component of the sediment transport becomes dominant again, leading to a net northward transport. This transport increases towards Den Helder. Stive (1989) attributes this increase to the influence of the Marsdiep. Van Rijn (1995) attributes this increase to the presence of breaker bars, an increasing steepness of the profile and the increasing tidal asymmetry. The positive correlation between profile steepness and longshore sediment transport was also found by Mil-Homens (2016). As discussed in Section 2.2 is erosion or accretion the result of a gradient in the sediment transport. According to Figure 4.3 should a large gradient exist near Egmond aan Zee. This can be recognized by the high nourishment quantities observed at Egmond in Figure 4.2.

4.1.3. Selection of two locations

In Section 3.6 it is concluded that tidal channel nourishments and shoreface nourishments are best suitable for the application of a continuous nourishment. From Figure 4.3 it can be observed that the estimated net transports increase in northward direction. Callantsoog is a suitable location for the application of a shoreface nourishment for two reasons. First, the coastal stretch at Callantsoog has a relatively large net transporting potential. Figure 4.2 shows that this stretch is subject to frequent and large nourishments. Secondly, Callantsoog is located away from the ebb-tidal features that could shelter NW waves. The tidal channel wall nourishment will be placed in the main Marsdiep channel. Which location suits best is dependent on the channel-specific hydrodynamics. These are treated in Section 4.3.

4.2. Description of Callantsoog

The bathymetry in the nourishment location, in front of Callantsoog, is characterized by a large sandbar with an alongshore length of approximately 6 kilometres and a crest height between -4.5 and -2.5 m NAP. Northward of this sandbar, the features from the Marsdiep tidal inlet system become apparent with shoals and steeply sloped channels. The most southward shoal is called the 'Franse Bankje', and the adjacent channel is called the Nieuwe Lands Diep (Elias & Van der Spek, 2017), see Figure 4.4b.

The coastline at Callantsoog has an orientation of 15 degrees north. SW and NNW waves are dominant. Figure 4.4a shows the wave rose for waves measured at IJmuiden. The highest NNW waves are sheltered by the features presented in 4.4b, which makes the transposition of the presented wave rose to Callantsoog not entirely valid. The grain size in the nearshore zone at Callantsoog lies between the 200 and 300 μm (Van de Graaff, 1984). The entire coastline north of Petten consists of groynes, placed approximately 200 m apart from each other. According to Rakhorst (1984), the effect of these groynes in this area is quite limited. One of the proposed explanations of this limited effect is that cross-shore transports move sediment seaward of the groynes, where a gradient in the alongshore transport exists that moves the sediment along the shore. South of Callantsoog the Hondsbossche Dunes are located.

(a) Wave rose IJmuiden munitiestortplaats (1990-2021)

(b) Bathymetry of area of interest
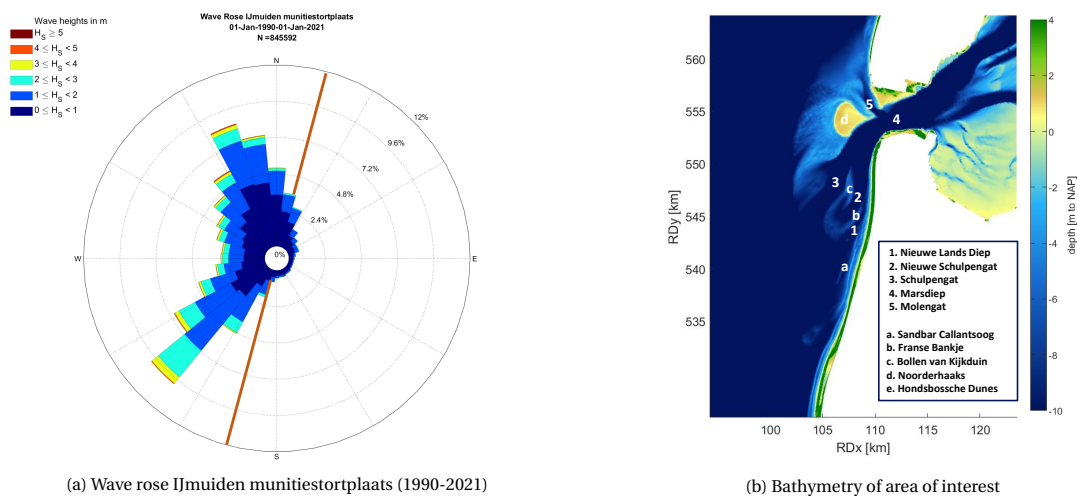
Figure 4.4: Wave rose for nearby measurement station (IJmuiden munitiestortplaats) and bathymetric features of the area, including names. The orange line in (a) indicates the orientation of the coastline at Callantsoog.

Figure 4.5 shows the development of the coastal profile of Jarkus transect 1303. In 2017, Rijkswaterstaat has executed a beach and shoreface nourishment of 400.000 m^3 and 1.000.000 m^3 respectively at the Callantsoog coast (Rijkswaterstaat, 2019c). The shoreface nourishment is visible as a 3m bar at 1500 m seaward of the MCL in Figure 4.5. In 2020, an additional 400.000 m^3 beach nourishment was carried out, as the 2017 shoreface nourishment is expected to become effective only in a few years. This slower development of the nourishment becomes apparent when looking into its development. In two years, the outer berm has eroded approximately 50 cm vertically, and the face has moved shoreward 20 m. The berm at x = 500 is more dynamic and has progressed 60 m in onshore direction between 2018 and 2020.
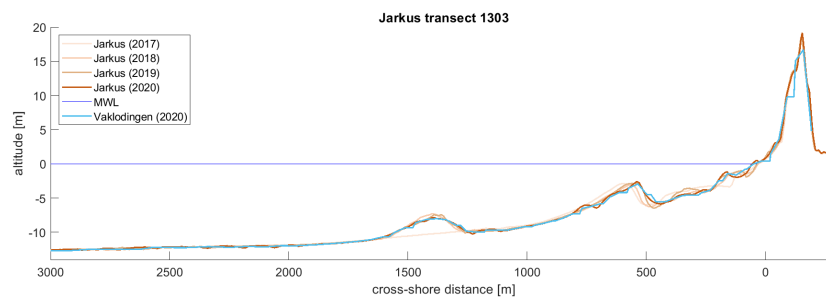
Figure 4.5: The measured Jarkus profile (1303) shows the morphological development between 2017 and 2020. Additionally, a transect based on the Vaklodingen is given.

4.3. Description of the Marsdiep

The closure of the Zuiderzee in 1932 led to a change in basin geometry and an increase in tidal range from 1.1 to 1.38 m at Den Helder. This led to a reorientation of the channels, which resulted in the erosion of the ebb-tidal deltas of Texel and its adjacent coasts (Elias et al., 2012). The system can be qualified as mixed energy wave-dominated, with an averaged wave height of 1.3 m and its 1.38 m tidal range (see Figure 2.10) (Elias & Van der Spek, 2017). This reorientation of the channels cut the sediment supply of the supra-tidal flat Noorderhaaks, making it more susceptible to the incoming waves. These are expected to be the primary driver of its current erosive behaviour. The reorientation of the channels is also expected to induce additional coastal losses. The position of the entire Marsdiep inlet channel has remained mostly stable due to a hard sea defence at the tip of North Holland, named the Helderse Zeewering. On average, the Wadden Sea has started importing sediment since its separation from the Zuiderzee. In the Netherlands, this behaviour is called 'Zandhonger', or sand hunger (Herman et al., 2016).
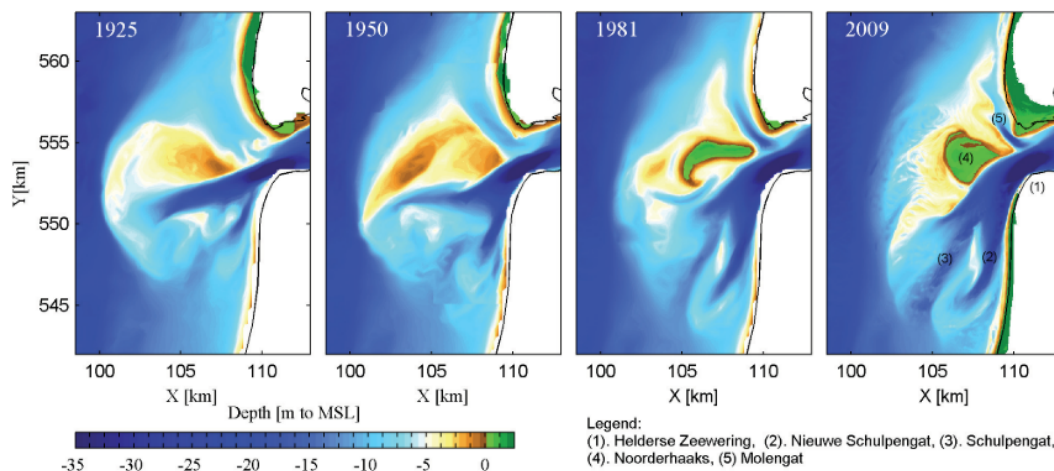
Figure 4.6: The development of the ebb-tidal delta after closure of the Zuiderzee. From Elias et al. (2012).

Since 1990, more than 30 million m^3 of sand has been nourished at the coastlines adjacent to the Texel inlet, making it the most maintenance demanding stretch of the Dutch coastal system. One way of satisfying the sand hunger of the Wadden Sea could be a direct nourishment in the Marsdiep. Such a nourishment could in principle be executed with the Sandwindmill. The exact exchange between the ebb-tidal delta, the channels, the coastline and the basin has been researched extensively. Yet, no thorough understanding of these flows and the governing processes is present. The same holds for the quantity of sediment imported through the Texel inlet, which is estimated to be between 2 - 6 million m^3/year (Van der Hout et al., 2009; Elias & Van der Spek, 2006; Elias & Wang, 2020; Van Rijn, 2015).

The sediment fluxes around the Marsdiep are very uncertain. For the sediment budget overview, the estimated transport between -8 m NAP and -20 m NAP is also given in Figure 4.3. These values are higher than the shallower transport because the cross-shore distance between -8 m NAP and -20 m NAP is higher than between +3m NAP and -8m NAP. The net sediment import by the Marsdiep has multiple possible explanations. Wang et al. (2018) make a distinction between barotropic and baroclinic mechanisms. Barotropic means that the density is a function of pressure only (hence almost constant). Most of the barotropic mechanisms are summarised below:

- **Residual flow**. There are a few processes that can cause a residual flow through a tidal inlet. The discharge from the IJsselmeer into the Marsdiep can contribute quite significantly to a residual flow. When the water level in the Wadden Sea is lower than the water level in the IJsselmeer, freshwater is discharged in the Waddensea. According to Van Rijn (2015), approximately 50% of the difference in ebb and flood volume through the Marsdiep can be appointed to this freshwater discharge. Secondly, Stokes drift can cause net residual currents directed seaward. Under progressive wave conditions, an

inland directed accumulation of water occurs. This leads to a water level gradient that is positive in the landward direction. This gradient is compensated by a seaward directed return flow. Guo et al. (2014) estimate that the magnitude of this return flow is in the order of cm/s, hence not very significant. Furthermore, winds can directly drive flows. Indirectly, winds and air-pressure differences can drive flows through the generation of set-up or set-down. Lastly, winds can stir up sediment through the generation of waves.

- **Tidal asymmetry**. In shallow seas, the tidal wave can deform. This can lead to a discrepancy between the period of the rising and the period of the falling tide. In the case of a flood-dominant system, the rising period is shorter than the falling period. This induces higher flood velocities. Due to the strong nonlinear response of sediment to flow velocities, this asymmetry can cause significant net transports. Another type of asymmetry is the duration of slack waters. When the duration of the high-water slack is longer, fines have more time to settle.

- **Jet-flow asymmetry**. When a tidal flow moves towards an inlet, it is fairly uniformly distributed (Oertel, 1988). Once the flow is constricted by the inlet, it accelerates and leaves the inlet as a jet. Upon reaching higher velocities, more sediment is eroded. As the flow leaves the inlet as a jet, the sediment can be transported quite far away from the inlet. When the tide turns, a slower uniform flow is being created again, not able to erode the sediment that has been deposited far away from the inlet by the jet. As waves are able to bring sediment into suspension on the seaward side of the inlet, the uniform flood flow moving towards the inlet might contain more sediment than the ebb flow moving towards the inlet. This jet flow could hence enhance the sediment import of tidal basins.

- **Dispersion and spatial asymmetry in deposition**. Waves stir up the sediment at the ebb-tidal delta. This results in a higher sediment concentration on the seaward side of the Marsdiep. Tidal currents induce mixing of the sediment, moving sediment from this higher concentration area towards the lower concentration at the Wadden Sea side of the channel. During flood, on both the flats and channels sediment is deposited. During ebb, the velocities on the flats are relatively lower, leaving a part of the sediment behind.

Baroclinic mechanisms and transverse flow are other drivers of net sediment transports in the Marsdiep channel. Spatial asymmetry becomes essential when looking at the baroclinic mechanisms, which are currents driven by differences in salinity and temperature. As freshwater has a lower density than saltwater, it will move on top of the saltier water. This movement induces a current in the direction of the saltwater higher in the water column and in the direction of the sweeter water lower in the water column.

- **Normal flow**. As the freshwater input occurs on the basin side of the inlet, the density gradient directly induces an eastward flow near the bed, leading to a further increase of the net import of sediment (Elias, 2006).

- **Transverse flow**. There is a spacial asymmetry in the dominant flow direction in the inlet, where the southward side of the channel is flood-dominant and the northward side ebb-dominant. The importance of this asymmetry becomes apparent when looking at the transverse transport gradients. Buijsman & Ridderinkhof (2008) state that the curvature of the channel, transverse density gradients and Coriolis forcing may induce cross-channel currents. Coriolis force is not expected to be significant for the Marsdiep inlet, which has an Ekman number of 1.4 (J. De Vries, 2015). This Ekman number quantifies the importance of frictional forces in a channel, where low frictional forces allow a larger influence of Coriolis. Huijts et al. (2006) show that for tidal estuaries, the density gradients become dominant over the Coriolis force for Ekman values >0.02. As the IJsselmeer freshwater discharges are present at the southern side of the Marsdiep channel, transverse density currents can drive sediment towards the southern side of the channel. As this is the flood-dominant part of the inlet, this density-driven current can increase the net sediment import by the Marsdiep. The curvature of the flow could also induce a net southward centrifugal force, increasing the southward and consequently eastward transports in the channel (Buijsman & Ridderinkhof, 2008).

The closure of the Zuiderzee, which has mainly driven the sediment import, has had the most effect on the barotropic characteristics. It is, therefore, safe to assume that these have the most considerable impact on the sediment transport through the Marsdiep (Wang et al., 2018).

5

Modelling approach

5.1. Model choice and description

This study aims to predict the behaviour of a nourishment on the timescale of a year. Three types of models could be used for predicting such behaviour: parametric, behaviour-based numerical models and process-based numerical models (Lopez De San Roman Blanco et al., 2019). Parametric models use simple formulae that have been derived chiefly from observations. Behaviour-based models use known behaviour, such as derived equilibria, to simulate developments. No thorough understanding of the governing processes is needed, neither for the model, nor for the modeller. Process-based numerical models use physical laws to reproduce natural behaviour. This requires a better understanding by the modeller and generally leads to higher computational times. Three types of numerical models can be distinguished to study the effects of a nourishment on a large coastal stretch: coastal profile models, one-line models and coastal area models (Payo et al., 2017).

Coastal profile models are simplified 2D models that entail the cross-shore distance and depth as dimensions. These models can calculate the change of the cross-shore profile due to hydrodynamic processes and sediment transport. Such models assume a uniform profile in the alongshore direction, which means that alongshore variability in bathymetry is not accounted for.

In one-line models, the morphology is often represented as a single contour that could shift as a whole depending on the forcings. When multiple transects are placed next to each other, the coastline change can be modelled. UNIBEST-CL+ is a commonly used one-line model. When the cross-shore profile is divided into multiple sections that can interact with each other, we speak of a multiple-line model (Hanson et al., 2003).

Process-based coastal area models are developed to take into account changes in both the cross-shore and alongshore direction. Taking into account this non-uniformity of the alongshore is necessary for mimicking gradients in the sediment transport. When the bathymetry is relatively complex or when in the vicinity of a tidal inlet, coastal area models can be applied (Roelvink et al., 2016). As a local nourishment will affect the bathymetry in all dimensions, using a coastal area model for this research seems to be the best option. Furthermore, it allows for the assessment of multiple forms and shapes of the nourishment. Lastly, the vicinity of the Marsdiep tidal further substantiates the choice for a coastal area model. Although these criteria all favour a coastal area model, there are also limitations.

Complications of using a coastal area model

In general, process-based models are computationally more demanding than equilibrium-based models. This makes them less suitable for long-term predictions (Hanson et al., 2003). Another complication is that the effect of many time-varying processes that are embedded in process-based models, such as waves and tides, may be averaged out on the longer term. Residual effects that are excluded from the process-based models might play a significant role on the longer term. Therefore, it is important to critically assess the representativity of the model's boundary conditions, preferably comparing it to measured data. Predicting morphological change is an even more complex task due to the complexity of the transport processes and their sensitivity to natural forcings De Vriend (2003).

5.1.1. Delft3D

Although predicting long-term morphological change with a process-based model can be difficult, novel models enable us to make long-term predictions. One of such models is D-Flow Flexible Mesh (D-Flow FM), which is used for this study. Whereas the previous version of Delft3D uses structured grids, does this newest version use a flexible mesh. This allows the modeller to locally refine or coarsen the grid without the need of coupling multiple model grids (Deltares, 2021a). This coupling has resulted in not all information being passed on from one to the other domain. This issue does not persist in the flexible mesh version, as only one domain can be used at multiple resolutions. Another advantage of FM is using a coordinate system for the grid administration instead of using grid indices. This allows the modeller to easily change the grid without having to alter the model input too. The new grid definition requires using an alternative to the finite differences as a solver for hydrodynamic equations. Although this new finite volume method is less efficient, the ability to efficiently design the mesh leads to lower computational times. D-Flow FM solves the Navier-Stokes equations for incompressible fluid under the Boussinesq assumptions (which states that the density is neglected in all terms except the gravitational term). Furthermore, a hydrostatic pressure distribution is assumed, neglecting vertical accelerations in the fluid. Reynolds averaging is applied, which has been addressed in Section 2.2.2.

D-Flow FM, which is responsible for the hydrodynamic calculations using user-defined boundary conditions, can communicate with D-Waves. The latter uses the numerical Simulating WAves Nearshore (SWAN) model to compute the evolution of wind-generated short-crested waves in coastal areas (Deltares, 2019). The flow and wave modules can communicate, as both flows and waves can alter each other. The communication takes place at a user-defined interval.

The D-Morphology module can calculate the sediment transport induced by the combination of flow and waves. This module can use many of the transport formulations that have been derived in the past (Deltares, 2021b). The default option is the formulation by Van Rijn (1993) (also referred to as TRANSPOR1993). The most recent version of D-Flow FM also allows the use of the more recent formulation by Van Rijn, the TRANSPOR2004. The most important changes are the recalibration and the inclusion of a bed roughness predictor. In Appendix C the used formulations are treated in more detail.

5.2. Basic model set-up

As a basis, the Delft3D-FM WadSea model that Laan (2019) developed has been used. This model has been used for the assessment of sediment transport patterns in the Dutch Wadden Sea. It could therefore serve as a valuable basis for this study. In this section, the WadSea model and applied adaptations to this model are discussed.

5.2.1. Grid and bathymetry

As a basis, the coarse grid of Laan (2019) has been used. For this thesis, the two main areas of interest are the North Sea coast near Callantsoog and the Marsdiep inlet. As different mechanisms are expected to be the main driving force for spreading the nourishment, both nourishments can be modelled separately. Section 5.6.1 treats this separation in more detail. Since strong grid refinements in an area other than the area of interest would be a waste of computational effort, separate grids for both locations have been created. Furthermore, the eastern part of the grid has been cut off to reduce computational time. Figure 5.1 shows the two different grids and the original grid from Laan (2019).
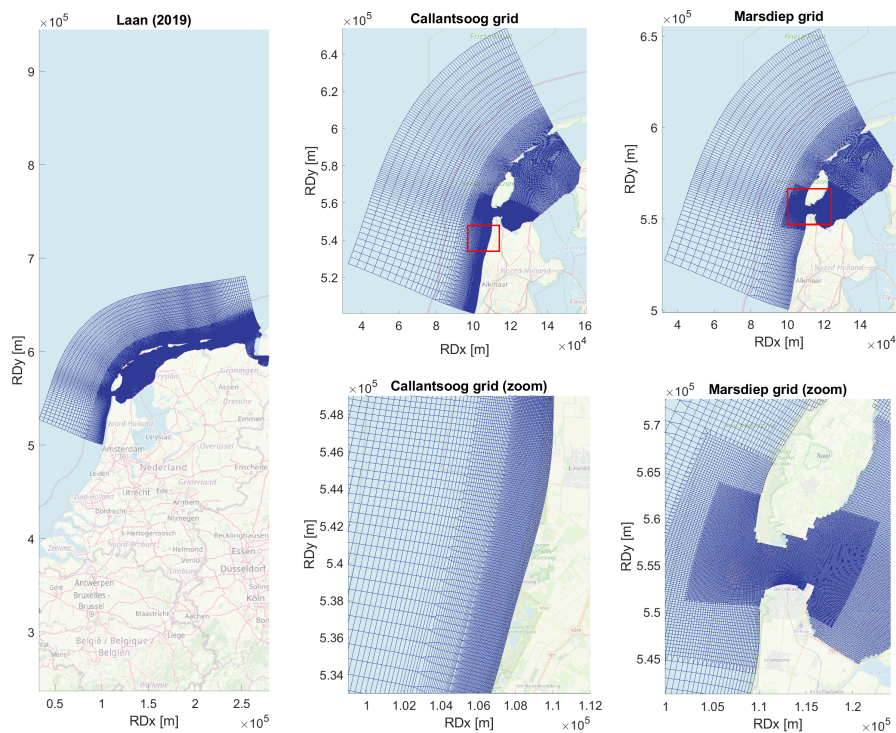
Figure 5.1: The Callantsoog and Marsdiep FM grids that are created based on the grid of Laan (2019).

Roelvink et al. (2016) state that when process-based models are used for analysing developments on a time scale of months to years, details in the surf-zone can usually not be represented very well. The resolution should be at least enough to be able to represent the currents and alongshore transports. This could be effectuated from a resolution of 5-10 grid cells across the surf zone. Also, some cross-shore processes must be taken into account, as the cross-shore profiles must stay in a reasonable shape. For the Dutch coastline, the surf zone extends to a distance of approximately -8 m NAP. The Callantsoog model has approximately 20-25 cells in the surf zone, with a cross-shore dimension of 35 m and an alongshore dimension of 170 m. A higher resolution than suggested by Roelvink et al. (2016) has been chosen, as the result of 10 cells in the surfzone in the MOHOLK model by Van der Hout et al. (2009) led to unrealstic behaviour in the foreshore. However, an even higher resolution led to unreasonable computational times, as the time step is dependent on the smallest grid size. This is the result of the CFL criterium that is being used in D-Flow FM (in contrast to the structured version, where a time step should be set by the modeller). A CFL value of 0.7 has been used, as suggested by Deltares (2021a). After the addition of the bathymetry and water level boundaries, the network has been enhanced by the displacement and resizing of cells that were limiting the computational time step, as suggested by Zijl & Groenenboom (2019). The maximum orthogonality of the grid, which must

be limited for computational efficiency, is 0.119. The orthogonality indicates the degree of perpendicularity of two adjacent grid cells and is calculated through the cosine of the angle of two circumcenters, see Figure 5.2. The smoothness is an indicator for the ratio of the size of two adjacent grid cells. The smoothness in the area of interest stays below 1.1, but reaches values up to 18 at the triangular transition between a finer and rougher part of the grid. Although the grid has sufficient computational times, these values can be improved for future model applications. The grid of the Marsdiep model has a maximum smoothness of 6 and a maximum orthogonality of 0.103. The minimum grid size is 40 m perpendicular to the channel and 70 m parallel to the channel. For both the Callantsoog and Marsdiep grid, it holds for the rectangular cells that the smallest side of each rectangle applies in the direction of the largest morphological gradients.
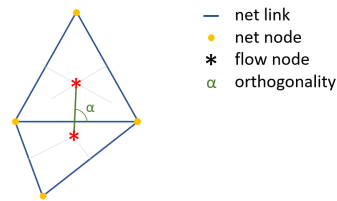
Figure 5.2: Clarification of orthogonality and smoothness, where $\cos(\alpha)$ indicates the orthogonality.

As a basis, the bathymetry of Laan (2019) has been used. As the bathymetry of the North Holland coast dated from 2011, it has been updated using the 2020 Vaklodingen from Rijkswaterstaat. The bathymetry at the boundaries between the 2020 and the 2016 data has been carefully smoothed in order to remove large jumps in the bed level. Although more recent Vaklodingen for a part of the Marsdiep are available, it is decided not to use these as the difference with the 2016 bathymetry of the other Marsdiep parts would be too large. Figure 5.3a shows the maturity of the bathymetry of the model. For a specification of the 'other' bathymetry, reference is made to Laan (2019).
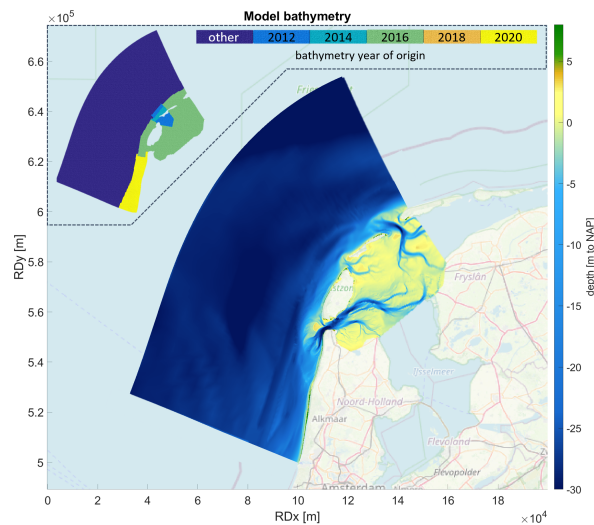
Figure 5.3: Bathymetry that is used for the North Holland and Marsdiep models. Additionally, the years from which the bathymetry measurements are dated is given.

For the WAVE model, three nested grids are used. The three grids are presented in Figure 5.4. The intermediate grid exceeds the FM grid with one cell to avoid boundary problems. The resolution of the surf zone near Callantsoog has been set at 20 m x 60 m in cross-shore and alongshore direction, respectively. This is fine enough to correctly represent the influence of morphology and morphological changes on the behaviour of waves. The smallest grid extends to a depth of approximately 15 m. The northern lateral boundary of the smallest wave grid is located near Julianadorp. When the grid was extended more northwards, model instabilities occurred. This might have to do with the complex bathymetry near the Marsdiep. The maximum orthogonalities are 0.001, 0.134 and 0.044 from the largest to the smallest grid.
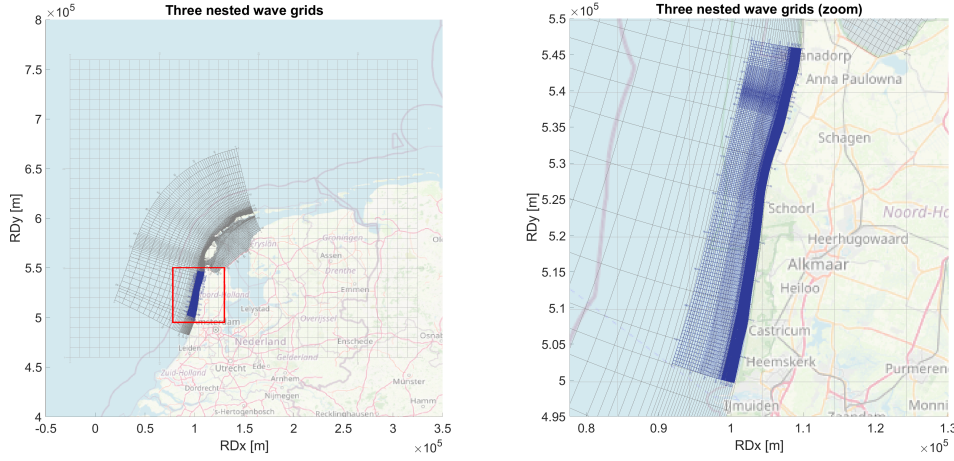
Figure 5.4: Grids for the WAVE model. Blue colour indicates the smallest of the three grids.

5.2.2. Boundary conditions and model input

In this subsection the boundary conditions and other model input is discussed. The forcing conditions of 2017 have been used as these were available and partly calibrated for the domain of interest. Section 5.3 treats the representativity of this year, comparing it to measurements between 1990 and 2020.

Water level

The water level boundaries are deducted with the use of the DCSMv6-ZuNov4 model for the offshore and two lateral boundaries of the grid of Laan (2019). The DCSMv6-ZuNov4 model is well capable of representing the surge and tide in the Dutch coastal waters (Zijl et al., 2013, 2015). The boundaries are time series of water levels, consisting of both the tidal and non-tidal residual, applied at 86 points around the mesh. As the mesh has been adapted for this research (see Figure 5.1), new water level boundaries have been deducted for the new eastern boundary. This has been done by executing a full simulation on the original grid and extracting water level data on multiple points along the new boundary. No significant change in model performance (water levels and velocities) resulted from this new boundary deduction.

The water level boundary conditions led to a disturbed velocity profile at the lateral model boundaries. This disturbance had a significant influence along the entire North Holland coast, leading to skewed current velocities and extreme erosion at the boundaries. As the alongshore current velocities are important for the transport of sediment, the lateral boundary conditions have been adapted towards Neumann boundaries, as suggested by Kaji et al. (2014). With Neumann boundaries, a gradient of the water level in alongshore direction is imposed on the lateral boundaries (Deltares, 2014). The Neumann boundaries have been determined by dividing the water level difference between two offshore boundary points near the grid corner by the distance between them, for each time step, see Figure 5.5 and Equation 5.1. These time series of water level gradients have been applied uniformly to the lateral boundary. The performance of the model with regards to the hydrodynamics changed slightly due to this adaptation. The performance on the water levels improved for some points and worsened for some others. The alongshore tide driven velocity improved significantly, and the unrealistic erosional behaviour at the boundaries diminished. Section 5.4 goes into further detail with regards to the model performance.

$$\nabla_{Neumann,t} = \frac{\eta_{Xout,t} - \eta_{Xin,t}}{\Delta X} \tag{5.1}$$

where:

$\nabla_{Neumann,t}$	Neumann gradient at time t [-]
$\eta_{Xout,t}$	water level at point Xout at time t [m]
$\eta_{Xin,t}$	water level at point Xout at time t [m]
ΔX	distance between grid points [m]
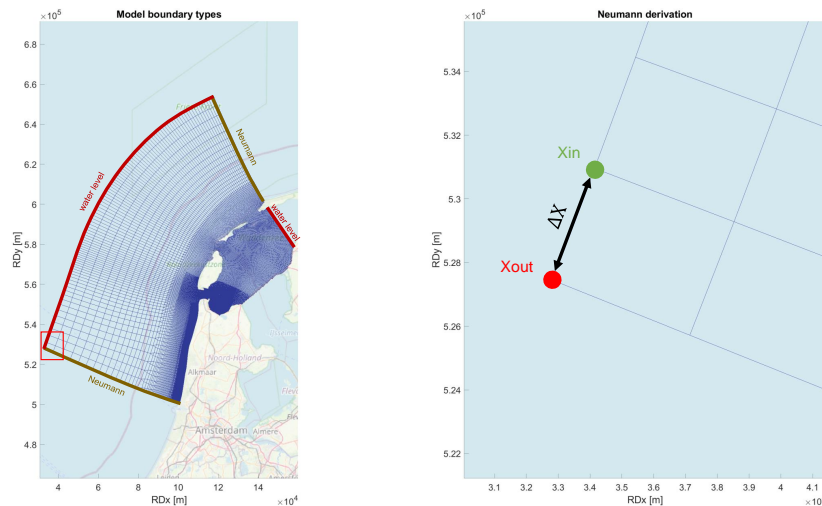
Figure 5.5: Classification of model boundary conditions. The right figure indicates the parameters that are mentioned in Equation 5.1.

Waves, wind and atmospheric pressure

The wave, wind and pressure boundary conditions originate from the ERA5 atmospheric reanalysis (Hersbach et al., 2020). The wave boundary conditions are applied as a time series containing H_s, T_p, the direction and the spreading and imposed at the largest Delft3D-WAVE grid, see Figure 5.4. The wind, atmospheric pressure and applied have a spatial resolution of 31 kilometres and are updated every hour. The Charnock constant, which links the sea surface roughness with the surface shear stress, is updated with the same time interval at the same resolution (Zijl et al., 2018).

Sediment

From the Sedimentatlas it can be seen that the D_{50} of the North Holland coastline varies between 180 and 450 μm. For the Marsdiep basin, values vary much more with median grain sizes of 22 μm on the flats and up to 480 μm in the tidal channels (see Figure 5.6). For the North Holland model, a value of 250 μm has been chosen, which is in correspondence with the value used in similar researches on the Holland coastline (see e.g. Van der Hout et al. (2009); Elias et al. (2006)). For the Marsdiep model, a value of 350 μm has been chosen as the grain size of 250 μm led to a too-rapid erosion of the channels. Note that these values are relevant mostly for calibration of the hydrodynamics and the validation. The grain size of the nourishments can be set independently of the bottom grain size.
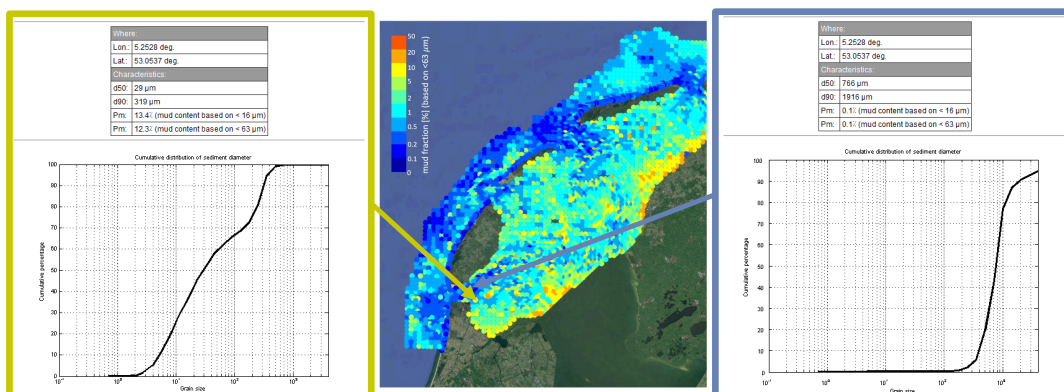
Figure 5.6: Grain size distribution in and around the Wadden Sea, indicated by the mud fraction in sediment samples. Cumulative distributions of two samples 400 m apart from each other are given to indicate the high spatial variability.

The (default) sediment transport formula of Van Rijn (1993) has been used, which makes a distinction between bed-load and suspended load transport. Except for a correction factor of the wave-induced transports, all default Delft3D settings for sediment and morphology have been used. Section 5.4 treats the calibration of these factors.

Other settings

The horizontal diffusivity and horizontal eddy viscosity are incorporated in Delft3D to account for small-scale turbulent motions (Deltares, 2021a). For similar applications and grid sizes, a diffusivity value of 0.1 m^2/s has been used (see e.g. Walstra et al. (2004) and Luijendijk et al. (2017)). A value of 1 m^2/s is used oftentimes for the viscosity and therefore adopted for this research. A sensitivity study showed no large influence of the variation in these parameters between values of 0.05 and 2 m^2/s on the hydrodynamic and morphodynamic behaviour. For stability reasons, the maximum timestep has been set at 6 seconds, and the coupling interval between the WAVE and FLOW module has been set at 20 minutes. In this research, Delft3D is used in depth-averaged mode (2DH). Adding vertical layers to the mesh would lead to unacceptable computational times given the size of the mesh and the time scale of interest. The main expected implications of the use of a 2DH model are the poor representation of offshore processes (offshore directed undertow) and the assumption of a vertical concentration profile (Grunnet et al., 2004; Huisman et al., 2019). This choice is expected to have the largest influence on the modelling of the shoreface nourishment at Callantsoog, as depth-averaged results for morphological development around tidal inlets are quite promising (Nederhoff et al., 2019).

5.3. Representativity of 2017

The boundary conditions are based on data from the year 2017. As atmospheric conditions can vary from year to year, an analysis on the representativity of the year 2017 is conducted. First, the wave heights of 2017 are compared to the wave heights of 1990-2020. Then the directions are included, concluded by an analysis of the sediment transporting capacity of the wave climate based on the CERC equation (2.21). The results of the analysis are summarised in Figure 5.7. For the elaboration of the figure, reference is made to Appendix B.
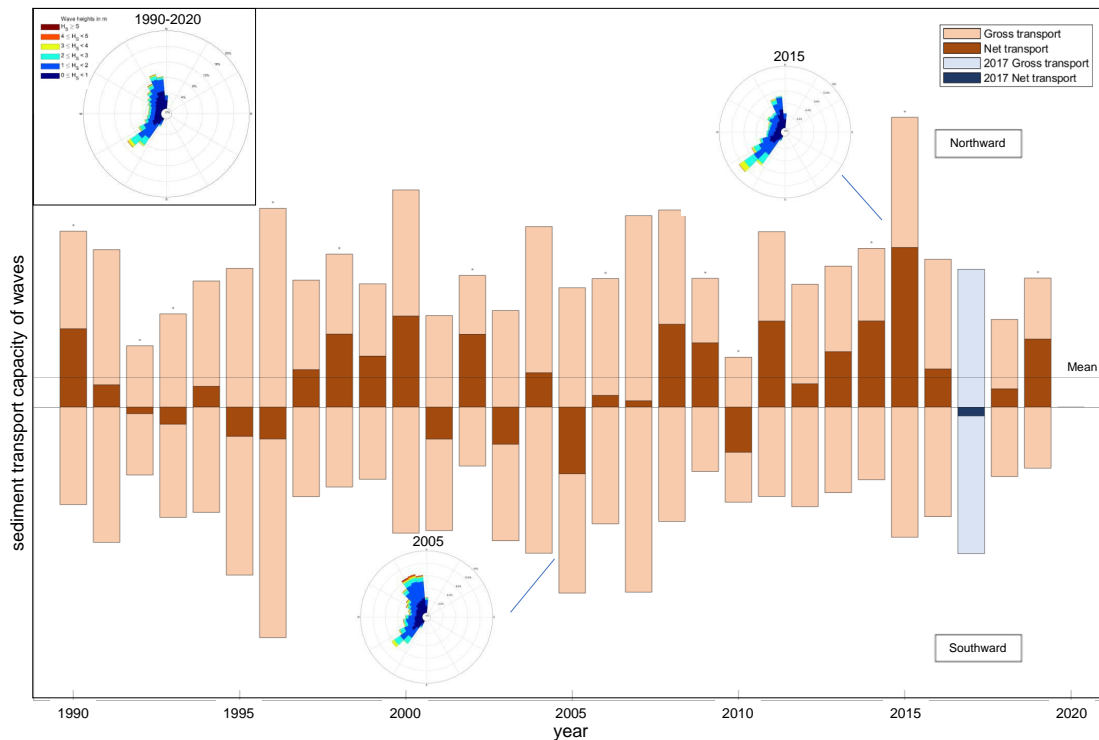
Figure 5.7: Gross and net sediment transports at the Callantsoog coast according to the CERC formula, based on wave measurements at IJmuiden munitiestortplaats between 1990-2020. Bars marked with a '*' indicate years where >30% of the data was missing (either Hs, Dir, or both).

Figure 5.7 shows that the mean net transport according to the CERC formula over the 30 years is directed northward. This is in agreement with the findings in Section 4.1. As expected based on the wave roses does the wave-driven sediment transport in 2017 comes out lower than the average and appears to be even negative. The gross transports in 2017 are in correspondence with the 30-year average. This suggests that the sediment dispersion due to waves in 2017 has a smaller net direction but has a similar magnitude as the 30-year average. In the validation of the sediment transports of the Delft3D-model, the atypical net behaviour of 2017 should be taken into account.

5.4. Calibration

The WadSea FM model has been developed to reproduce the processes in and around the Wadden Sea. For this research, the area of application is extended towards the North Holland coastline. The hydrodynamic and morphodynamic settings are thus re-examined to also represent the conditions along the North Holland coastline to a satisfactory extent. In Section 5.4.1 the hydrodynamics are calibrated, which are important for the sediment transports. The sediment transports with the calibrated hydrodynamics were only calibrated on the grain size. A median grain size of 250 μm for the North Holland model and 350 μm for the Marsdiep model led to accurate results. Section 5.4.2 briefly goes into morphodynamic calibration. Subsequently, Section 5.5 treats the validation of aspects that have not been taken into account in the calibration, such as sediment transports and transport patterns.

5.4.1. Hydrodynamics

In this section, the hydrodynamic calibration is discussed. An often-used parameter for calibration of hydrodynamics is the bottom roughness (e.g. in the development of the DSCM models (Zijl et al., 2013; Zijl & Groenenboom, 2019)). In Delft3D in depth-averaged mode, the shear stress at the bed is calculated by a quadratic friction law, see Equation 5.2. Note that the Manning and Chézy coefficients are negatively correlated, where an increasing Manning value is inherent to a higher roughness.

$$\tau_b = \frac{\rho_w g U |U|}{C^2} \qquad C = \frac{\sqrt[6]{h}}{n} \tag{5.2}$$

The roughness value is, amongst others, depending on the depth and bottom composition and bed forms (Coon, 1998). Instead of determining a spatially varying roughness based on this information, a uniform roughness value is selected based on hydrodynamic model performance for different coefficient values. Coefficient values of 0.021, 0.024 and 0.027 s/m$^{1/3}$ are used as they correspond to values used in similar researches (e.g. M. J. P. Van Duin et al. (2004); Laan (2019); Lesser (2009)). These roughness values are used to calibrate the model performance on tidal constituents, water levels, tide-driven alongshore currents and the residual discharge through the Marsdiep. The justification of the selection of these indicators is stated below.

Tidal constituents

As explained in Section 4.3 can tidal asymmetry lead to a net sediment transport due to velocity differences between flood and ebb. For an understanding of this asymmetry and the manner in which it has been analysed, a small explanation of the tide is given first.

The tide is being caused by the gravitational pull of the sun and the moon on the oceans of the earth (Bosboom & Stive, 2015). This forcing combined with Coriolis leads to a standing (Kelvin) wave that moves around an amphidromic point, which is a point in the sea/ocean without any tide. The North-Sea tides are mainly forced by oscillations near Scotland. The tidal wave propagates along the British coast towards the English Channel, where it is reflected and turns counterclockwise along the French, Belgium and Dutch coast (Buijsman & Ridderinkhof, 2007). As the astronomical trajectories of the earth, moon and sun are fixed, one is able to predict the water level very well. A simplified approach, ignoring the 18.6-year cycle is:

$$\eta(t) = A_0 + \sum_{n=1}^{N} a_n \cos(\omega_n t - \alpha_n) \tag{5.3}$$

where:

$\eta(t)$	water level at time t	[m]
A_0	mean water level w.r.t. reference	[m]
N	amount of harmonic components	[-]
a_n	amplitude of component n	[m]
ω_n	angular velocity of component n	[°/h]
t	time	[h]
α_n	phase angle of component n	[°]

The tidal signal is thus made up of multiple components, each of which having its own angular velocity. The amplitude and phase of each component are dependent on the location, as the distance to an amphidromic point, local bathymetry and coastal orientation can highly influence these characteristics. The Dutch coastline has a semi-diurnal tide. This is mainly due to the M$_2$ component, which has a frequency of 28.98 de-

grees/hour (hence a period of 12.42 hours) and is the largest contributor to the tidal amplitudes at the Dutch coast. The most important components of the locations IJmuiden and Den Helder are presented in Table 5.1.

	IJmuiden			Den Helder	
constituent	frequency [cycle/hour]	amplitude [m]	constituent	frequency [cycle/hour]	amplitude [m]
M_2	0.08	0.67	M_2	0.08	0.64
M_4	0.16	0.21	S_2	0.08	0.17
S_2	0.08	0.17	M_4	0.16	0.11
O_1	0.04	0.11	N_2	0.08	0.10
N_2	0.08	0.10	O_1	0.04	0.10
SA	0.00	0.10	μ_2	0.08	0.08
μ_2	0.08	0.08	K_1	0.04	0.07
K_1	0.04	0.08	L_2	0.08	0.06
MN_4	0.16	0.07	MS_4	0.16	0.06
L_2	0.08	0.07	M_6	0.24	0.06

Table 5.1: Constituents obtained with the harmonic analysis of water levels at IJmuiden and Den Helder, using the measured water levels between 01-07-2019 and 01-07-2021. Components that contribute most to the amplitude of the tide are depicted in the table. Data obtained from Rijkswaterstaat (n.d.).

The modelled water levels of 2017 have been evaluated using a harmonic analysis. The obtained results for the most important constituents have been compared to the measured water levels during the same period. The result is depicted in Figure 5.8. From the figure, it becomes apparent that the amplitude error increases with the roughness. For the phases, a relatively large error in the M4 constituent can be observed. As this constituent, which is a higher harmonic of the M2 component, results in a tidal asymmetry and is a relevant contributor to the behaviour of sediment transport through the Marsdiep, it is important to have the phase error for this constituent as low as possible (see Bonekamp et al. (2002) for an analysis of the response of the Marsdiep transport field to the interaction of the constituents). The S_2 component phase, which is responsible for the spring-neap variability due to its interaction with the M_2 component, is represented well for all roughness values. Based on these results, a uniform roughness of 0.021 s/m$^{1/3}$ seems to be the most appropriate choice.
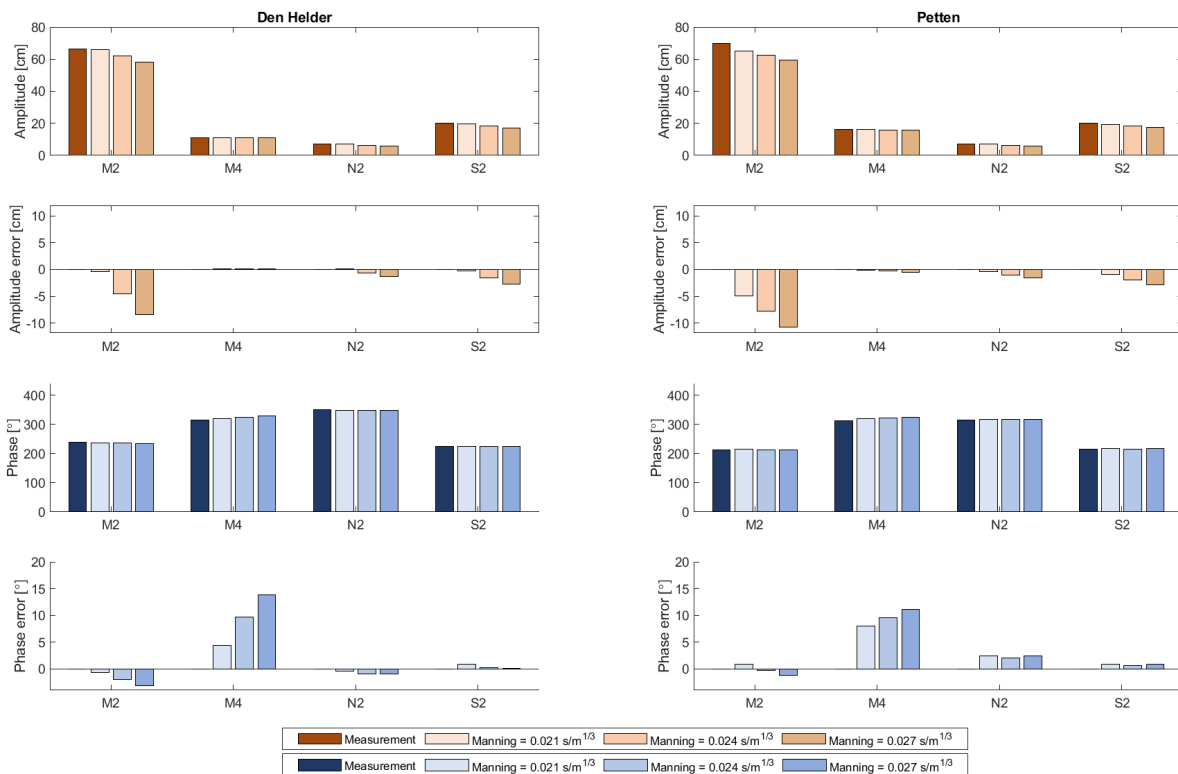
Figure 5.8: Comparison at two locations of modelled and measured phases and amplitudes of important tidal constituents for the Dutch coast.

Water levels

Apart from the tidal forcing, there are other mechanisms that induce a variation in the water level. Winds and air pressure can induce a large variability in the water levels. In order to capture the performance of the model for different roughness values on this residual water level change, the tidal signal has been separated from this non-tidal residual (NTR), which is also referred to as surge (Nederhoff et al., 2019). Apart from determining the performance on this NTR, this separation allows for an evaluation of the water level performance on more tidal components at the same time (as the tidal signal is composed of more components than the four evaluated in the previous section).

The NTR is deducted by subtracting the tidal signal from the full signal for both modelled and measured water levels. In Table 5.2 the model performance on the water levels is quantified. The equations used for calculating the performance are given in equations 5.4 and 5.5.

$$RMSE = \sqrt{\frac{\sum_{t=1}^{J}(x_t - \hat{x}_t)^2}{J}} \tag{5.4}$$

$$Bias = \frac{\sum_{t=t}^{J}(x_t - \hat{x}_t)}{J} \tag{5.5}$$

with:

J   number of data points [-]
x_i observed value at time t []
$\hat{x}_i$ modelled value at time t [-]
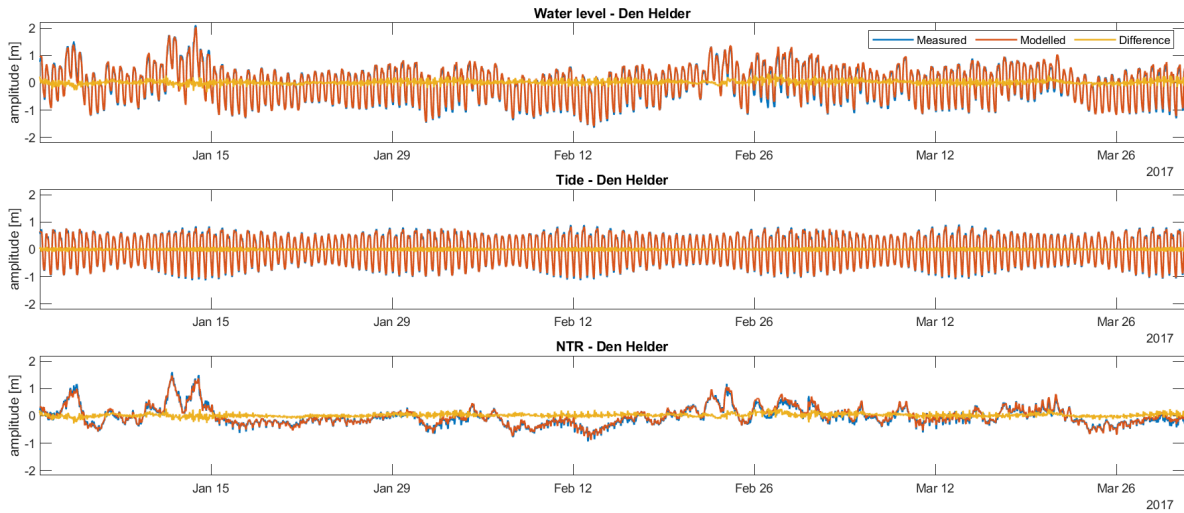
Figure 5.9: Tidal signal analysis of the water level in Den Helder and a Manning roughness of 0.021 s/m$^{1/3}$ during six spring-neap cycles.

Manning roughness [s/m$^{1/3}$]	Den Helder				Petten			
	RMSE$_{total}$ [cm]	RMSE$_{tide}$ [cm]	RMSE$_{NTR}$ [cm]	Bias$_{total}$ [cm]	RMSE$_{total}$ [cm]	RMSE$_{tide}$ [cm]	RMSE$_{NTR}$ [cm]	Bias$_{total}$ [cm]
0.021	7.74	3.81	6.80	-2.65	12.82	8.26	9.81	-4.57
0.024	8.41	5.60	6.36	-2.96	12.86	9.29	8.85	-3.85
0.027	10.34	8.25	6.31	-3.16	13.9	11.03	8.38	-3.26

Table 5.2: Model performance at Den Helder and Petten on tide and surge for three different roughness values.

From Table 5.2 it becomes apparent that the RMSE at Den Helder increases with increasing roughness. Mainly the tidal part of the water level deforms significantly with higher roughness values. For Petten the performance also decreases for higher roughness values. The bias does decrease for the higher values. As in the constituent analysis, the roughness of 0.021 s/m$^{1/3}$ performs the best.

Maximum alongshore velocity

Currents driven by the tide are partly responsible for alongshore sediment transport. Van Rijn (1995) attributes 15-40% of the yearly longshore transport in the surf zone to the tide-induced currents. Currents alone will not have a large influence on the sediment transport. However, they do contribute to both the advection of suspended sediment and the magnification of the bed shear stresses and hence the stirring up of more sediment. Figure 5.10 shows the maximum alongshore currents for ebb and flood, solely driven by the tidal forcing. As a reference, data from the Coast3D measurement campaign in 1998 (Van Rijn et al., 2002) and models from Grasmeijer et al. (2019) and Rijkswaterstaat (1993) is used. Lower roughness values lead to both an increased flood and ebb velocity. As the increase in the flood velocity is larger in an absolute sense, the net velocity increases with a decreasing roughness. The net velocity falls within the range of the benchmark values at both Egmond aan Zee and Callantsoog. It is hence difficult to assign a roughness value that leads to the correct tide-driven current velocities.
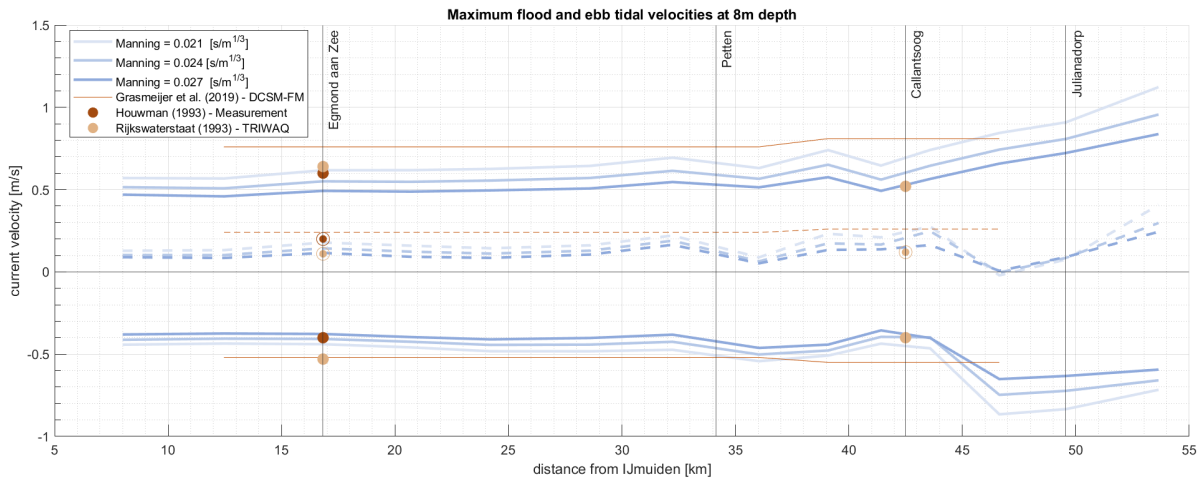
Figure 5.10: Maximum flood and ebb velocities driven by the tide for three roughness values. The dashed lines indicate net velocity (flood - ebb).

Cumulative discharge Marsdiep

The Marsdiep has a tide averaged net seaward water flux, resulting from the difference of huge ebb and flood volumes. The net flux is in the order of 20 Mm^3/tide, whereas the gross fluxes are in the order of 1,000 Mm^3/tide (Buijsman & Ridderinkhof, 2007). As the net flux is the resultant of two large fluxes, it is sensitive to changes in forcing. Nauw et al. (2013) showed that meteorological forcings can induce a change from exporting to importing. Another driving force are tidal gradients, although these are expected to have a smaller effect than the winds (Elias & Van der Spek, 2017). As in the case of the alongshore current, a higher roughness has a larger reducing effect on the (higher) flood current than on the ebb current. This leads to an increasing residual discharge with increasing roughness. Table 5.3 shows the model and benchmark values. Meteorological forcing was included in the modelling. Van Rijn (2015) expects the influence of freshwater discharge through sluices in the Afsluitdijk to contribute 50% to the net yearly discharge. These discharges are not included in the Delft3D model.

		Net discharge [m^3/s]
D-Flow FM	Roughness = 0.021 [$s/m^{1/3}$]	-400
	Roughness = 0.024 [$s/m^{1/3}$]	-780
	Roughness = 0.027 [$s/m^{1/3}$]	- 1,110
Benchmark	Duran-Matute et al. (2014)	-381
	Buijsman & Ridderinkhof (2007)	-3,000
	Van Rijn (2015)	-2,240

Table 5.3: Averaged discharge through Marsdiep due to tides and meteorological forcing.

From Table 5.3 it can be concluded that the model results for all roughness values are well in line with the benchmark values that are based on acoustic Doppler current profiler (ADCP) measurements between 1998-2002 and models. Therefore no specific roughness value can be chosen based on this analysis, as in the case

of the alongshore velocities.

Conclusion on calibration
The model's performance for different roughness values has been assessed, based on water levels and velocities at the Holland coast and Marsdiep, as well as the net discharge through the latter. From both the water level analyses, it can be concluded that a Manning roughness of 0.021 s/m$^{1/3}$ seems most appropriate. From the velocity and discharge analysis it appeared that the model results are between the benchmark values for all roughness values. For the remainder of this research, a Manning value of 0.021 s/m$^{1/3}$ is thus selected.

5.4.2. Morphodynamics

When modelling in 2DH, the model assumes a logarithmic velocity profile over the vertical (Deltares, 2021a). Processes like undertow and density-driven currents are thus not taken into account. The absence of undertow in a morphodynamic model can lead to unrealistic steepening of the profile (Huisman, 2019). One solution to this behaviour is applying a factor on the wave related suspended and bed transports, susw and bedw, respectively. In comparable 2DH morphodynamic coastal models, this scaling factor is sometimes used to account for, amongst others, the absence of undertow. Van der Hout et al. (2009) and Tonnon et al. (2009) set both values at 0.2. Figure 5.11 shows that this indeed slows down the extreme steepening of the foreshore and the onshore movement of the breaker bar, hence both values are set at 0.2.
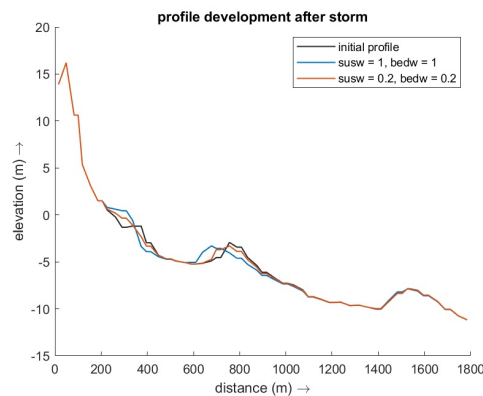
Figure 5.11: Influence of susw and bedw parameters on the development of the bed.

5.4.3. Conclusion on calibration

The calibration of the hydrodynamics shows that a Manning roughness value of 0.021 s/m$^{1/3}$ leads to the best performance. For this research, the Neumann boundaries have been deducted in a simplified manner (as explained in Section 5.2.2). The water level performance of the model with a water level forcing on all boundaries was better for some locations (amongst which Petten). As the Neumann boundaries significantly improved alongshore velocities, these are assumed to be better for the current model application. It is advised to deduct a spatial non-uniform Neumann boundary for better hydrodynamic performance. For the morphodynamics, only the susw and bedw parameters have been calibrated. Other parameters could further improve the morphological performance. Adding these parameters to the calibration and comparing the modelled profile development with measurements is advised.

5.5. Validation

In this section, some model aspects are validated to measurements, theories and results from comparable computational models. The model characteristics that have been treated in Section 5.4 are not addressed in this section. First, the model performance on the wave representation is treated. Next, the tide and wave-driven current velocity fields for the coastal stretches and the Marsdiep are treated. Lastly, the modelled sediment transports are validated, both alongshore the North Holland coastline as around the Marsdiep.

5.5.1. Waves

Along the Dutch coast, waves are the most important driver of alongshore sediment transport in the nearshore zone (Van Rijn, 1997). Both the height and the wave direction should thus be represented well by the model. Figure 5.15 shows the RMSE and bias (see equations 5.4 and 5.5) for the waves at the Eierlandsegat and IJmuiden Munitiestortplaats. The model results are compared with data obtained with offshore measurement buoys at these locations. As there are no nearshore wave measurements in the researched domain for 2017, the propagation of the waves in the shoreface as simulated by SWAN cannot be validated.

(a) IJmuiden munitiestortplaats.

(b) Eierlandsegat.
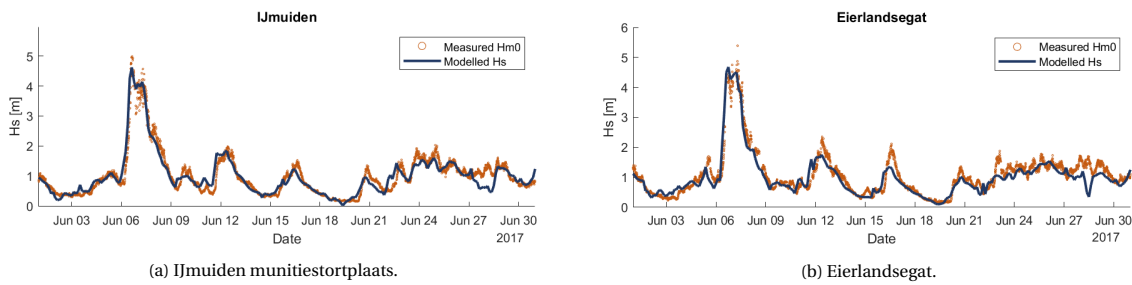
Figure 5.12: Model performance on the wave heights for the month June. Performance on all months is shown in Figure C.1.

Not all wave heights contribute equally to the alongshore sediment transport. Figure 5.13a shows the probability of occurrence of certain wave classes based on 30-year measurement data from IJmuiden munitiestortplaats. Figure 5.13b shows the transport capacity of each wave class after applying the CERC equation and the refraction method for the Callantsoog coast as explained in Section 5.3. High waves with an oblique incidence lead to the highest transports. Lastly, Figure 5.13c combines the first two figures, showing the expected dominant wave classes for sediment transport at Callantsoog. The estimated transport of waves with Hs < 1 m is low, despite them occurring the most frequently. Waves with a height between 1 and 4 metres show a much larger calculated transport. It is therefore important that these waves are represented well by the model. Kaji et al. (2014) found that the long-term development of the Sand Engine was dominated by waves of height 2.5 - 3 m, which is in line with the findings in Figure 5.13.

(a) Occurance of waves at IJmuiden.

(b) Transport potential per wave class.

(c) Transport potential of waves at Callantsoog.
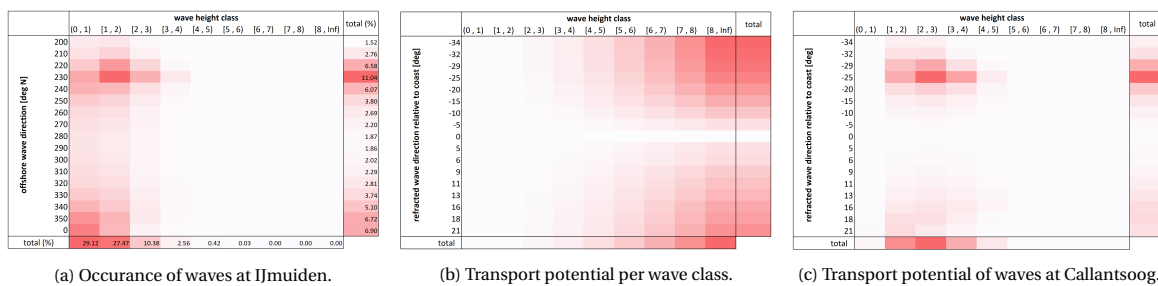
Figure 5.13: Theoretical sediment transporting capacity at Callantsoog of waves measured between 1990 and 2020 at IJmuiden munitiestortplaats. Snell's law and CERC formula have been used for the derivation.

From Figure 5.14 it becomes apparent that the absolute RMSE increases with the wave height. When looking at the RMSE relative to the height of the class, it stands out that the relative error of the smallest class (Hs = 0 - 1 m) is twice the relative error of all other classes, which is approximately 18%. As these smaller waves have barely any influence on the transport, this is deemed acceptable. The error values at IJmuiden (RMSE = 37 cm, R^2 = 0.85) and Eierlandsegat (RMSE = 33 cm, R^2 = 0.81) are in congruence with comparable models (see e.g. Luijendijk et al. (2017)) and thus regarded sufficient.

(a) IJmuiden munitiestortplaats.

(b) Eierlandsegat.
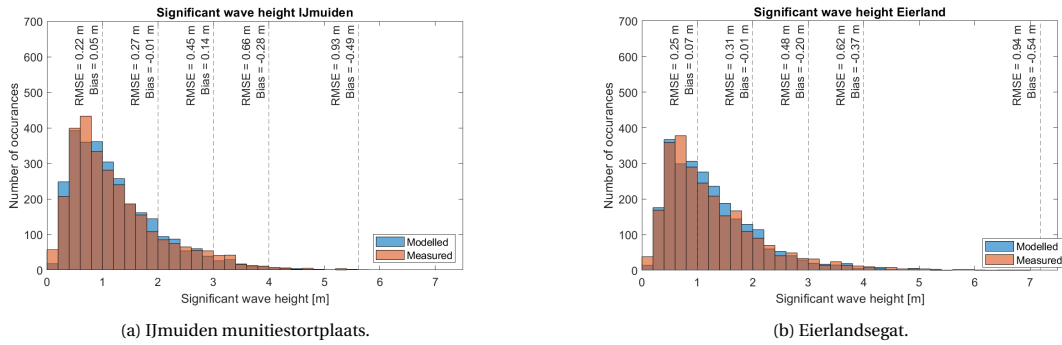
Figure 5.14: Model performance per wave height class. The waves classified per meter Hs, except for the waves with Hs > 4 m, which are assigned the final class.

(a) IJmuiden munitiestortplaats.

(b) Eierlandsegat.
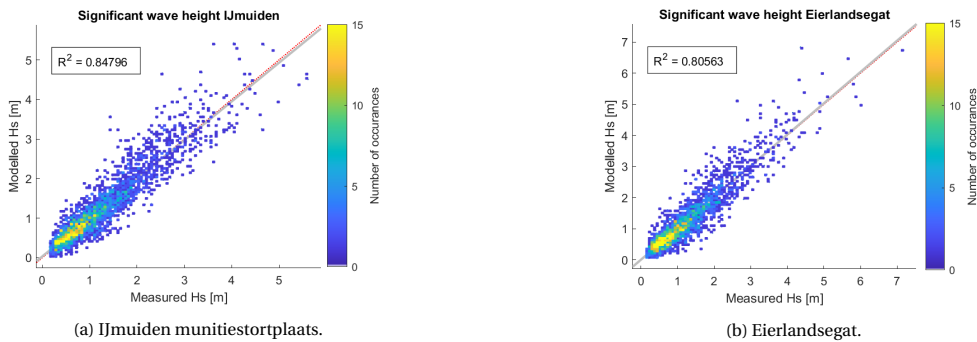
Figure 5.15: Correlation between measured and modelled wave heights. The red dash line indicates reference line.

Figure 5.16 shows the comparison between the measured and modelled wave direction. In the calculation of the RMSE, it is taken into account that the difference between waves from 350° and 10° = 20° and not 340°. In general, the model performance is good. Waves between 0 and 100 degrees are not represented very well. For IJmuiden, this can be attributed to the fact that these eastern waves are mostly very small and hence less easy to measure with a wave rider buoy. The discrepancy in this directional domain is not problematic, as these low eastern waves barely influence transports at the Holland coastline.

(a) IJmuiden munitiestortplaats.

(b) Eierlandsegat.
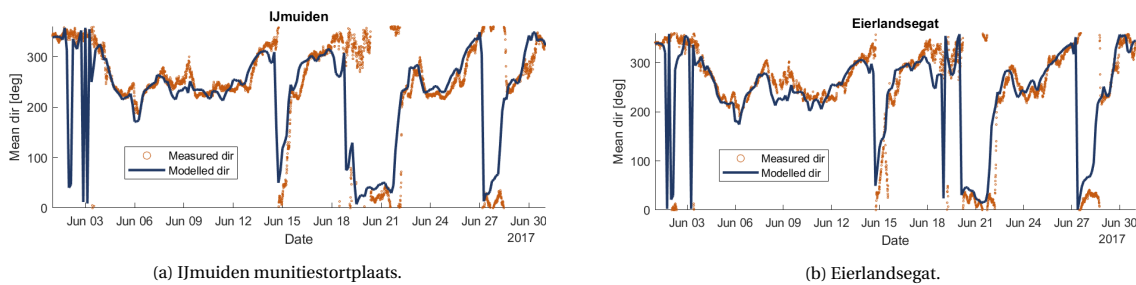
Figure 5.16: Model performance on wave direction for the month June. Performance on all months is shown in Figure C.2.

Based on the offshore wave height and direction, it can be concluded that the model performs well. As nearshore measurements are non-existent, concluding on the wave propagation through the domain is challenging. However, based on visual observation of this propagation, it has been concluded that there are no oddities in the primary processes such as refraction and wave breaking.

	RMSE	Jan	Feb	Mar	Apr	May	Jun	Jul	Aug	Sep	Oct	Nov	Dec
IJmuiden	H_S **[cm]**	35	47	31	20	25	23	28	25	27	37	33	36
	Dir [deg]	49	33	50	44	52	44	38	40	32	24	19	20
Eierlandsegat	H_S **[cm]**	44	50	33	26	29	29	32	26	37	NaN	34	37
	Dir [deg]	34	45	50	34	55	38	46	41	26	NaN	18	26

Table 5.4: Summary of the RMSE of the modelled wave height and direction at IJmuiden munitiestortplaats and Eierlandsegat.

5.5.2. Velocities

In this section the velocities driven by currents and waves are discussed. First, the velocities at the Callantsoog coastline are assessed. Afterwards, the velocity field in the Marsdiep is evaluated.

Callantsoog

In Section 5.4 it was explained that tide-driven currents contribute to the sediment transport by advection and the amplification of bed shear stresses. Wave driven currents are a more significant driver of sediment transports at the North Holland coast. Figures 5.17a and 5.17b depict both currents, which are in correspondence with the theoretical velocity profile discussed in Section 2.1, see figures 2.2b and 2.3. From the tide-driven current, the influence of the offshore bar is visible. The wave-driven currents resemble clearly the depth-induced breaking for different wave heights and water levels. There are no steep gradients in the velocity profiles, which is required for modelling the nearshore processes. The maximum magnitude of the wave-induced current at a breaker bar for waves of Hs = 2.5 m ($\sim$ 1.1 m/s) is in correspondence with values described by Van Rijn et al. (2002) based on measurements at Egmond aan Zee. The velocity magnitudes of the tide-induced current have been treated in Section 5.4.
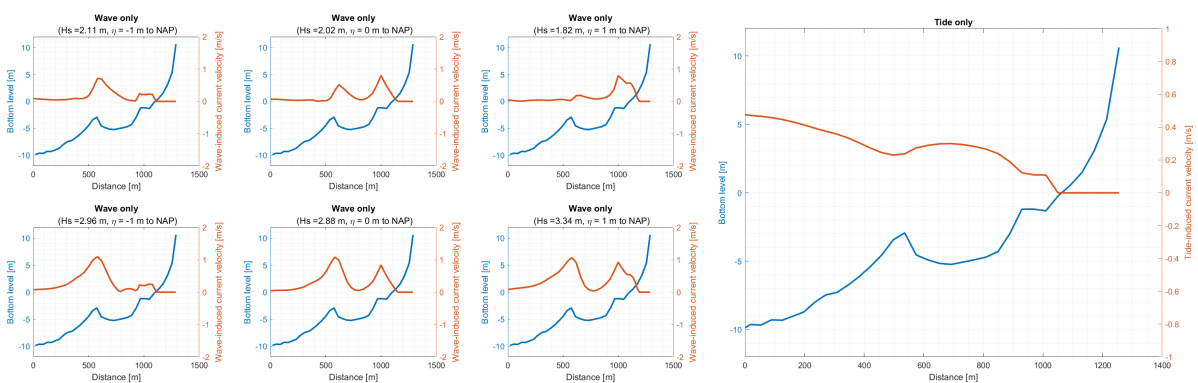
Figure 5.17: Modelled cross-shore velocity profiles of wave- and tide-induced currents at Callantsoog coast.

Marsdiep

The velocities in and around the Marsdiep basin should be represented well as they influence the spreading of a tidal channel nourishment applied in that region. For assessing the tidal channel nourishment, waves are not considered, as this leads to high computational times. Both research with the used model as research by Elias (2006) shows that the influence of waves east of the Noorderhaaks is minimal. The maximum wave heights in the inlet are generally below 1 m, hence not enough to significantly contribute to the sediment transports (see Section 5.6.1 for an elaborated explanation).

Figure 5.18 shows the comparison between the model used in this thesis, the model used by Elias et al. (2006) and a velocity field which is based on measurements executed by the Royal Netherlands Institute for Sea Research (NIOZ). These measurements are obtained by an Acoustic Doppler Current Profiler (ADCP) mounted on a ferry. Velocity magnitudes and directions have been obtained under a high frequency for an extended period. By qualitatively comparing the models, many similarities can be observed.

- the strong southward directed net current along the Nieuwe Schulpengat[2] ; a less strong southward net current through the Schulpengat; a net eastward current in the southern section of the inlet; a net westward current in the northern section of the inlet; a net southward directed transport through the Molengat;

---

[2]see Figure 4.4 for nomenclature of bathymetric features

Quantitatively the only reference is the ADCP measurements executed by the NIOZ. Also here, there is a good resemblance with the model:

- a maximum westward velocity of ∼ 0.15 m/s in the northern section of the channel; a maximum east-ward velocity of ∼ 0.06 m/s in the southern section of the channel; a flip in the net velocity direction at Y = 555.5 km.

(a) Model result from this thesis   (b) Model result from Elias et al. (2006)   (c) NIOZ
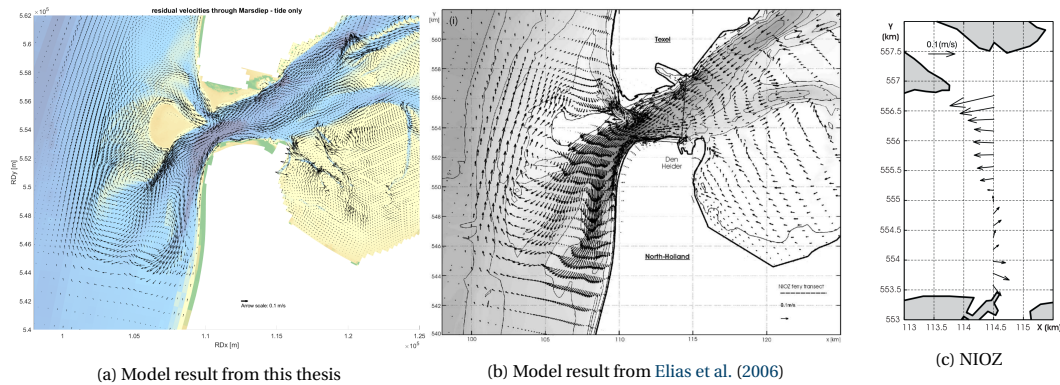
Figure 5.18: Residual velocity averaged under one spring-neap cycle and only tidal forcing.

5.5.3. Sediment transport

Now that we know that the water levels, waves and currents are well-incorporated in the model, it is time to look at the sediment transports. Validation on the sediment transports comes with more uncertainty than validation on hydrodynamics, as the former are more difficult to measure. Model results are hence compared to the results of other models and research, which are partly based on theoretical deduction of transports and partly on hydrodynamics and sediment budget studies.

Callantsoog

The alongshore suspended sediment transport along the entire coastal domain of the model has been determined for three different cross-sectional lengths. These lengths are perpendicular to the coastline. The upper two plots of Figure 5.19 stretch between (a) +3 and -8 m NAP (b) +3 and - 11 m NAP. The third one starts at +3 m NAP and has a constant length of approximately 1200 m. The first cross-section dimension is often used in literature for the description of sediment transport in the surf zone. The second and third dimensions are mainly interesting in the Marsdiep region, where strongly varying flow patterns occur on a small spatial scale (see Figure 5.18). The applied forcings are the water levels, winds and waves between 01-01-2017 and 01-01-2018. The simulation has been executed morphostatically, which means that the bed is not updated during the simulation. The gross transports (positive northward), net transport and transports per kilometre are given in kilograms. Recalculating to volume including pores can be done by dividing over the dry sediment density ($\rho_s = 2,650$ kg/m^3) and the porosity (p = 0.4).
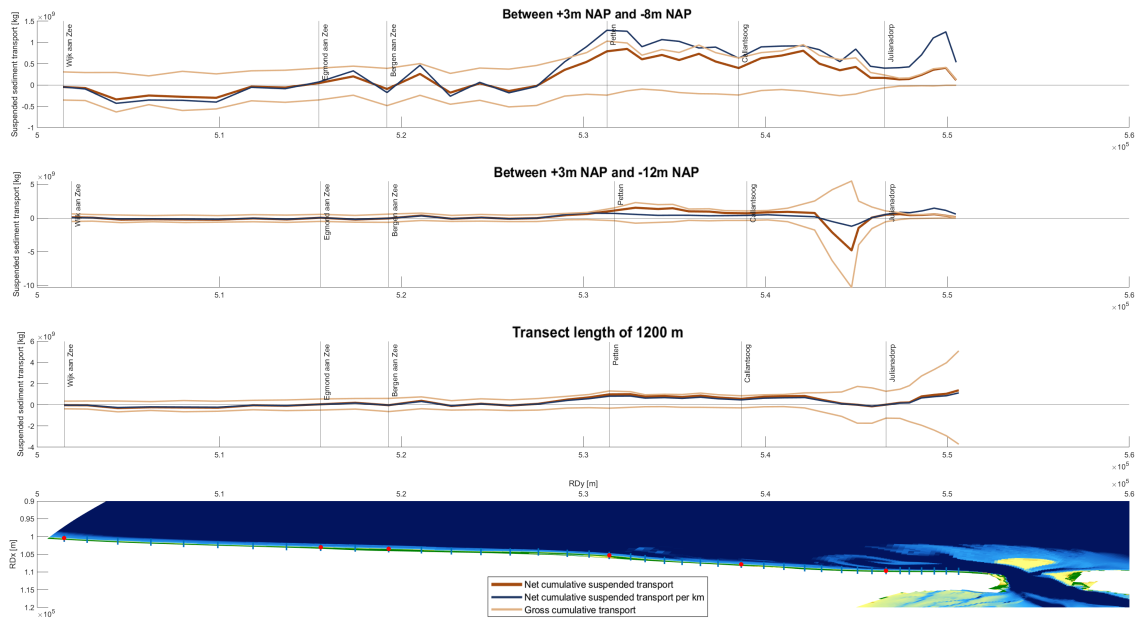
Figure 5.19: Modelled alongshore sediment transport for three different cross-sectional lengths. For each length, the transports are depicted a panel (upper three panels). A separation is made between gross and net transports.

The **gross southward transport** between +3 and -8 m NAP is mainly driven by waves and remains relatively constant, up to just south of Petten. It decreases in northward direction and eventually becomes almost zero near the inlet. The curvature of the North Holland coastline is such that NW waves enter more obliquely to the section between Wijk aan Zee and Petten, than north of Petten. Based on this, a southward increase of gross southward transport could be expected, which is resembled by the model well. The further decrease between Callantsoog and Julianadorp can be explained by the shadowing effect imposed by the features of the ebb-tidal delta. What stands out in the second plot is the large hump in gross transports between Callantsoog and Julianadorp. The high tide-induced currents can explain this hump in the Nieuwe Landsdiep, which are the result of the bathymetrically compressed ebb-flows from the Marsdiep (see Figure 5.18). Furthermore, the length of the cross-section implies that the transports are very large. The blue line, indicating the transports per kilometre, shows that the actual transports per unit length are not that high, though they have increased in magnitude. The increasing gross southward transport in the third plot is not only explained by the large flow velocities but also by the large depths and steep slopes over which the cross-sections span (up to 25 m depth, whereas the maximum depth of the cross-sections south of Callantsoog is 8 m).

The **gross northward transport** between +3 and -8 m NAP is quite stable between Wijk aan Zee and Bergen aan Zee, just like the gross southward transports. Towards Petten, the transports increase in magnitude. This increase can be ascribed to the changing coastline orientation just south of Petten (leading to a higher angle of incidence for the dominant SW waves), and to the presence of the large hump of sand of the Hondsbossche Dunes. The decrease that occurs when moving close to and northward of Julianadorp is mainly the result of the sheltering of the SW waves. The increase of northward transport around the 550 km coordinate is due to the 'taking over' of tide-induced transports. The reason that the gross northward transport is larger than the southward transport could be attributed to the northward increasing tidal asymmetry and that the ebb flow cannot sharply follow the curvature around the tip of North Holland.

The **net transport** is the difference between the gross transports and has been calculated by subtracting the gross southward transport from the gross northward transport. This results in net transport that wiggles around 0 in the southern half of the investigated area. Net transports in the surf zone increase strongly towards Petten, probably largely due to the changing orientation of the coastline (Van Rijn, 1997). The sheltering of the tidal delta leads to a decrease near Julianadorp, followed by an increase due to the steep coastal profile and strong tidal currents.
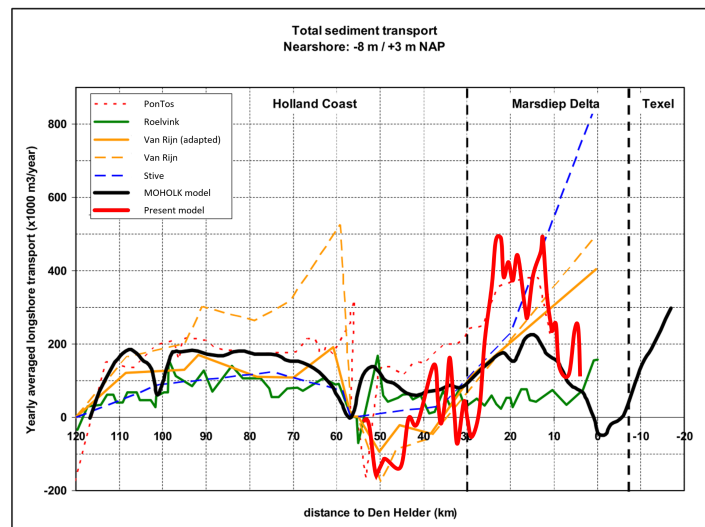
Figure 5.20: Comparison of model results with benchmark models. Adapted from Van der Hout et al. (2009).

In Figure 5.20 the result of a one year simulation is compared to other studies which used calibrated conceptual and computational models (PonTos by Steetzel & De Vroeg (1999), Roelvink et al. (2001), Stive & Eysink (1989), Van Rijn (1995), Van Rijn adated by Van de Rest (2004) and MOHOLK by Van der Hout et al. (2009)). A few things stand out and are treated below.

Between km 55 - 30: The southward directed transport just northward of IJmuiden (around km 55) is in resemblance with some other studies; southward directed. The physical explanation of this southward transport is different, however. The models used in this comparison include the harbour of IJmuiden, including its breakwaters. These breakwaters block northward currents, sediment transports and waves. In the current morphological model, IJmuiden is not included. Hence no blocking of waves occurs. As no sediment is fed to the system at the model boundaries, the blocking of northward directed transports is implicitly included. Another explanation for the discrepancy can be the wave climate of 2017, as specified in Section 5.3. The strong NW waves in January 2017 drive significant southward transports (see Figure C.5). When January is excluded from the analysis, the gross southward transports decrease, leading to an 'upward' shift of net transports with $0.15 \cdot 10^9$ kg (halving the southward transports between Wijk aan Zee and Egmond aan Zee). Comparison of the wave roses of 2017 (including and excluding January) and the 30-year period shows that 2017 without January better resembles the last 30 years.

Between km 30 - 10: The increase in net northward transport in the Marsdiep Delta is in agreement with the other studies, although the increase in the current model is somewhat higher than in the benchmark studies. The outlying value of Roelvink et al. (2001) can be explained by the short calibration period used in this study (1972-1980), which is a period where relatively little erosion occurred (Van de Rest, 2004). Furthermore, Roelvink et al. (2001) applied a 50% reduction in transports to account for the groynes in this section. Van Rijn (1995) applied a 20-50% reduction to account for these groynes. In the present model, no groynes are included and the transports shown in Figure 5.20 are not adapted afterwards. The reasoning behind this is that these groynes could induce numerical instabilities. Furthermore, the groynes only extend to a depth of approximately 1 m. Although they might indeed influence 15-50% of the alongshore transport, they are not expected to largely influence a shoreface nourishment, which is placed a few hundred metres offshore of the groynes. A study by Rakhorst et al. (2001) shows that the effect of these groynes on coastal erosion is limited. One other explanation of the relatively higher values for the present model could be the used sediment transport formulation, which is TRANSPOR1993 and based on formulations by Van Rijn et al. (1993). A sensitivity study for the MOHOLK model showed that the use of the TRANSPOR2004 formulation led to a reduction of alongshore transports of approximately 50% (Van der Hout et al., 2009). This could partly explain the difference between the MOHOLK model and the present model. Furthermore, the construction of the Hondsbossche Dunes had not taken place in the reference studies, whereas it is included in the bathymetry

of the model used in this study. The drop at km 17 can be explained by the nourished bar at Callantsoog, which lies outside of the +3 to -8 m zone (see Figure 4.5).

Between km 10 - 0: Lastly, it stands out that the transports decrease towards the Marsdiep. One explanation for this discrepancy is the definition of the surf zone. For this analysis, the definition is the transect between +3 and -8 m, as is in the MOHOLK model (which shows the same behaviour). The steep coastal profile in the north makes this transect short. Hence low transports seem to occur. When looking at the blue line in Figure 5.19, it can be seen that the transports per unit length are reaching the maximum alongshore value. The researches used for the comparison of Figure 5.20 point out that the largest uncertainties are present near hydraulic structures and inlets, hence near km 55 and around the Marsdiep delta (see e.g. Van Rijn (1995)).

Marsdiep
Figure 5.21 shows the tide-averaged transport field of suspended sediment. Qualitatively, the transport field of the current model corresponds well with the model by Elias (2006). A substantial import can be observed around the tip of North Holland. Sediments are imported mainly towards the northern channel inside the basin. The separation of net northward and net southward transport between the Franse Bankje en the Bollen van Kijkduin is also present. Net transports through the Schulpengat are northward directed in the current model, whereas transports are south in Elias (2006). The almost logarithmic scale used in the figure of the benchmark model slightly complicates the visual comparison. The southward transports through the Molengat and bypassing around the Noorderhaaks are - though hardly visible in the current presentation - present as well in the model. Quantitatively, the values of the transports correspond well, with a maximum in the order of magnitude of $0.0001 \text{ m}^3/(\text{m} \cdot \text{s})$. The values in the Molengat match as well, being a factor 10-20 smaller than the values around the tip of North Holland. The modelled net annual import of $2 \cdot 10^6 \, m^3$ is within the range of the values of $0.5 - 6.0 \cdot 10^6 \, m^3$ found by other studies (Elias, 2006; Van der Hout et al., 2009; Van Rijn, 2015). It should be noted that this is in the absence of waves, which contribute to the sediment import through the inlet (Elias et al., 2006). The contribution of the waves is expected to be well below the contribution of the tides and waves. Elias et al. (2006) calculated a 60% increase when adding waves to the tide and wind-driven transports. It is worth mentioning that a month of winter waves - containing high SW waves - were used for this calculation and that the expected annual contribution is thus expected to be lower.

(a) Model result of this thesis

(b) Model result of Elias (2006)
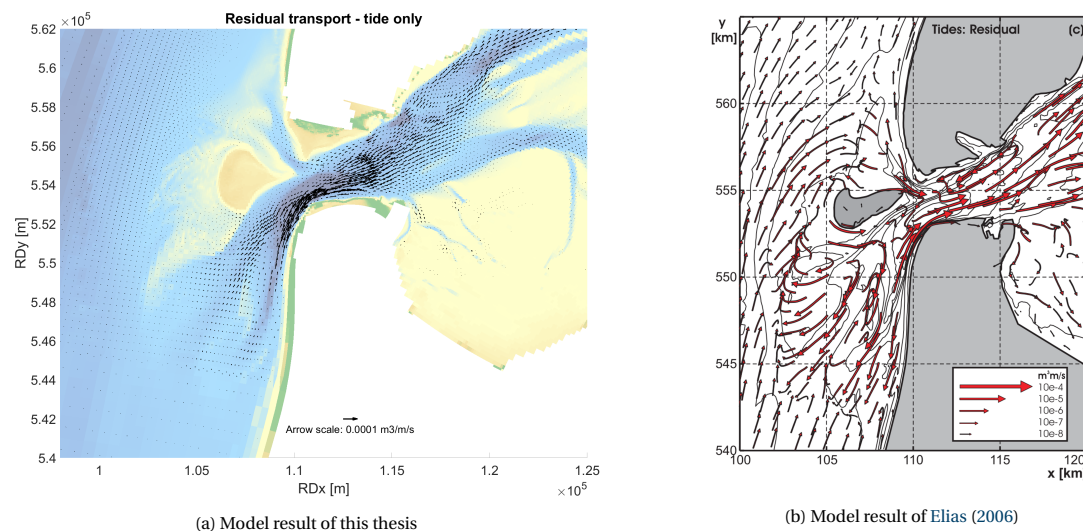
Figure 5.21: Comparison of the modelled tide-averaged transport field with the model by Elias (2006).

Morphological development
Lastly, the modelled morphological development of the Marsdiep is assessed. As a benchmark, the morphological development between 2009 and 2015 has been used. This development is retrieved by the subtraction of the 2009 Vaklodingen from the 2015 Vaklodingen, which have been obtained through Rijkswaterstaat and are the most recent successive measurements of the entire area. A morphological simulation of five spring

neap cycles without the influence of waves and with a morfac of 12 has been executed [3] . This represents the morphological development of 27 months. In order visually to compare the 6-year data with the 2.25-year data, the bed level changes have been divided over the period. In order to keep the channel position and development more realistic, the grain size has been increased to a uniform value of $D_{50} = 350 \ \mu$m, which is more in between the channel and flats values (see Figure 5.6). Despite this higher value of the grain size, the model seems to overestimate the sedimentation and erosion. In reality, there is a large variation in grain sizes, with significantly larger grain sizes in the channels. Although the morphological development in the channels seems to be over predicted, the flats show greater correspondence with the measurements. The latter is probably due to the oversizing of the grain size of these flats.
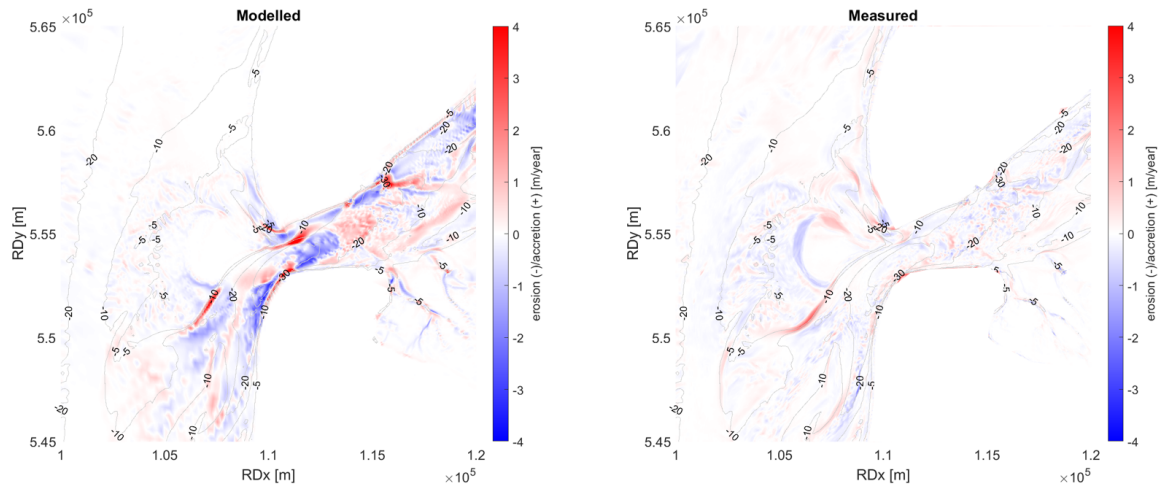
Figure 5.22: Comparison of the modelled and measured morphological changes around the Marsdiep. Measurements are based on the difference between the 2009 and 2015 Vaklodingen.

From qualitatively comparing the two figures, some similar features can be observed. The most prominent feature is the deposition of sediments at the southern tip of the Noorderhaaks. This deposition could be attributed to the decelerating ebb flows containing much sediment. Another feature that seems to be represented well in the model is the erosion of the Nieuwe Schulpengat.

What is missing in the modelled bathymetry is the erosion of the seaward side of the Noorderhaaks. This is caused by the absence of waves in the modelled situation. Another difference is the modelled strong morphological developments at the channels of the northwestern tip of North Holland. In the measured bathymetric data, no significant bed level difference is observed. When looking at the data from the Sedimentatlas, it can be seen that grain size distributions with a D_{50} between 450-600 are prevailing in this section. The strong erosion and accretion can be hence attributed to the modelled median grain size of 350 μm. Lastly, it should be noted that the measured developments had the 2009 bathymetry as a starting point, whereas the model uses the 2015 bathymetry. For a better comparison, the 2015 Vaklodingen should be compared to measurements executed at a later stage, which are not available yet at the moment of writing.

5.5.4. Conclusion on validation
The executed validation shows that the modelled wave climate and velocities correspond well with measurements and results from other researches in both magnitudes and directions. The validation of the sediment transports along the North Holland coast shows that the performance of the model is reasonably in line with the benchmark studies. To most abnormalities, a possible explanation has been given. However, the modelling of wave-, tide- and wind-induced sediment transports is inherent to many uncertainties. The validity of the proposed explanations is thus to be disputed. A further examination of the parameterisations and sensitivities could give more insight into the model behaviour but is beyond the scope of the research. The net alongshore transports around the shoreface nourishment location, Callantsoog, correspond with other

---

[3]It has been validated that the use of a morfac of 12 leads to the same morphological development as a simulation with 12 times the simulation interval and a morfac of 1.

studies. Hence no further optimisation is deemed necessary. The validation of the morphological devel-
opment implicates that making statements about the eventual bathymetry after a nourishment comes with
quite some uncertainty. One of the contributors to the discrepancies is probably the chosen uniform grain
size. This would therefore not necessarily imply that the morphological modelling around the Marsdiep is
performing poorly. One way of dealing with this complexity of the Marsdiep morphology and composition
is by looking at the difference in bed level before and after a nourishment. In that way, the nourishment
development can be considerably isolated from the 'base-case' bathymetric developments. Validation on
transport patterns in this region confirms that this would allow for reasonably accurate predictions.

5.6. Acceleration techniques

Morphological, process-based coastal area models can be computationally demanding (Luijendijk et al., 2019). The frequent communication between the D-Waves and D-Flow modules, desired for an accurate representation of the interaction between the governing processes, contributes to high computational times. In the case of the assessment of the shoreface nourishment at Callantsoog, this coupling is required. In order to reduce the computational times of the model, some acceleration techniques are assessed.

5.6.1. Separation Callantsoog and Marsdiep

As discussed in the model setup, the nourishments at Callantsoog and the Marsdiep are separately modelled to reduce computational times. A brief justification for this choice is given in this section.

Section 4.3 explains the contribution of many processes to the sediment behaviour in and around the Marsdiep inlet. Many of the dominant processes are the result of the tide. The contribution of waves is twofold. Most of the waves that approach the Marsdiep break on the shallow ebb-tidal features (Elias, 2006). This breaking leads to the stirring of sediment, making it susceptible to being transported through the inlet. This effect does influence the sediment transport in the region. However, a higher sediment concentration originating from the outer delta is expected to have just a limited influence on the dispersion of the nourishment. A minor effect of hindered settling could occur, but its effect will be negligible compared to the hindering effect of the nourishment itself. Secondly, waves contribute to the current velocities that prevail in the region. This effect could play a role in the dispersion of the sediment. However, (Elias, 2006) accounts 20% of the net sediment import to waves. Taking into account that part of this 20% is due to the enhancement of the sediment concentration, leaving out the waves for the tidal channel nourishment is assumed to be a valid choice for the significant reduction of computational times. Model results of the model developed for this thesis substantiate this choice, showing little influence on the Marsdiep transport pattern by the addition of waves (see Appendix C.3).

5.6.2. Different techniques

Luijendijk et al. (2019) have evaluated different techniques for the acceleration of a morphodynamic coastal Delft3D model for medium to long-term application. The techniques are evaluated using a calibrated Sand Engine model. One fundamental principle is the morphological acceleration factor, or morfac, developed by Lesser et al. (2004). When applied, the bed level changes after each hydrodynamic time step are multiplied by the morfac. It must be assumed that the response of the bed to the hydrodynamic forcing is linear during one morphological time step (Ranasinghe et al., 2011). For example, in the case of a more complex bed stratigraphy, where the lower bed layers are more resistant to flows as they are compressed or coarser, the erosion of the first layer cannot always simply be extrapolated. Applying a morfac could also be unsound if a morphological change significantly alters the flow on the hydrodynamic timescale. Lesser et al. (2004) show that values up to the order of 50-100 could be used for simulations with waves and tides. Brière et al. (2011) demonstrate that the appliance of a morfac is also useful in the case of modelling bar behaviour.

Luijendijk et al. (2019) make a distinction between brute and representative forcing. The first entails the use of unfiltered time series of forcings such as water levels, waves and wind. The second category uses representative conditions. In that case, a wave climate could be generated that represents the gradient in alongshore sediment transports (see Figure 5.19). Another method could be the determination of common wave classes based on the offshore wave climate. In the case study of Luijendijk et al. (2019), the use of representative conditions resulted in the smallest computational times (1-1.6% of the reference case). However, the use of representative conditions induced inadequacy in accurately predicting the short term (< 2 years) morphological developments. The RMSE error of the representative conditions was calculated to be 10 times the RMSE of the brute forced conditions. Although this might be partly attributed to the low amount of representative conditions selected (O(10)), it is decided not to derive representative conditions for this study. As there are already multiple uncertainties regarding the model performance, adding more large uncertainties at the win of computational time is not desired nor needed.

With regards to the brute forced accelerations, three methods are researched next to the standard brute forcing (BF); the brute force filtered (BFF), brute force filtered and compressed (BFFC) and brute force merged (BFM) approach. In the case of BFF, certain conditions are filtered out of the input data. In the case study by

Luijendijk et al. (2019), waves with Hs < 1 m were left out as they are not expected to contribute significantly to the morphological development of the Sand Engine. In the case of the Sandwindmill, where sediment is added to the system in suspension, these waves could have a larger influence as they can keep the sediment in suspension through the wave orbital velocities. For a stationary nourishment like the Sand Engine, a threshold velocity should be exceeded before the sediment is brought into suspension. Although the magnitude of this effect has not been quantified, it is chosen not to remove the lower waves from the input data.

In the BFFC approach, the filtered conditions are compressed as well. This means that the duration of each forcing condition is reduced with a factor X, and so is the computational time. To offset the decreased duration of each condition, an equal morfac is applied. The compression can be applied to waves and wind, which should be simulated synchronised as winds induce wave growth. The compression of the water levels (consisting of tide and a NTR) is more complicated. If the vertical tidal signal is compressed, unrealistic tidal velocities may be produced (tidal velocities are also described as the horizontal tide). Especially with the filling and emptying of the Marsdiep basin, these velocities could become unrealistically high. Not adapting the water levels is not a good option either; the NTR (or surge) has a significant correlation with the wave height (Petroliagkis et al., 2016). Decoupling the two would lead to unrealistic behaviour, as high waves would not coincide anymore with high surges. This would lead to a skewed depth induced breaking, where modelled high waves would break more offshore due to the missing of the right level surge. As the wave breaking is expected to be key to the sediment transports of the Callantsoog nourishment, the surge signal should be fed to the model synchronous to the waves and wind. A decoupling of the tide and surge level is required for this. Section 5.6.1 treats this decoupling for the current model.

The last technique discussed by Luijendijk et al. (2019) is the BFM approach. In this approach, the wave time series is split up into multiple separate time series. These series are distributed over several processors, which calculate the bed level change in parallel. After a specified interval, the bed level changes of all processors are weighted, merged and fed back to the processors. This technique is computationally fast (4.5% relative to the reference BF simulation), leading to the same error measure as the other BF acceleration methods. As the scenarios that will be assessed include the time- and condition-dependent execution of a nourishment, such a merging process becomes too complex. For that reason, the BFM method is not used in this research.

From the description of the acceleration methods and their applicability to the current research, solely applying a compression and equal morfac appears to be the best technique (BFC). This conclusion is partly based on assumptions, such as that the omitting of lower waves could result in a decreased initial sediment dispersion. Testing these assumptions could result in a computationally more effective model and is recommended for any further research.

5.6.3. Application of BFC method
The discussed acceleration methods are mainly effective in simulations that include the effect of waves. As the assessment of the tidal channel nourishment at the Marsdiep does not include any waves, applying the morfac would be satisfactory. For assessing the shoreface nourishment at the open coast, the compression of the forcings appears to be the best method. An acceleration factor of 3 has been chosen. Applying a higher morfac could lead to high velocities imposed by the compressed surge. First, wave compression is treated. Afterwards, the separation and compression of the surge signal is discussed.

Waves
The compression of the wave (and wind) forcings is a relatively simple task. The interval between the wave conditions is decreased with a factor of 3. The compressed wave series is compressed towards the starting point, here 31-12-2016. See Figure 5.23.
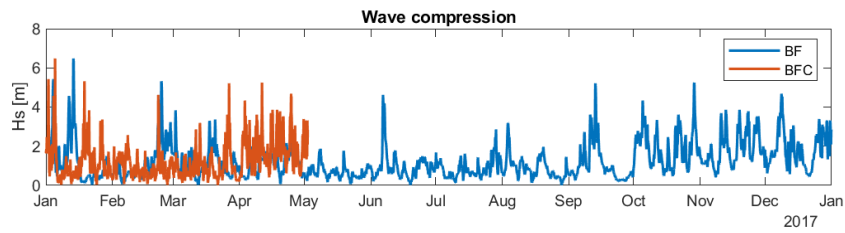
Figure 5.23: Example of wave compression with a factor 3.

To inspect if the adaptation of the input conditions is captured well by the model, the model output (Hs) of the compressed and uncompressed series are compared for an offshore measurement point. The compression results in a shorter duration of each wind and wave condition. Consequently, the wind is given a shorter time to exert shear stress on the water body and let the waves grow.
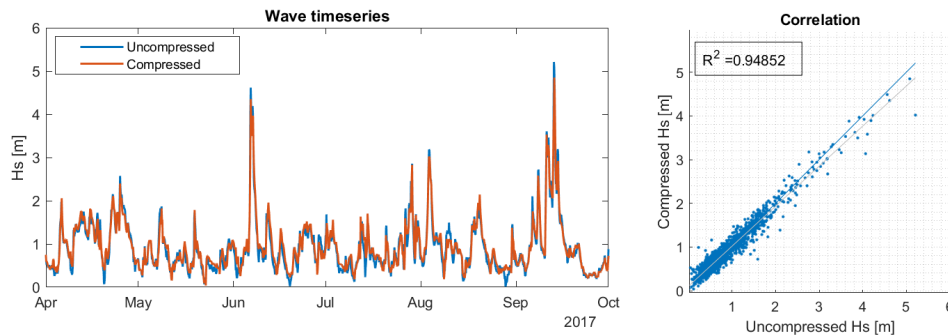
Figure 5.24: Performance of compressed wave series. The orange line shows the model output of the compressed wave series, which is manually transformed to a non-compressed series for comparison with the reference model output (blue line). In the correlation figure, the blue line is the reference line, indicating a perfect correlation.

In Figure 5.24 the model output of the compressed and uncompressed wave time series are compared. In order to visually compare, the times of the compressed output have been manually extended such that the series have a good overlapping. From the comparison it can be seen that overall, the compressed wave time series correlate well with the uncompressed series. As expected, the model with compressed boundaries slightly under predicts the magnitude of the higher waves.

Surge

To compress the surge, separation of the NTR with the tide has been executed through a harmonic analysis of all water level boundary conditions (time series). For a good synchronisation with the waves, the starting time has also been set at 31-12-2016. A simulation with the resulting tide-only signal has been analysed and shows acceptable correspondence with the tidal constituents presented in Table 5.1. After separating the tide and the NTR, the NTR of a single boundary condition point has been compressed with a factor of three and added to the tide-only signals of all other boundaries. The NTR of a single point has been applied to all boundary condition points to reduce the spatial gradient in the surge. This spatial gradient could lead to unrealistic velocities as the signal is compressed. Lastly, Neumann boundaries are derived in the same manner as described in Figure 5.5. The performance of the hydrodynamics of the model after these adaptations was rather poor. Comparing water levels with measurements is a difficult task, as surge and tidal signals are no longer synchronised. However, the velocities seemed to be significantly higher than the values tested in Section 5.4. The main reason for this is that not all harmonic components were captured well by the harmonic analysis. The surge signal contained some noise, of which the frequency and amplitude were high enough to skew the velocity signal when compressed by a factor 3, see Figure 5.25. A new signal has been produced by calculating the moving average over a period long enough to both capture surge extremes as to provide a smooth signal.
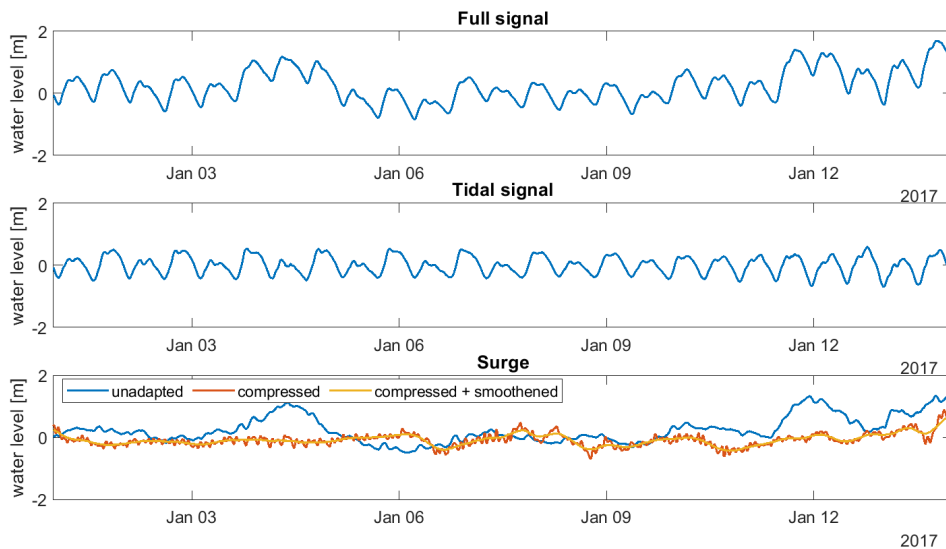
Figure 5.25: Result when surge is filtered from the tidal signal, compressed and smoothed. The upper panel depicts the full water level signal, the middle panel the isolated signal and the bottom panel the isolated surge.

5.6.4. Conclusion on acceleration

The difference in characteristics at the Marsdiep and Callantsoog allows for a separation into two models. As tidal influences are dominant in the Marsdiep region, waves can be omitted from the modelling without considerable implications on the results. For Callantsoog, waves are the dominant mechanism for sediment transport. As the online modelling on the current spatiotemporal scale and resolution is computationally expensive, multiple acceleration methods are discussed. It is concluded that compression of the wave-, surge- and wind-signal leads to the most efficient and robust acceleration method for the intended assessment. Two limitations of the method are the underestimation of higher waves and the loss of information during the separation of the tidal and surge signal. The under-representation of high waves could lead to an underestimation of transports. However, the altered water level signal is less critical, as tidal velocities are of minor importance at the closed coastal system that is assessed.

6

Nourishment design

Section 3.6 discusses that tidal channel and shoreface nourishments are the most cost-effective applications for the Sandwindmill. The assessment of the study area in Chapter 4 shows that the Marsdiep inlet and the coastline near Callantsoog are well-suited for these respective nourishment methods. In this chapter, different nourishment designs are analysed. First, the nourishment goals are defined in Section 6.1. Based on the goals, the scenarios are set up in Section 6.2. The scenarios are evaluated with the use of the D-Flow FM and D-Waves models that are examined in Chapter 5. The simulation results are summarised in Sections 6.3 and 6.4. In Section 6.5, the performance of each scenario is evaluated in accordance with the criteria from Section 6.1.

6.1. Nourishment goals

As stated in Section 1.2, the Dutch coastal system needs approximately 7 Mm^3 to keep up with every millimetre of sea-level rise (Veerman et al., 2008). Therefore, for the entire coastal system, it holds that every m^3 of added sediment contributes to keeping up with SLR. With regards to the Marsdiep, it is believed that the feeding of the Wadden Sea could slow down coastal erosion in adjacent regions (Wang et al., 2018). Adding sand to the Wadden Sea and the coastal foundation is therefore one of the nourishment goals. From a technical-economical point of view, it is optimal when much sediment can be placed within a small area. Fast erosion of the added sediment at the nourishment location is thus an critical parameter for determining the potential of a nourishment strategy. Another goal is the sufficient spreading of the added sediment. When the material is eroded from the dumping location, it would be beneficial if it could cover a significant reach, rather than staying around the nourishment area. Widely spread, moderate accretion is therefore preferred over concentrated, large accretion. This spread accretion is furthermore preferred from an ecological point of view, as marine species could better keep up with smaller accretion rates. For the Callantsoog nourishment, another measure of this spreading is the alongshore development of the bed level change. As the cross-shore modelled processes are less reliable (see Section 5.4.2), these are not addressed. Lastly, a goal of the Marsdiep nourishment is supplying sediment to the base of the Helderse Seawall to maintain the stability of the wall (Rijkswaterstaat, 2019a).

Measuring the nourishment success

A qualitative assessment of each scenario contributes to a better understanding of the hydro- and morphological developments. However, with the aim of determining the performance of each strategy, each criterion should also be made quantifiable. Therefore, each of the stated nourishment goals is assigned a key performance indicator (KPI).

For the Marsdiep nourishment, the amount of sediment entering the Wadden Sea can be measured by determining the sediment volume change in a polygon in the basin. Whether the nourishment adds to the stability of the Helderse Seawall can be monitored by assessing the sediment volume change in the area nearby the wall. The fast local erosion of added sediment can be determined based on the bed level change at the nourishment location. Whether the nourishment disperses regionally can be measured by categorizing the bed level change into accretion-classes, and by looking at the contribution of each class to the total amount of ac-

cretion. As stated before, moderate regional accretion O(cm) is preferred over concentrated accretion O(m), also from an ecological point of view.

For Callantsoog, every m³ of sediment directly contributes to the coastal foundation. As this value is directly dependent on the sediment input, this goal is not measured. The local and regional dispersion can be measured in a similar fashion as for the Marsdiep. The alongshore distribution can be measured by looking at the distance to e.g. a 10 cm bed level increase. The goals, their name and the KPI of the goal are summarised in Table 6.1. The performance of all nourishments on the KPIs is elaborated in the result analysis. In Section 6.5, the results are summarised for both the shoreface and tidal channel nourishment.

	Goal	Name of goal	KPI
Tidal channel	Add sediment to the Wadden Sea	Wadden Sea	Volume change in polygon [m³]
	Feed foundation of Helderse Seawall	Helderse Seawall	Volume change in polygon [m³]
	Limited local accretion of added material	Local accretion	Bed level at nourishment location [m]
	Large regional dispersion	Regional dispersion	Share of small and medium accretion in total [%]
Shoreface	Limited local accretion of added material	Local accretion	Bed level at nourishment location [m]
	Large regional dispersion	Regional dispersion	Share of small and medium accretion in total [%]
	Large alongshore distribution	Alongshore distribution	Spreading of 10 cm depth contour [m]

Table 6.1: Key Performance Indicators (KPIs) for determining the degree of success of each nourishment design.

6.2. Scenario set-up

Section 6.2.1 provides an overview of the executed nourishment scenarios. In Section 6.2.2, the nourishment scenarios for the Marsdiep are discussed. Afterwards, the scenarios for the shoreface nourishment at Callantsoog are treated in Section 6.2.3.

6.2.1. Overview of nourishment scenarios
In Table 6.2, an overview is presented of the executed nourishment scenarios.

		Yearly in-situ [m³]	D_{50} [μm]	$L_{cross-shore}$ [m]	$L_{alongshore}$ [m]	Location	Other
Tidal channel	A0	1,500,000	350	200	110	Marsdiep (south)	None
	A1	1,500,000	**150;250**	200	110	Marsdiep (south)	none
	A2	**3,000,000**	350	200	110	Marsdiep (south)	none
	A3	1,500,000	350	220	110	Marsdiep (south)	**Dependence on velocity**
	A4	1,500,000	350	220	110	**Marsdiep (shift offshore)**	none
	A5*	1,500,000	350	220	110	Marsdiep (south)	**6 year prediction**
Shoreface	B0	100,000	250	70	200	Callantsoog (outer bar)	None
	B1	100,000	**150**	70	200	Callantsoog (outer bar)	None
	B2	**200,000**	250	70	200	Callantsoog (outer bar)	None
	B3	100,000	250	70	200	Callantsoog (outer bar)	**Dependent on wave height**
	B4	100,000	250	70	200	**Petten (outer bar)**	None
	B5	100,000	250	70	200	**Julianadorp (channel wall)**	None
	B6	100,000	250	70	200	**Callantsoog (nourished bar)**	None
	B7	**500,000**	250	70	**1,000**	Callantsoog (outer bar)	None

Table 6.2: Overview of the assessed nourishment scenarios. The bold cells indicate a deviation from the base case. Scenario A5 is excluded from quantitative comparisons with other simulations.

6.2.2. Tidal channel nourishment
The first nourishment to be assessed is a tidal channel nourishment in the Marsdiep region. This region is of importance as sediment is imported towards the Wadden Sea, leading to erosion of the outer delta and coast. The optimal location satisfies two criteria. Firstly, high flow velocities must occur, as this is fundamental to the transporting potential of the location. Secondly, it would be beneficial if the nourishment can contribute to the stability of the Helderse Seawall, apart from feeding the Wadden Sea. A location that satisfies all these goals is the tidal channel adjacent to the Helderse Seawall. The highest tide-induced flow velocities of the region are expected to occur here (Elias et al., 2006). An additional motivation to select this location is that Rijkswaterstaat wants to improve the knowledge on the effect and interaction of nourishments placed here (Rijkswaterstaat, 2021).

Scenario A0: Base case
Scenario A0 is used as a base case and reference for the other scenarios. As the dominant sediment trans-

port direction is towards the Marsdiep, the nourishment should be placed slightly on the outer side of the North Holland tip. However, placing the nourishment too far to the west/south could make it insusceptible for the ebb currents. As explained in Section 4.3, the flow streams through the inlet like a jet. As the ebb-flow jet cannot sharply follow the curvature of the tip of North Holland, the nourishment should be placed just before the part where the jet detaches. In that way, the stronger ebb currents can reach the sediment as well, contributing to the goal of limited local accretion. Furthermore, orbital velocities of southwestern waves could stir up the nourished sediment, keeping it in suspension for a longer time and increasing the spreading.
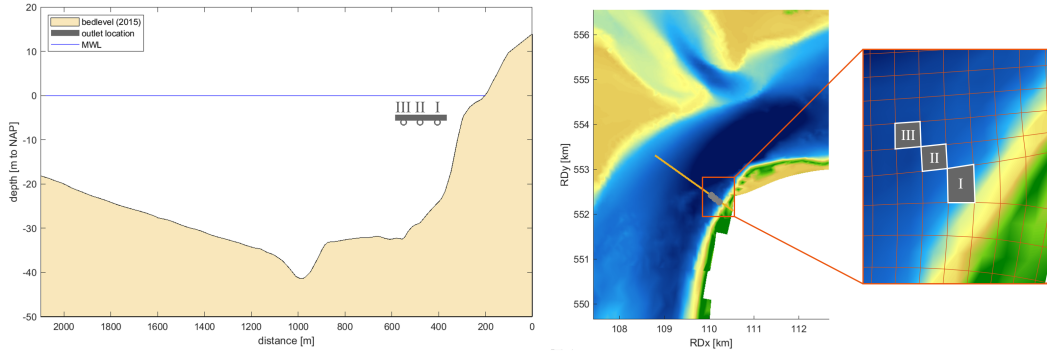
Figure 6.1: Nourishment location of the tidal channel nourishment. The cells I, II, and III are the cells in which the nourishments take place. These are used as a reference in the description of the nourishment behaviour. The sizes are I: 9,600 m^2; II: 6,400 m^2; III: 6,500 m^2. The cross-section of the left panel is indicated by the orange line in the right panel.

The location of the nourishment for this study is shown in Figure 6.1. The nourishment location is chosen such, that it is just landward of the shipping channel. The influence of the nourishment on the shipping traffic must be closely monitored, as both a port and a naval base are located at Den Helder. The nourishment in the base scenario spans two computational cells. For this base scenario, 1,500,000 m^3 of sediment will be placed. This regards the annual volume including pores (also called in-situ). With a safe volumetric concentration of 10% (see Section 3.4), this requires a mixture discharge of approximately 0.1 m^3/s per cell. Without erosion, this would lead to a yearly bed increase of approximately 90 metres, which is three times the depth. 1,000,000 m^3 is added to cell I and 500,000 m^3 to cell II, as cell I is more critical regarding the seawall stability. The grain size has been set equal to the bed grain size, at $d_{50} = 350$ μm. As explained in Section 5.6, both the water level and atmospheric forcing of 2017 are applied.

Scenario A1: Variable D_{50}
The second scenario assesses the variability in nourishment grain size [4] . There are multiple reasons to assess the influence of the grain size on the sediment distribution. Section 3.4 shows that a smaller grain size is beneficial in both energy requirements as in the abrasion of the transport pipes. Another reason is that smaller grain sizes are being transported more easily (see Section 2.2). As a large sediment dispersion is desired for the feasibility of the Sandwindmill, smaller grain sizes seem to have significant potential. For this scenario, two simulations with median nourishment grain sizes of 150 and 250 μm are executed.

Under default settings, Delft3D works with a uniformly mixed bed (Deltares, 2021b). In the case of deposition of sediment from a different fraction, the new fraction will be mixed through the entire original sediment layer. Bookkeeping of layers is required to ensure that sediment fractions do not mix up in the entire bed layer. In Delft3D, underlayering can be applied to do this bookkeeping. This underlayering works as follows. On the top of the bed, there is an active layer with a user-defined, constant thickness. When accretion occurs, the sediment in this layer is mixed proportionally. The transport layer then passes the volume of accreted sediment with the new mixture towards the layer beneath it. This layer is called the exchange layer. When the threshold height of the exchange layer is reached, a new exchange layer is created between the old one and the transport layer. The old exchange layer is now called an underlayer. An active layer thickness of 0.2 m and a maximum exchange layer thickness of 0.1 m have been used.

---

[4]The nourished grains are not uniform fractions. When reference is made to the 250 μm grains, a sediment fraction with $D_{50} = 250$ μm is intended.

Scenario A2: Larger discharge

The A2 scenario evaluates the application of a nourishment twice the volume applied in the base scenario. This is done by keeping the concentration constant (due to the blockage risk) and doubling the discharge to $0.2 \text{ m}^3/\text{s}$. This results in a one-year discharge of $3,000,000 \text{ m}^3$ including pores.

Scenario A3: High velocity nourishment

As the pipe outlet is considered static, steering the distribution is challenging. Another way of directing the nourishment can be the application of an interval nourishment. When a nourishment is only applied at higher current velocities, the expectation is that relatively less sediment will be deposited at the nourishment location. The higher velocities are be able to keep the sediment in suspension, preventing the sediment from being deposited at the bottom. Figure 2.7 shows how the increase in velocity can affect the concentration near the bottom, which has a direct effect on the deposition rate. The velocity threshold for nourishing is set at the 50% highest velocities of both flood and ebb. In order to compare this scenario with the other scenarios, the nourishment discharge is set such, that the annual nourishment volume is kept the same as in the A0 case.

Scenario A4: Displacement of outlet

Scenario A4 evaluates what happens if the outlet is placed slightly more in the channel direction, away from the Helderse Seawall. The larger depth beneath the nourishment location offers a higher accommodation space for the nourishment and provides a longer settling time, which allows the particles to be dispersed better initially. The 1 Mm^3 nourishment of cell I is placed towards cell III.

Scenario A5*: Long-term development

The last scenario evaluates the nourishment development on a larger timescale. Using a morfac of 12, the nourishment development during six years is assessed. As the Sandwindmill system will be built for long-term use, looking further than one year could provide relevant information. This scenario will not be compared to the other scenarios, as the timescale is different. The results are presented in Section D.1.5, however.

6.2.3. Shoreface nourishment

The second type of nourishment that will be assessed is the shoreface nourishment. In Section 4.1, Callantsoog has been selected as a good location for the execution of such a nourishment through the Sandwindmill.

Scenario B0: Base case

For the base case, the nourishment position is located just outside the breaker bar (see Figure 4.5), above approximately 5 metres depth. This location is chosen as many waves break over this bank, leading to significant wave-induced currents (see Figure 5.17). A nourishment with an in-situ discharge of $100,000 \text{ m}^3/\text{year}$ is placed, distributed over two computational cells of 35x200 m each. The nourishment will thus be distributed over 70 m in the cross-shore and 200 m in the alongshore direction. It is assumed that it is technically possible to ensure such a spreading in reality. The bed level increase would be 7 metres if no dispersion occurs. For the B0 simulation, a fraction with a D_{50} of 250 μm is used, which is the same size as the native bed material.
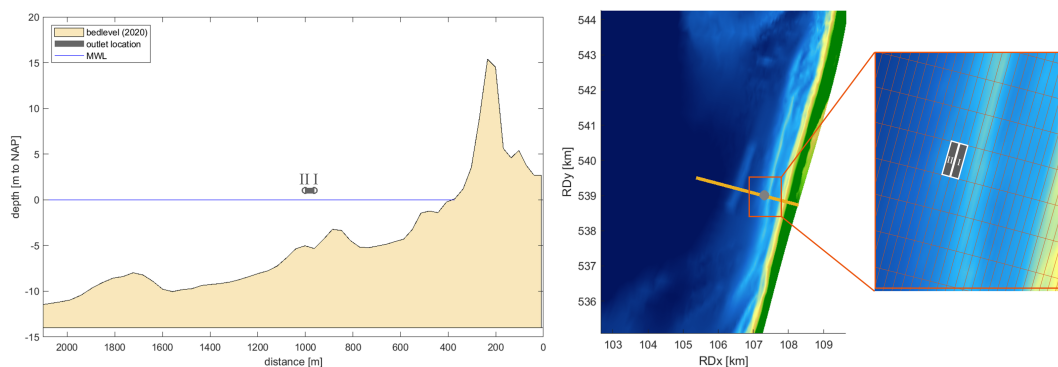
Figure 6.2: Nourishment location of the shoreface nourishment. Both cells I and II have an area of 6,000 m^2. The cross-section of the left panel is indicated by the orange line in the right panel.

Scenario B1: Variable D$_{50}$
In scenario B1, a variation in nourishment grain size is tested for the same reason as in scenario A1. Next to the reference value of D$_{50}$ = 250 μm, the influence of the application of grain sizes with D$_{50}$ = 150 μm is assessed. The 350 μm fraction is not tested, as the application of coarser material than the original material is deemed unviable for the Sandwindmill application.

Scenario B2: Larger discharge
For the B2 scenario, the discharge is doubled, whereas the concentration is kept the same. This results in a yearly in-situ nourishment of 200,000 m^3.

Scenario B3: Wave height dependent
For scenario B3, the nourishment is only applied if the offshore significant wave height is larger than 1.5 metres. As high wind velocities and high waves often coincide, this represents the plausible situation of system downtime in case of low winds. The fact that the system can be operable under higher Eastern winds that do not drive significant waves at the Holland coast, is herein neglected. In the case of the coincidence of high waves and a sediment nourishment (where a high concentration of sediment persists in the water column), the turbulence and velocities induced by the waves would keep the sediment in suspension. This should enhance the initial dispersion of the sediment, leading to a larger nourishment capacity. To compensate for this downtime (65%), the discharge has been increased by a factor 2.7. In that way, the annual volume is equal to the volume of the base case.

Scenario B4: Petten
Figures 5.19 and 5.20 show the alongshore variability in longshore sediment transport at the North Holland coastline. To assess the influence of the alongshore location of the nourishment, one nourishment is placed near Petten. This location shows to have a larger transporting potential than Callantsoog. The nourishment is placed at 5 m depth as well, with the same quantity as in the base case. What makes the comparison difficult is the different bathymetries of the locations. The nourishment falls between two sand bars, with their crest at -4 m (outer bar) and -2.5 m (inner bar).

Scenario B5: Julianadorp
In scenario B5, the nourishment is placed more in the direction of the Marsdiep, near Julianadorp. Assessing a nourishment at Julianadorp provides insight in the nourishment dispersion in an area that is more dominated by the tide. The nourishment is placed at the tidal channel wall at approximately 8 m depth.

Scenario B6: Elongated bar
Scenario B6 evaluates the dispersion of the nourishment if it is shaped like an alongshore bar. The nourishment is extended two cells in the northern direction and two cells in southern direction, leading to a dimension of 70 x 1000 m in cross and alongshore direction, respectively. The same Q and C per cell as in B0 are used, which results in an annual in-situ nourishment volume of 500,000 m^3. As described in Section 2.2, the analysis of 19 shoreface nourishments by Huisman (2019) points out that alongshore elongated nourishments erode relatively less than shorter nourishments. No relation is found for the cross-shore length of a nourishment. It will be evaluated if this relationship can be also observed in the model results.

Scenario B7: Cross-shore location variation
Scenario B7 assesses an offshore movement of the nourishment location. The initial benefit of a more offshore placement is that sediment has more time in the water column before it settles. Hence, there is more time for each sediment particle to be picked up by the currents. However, at the larger depth, wave-induced currents are smaller. Tidal currents thus become more important in the sediment dispersion. Eventually, when the bed level increases at the nourishment location, these waves will become more important. For scenario B7, the nourishment is placed just inside of the nourished bar, at 1600 m in Figure 6.2.

6.3. Results tidal channel

In this section, the results of the base scenario A0 are discussed on a local and regional scale. The mechanisms that are governing for the morphological developments are also discussed. The results for scenarios A1 to A6 are elaborated in a similar fashion in Appendix D.1. A summary of these results is given in this section, as well as a qualitative and quantitative comparison of the different scenarios. The goal is to extract the parameters that can lead to an improved design of the continuous nourishment.

6.3.1. Scenario A0: Base case

First, the behaviour at the nourishment location is evaluated for scenario A0. Secondly, the regional dispersion of the bed level change is assessed.

Local morphological behaviour

Figure 6.3 shows the bed level development over time for the entire cross-section and the nourishment cells (most right figure). The erosive behaviour of the tidal channel between 200 and 600 m can be attributed to the combination of high (residual) flow velocities (see Figure 5.18) and the uniform grain size that has been used. In reality, the grain size distribution in the region is highly non-uniform, with coarser fractions in the deeper channels (see Section 5.5.3). The steeper development of the nourishment at cell I (which is the nourishment cell at the inner side of the bend, at X = 75 m) can be particularly attributed to the higher assigned nourishment discharge. Another factor that plays a role is the 'autonomous' increase in bed level at this section. For the nourishment at X = 150 m, the 'autonomous' decrease in bed level is converted to a bed level increase in the situation with a nourishment. The wiggly behaviour of both lines can be explained by the variability of current velocities during a spring-neap tidal cycle. The erosive behaviour coincides with spring tides, as its higher velocities are better capable of transporting the nourishment.
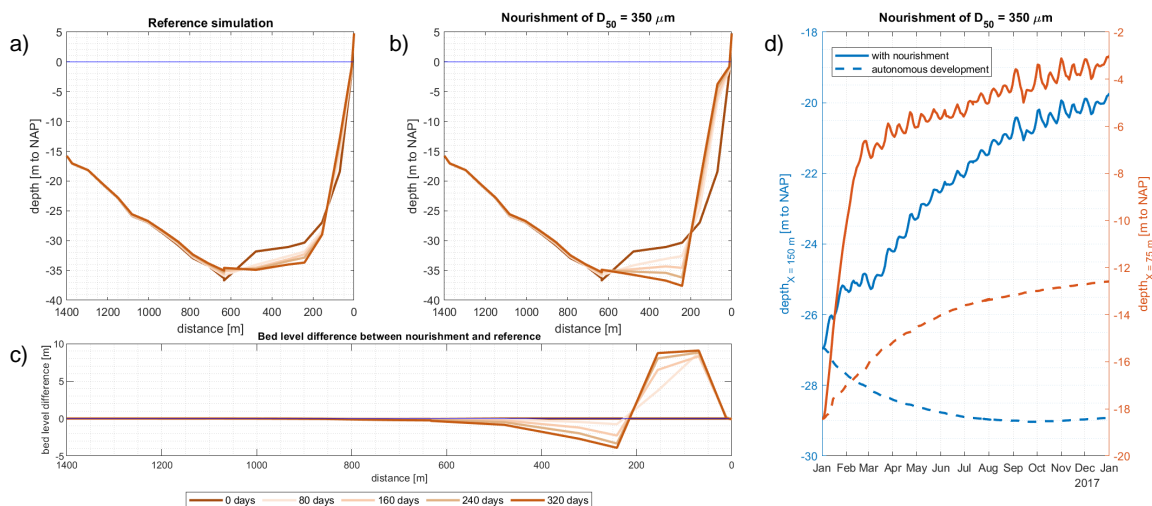
Figure 6.3: Development of the bathymetry during the reference (a) and A0 (b) simulation. Nourishment locations are located at 75 and 150 m, or cell I and cell II in Figure 6.1, respectively. Pane (c) depicts the difference between the reference and A0. The dashed line in (d) indicates the autonomous bed level development. Note the two y-scales for in (d).

Figure 6.3 shows that after some time, the bed level of both the reference simulation and nourishment simulation seem to move towards an equilibrium. Whereas the reach of the equilibrium of the nourishment simulation at the shallower part (X = 75 m) can be partly explained by the autonomous development (orange lines), this does not hold for the development of the equilibrium of the nourishment at X = 150 m (blue lines). The change in bed level development is governed by a changing ratio of the deposition and erosion fluxes. These fluxes are governed by the fall velocity, bed-shear stresses induced by currents, turbulence and the distribution of the sediment concentration over the vertical. As a result of the decreasing depth and constant sediment discharge, the concentration in the water column increases over time. Equation 2.6 denotes the theoretical fall velocity. In reality, the fall velocity is impeded by an increasing concentration. This principle is called hindered settling and may lead to slower sedimentation, as more sediment particles stay in suspen-

sion as the concentration increases. Next to the direct reducing effect on the deposition term, the decrease in fall velocity also leads to a different concentration distribution over the water column. Furthermore, the bed-load transport increases for steeper bed slopes. The steepening of the profile due to the nourishment also increases the transports locally. Lastly, the hydrodynamic forcing directly influences the erosion through the magnitude of the erosion flux (parametrized as the fluid mixing coefficient ϵ_f in Delft3D). Indirectly it affects the sediment distribution in the water column, which is parameterized through the Rouse number.

Regional morphological behaviour

Figure 6.4 depicts the change in hydrodynamic forcing due to the nourishment after 180 days. Apart from a marginal increase in current velocities in the main channel, is a significant increase in flow velocities visible at the nourishment location. Mainly during flood, the local velocities increase from 1.5 to 1.75 m/s (17%) in the direct vicinity of the pipe outlet. One mechanism that can lead to these higher flow velocities is the constriction of the flow. According to Van Rijn et al. (2007), this velocity increase can increase the bed load transport with 80% for 300 μm grains at 10 m depth. The suspended load of grains between 200-400 μm would increase with 100%. Also, a lee effect can be observed, mainly for the ebb current. The maximum ebb velocity along the North Holland tip decreases with approximately 10%. This velocity decrease can result in smaller gross southward transports, leading to a larger net northward sediment transport along the coastal section. The effect of this velocity change on the erosion of the coastal section south of the seawall should be investigated. If the sedimentation of the section resulting from dispersion of the nourishment is large enough, the potential erosion due to the reduction of the ebb velocities could be counterbalanced.
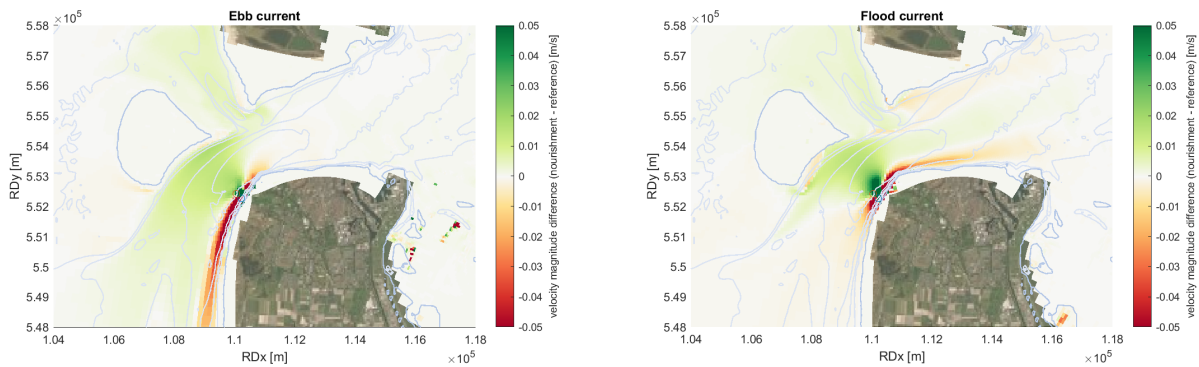
Figure 6.4: Difference in current velocities during flood (left) and ebb (right) between reference and nourishment scenario after 180 days.

When looking at the distribution on a regional scale (see Figure 6.5), it can be seen that in the first weeks, the main accretion occurs at the nourishment location itself. After a time, the nourishment starts to spread. This is presumably due to the mechanisms described above. After one year, the nourishment has spread reasonably well. A bed level increase of 2 m relative to the reference simulation is observed within a distance of 1.5 km. Sedimentation along the seawall is observed, which is one of the desired effects. Seaward of the nourishment an erosion pit is observed. The increased flow velocities can be the driving mechanism of this relative erosion. The regional behaviour will be more extensively assessed in the comparison with the other scenarios.
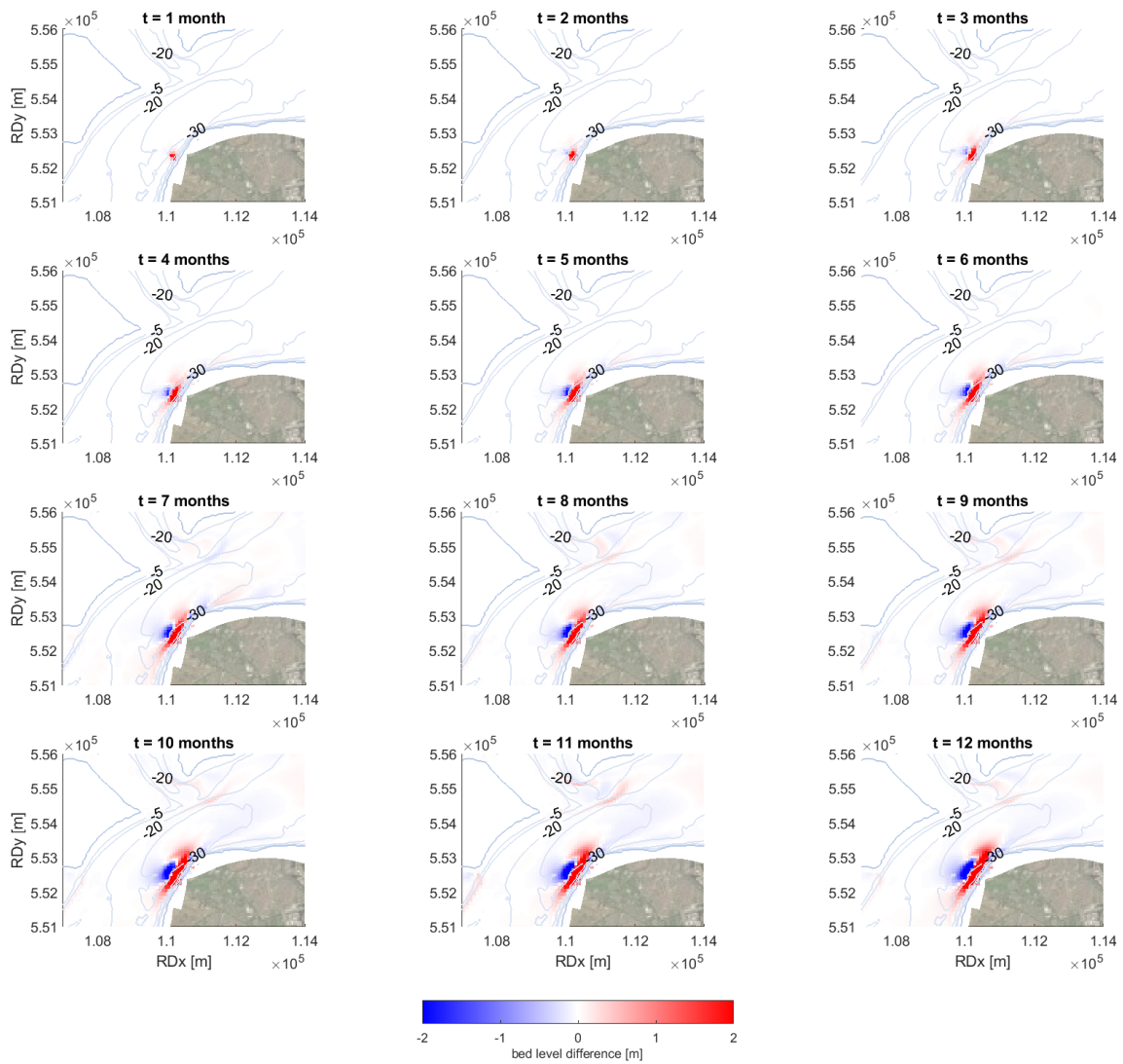
Figure 6.5: Development of bed level change relative to the reference simulation (A0 - reference) over the simulated period.

6.3.2. Results of A-scenarios

In this section, some of the findings of the different scenarios are discussed. A more extensive analysis of each separate scenario can be found in Appendix D.1. First, the behaviour at the nourishment location is evaluated, as a limited accretion is one of the nourishments' goals. Next, the distribution of the bed level change after one year is qualitatively assessed. Finally, three quantitative analyses are discussed that are can express the score on the chosen KPIs.

Local behaviour

First, the short-term local behaviour of some of the different nourishment strategies is discussed. This allows to understand better the longer-term morphological developments, which are discussed afterwards.

Figure 6.6 shows the initial response of the bed to the nourishment with different fractions. The nourishments start after twelve hours. The centre figure shows the amount of nourished sediment in the nourishment cell II. The figures left and right of the centre figure show the amount of nourished sediment in the adjacent NE and SW cells. The current velocity through the Marsdiep is added to the figure to show the response of the bed level to the velocities. From this figure, some conclusions can be drawn. First of all, it is visible that the bed level change for the coarser fractions is larger than for the finer fractions. As visible in Figure 6.3, this effect diminishes on the longer term: extrapolating the increase of sediment would lead to a yearly bed level increase of 18 m (assuming a porosity of 40%), whereas the modelled increase at this location is approximately 10 m. Secondly, it can be observed that the largest sedimentation occurs around slack water, where the horizontal tidal velocities are zero. The duration of this sedimentation period differs significantly between the different fractions. The coarser fractions are less sensitive to the lower velocities, leading to a longer period during which the bed level increases. During the higher tidal velocities, the bed level slightly decreases for all fractions, this time with a longer duration for the finer fractions. The figure also shows the difference between flood and ebb currents. It should be noted that the used velocities are the velocities through the Marsdiep. The maximum velocities at the nourishment location are approximately 1.8 m/s and 1.25 m/s for flood and ebb, respectively. The higher flood velocities are better capable of eroding the sediment than the ebb velocities.
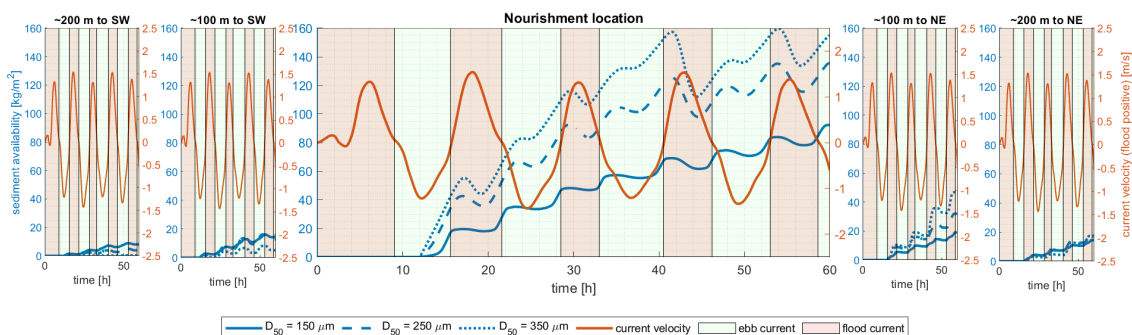
Figure 6.6: Initial response of the availability of nourished sediment of three different fractions in the transport layer. The development over time is given for the nourishment location and two adjacent cells in both flood and ebb direction (southwest for ebb and northeast for flood).

The growing availability of sediment during flood (shaded in red) 100 m northeast of the nourishment location shows that the sediment that is eroded at the nourishment is transported in the direction of the currents. The larger erosion of coarser fractions at the nourishment location can be recognized with the larger accretion of these fractions in this adjacent north-eastern region. Further northeastward, equal sedimentation of the different fractions can be observed, which can be attributed to the limited transportability of the coarser and heavier fractions. These initial developments suggest the anticipated larger spreading of the finer fractions. For the southwestern region the accretion during ebb (highlighted in green) is well-visible. The smaller magnitude of the ebb velocities show that the southward transport is more limited for all fractions, but again mostly for the coarser fractions.

In most scenarios, the relative bed level change at the nourishment location seems to go towards an equilibrium. The mechanisms that explain this behaviour are, amongst others, hindered settling, the transverse transports of sediment due to the steepening of the profile and the increase of local flow velocities due to a contraction of the flow. The assessment of the difference in grain sizes on a smaller timescale (Figure 6.6) shows that a clear distinction can be made in the response to the hydraulic forcing. Whereas the initial response shows a clear difference with the A0 case, the long term difference does not show big differences (see Figure 6.7). Although the bed grows at a different rate initially, the equilibrium depth appears to be approximately the same for the different grain sizes and for the nourishment timing case.

Under a doubling of the discharge in both cells, the described equilibrium effects appear to be not strong enough, leading to the piling up of sediment above MSL in cell I. The displacement of the outlet from cell I to cell III (scenario A4) leads to a smaller accretion in cell II. This suggests that under the base case, a part of the nourishment in cell I is transported in transverse direction towards the deeper part of the channel. The assessment of the six-year development shows that after 16 months, the bed level at cell I will approximate mean sea level. Applying one million m^3 of sediment annually on a 9,600 m^2 area (cell I) appears to be too much for the inlet system to distribute on a longer timescale. Applying a smaller volume, displacing the outlet or spreading out the nourishment over a larger area seems to be required to guarantee a longer-term applicability of the Sandwindmill system.
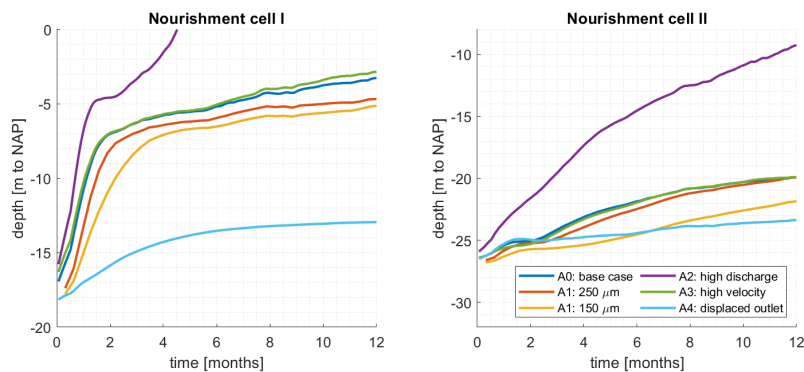
Figure 6.7: Development of the bed level at the two nourishment locations in the Marsdiep. Cell numbering is depicted in Figure 6.1. For improving the comparison, the development has been smoothed by taking the moving average over 30 days. This results in the missing of some of the presented data in the first weeks.

Qualitative regional comparison

Regionally, most of the bed level changes occur in the adjacent areas of the nourishment. For all scenarios, the bed level in alongshore direction of the nourishment shows a relative growth and in transverse direction some erosion due to the changing flow velocities. The six-year simulation (presented in Appendix D.1.5 shows that the pattern of the development is the same as the observed pattern after one year. It should be assessed whether the further deepening of the channel adjacent to the nourishment location posed a threat for the seawall stability.
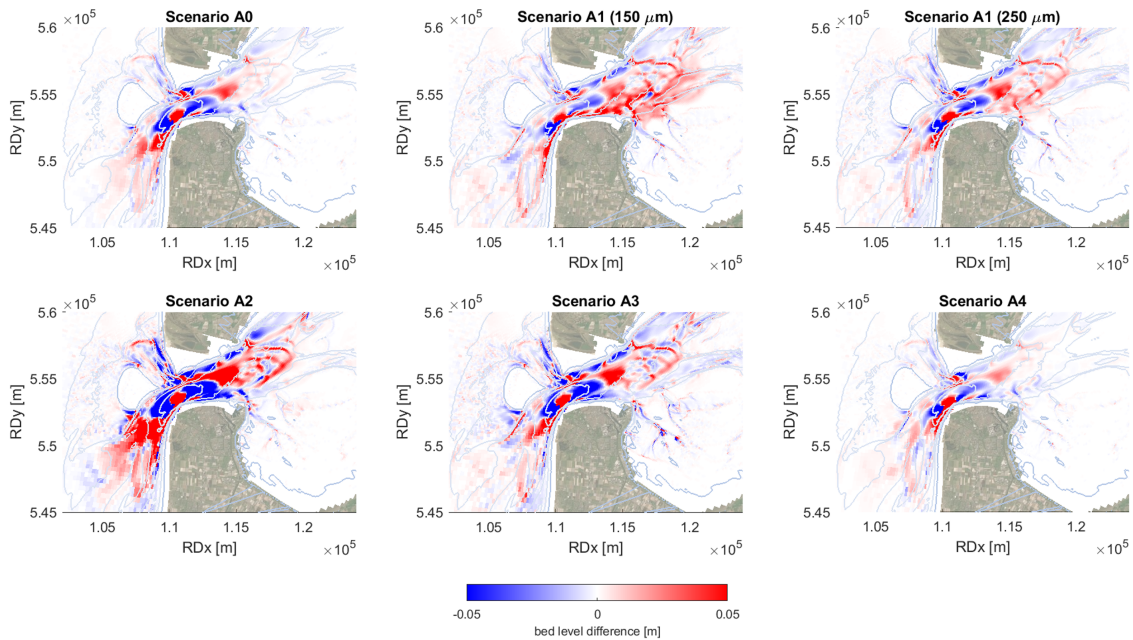
Figure 6.8: Bathymetric changes relative to reference simulation for scenarios A0 to A4. A0: Base case; A1: Variable D_{50}; A2: Larger discharge; A3: High velocity; A4: Displaced outlet.

From Figure 6.8, it becomes apparent that the bed level changes in the region away from the nourishment location are somewhat larger for smaller grain sizes, a larger discharge and the high-velocity nourishment. This is in line with the expected behaviour that is described in section 6.2.2. The displaced nourishment (A4) seems to lead to a smaller spreading of the sediment. More sediment is deposited in the deeper part of the channel, where it remains. The smaller velocities that prevail in this deeper section might not be able to pick up the sediment from the channel bottom. Lastly, it can be seen that the smaller grain sizes induce a larger bed level change at the coastal section south of the nourishment. The smaller ebb velocities are more capable of transporting the finer fractions, leading to a better distribution of these particles.

Next to looking solely at the bed level change, the application of the underlayering method allows to track the nourished sediment particles. Figures 6.9a to 6.9c show this dispersion for the three different grain fractions. From these figures, a significant difference can be observed in the dispersion of the nourished sediment. The maximum distance between two points that contain 32 kg/m^2 are 6.7, 10 and 12.3 kilometres for D_{50} = 350, 250 and 150 μm.

(a) Nourishment sediment fraction of $D_{50} = 350\ \mu m$.

(b) Nourishment sediment fraction of $D_{50} = 250\ \mu m$.

(c) Nourishment sediment fraction of $D_{50} = 150\ \mu m$.
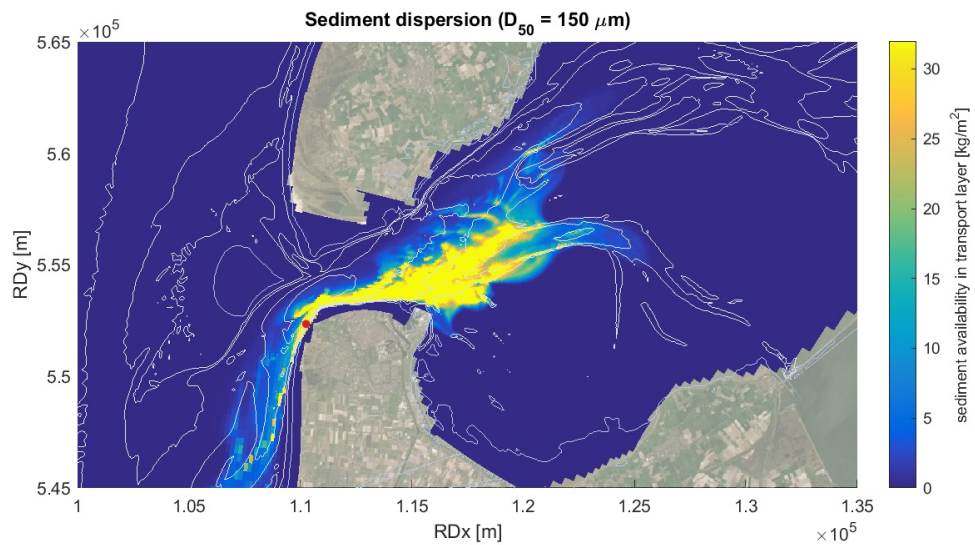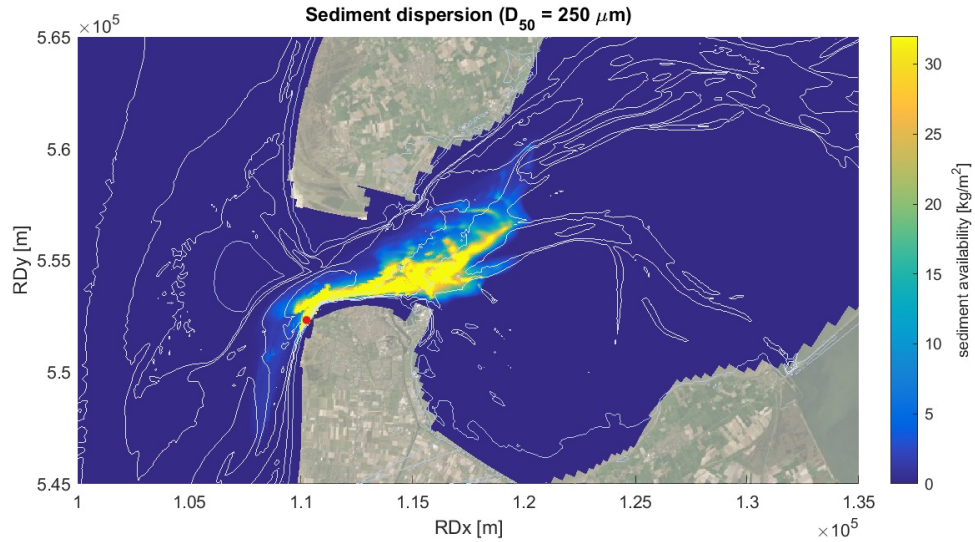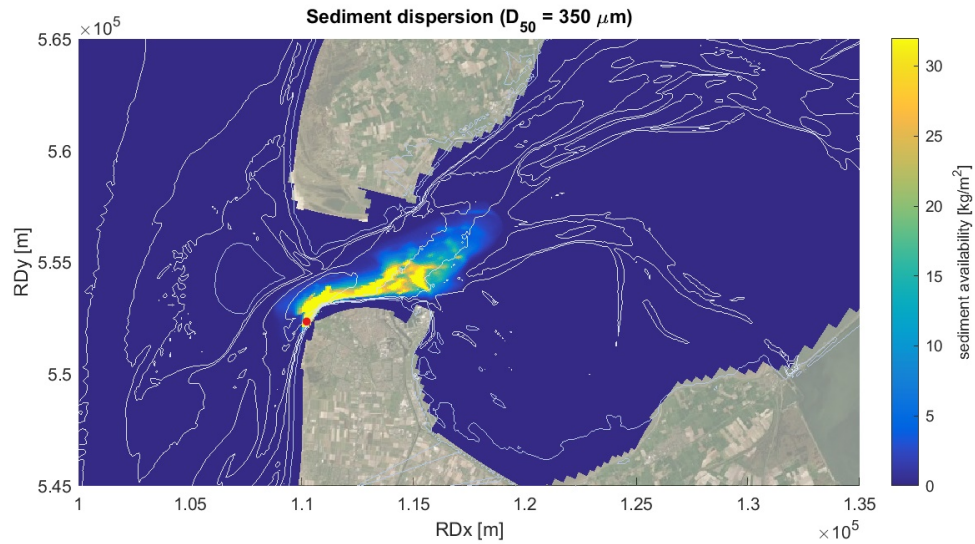
Figure 6.9: Dispersion of the nourished sediment after a one-year continuous nourishment of 0.045 m^3/s, or 1,500,000 m^3 annually. 32 kg/m^2 corresponds with a sediment thickness of 2 centimetres. The system is mass-conserving: in all figures, an equal amount of sediment is added. Depth contours indicate depth between 0 and -30 m NAP with steps of 10 m, and the -5 m contour additionally. The red dot indicates the nourishment location.

Quantitative regional comparison

Figure 6.10 shows the difference in volume per section (P1-P4) compared to the reference simulation. The total volume change of all four sections corresponds well with the nourishment volume of these scenarios, implicating that the nourishment is contained almost entirely within these four sections (see Table 6.3).

What stands out for area P1 is that the smaller grain sizes lead to a smaller volume change than the larger grain sizes, which is not expected based on the qualitative analysis. For the 150 μm fraction, the difference in volume is not that large. The volume for this fraction in P1 was expected to be higher due to the large tail at the North Holland coastline visible in Figure 6.9c. For the 250 μm nourishment, most of the sediment is transported towards sections P3 and P4: in flood direction. Howerver, the 250 μm fraction is more easily transported to the south by the lower ebb currents than the 350 μm fraction. One explanation for this behaviour is the resuspensioning of the sediment. When the 350 μm fractions are deposited initially during ebb (south of the nourishment location), flood currents might not be well capable of resuspending the particles and transporting them northward. For the 250 μm fractions, the flood velocities might be sufficient to resuspend the material and transport it northward. The initial southward transport in Figure 6.6 does show that the smaller fractions are transported southward more easily, which would substantiate this hypothesis of resuspensioning material. The southward ebb velocities might be high enough to also resuspend the 150 μm grains, explaining the higher southward transport.

Finally, it becomes apparent that the finer fractions are able to reach the P4 area, where lower velocities prevail. The volume decrease in this section for the other scenarios could be explained by the lower flood velocities reaching this area (Figure 6.4) and the blocking of sediment by the nourishment hump.
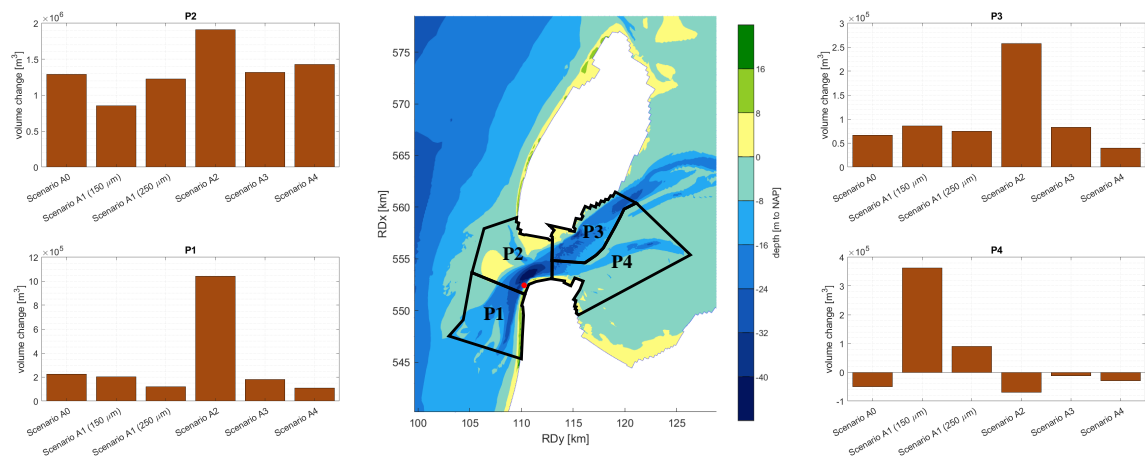
Figure 6.10: Volume change near the Marsdiep relative to reference development under the different scenarios. Areas P3 and P4 are indicate the import by the Marsdiep and are divided based on the basin geometry. Section P1 indicates the southward transports and P2 comprises the residual area. A0: Base case; A1: Variable D$_{50}$; A2: Larger discharge; A3: High velocity; A4: Displaced outlet.

| | **Average bed level change [mm]** | | | | **Volume change [·10^4 m^3]** | | | | |
	P1	P2	P3	P4	P1	P2	P3	P4	Σ
Scenario A0	4.7	31.6	2.6	-0.9	23	130	6.6	-5.0	153
Scenario A1 (150 μm)	4.2	20.9	3.3	6.2	20	85	8.6	36	150
Scenario A1 (250 μm)	2.5	30.1	2.9	1.5	12	120	7.5	9.0	151
Scenario A2	21.6	46.8	9.9	-1.2	100	190	26	-7.0	314
Scenario A3	3.7	32.2	3.2	-0.2	18	130	8.3	-1.2	157
Scenario A4	2.3	35.0	1.5	-0.5	11	140	4.0	-3.0	155

Table 6.3: The average bed level change for each region in millimetres, calculated by dividing the volume change by the section area. The volume changes are given in the right-hand side of the table.

Quantitative comparison near Helderse Seawall

Next to feeding the Wadden Sea, one of the nourishment goals is providing sediment at the wall and toe of the Helderse Seawall. Therefore, the volume change in the area is calculated. The nourishment and adjacent cells have been excluded, as this might distort the view on the dispersion along the wall (see the red-shaded area in Figure 6.11). The volume change in the selected region after one year is presented in Table 6.4. The quantitative difference for the different grain sizes are minor (+ 10%). The displacement of the outlet leads to a larger increase of the volume (+ 30%), as much of the deposited sediment remains where it is placed. Lastly does the doubling of the discharge lead to a doubling of the volume increase at the area.
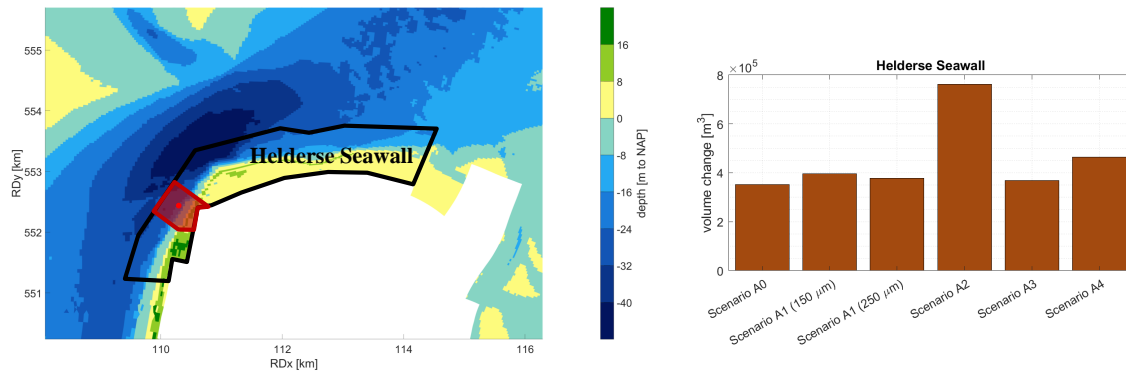
Figure 6.11: The area at which the volume change around the Helderse Seawall is calculated is marked in the map. The red area is excluded from the analysis, as this area is too close to the nourishment location. The distance from the deep part to 0 m NAP is approximately 500 m along the entire stretch. Red dot indicates the nourishment outlet position.

	Average bed level change [mm]	Volume change [$\cdot 10^5 \mathrm{m}^3$]
Scenario A0	46	3.52
Scenario A1 (150 μm)	52	3.96
Scenario A1 (250 μm)	49	3.78
Scenario A2	99	7.62
Scenario A3	48	3.68
Scenario A4	61	4.65

Table 6.4: The average bed level change for each region in millimetres, calculated by dividing the volume change by the section area. The volume changes are given in the right-hand side of the table.

Distribution of sediment thickness

The final goal that is set, relates to the spreading of the nourished sediment. To that end, the accretion and erosion has been classified into small (0.01 - 0.05 m), medium (0.05 - 1.0) and large (>1 m) bed level changes (see Figure 6.12). The larger the contribution of small and medium sedimentation to the total sedimentation, the better.

Figure 6.12 shows that the use of coarser grains leads to relatively more 'large' erosion and accretion (> 1 m). The sedimentation classes for the finer grains are more evenly distributed. The high sedimentation (> 1 m) induces hydrodynamic accelerations, leading to more erosion. The finer fractions are thus not only distributed over a larger distance, they also induce less erosion. For some locations, e.g. the feet of the seawall, this erosion might be undesired. Lastly, the smaller grain sizes seem to stick better to the Helderse Seawall, inducing 'medium' sedimentation along the entire wall. The doubling of the sediment discharge leads to a large increase in the erosion. From Figure 6.10, it can be observed that much of this sediment is transported towards polygon P3. The timing of the nourishment (A3) shows to lead to a slightly wider regional spreading, as well as a differently distributed sedimentation/erosion pattern compared to A0. Lastly, the deeper-placed nourishment (A4) shows to have the most concentrated sedimentation, as was also observed from Figure 6.8.
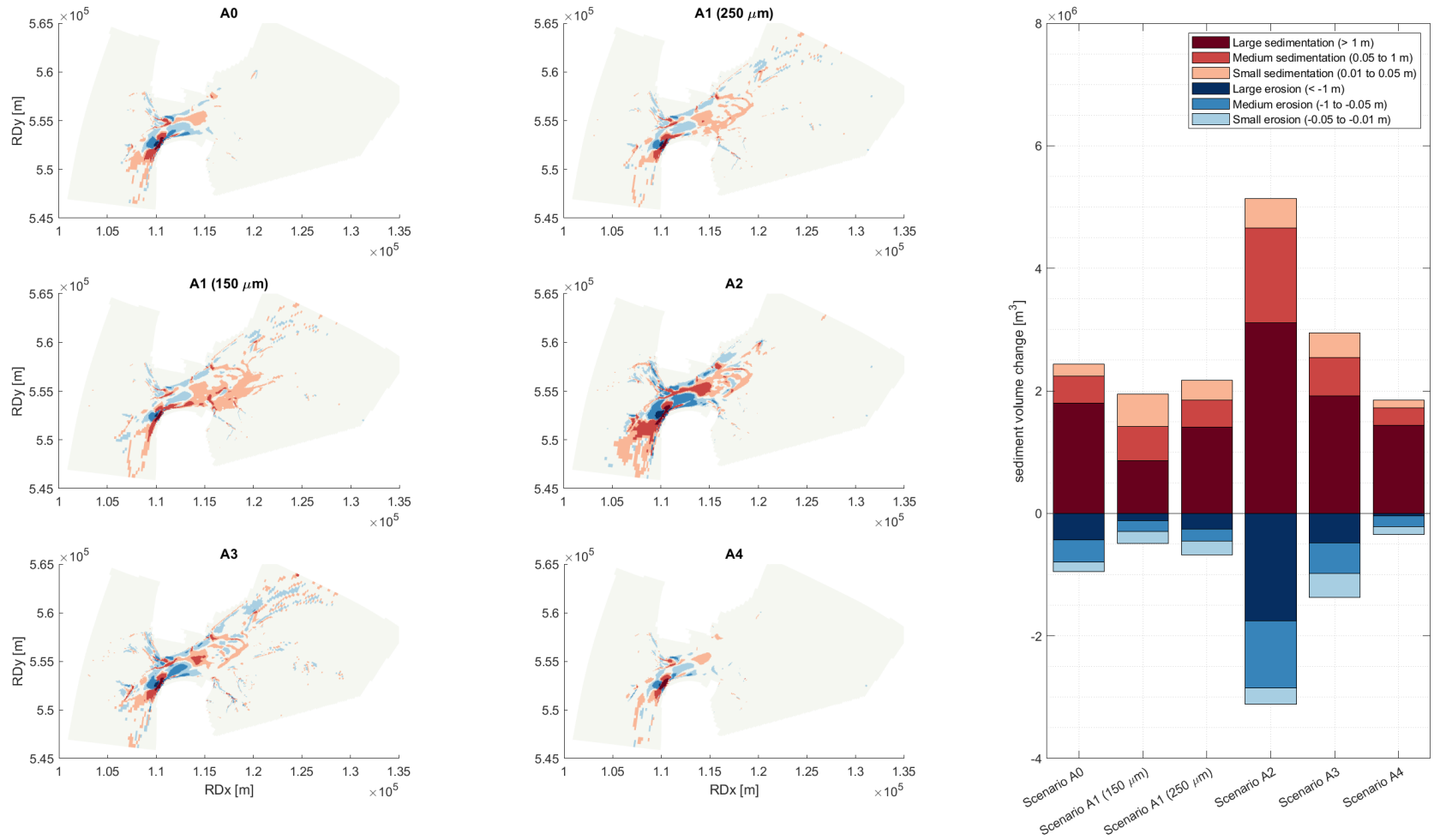
Figure 6.12: Regional comparison of the Marsdiep scenarios, categorised in three bed level change classes. A0: Base case; A1: Variable D_{50}; A2: Larger discharge; A3: High velocity; A4: Displaced outlet.

6.4. Results shoreface

In this section, the results for the shoreface nourishment are assessed. First, the results of the B0 scenario are analysed. Subsequently, the differences between the different scenarios are treated. A more extensive analysis of each scenario can be found in Appendix D.2.

6.4.1. Scenario B0: Base case

In this section, the results of the base scenario B0 are discussed: a nourishment of 100,000 m^3 with a grain size of 250 mu. Except for Figure 6.13a, which shows the absolute bed level development, the morphological developments relative to a simulation without a nourishment are used. This is done to account for model errors in predicting the autonomous morphodynamic development.

Local behaviour

(a) Unfiltered bed level change   (b) Filtered bed level change
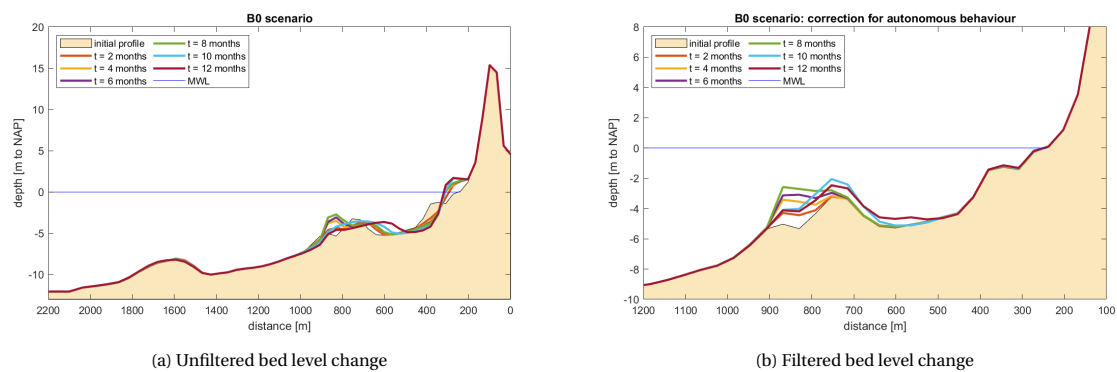
Figure 6.13: The development of the cross-shore profile over a morphological year. The implication of the model set up on the cross-shore behaviour, which is discussed in Section 5.2, leads to a visible flattening of the foreshore and steepening of the beach. This effect has been filtered out in Figure 6.13b, where the autonomous morphological behaviour is subtracted from the behaviour with a nourishment.

From Figure 6.13 it can be observed that the bed level increases in the first months at the nourishment location (X = 800). Over these first months, the rate accretion reduces. One explanation is the increase of depth-induced wave breaking as the bottom level increases. This implicates that the first-year growth of the nourishment is not representative for the longer term, as the erosion rates could grow due to the increase of wave breaking. Furthermore, the seasonality becomes apparent. A diminishing of the hump during the winter months (months 10 and 12) is visible. Figure 6.13 implicates that a nourishment of 100,000 m^3/year distributed over 12,000 m^2 can be distributed by nature in the cross-shore direction. However, as the cross-shore processes are not resolved accurately, these conclusions should be considered carefully.

Regional behaviour

The bed level directly around the nourishment location increases. This can be attributed to the increase in sediment availability. At the nearshore tips of this region of accretion, some decrease in bed level change can be seen. This decrease can be attributed to the changing hydrodynamic conditions around the nourishment location. The change in wave breaking location can induce erosion if the supply of sediment is not enough to compensate for this altered wave breaking. The small erosion at the NAP = 0 m line northward of the nourishment could be the result of a lee-side effect. Van Rijn & Walstra (2004) describe the blocking of a net alongshore transport by breaker bars, leading to the deposition of the alongshore transported sediment shoreward of these bars. The subsequent reduction in sediment availability downdrift of the bar leads to local shoreline erosion. With a northward going residual tidal velocity and transports at Callantsoog, the occurrence of this phenomenon is probable. It is expected that this lee-side effect becomes more apparent if the nourishment is stretched in alongshore direction, as is tested in scenario B6.
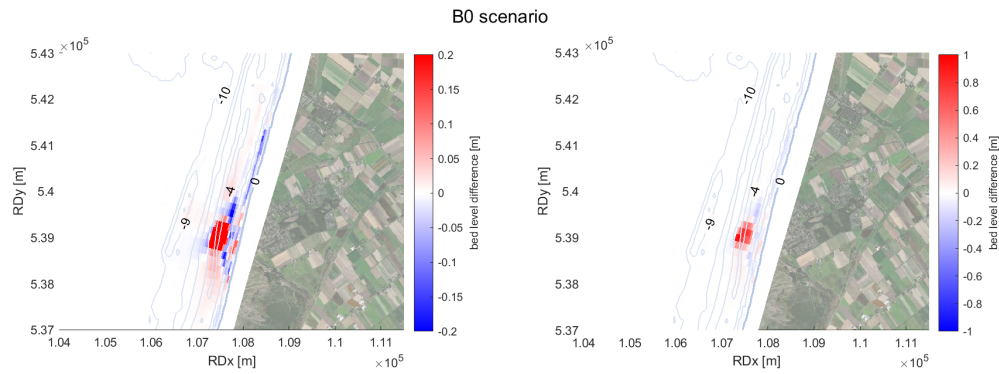
Figure 6.14: The regional development of the bed level around the nourishment location after one year, for two different color scales.

Another effect described by Van Rijn & Walstra (2004) is the feeder effect, where the onshore directed transports due to wave asymmetry transport the nourishment in onshore direction. Return currents directly landward of the nourishment can transport the sediment in alongshore direction. In Figure 6.15 this onshore movement of the nourishment in time can be observed. Between the nourishment and the beach, a small relative erosion is visible. This relative erosion can be the effect of these return currents. The figure furthermore shows the large influence of waves. Most of the smudges - in both alongshore and cross-shore direction - of the bed level coincide with high waves.
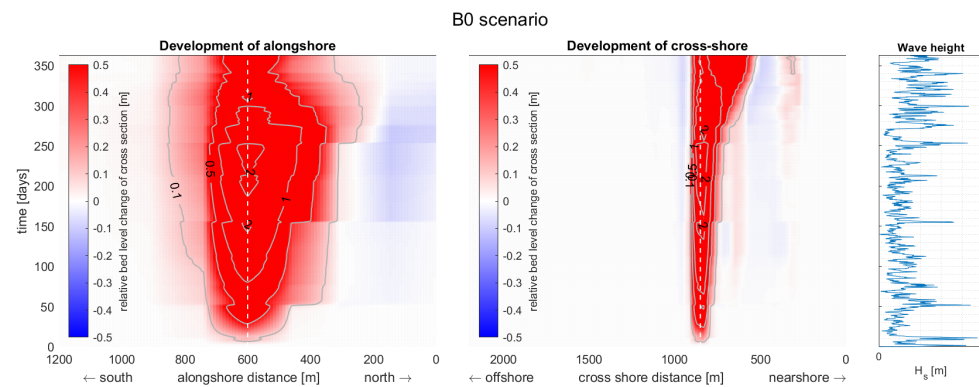
Figure 6.15: The development in time of the bed level at cross-sections through the nourishment location in alongshore direction and cross-shore direction. The cross-shore profile corresponds to the profile shown in Figure 6.13. The alongshore section extends 600 m north and 600 m south of the nourishment centre of gravity (white dotted line). The 10 cm accretion contour extends 270 m in N direction and 220 m in S direction of the nourishment centre of gravity.

The migration of shoreface nourishments in the Netherlands has been studied extensively in the past. The alongshore movement of 250 μm nourishments in the order of 200-400 metres per year for the North Holland coast is observed by multiple researches (Van Rijn & Walstra, 2004; Spanhoff et al., 2003). Hoekstra et al. (1997) traced the development of a nourishment at Terschelling which is placed between two bars at a depth of -4 to -7 metres, which is in correspondence with the nourishment placement in most of the B-scenarios. A migration rate of 300-400 m/year is observed by Hoekstra et al. (1997). These distances are in correspondence with the alongshore migration of the modelled point source nourishments. Spanhoff et al. (2003) observe a distinctive northward transport at Callantsoog. Whereas no clear reason is mentioned, the shown sensitivity to waves suggests that SW waves were more dominant in this period than in 2017. As explained in 5.3, the 2017 wave-induced transports are expected to have a less distinctive direction, which would explain the somewhat more symmetrical development of the 0.1 m depth contour in Figure 6.15. The slight skewness to the north can be explained by the fact that many of the strong NW waves in 2017 occurred in the first weeks of the year, when the nourishment volume was still limited. Visual comparison of the wave roses of both periods confirms this difference in wave climate.

Huisman (2019) observed that shoreface nourishments mostly react to severe wave conditions ($H_{m0} > 3$ m).

This is in line with the modelled response of the nourishment to wave heights. Huisman (2019) furthermore states that shoreface nourishments propagate mainly towards the coast in the first years after construction, which is in line with the model results. Limitations in the representation of cross-shore processes can partly explain the modelled onshore behaviour, however.

6.4.2. Results of B-scenarios

In this section, the most notable results of the executed scenarios are discussed. A more extensive analysis of each scenario is presented in Appendix D.2.

Local behaviour

The bed level increase at the nourishment location is determining in the volume of the nourishment that can be applied, and is therefore one of the selected criteria. If the erosion of the bed is not sufficient, the piling up of sediment would require a lower discharge or the displacement of the pipe outlet. This induces a higher cost per m^3 and is thus undesired.
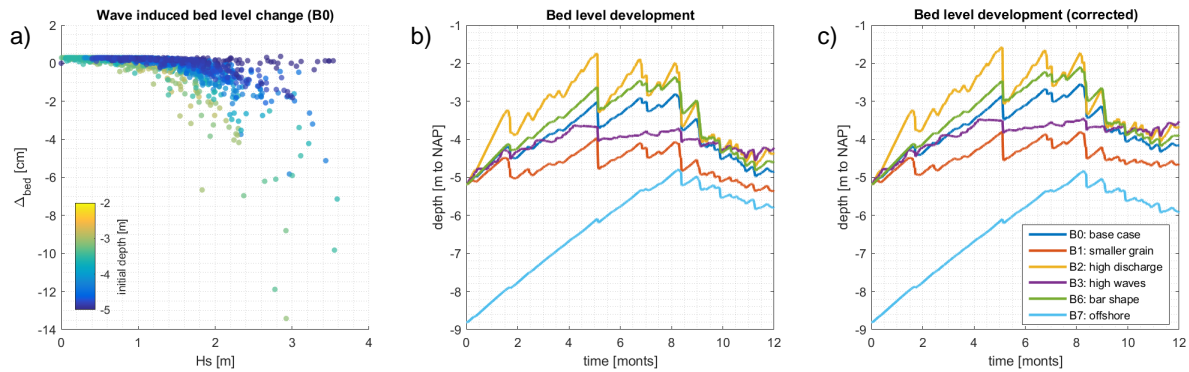
Figure 6.16: In figure a the bed level change per 4 hours under a certain wave forcing is given. Wave heights are model results at 11 m depth at Callantsoog. The bed level increase during mild conditions O(0.1 cm) is due to the nourishment placement. Figure b depicts the absolute bed level development (as in Figure 6.13a). Figure c depicts the bed level development corrected for the autonomous behaviour (as in Figure 6.13b).

From Figure 6.16a it can be observed that the bed level hardly decreases for waves lower than 0.75 m. The most significant erosion occurs at the higher waves. The color scale shows that for a given wave height, the highest erosion occurs if the bed is higher. This is the result of increased energy dissipation on the shallower bed. This effect can be observed in Figures 6.16b and 6.16c. The highest bed levels erode the most in case of storms. The seasonality is also visible. In the winter months, the long-term bed level is stable, whereas the same sediment discharge is applied as in the calmer months.

The effect described above results in a relatively limited bed level increase for the double discharge scenario; the doubling in the discharge (200,000 versus 100,000 m^3) leads to a 50% difference in bed level change after one year (+1,51 versus +1,01 m). The bed level at the centre of the bar (B6) accretes 25% more than in the reference (B0). This is explained by the fact that the largest transport gradients occur at the alongshore edges of the bar. The grain size of 150 μm shows to be more sensitive to waves, resulting in an almost zero bed level change after one year. Applying the nourishment only in the case of high waves results in a lower bed level during the summer months. During the winter months, the area is loaded with more sediment. This results in a bed level increase and eventually a higher bed level than with a continuous nourishment. Lastly, the more offshore placed nourishment grows during the first 8 months, as waves do not break at the prevailing height yet. From month 8 onward, waves break on the profile and erosion occurs.

The main findings of this local analysis are that energetic periods and the induction of depth-induced breaking push the bed in the direction of an equilibrium. This results in a 50% increase of the bed level with a 100% increase in nourishment volume. Whether this relation is linear and holds for a further increase in nourishment volume should be examined. This would imply that a 500,000 m^3 nourishment would result in a 5.06 m bed increase, which is still below MSL. During the summer months, however, the bed level would exceed MSL. Looking at this equilibrium at a multi-year timescale would give insight into the length of the period in which the pipe outlet would not have to be removed. Figure 6.17 illustrates this effect. Lastly, the smaller grain size induces only a 0.5 m bed level increase, which is half of the increase of the basic scenario.
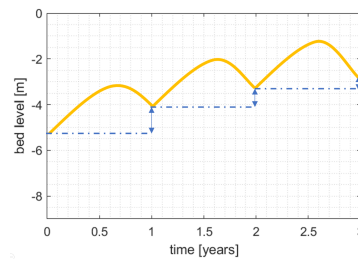
Figure 6.17: Illustration of the long-term equilibrium effect. If the first months of each year contain energetic periods, the steepness of the increase would also decrease in time.

Qualitative regional comparison

Figure 6.18 shows the regional morphological development after one year. In scenarios B0 to B3, the nourishment takes place at the same location. Scenarios B4 to B7 show the application of the nourishment at another location.

The nourishment with a smaller grain size (B1) leads to a significantly higher spreading of bed level changes than in the B0 scenario. The doubling of nourishment volume does not have a large effect on the spatial distribution of bed level change. The magnitude of the changes does alter compared to B0. Lastly, the timing of the nourishment based on the prevailing wave conditions changes little in the distribution of the sediment (both magnitude and space). At Petten, the bed level change takes place mainly in the northward direction. The orientation of the coastline leads to a higher obliqueness of SW waves and a smaller obliqueness of NW waves. This could explain the difference in sediment distribution. Van Rijn (1993) stipulates that in this region, small coastline changes ($O(5°)$) can induce large changes in wave-induced alongshore transport ($O(50\%)$). The nourishment at Julianadorp in scenario B5 shows similarities with the nourishments evaluated in the A-scenarios: accretion in the direction of the currents and locally erosion perpendicular to the tidal currents. Furthermore, the asymmetry of the tide is visible through a northward-dominant dispersion.

In the B6 scenario, 500,000 m^3 has been nourished at an area of 70 by 1,000 metres. The lee-side effect is more pronounced than in the B0 case, as the length of the bar induces a larger shadow zone. Inspection of the distribution of the grains shows that this deposited sediment is not originating from the nourishment. The deficit of sediment updrift (northward) leads to coastal erosion. Lastly, the offshore placed nourishment induces little regional morphological change.
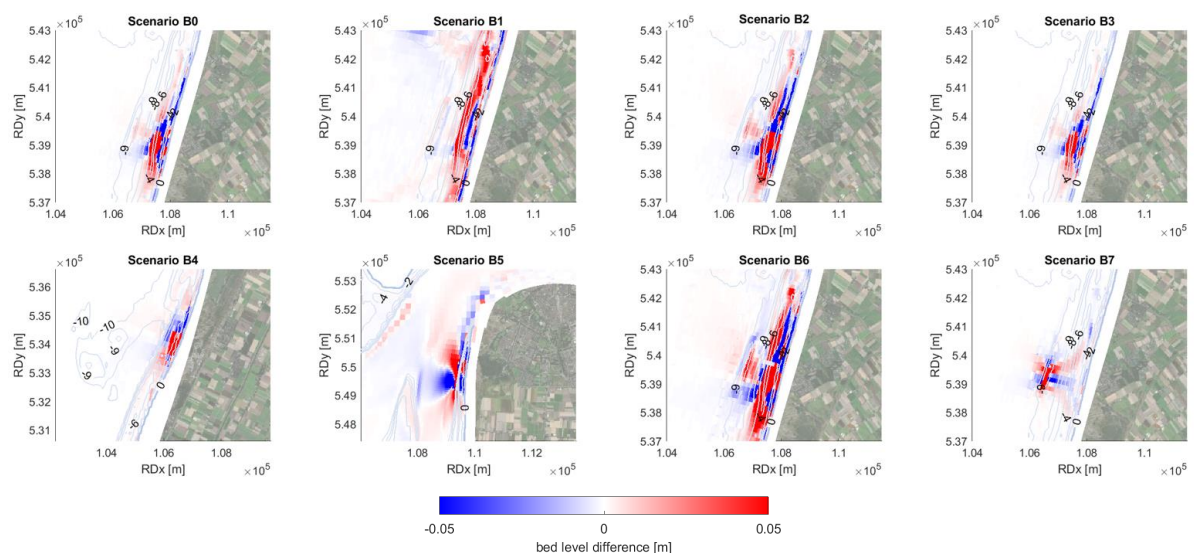
Figure 6.18: Regional morphological development after one year for all scenarios. Note that scenario B4 and B5 are not located at Callantsoog. B0: Base case; B1: Variable D$_{50}$; B2: Larger discharge; B3: High waves; B4: Petten; B5: Julianadorp; B6: Elongated bar; B7: Larger depth.

Figure 6.19 shows where the nourished sediment is deposited after one year, whereas Figure 6.18 shows the bed level differences after one year. From Figure 6.19, it can be read that a part of the nearshore transported sediment is originating from the nourished material, for both the grain sizes. Furthermore, it can be observed that the transports are mainly in northward direction. As explained in Section 6.4.1, the predicted symmetrical gross transports of 2017 are mainly due to the NW storms in January. As the nourishment only started in January, little nourished sediment was available in this period for dispersion. The sediment that had been transported south, could have been transported north again in the later months.

For the 250 μm fraction, the dispersion of the 2 cm layer is approximately 2.5 kilometres. For the same grains, a dispersion of approximately 10 kilometres is observed for the Marsdiep case in Figure 6.9b. This indicates that the reach of the nourishment of the Marsdiep is four times the reach of the nourishment at Callantsoog, for this grain size. For the 150 μm fraction, the Marsdiep maximum distance between two 2 cm points is approximately 3 times the Callantsoog value (15 km against 5.8 km). It must be noted that the distance travelled by the nourished sediment does have direct implications on the distance travelled by the accretion.

The results show 2 cm of the nourished material has travelled approximately 2.5 km after one year. From figure 4.2 it follows that the coastal stretch between Callantsoog and Julianadorp needs approximately 60,000 m^3/year/km. With a 100,000 m^3/year discharge, placing the outlets 1.6 km from each other would provide this volume. The results show that the nourishment is capable of travelling a larger distance. When the annual discharge would be 200,000 m^3/year, the outlets could be placed 3 km apart from each other. As most of the sediment stays in the vicinity of the outlet, placing the outlets further apart would leave gaps along the coast, which could form a weak link in the coastal protection.

(a) Scenario B0 (b) Scenario B1
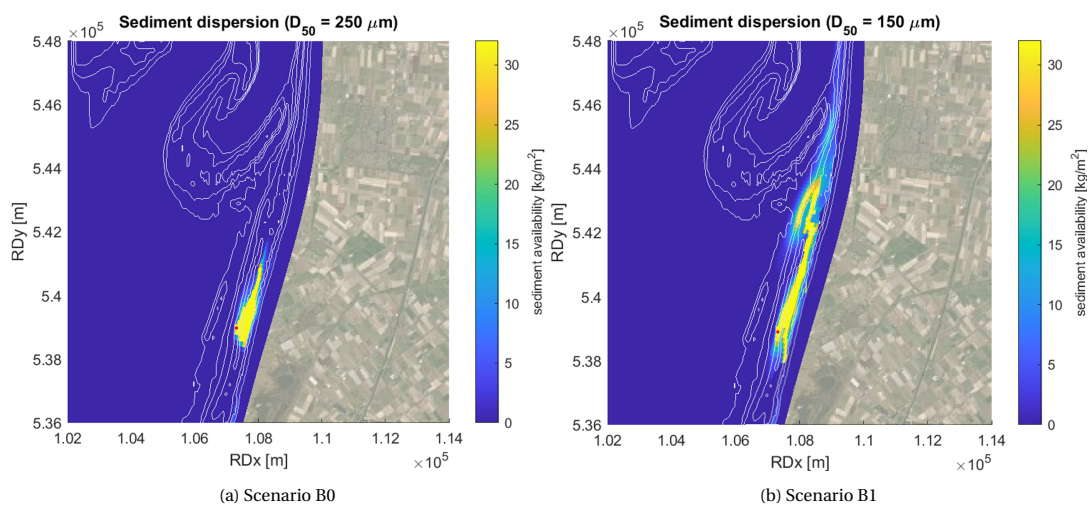
Figure 6.19: Dispersion of the nourished sediment after a one-year continuous nourishment of 100,000 m^3 annually. 32 kg/m^2 corresponds with a sediment thickness of 2 centimetres. The system is mass-conserving: in both figures, an equal amount of sediment is added. Depth contours indicate depth between 0 and -10 m NAP with steps of 2 m, and the -9 m contour additionally. The red dot indicates the nourishment location.

Quantitative regional comparison

In Figure 6.20 and Table 6.5, the results of the quantitative analysis are presented. To ensure the comparability of the results, only the scenarios in which the nourishment has taken place at the same location have been adopted.

The main findings of this comparison are that the northward transports increase significantly for the larger nourishment volume, whereas the transports in the southward direction are less affected by this volume increase. The nearshore transport in case of a finer grain nourishment is almost a factor 10 smaller than the nearshore transport of the 250 μm grains. This could be attributed to the limited lee-side effect, as the sediment hump is constantly smaller compared to B0. Lastly, the accelerating currents and the breaking waves erode the bed seaward of the nourishment. In the presence of a better representation of undertow, this erosion could have been smaller. The offshore erosion is smaller for the finer grains as the bed level at the nourishment develops slower, leading to less depth-induced breaking and a more limited increase of current velocities.
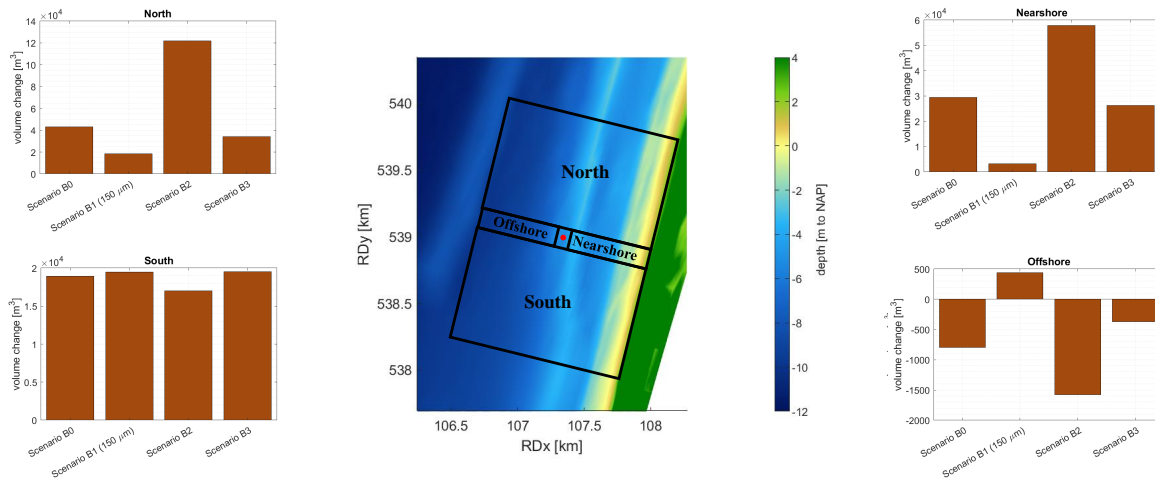
Figure 6.20: Volume change near Callantsoog relative to reference development under the different scenarios. The B4-B7 scenarios have been left out of the analysis as a different placement makes the comparison for the chosen sections impracticable. B0: Base case; B1: Variable D_{50}; B2: Larger discharge; B3: High waves.

	Average bed level change [mm]					Volume change [$\cdot 10^3$ m^3]					
	Nearshore	Offshore	North	South	Centre	Nearshore	Offshore	North	South	Centre	Σ
Scenario B0	199	-5.4	20	8.7	1,012	29.4	-0.797	43.0	18.9	12.1	103.5
Scenario B1	21.8	3.0	8.7	8.9	510.6	3.22	0.442	18.3	19.5	6.12	47.6
Scenario B2	392	-11	58	7.8	1,477	57.9	-1.58	122	17.0	17.7	213
Scenario B3	178	-2.5	16	8.9	1,573	26.3	-0.373	34.1	19.5	18.9	98.4

Table 6.5: Numerical results of the quantitative analysis depicted in Figure 6.20. It should be noted that expanding the north and south sections in alongshore direction leads to a correct volume balance for the B1 scenario. When the distance is doubled, the volume in section north increases with 60% and south with 48%. Scenarios B4-B7 are omitted as these nourishments do not take place at the indicated location.

Distribution of sediment thickness

A categorised regional analysis for the Callantsoog results is presented in Figure 6.21. Alike the Marsdiep case, a finer fraction leads to less concentrated accretion. Surprisingly, the erosion is somewhat larger for the B1 scenario compared to the B0 scenario. As the difference is limited, no physical explanation is sought. The timed nourishment leads to a higher share of the 'large' category, as during the last energetic months of the simulation, much sediment was deposited. The deeply placed nourishment (B7) shows large concentrated accretion, as most of the sediment is placed too deep to be dispersed by the breaking waves.

The nourishment at Petten shows a similar distribution of the accretion classes. At Julianadorp, the nourishment is more concentrated and leads to a more erosion in the region. The increase in local flow velocities cause this behaviour, similar to the behaviour of the nourishments at the Marsdiep.
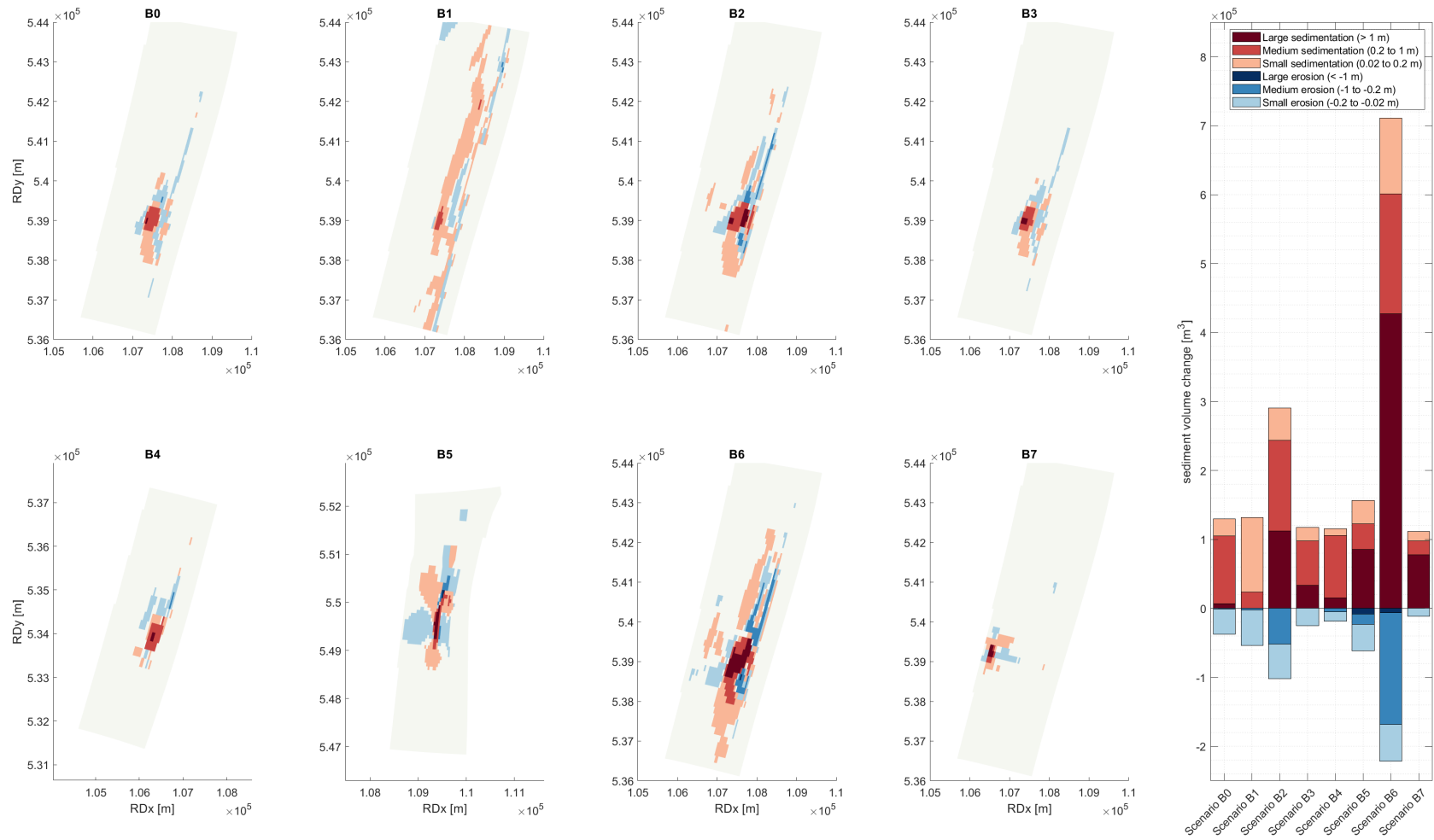
Figure 6.21: Regional comparison of the Callantsoog scenarios, categorised in three classes. The B4 and B5 scenarios have been left out, as they are applied at a different part of the coast. B0: Base case; B1: Variable D_{50}; B2: Larger discharge; B3: High waves; B4: Petten; B5: Julianadorp; B6: Elongated bar; B7: Larger depth.

6.5. Conclusions

In this section, the performance of each scenario is scored using the selected KPIs. Finally, additional general conclusions are drawn based on the results of this chapter.

6.5.1. KPI scores

In Section 6.1, KPIs are selected that can measure the success of the nourishment according to the goals set in this thesis. Whether the nourishment feeds the Wadden Sea can be determined based on the volume change of the P3 and P4 polygons of Figure 6.10. For A0, the score is thus $(6.6 - 5.0) \cdot 10^4 = 1.4 \cdot 10^4$ m^3. The higher the volume, the better the nourishment performs. Whether the nourishment contributes to the stability of the Helderse Seawall can be determined based on the volume change depicted in Table 6.4. The local erosion is measured based on the development of the bed level at the nourishment locations (Figure 6.7). The lower the bed level increase one year, the better the nourishment performs. The bed-level increase of A0 for cell I is -2.99 - -18.41 = 15.42 m. Lastly, the measure of dispersion can be derived from the proportion of small and medium sedimentation to the total sedimentation of Figure 6.12. For A0 the total sedimentation is 2.4 Mm^3, of which 0.44 + 0.19 = 0.63 Mm^3 sedimentation between 0.01 and 1 m. The assigned score is thus 0.63/2.4 = 26%.

From Table 6.6 it can be read that using smaller grains contributes to all of the chosen nourishment goals. Under a doubling of the discharge, a more significant fraction of the added sediment ends up in the Wadden Sea. As explained in Section 6.3.2, a large part of this accretion can be attributed to sediment losses near the nourishment. It is unknown whether this sediment displacement from the channel towards the Wadden Sea leads to undesired effects. Executing the nourishment only during higher flow velocities positively affects the imports to the Marsdiep. On the other KPIs, the difference with A0 is less significant. Lastly, the displacement of the outlet does not positively affect most of the KPIs.

	Goal	KPI	Source	A0	A1 (150 μm)	A1 (250 μm)	A2	A3	A4
Tidal channel	Wadden Sea	Volume change in polygon [$\cdot 10^4$ m^3]	Fig. 6.10	1.60	44.6	16.5	19.0	7.10	1.00
	Helderse Seawall	Volume change in polygon [$\cdot 10^4$ m^3]	Fig. 6.11	35.0	39.6	37.8	76.2	36.8	46.5
	Local accretion cell I	Bed level at nourishment cell I [m]	Fig. 6.7	15.4	13.4	13.9	119*	15.8	5.47*
	Local accretion cell II	Bed level at nourishment cell II [m]	Fig. 6.7	7.22	5.20	7.14	18.0	7.16	3.77
	Regional dispersion	Share of small and medium accretion [%]	Fig. 6.12	26.5	56.1	35.6	33.8	35.2	22.6

Table 6.6: Scores of nourishment scenarios A0 to A4 on the KPIs selected in Section 6.1. The bed level at cell I for A2 is not coloured as this would change the colour scales too much. The local bed level change at A4 is not coloured either, as the A4 nourishment does not take place at cell I (but in cells II and III). A0: Base case; A1: Variable D$_{50}$; A2: Larger discharge; A3: High velocity; A4: Displaced outlet.

For Callantsoog, the local erosion and regional dispersion are measured in the same manner as for the Marsdiep, based on the result presented in Figures 6.16 and 6.21. As every bit of sediment that is placed adds to the coastal foundation per definition, this criterion is not measured. The alongshore distribution is measured based on the dispersion of the 10 cm depth contour, as in Figure 6.15. The score for the A0 scenario is thus 270 + 220 = 490 m.

As in the case of the tidal channel nourishment, a smaller grain size leads to a better score on all KPIs. The doubling of the discharge leads to less than a doubling of the local bed level, but the dispersion and along-shore spreading are not affected positively compared to B0. The timing of the nourishment (B3) leads to a more concentrated accretion after one year. As explained in Section 6.4.2, the seasonality explains this behaviour. The deeper placement of the nourishment (B7) worsens the score on all KPIs, except for the along-shore distribution. This is not entirely in line with the limited dispersion observed in Figures 6.18 and 6.21. This shows a limitation of the applied approach; the alongshore distribution on one line with the nourishment can differ from the alongshore spreading along a line closer to the coast. Furthermore, the results show that the deeper-placed sediment behaves like the shallower placed sediment after some time. Whereas the score of B7 on the chosen KPIs is rather poor, does the increase in accommodation space by the larger depth provide more room for the nourished sediment. This requires a less frequent outlet displacement. Comparing the B7 results to the other scenarios might therefore be not appropriate.

	Goal	KPI	Source	B0	B1	B2	B3	B4	B5	B6	B7
Shoreface	Local accretion cell I	Bed level at nourishment cell I [m]	Fig. 6.16c	1.14	0.54	1.62	1.77	-	-	1.51	3.38
	Local accretion cell II	Bed level at nourishment cell II [m]	Fig. 6.16c	0.91	0.48	1.93	1.53	-	-	1.10	4.02
	Regional dispersion	Share of small and medium accretion [%]	Fig. 6.21	95.2	100	61.6	72.4	86.6	54.9	40.5	30.9
	Alongshore distribution	Spreading of 10 cm bed contour [m]	Fig. 6.15	490	960	490	520	750	440	1340	550

Table 6.7: For the local erosion, the bed level change has been corrected for the autonomous bed level change. Alongshore distribution can be found in Figures D.20, D.23, D.26, D.29, D.32, D.35, D.38. B0: Base case; B1: Variable D_{50}; B2: Larger discharge; B3: High waves; B4: Petten; B5: Julianadorp; B6: Elongated bar; B7: Larger depth.

6.5.2. Summarizing remarks

Overall, the Marsdiep has a large capacity of locally eroding the nourished material. In cell II of the Marsdiep, where 500,000 m^3 of 250 μm material is nourished over 6,400 m^2 (78 m^3/m^2), the accretion is just 10% of the added material. At Callantsoog, this ratio is approximately 15%. As both the Marsdiep and Callantsoog models are not performing very well on autonomous morphodynamics, these results should be used carefully. For both locations, a change in grain size positively affects all KPIs. Therefore, looking at the grain size in the search for borrow-locations is recommended, regardless of the area of application. Under the considered conditions, the timing of the nourishment has no distinctive effect on the KPIs, except for the import by the Wadden Sea. The bed level development in time does show that timing at Callantsoog can prevent a hump from forming during the calmer months (Figure 6.16). A change in the outlet location significantly influences the dispersion, mainly for the Marsdiep, where a high spatial variability in flows exists. Lastly, increasing the discharge does not lead to a 1-on-1 increase in bed level for both locations. Furthermore, this discharge increase mostly leads to an increase of the erosion and sedimentation magnitudes compared to the base cases, rather than in a different erosion/sedimentation pattern.

Part IV

Conclusions

<div style="text-align: right; font-size: 3em; font-weight: bold;">7</div>

<div style="text-align: right; font-size: 2em;">Discussion</div>

In this chapter, the research approach and results are discussed. Section 7.1 discusses how the applied nourishment volumes fit in with the transporting capacity of the natural system. In Section 7.2, the degree of choice for the mining of a certain grain size is discussed. Section 7.3 discusses the approach of Chapter 3. The modelling of the nourishment development with Delft3D comes with simplifications and assumptions regarding relevant physical processes. These shortcomings are treated in Section 7.4. Section 7.5 discusses the influence of morphological adaptations on the dynamics of a tidal inlet. The chapter is concluded by Section 7.6, which treats the expectation on the longer-term development of the nourished region.

7.1. Natural system demand and interaction

The analysis of the entire Sandwindmill system in Chapter 3 showed that a large nourishment volume is required for the system to be economically competitive to traditional methods. This conclusion set the main goal for the subsequent chapters: developing a strategy that allows for a large dispersion of the nourished sediment. Subsequently, regions were identified that have a large sediment demand. The primary reason for this demand is the large transport capacity, governed by high flow velocities and the susceptibility to oblique wave attack. Gradients in the large transports induce erosion in these regions. The growing sediment demand due to the rising sea level and – for the Marsdiep – the closure of the Zuiderzee are another motivation for adding sediment to the system.

Within these regions, a small area has been selected with a large transporting capacity that can allow for the local erosion of the added sediment. For the Marsdiep, this is the location where the highest tidal velocities occur. For Callantsoog, a location has been chosen where storm waves break. The applied nourishment volumes have been selected based on the geometry of the location. Whether the applied nourishment volumes fit in with the capacity of the natural system has barely been taken into account.

7.1.1. Marsdiep

For the Marsdiep, the 1.5 Mm^3 nourishment is applied at approximately 16,000 m^2, leading to a bed level increase of 90 metres if the sediment would fall down vertically and no erosion would take place. With a depth of 30 metres, this would mean an exceedance of MSL by 60 metres. Due to the large falling height, which allows time for the initial dispersion, a volume three times the accommodation space has been chosen. When looking at the capacity of the natural system, this 1.5 Mm^3 seems a significant value. Net sediment transports through the entire Marsdiep inlet are expected to be a factor 1.5-4.0 higher. On the other hand, most of these net transports pass through a very small area, which is where the nourishment is applied. In that sense, the 1.5 Mm^3/year is more in line with the system capacity. Another way of determining the transport capacity of the system, is by looking at the response to nourishments in the past. Little measurement data is available for the Marsdiep. Elias et al. (2013) analyse a 1.0 Mm^3 nourishment in the deepest part of the Nieuwe Schulpengat. 77% of the added sediment is eroded after three years. As the nourishment in this thesis takes place at the channel wall rather than in the deepest part of the channel, a wall nourishment executed at Ameland (the Borndiep channel) also provides valuable insights. There, a 2.5 Mm^3 nourishment has been applied between -10 and -22 m NAP. 75% of this sediment has eroded from the nourishment location after two years (Van On-

selen & Vermaas, 2020). The estimated net transports through the Ameland inlet are expected to be smaller in magnitude than the transports through the Marsdiep (Elias & Vermaas, 2018). With larger net transports at the Marsdiep, a 1.5 Mm^3/year nourishment might be fairly in accordance with the local system capacity. It should be noted that the averaged transports over an inlet do not directly say something about the local transports that are assessed here, due to the very high spatial variability that is observed in each inlet. This variability is also observed for the Ameland inlet by McLaren et al. (1998), which even consists of two different channels. Local flow velocities could be a better indicator of the similarity of the capacity of the Marsdiep and the Borndiep. Peak ebb and flood velocities at the Bordiep are approximately 1 m/s, whereas velocities of 1.8 m/s are measured at the Marsdiep (Elias et al., 2019; Buijsman & Ridderinkhof, 2007). The strong non-linear response of sediment transport to flow velocities suggests a much higher transporting capacity for the Marsdiep, supporting the choice of a 1.5 Mm^3/year nourishment. Naturally, the area over which the sediment is placed also determines the system's capacity of processing the nourishment.

Nourishment goal

The primary goal of the Borndiep nourishment was adding sediment to the coastal foundation (seaward side of the channel). The offshore movement of the sediment thus proves that the nourishment is successful. Secondly, the effect of the nourishment on the position of the channel was addressed. For the Marsdiep case, the stability of the wall would benefit the stability of the Helderse Seawall. It is concluded by Van Onselen & Vermaas (2020) that a shift in channel-wall position would require a very intensive nourishment scheme, suggesting the use of hard materials (stones) or a hybrid solution. The Sandwindmill provides a soft solution with an intensive nourishment scheme, an option that is (understandably) not considered an option by Van Onselen & Vermaas (2020).

The other goal of the nourishment in this research is the increase of sediment volume in the Marsdiep basin, which is not part of the coastal foundation and therefore differs from the goal of the Borndiep nourishment. It is believed that the current sediment import by the Western Wadden Sea leads to erosion of the adjacent coastline (Mulder & Tonnon, 2011). According to Wang et al. (2018), this import is governed by a balance of (1) sediment supply, (2) transport capacity and (3) sediment demand by the Wadden Sea. Wang et al. (2018) hypothesise that currently, the import is limited by the transporting capacity. This suggests that the addition of sediment will not lead to larger import rates, but would contribute to the preservation of the outer delta and the coastal region (Van Oeveren et al., 2020). The modelled scenarios show that, mainly for finer fractions, the import by the Wadden Sea does increase with the addition of sediment. How much sediment the Wadden Sea would need to make (3) the limiting part of the system should be researched. When this is achieved, reduced coastal erosion in the future is expected (Mulder & Tonnon, 2011). If the nourishment goal would be to feed the coastal foundation, the nourishment should be placed more northward, as the importing transports are less dominant. Based on residual transport patterns, it is expected that the sediment will be transported into the (Nieuwe) Schulpengat channels, rather than being transported towards the shoreface of the coastline. This is also shown by Elias et al. (2013), who modelled the dispersion of sediment when placed at different positions in the area.

7.1.2. Callantsoog

For the base case of the Callantsoog nourishment, 100,000 m^3 has been applied over 14,000 m^2 at 5 m depth. The bed level would thus exceed MSL by approximately 2 metres if no erosion or initial dispersion would occur. Due to the smaller depth, the initial dispersion due to diffusion and advection is expected to be significantly smaller than at the Marsdiep. Furthermore, the estimated transport rates per metre at the Marsdiep are a few orders higher than at Callantsoog (Van de Rest, 2004). For that reason, a potential exceedance of MSL of only 50% the depth is chosen, over 200% for the Marsdiep. As for the Marsdiep, a 100,000 m^3 annual nourishment is rather large compared to the net averaged transports over the surf zone, estimated at approximately 300,000 m^3/year. Also, when assessing the historical nourishment data, presented in Figure 4.2, it can be seen that the average over the past 30 years in this region lies at 10,000 m^3/(year · 100 m). The nourishment is applied at a rate of 50,000 m^3/(year · 100 m). It should thus be questioned whether the coastal system is capable of handling these amounts of sediment in the longer term.

Nourishment goal

The goal of the Callantsoog nourishment is to supply the coastal foundation with sediment and directly protect the coastline from retreating. The continuous nourishment thus has a similar goal as a regular shoreface

nourishment. It is observed in the model results that the continuous nourishment shows similar behaviour as regular shoreface nourishments in terms of alongshore migration and the occurrence of the lee-side effect. As long as the sediment ends up in the surf zone, it contributes to long-term coastal safety.

7.2. Choice for grain sizes

The use of different grain sizes for the nourishment has been researched without an actual assessment of the degree of choice in nourishment grain size. On a large scale, Eisma (1968) found a significant difference in grain composition in the Dutch lower shoreface. At the 20 m depth contour in front of North Holland, a gradient between two grain classes exists, which would allow for some choice. Cheng et al. (2020) researched variability in sediment characteristics at a smaller spatial scale. At a sand wave field offshore of Texel, they found a significant difference of 25% in the median grain size between the trough and crest of these waves. With a sand wavelength of approximately 250 metres, this would also provide the freedom of selecting a certain sediment fraction. Both the tidal channel nourishments and the shoreface nourishments have shown to become more responsive to forcings after an initial bed level increase. This initial filling can be effectuated with the coarser fractions, whereas the more dispersive finer fractions can be added on top of this coarser layer. More research on such spatial grain size variability would provide more confidence in the freedom of choice for a certain nourishment grain size.

7.3. Integral system approach

In Chapter 3, all four subsystems (winning, energy, transport and nourishment) have been treated separately. It is shown how complex the designing of the entire system can be, even under the simplified applied approach. This section discusses some of the simplifications of the applied approach.

Parameter values such as costs, efficiencies and safety margins have been set based on gross estimates. The efficiency is considered constant, whereas it depends on many characteristics of the flow, the mixture and the pumping systems used (Matoušek, 2004). Furthermore, it is assumed that the pumps can be only switched on to their maximum capacity. Depreciation and the lifetime of the different parts have not been taken into account. The mining systems are costly, and it is shown that this system is determining in the design of the other subsystems. A more elaborate analysis of these options is therefore crucial. Also, other implications of design set-ups, such as maximum pressures in the transport pipelines and the occurrence of cavitation, have not been taken into account. Creating a more elaborate and complete causal relation diagram, including uncertainties, can contribute to designing an efficient system. In this research, a framework has been established that allows for further, detailed elaboration.

Another assumption relates to the displacement of the outlet. The static character of the nourishment outlet is one of the main boundary conditions in the research. The establishment of a movable outlet is considered impractical and expensive. The relatively high price for lower volumes could make a dynamic outlet a viable option. A spray pontoon system that can manoeuvre like the autonomous raft would allow for a relatively easy sediment distribution. Such a system should therefore be taken into account when assessing the feasibility of the entire system. As for the supra-marine mining equipment, such a spray pontoon would be weakly resistant to high and breaking waves. The application of such a pontoon in the surf zone might therefore be not optimal. Being non-operational during harsh conditions might be costly due to the missing on a prevailing energy surplus. Placing the sediment more offshore during these conditions might be a solution, as less wave breaking and a smaller shoaling of waves occurs at a larger depth. Another solution would be operating landward of a nourished bar, as the bar will provide shelter from the higher waves.

7.4. Model shortcomings

The assessment of the nourishment distribution with Delft3D has given useful information. The model has been set up in such a way that the essential processes are incorporated. In Section 7.4.1, the limitations in the model set-up are discussed. Subsequently, Section 7.4.2 treats some parameter settings that could have been improved. In Section 7.4.3 the drawback of the used vertical schematisation of the concentration profile is discussed. Section 7.4.4 treats the application of the model on different timescales. Section 7.4.5 concludes with a discussion of the model validity.

7.4.1. Model set up

This section treats the limitations of the simplifications and assumptions that have enabled the set-up of the numerical model in the available time.

Cell size

During the model set-up, some choices have been made that influence the model result. As explained in Section 5.2, D-Flow FM follows the Courant number criterion, in which the applied time step is dependent on the cell size to ensure model stability. The smaller the cell size, the smaller the applied time step. The grid size in the areas of interest has been set at a value large enough for reasonable computational times and small enough to represent the most important coastal processes (see e.g. Van der Hout et al. (2009); Luijendijk et al. (2019)). The choice of the cell size has some implications.

The first implication of the cell size is related to the initial dispersion. As the nourishment is assigned to a grid cell, Delft3D represents the nourishment as being evenly distributed over the entire cell. The sediment will be deposited at a much smaller area if one pipe outlet is used in the real/physical case. Spray pontoons might be needed to prevent such flows from happening and ensure an initial spreading of the sediment as it is modelled. Such a pontoon would be needed mainly at the shoreface nourishments, where the sediment has a limited falling height. Another option would be the frequent displacement of the outlet. A smaller cell size would allow to evaluate the dispersion in the case of a limited initial distribution. Secondly, the use of too large grid cells in the surf zone leads to unrealistic behaviour of the coastal profile, as is observed in the applied model and in Van der Hout et al. (2009).

Sea groynes

Based on research by Rakhorst (1984), it is assumed that the exclusion of the sea groynes between Petten and Den Helder has a limited effect on the modelled sediment transports. The research states that the limited effect is mainly due to offshore directed transports. These transports move sediment seaward of the groynes, where the alongshore currents can transport the sediment away. The offshore directed transports due to undertow are poorly represented as a result of the depth-averaging (Grunnet et al., 2004). This underestimation of offshore transports would make the modelled effect of the groynes stronger than it would be in reality, substantiating the choice of omitting them.

Neumann boundaries

Two of the lateral boundaries of the model have been transformed from water level towards Neumann boundaries. Both of these Neumann boundaries have been deducted using two offshore boundary points and were applied uniformly at the lateral boundaries. The resulting water level representation at Petten has worsened compared to the water level boundaries. The RMSE has increased from 6 cm towards 12 cm for the applied 2017 forcings. On the other hand, the alongshore tidal currents and boundary instabilities have significantly improved. The implication of the less accurate water level representation on the model results of Callantsoog is assumed to be minor, as waves are the primary driver of sediment transports in this region. However, the deduction of spatially-varying Neumann boundaries with the use of the DCSMv6-ZuNov4 or the newer DCSM-FM model of Zijl & Groenenboom (2019) would result in a more accurate representation of the water levels (Deltares, 2021a).

Waves at the Marsdiep

The choice of not including waves in the Marsdiep model has been substantiated with model results of the model by Elias (2006) and of the model used in this thesis. It has been explained that the role of waves is the stirring up of sediment in the outer delta and the alteration of current velocities. The latter could influence the dispersion of the nourished sediment, although this effect is expected to be limited. The degree of effect

that these waves have is not examined any further. As southwestern waves, the primary waves reaching the nourishment location, would enhance flood currents and weaken ebb currents, a higher net northward transport could be expected. The extent to which both current directions are altered could play a role in the piling up of sediment at the discharge point. Based on both transport theory and the Callantsoog model results, it can be expected that the nourished grain size is an essential factor in the sensitivity to the presence of waves in the Marsdiep.

Transport formulation
The choice of the used transport formulation can significantly alter the model results. In this thesis, the TRANSPOR1993 formulations by Van Rijn (1993) have been used as they were also used by the WadSea FM model from Laan (2019). Van der Hout et al. (2009) show that the use of the newer TRANSPOR2004 formulations can have a significant effect on the calculated alongshore transports, as was discussed in Section 5.5.3. One of the differences between the two transport models is that TRANSPOR2004 uses a sub-grid model that can better represent the concentration profile near the bed. Furthermore, the more recent TRANSPOR2004 model includes a bed roughness predictor, which calculates a spatial and temporal varying roughness that can also improve model performance on bar dynamics (Walstra et al., 2004). The use of multiple transport formulations could have added robustness to the model results.

Wave model
The set-up of the wave model also requires some discussion. Long (infragravity) waves are not included in the model, while they can play a significant role in the cross-shore transport of sediment (Van der Steen, 2015). Together with the poor representation of the undertow, this makes the cross-shore distribution of the nourished sediment more uncertain. Regarding the breaking of short waves, the absence of a roller model could lead to too large gradients in the wave-induced sediment transport. A roller model spreads out the energy dissipation of breaking waves (Grunnet et al., 2004). The absence of this roller model could induce an overestimation of the energy dissipation due to depth-induced breaking at the nourishment. The higher simulated alongshore currents at the nourishment location would lead to an overestimation of the alongshore distribution of the nourishment (Mil-Homens, 2016). The limited availability of nearshore measurements makes the validation of the wave propagation and nearshore behaviour difficult. Measurement data would contribute to the calibration of the wave propagation and the (spreading of) wave-induced currents. For this thesis, the measurement data from Van Rijn et al. (2002) is considered acceptable. The influence of the bathymetric changes between 2002 and 2020 on the flows has thereby been neglected.

7.4.2. Parameter settings
Some model parameters could have been calibrated more extensively. For example, the uniform grain size leads to unrealistic morphological behaviour in the Marsdiep inlet. Applying a spatially varying sediment field with coarser fractions in the channels would have improved the modelled morphodynamic behaviour of this area. The morphology of the tidal delta has a considerable influence on the flow field and vice versa. A better (autonomous) morphological development would contribute to a better representation of the nourishment dispersion.

Another parameter that could have been applied in a spatially varying manner is the roughness. Arcement & Schneider (1989) show how roughness values are dependent on the channel geometry and grain size, with higher values for coarser bed material. In this research, the roughness values have been calibrated without this physical substantiation. Given the water level boundary conditions, the spatially varying roughness field would allow for a more local calibration.

Furthermore, the α_{bn} factor could have improved the model results. In Delft3D, the effect of bed slope is taken into account. Herein a distinction is made between the slope in the flow direction and the slope perpendicular to the flow direction (see Appendix C.5 for the formulations). The transport in transverse direction can be tuned with the α_{bn} calibration coefficient. Through increasing this factor, the development of tidal channels and bar systems can be calibrated (see e.g. Visser (2014); Walstra et al. (2004)). A higher value for α_{bn} increases the transverse transports, leading to shallower channels and gentler channel slopes. The unrealistic modelled deepening of the Marsdiep channel could be calibrated using this factor. Using the grain size for this should be prioritised, as there is a physical foundation for changing this value. An increase in the α_{bn} could also lead to a somewhat smoother surf zone development at the Callantsoog coast (Walstra et al., 2004).

7.4.3. Model schematization of sediment concentration

Next to the poor representation of offshore directed transports, the representation of the concentration profile by Delft3D is expected to lead to a significant under-prediction of the initial sediment dispersion. In Section 2.2.2, the Rouse concentration profile is discussed. Delft3D calculates this profile for every time step, given the sediment and flow properties (Deltares, 2021b). The addition of sediment to the water column will lead to an initial concentration increase in the upper part of the column, whereas Delft3D interprets this addition as the shift of the entire profile. The relevance of the initial dispersion follows from a simplified calculation. A particle with a diameter of 350 μm (150 μm) has a fall velocity of 0.04 m/s (0.02 m/s), according to Van Rijn et al. (1993). If the particles are released at a horizontal current velocity of 1.5 m/s and at the height of 30 metres, they can travel 1100 m (2200 m) when they fall directly towards the bottom. Turbulent forces can alter the time that the particles are in suspension. Whereas in reality all particles get the opportunity to fall over this height, Delft3D distributes the particles in such a way over the vertical that many particles start near the bottom when deposited. This is mainly the case for the larger fractions, which have higher concentrations near the bottom according to the Rouse profile (see Figure 2.7). This modelled concentration profile implicates an underestimation of the dispersion of larger grains compared to the smaller grains.

7.4.4. Model application at different timescales

The models developed for the assessment of the shoreface and channel wall nourishment can be considered applicable for a month to year timescale. The simulation times for one morphological year are approximately 15 days and 6 days for the coupled and flow-only model, respectively. The simulations of the Marsdiep region have shown that acceleration using a morfac is possible, allowing to simulate the development over several years. Other than the BFC, the Callantsoog model has not been accelerated any further. Although the model can show the impact of storm events on the nourishment dispersion, a higher grid resolution would give more confidence on the timescale of storms. For larger time scales, the model would have to be further accelerated with the methods discussed by Luijendijk et al. (2019), such as a schematisation of a representative wave climate.

7.4.5. Model validity

The validity of the model has been checked using measurements of water levels, current velocities and offshore wave characteristics. The sediment transports have been validated with the use of other researches, which mainly based the transports on sediment budget and modelling studies. Mainly the model performance on bathymetric developments is disputable. The model performance on hydrodynamics and sediment transports is good enough to make statements about the sediment dispersion of the nourishments with some confidence. The uncertainties in the nearshore wave propagation, the consequences of 2DH modelling and the development of the tidal channels in the Marsdiep model make that all conclusions drawn based on the Delft3D study should be treated carefully. A further calibration and validation using the parameters discussed in Sections 7.4.1 and 7.4.2 could lead to results of higher confidence. The importance of the right representation of nearshore waves can be derived from the formulations explained in Section 2.2.

A few critical notes should be made with regards to the validation of the nourishment behaviour with measurements of shoreface nourishments by Spanhoff et al. (2003) and Hoekstra et al. (1997). Firstly, the modelled onshore movement of the sediment can also be attributed to the poor model representation of undertow. Secondly, the difference in shape makes the comparison of a 'point nourishment' with a bar-shaped nourishment less valid. The importance of nourishment shape is stipulated by Huisman et al. (2019). Lastly does the comparison use measurements made during periods with a different forcing and a different morphology. These benchmarks could thus mainly provide in confirming that the modelled behaviour does not significantly differ from observed behaviour.

7.5. Tidal inlet dynamics

The dynamic behaviour of the Marsdiep channel offers a large transport capacity for the continuous nourishment. Escoffier (1940) designed a curve that demonstrates the behaviour of a tidal inlet in the case of a distortion. At one side of the curve, the velocity change due to an alteration in the cross-sectional area leads to a restoration of the equilibrium. At the other side of the curve, the velocity changes to such an extent that a new combination of velocity and the cross-sectional area will become the equilibrium (being a total

closure or a widening of the channel). The simulations of the channel wall nourishment show a velocity increase and a deepening of the channel adjacent to the nourishment. Through this deepening, the inlet tries to maintain its equilibrium between the velocity and the cross-sectional area. This is in line with the stabilising behaviour described by Escoffier (1940). The effort of nature to stabilise the cross-sectional area implicates the displacement of the sediment that is added, which is the desired long-term effect of the Sandwindmill. The velocity change can furthermore increase the jet-effect described by Oertel (1988) and Wang et al. (2018) (treated in Section 2.4). As this jet-flow asymmetry increases the sediment importing by the inlet, this would act as a secondary effect, further increasing the sediment import by the Marsdiep. A better understanding of the long-term consequences of the continuous nourishment on the Marsdiep dynamics would help in predicting the long-term effect of the Sandwindmill.

7.6. Morphological development on longer term

The developments of the nourishments have been assessed on a one-year timescale. The Sandwindmill system will be built for a much longer-term application. It should therefore be evaluated to what extent the findings hold for the subsequent years. Due to the many dissimilarities between the Marsdiep and Callantsoog cases, a distinction is made in the discussion of the expected longer-term behaviour.

7.6.1. Marsdiep

A distinction is made between the local and regional developments, following the structure of the result analysis in Chapter 6. First, the expected longer-term behaviour on the local scale is discussed. With local, the bed level at the nourishment location is indicated. Subsequently, the longer-term regional effects are discussed.

Local

During the first year, the rate of accretion at the nourishment location decreases over time. The change of local flow velocities is expected to be one of the main drivers of this development. However, for an annual volume of 1.5 Mm^3, simulation A5 shows the exceedance of MSL by the bed after 18 months. Whereas the nourishment can significantly increase the local transport capacity, this capacity increase does not always lead to the development of an equilibrium between the sediment supply by the SWM, and the erosion by natural forces. For a given nourishment area (here 15,000 m^2), a lower nourishment volume could exist that eventually induces a new balance between the sediment supply and erosion. This would allow for a continuous nourishment without the displacement of the outlet, as all supplied sediment can be transported away. Due to the different response to forcings for different grain sizes, this 'equilibrium discharge' can be dependent on the supplied grain size, as shown in scenario A1. As reducing the volume is undesired financially, another option to deal with this equilibrium in the long term would be shifting the pipe mouth more towards the inlet after time. This would induce an even larger contraction of the flow, further increasing the local transport capacity. Placing one pipe with multiple outlets and a different discharge per outlet could also steer the hydro- and morphological behaviour without the need of displacing the outlet.

Regional

The bed in regions adjacent to the nourishment location is influenced by the change in local hydrodynamics and the sediment supplied by the nourishment. The former makes the longer-term prediction of the regional development challenging. The local concentration of energy can erode sediment, nourishing the nearby areas where the transporting potential diminishes again. This interaction between the regional flow behaviour and the morphology is dynamic, making it difficult to predict the effect on the longer term. Outside of the influence of the change in local hydrodynamics, the long-term bathymetric changes due to the addition of sediment are expected to be more constant in time. These developments can be attributed to the direct disposal of sediment and to the resuspensioning of sediment. For a significant part of the area influenced by the nourishment, the bed level change is in the order of centimetres or millimetres (see Figure 6.12). These relatively small morphological changes will barely influence the flow, allowing to extrapolate the observed changes after one year. The model results of scenario A2 partly substantiate this, showing mainly a magnitude change for larger nourishment volumes, rather than a change in the spatial distribution of the nourishment (visual comparison Scenario A0 and A2 from Figure 6.8).

7.6.2. Callantsoog
As for Section 7.6.1, the local and regional longer-term developments are treated below.

Local
The expected local longer-term development at Callantsoog has been illustrated in Figure 6.17. Depth-induced breaking slows down the bed level increase at the nourishment location. The predicted accretion in the following years is thus expected to be smaller than in the first year. Furthermore, changes in tidal flow due to further growth of the sand hump can induce new transport gradients. Mostly finer materials would react to this change, as the tidal velocities are hardly able to erode any of the native sediment (Van Rijn, 1995). As for the Marsdiep case, a nourishment discharge can be sought that leads to a balance of supply and erosion. Hereby the timing of the nourishment shows to be an effective remedy to prevent the bed from exceeding MSL during calmer periods. This is shown in the result of scenario B3 in Figure 6.16, which reflects the more realistic scenario of system activity during more energetic conditions. Lastly, the representativity study shows that the interannual variability in wave climate could affect the dispersion during a certain year. This would imply that the applied nourishment volume could vary from year to year, being lower in calmer years.

Regional
The bed surrounding the nourishment location evolves vertically at a slower pace than the bed beneath the outlet. Therefore, the bed is expected to develop more constantly over time. After the first years, a retreat of the coastline downdrift of the nourishment can occur due to the nourishment's sheltering effect. This effect is already observed in the model results and is often observed near shoreface nourishments (Giardino et al., 2010). Lastly, the nourished material would be transported further away from the nourishment due to the resuspensioning by waves and - for the finer material - tidal currents. The grain size shows to have a significant influence on the distance that the nourished material can travel. Based on observations and the executed analysis of the wave climate between 1990-2020, a net movement in northward direction is expected.

7.7. Limited scenario quantity
A part of this research tends to optimise the dispersion of the nourished material. To that extent, a numerical model has been set up. With this D-Flow FM model, 15 alternative nourishment strategies have been analysed. The simulations allow to draw some conclusions about the sensitivity of the dispersion to a change in the nourishment characteristics. Many of the assumptions and limitations that are discussed in Section 7.4 impede the robustness of these conclusions.

An increase in the number of evaluated strategies could contribute to the reliability of the drawn conclusions. The model lends itself well to assess a wide variety of set-ups. First of all, a wider range of parameter values could provide more insight into the natural system's capacity to disperse the nourishment. For Callantsoog, the simulation of a nourishment with a larger volume than 200,000 m^3 could give an improved view on the equilibrium behaviour by wave breaking at a one year timescale. Secondly, for each scenario, only a single parameter is changed with regard to the user-defined base case (A0 and B0). The morphodynamic processes are complex. A simultaneous change of two parameters could give an entirely different outcome than anticipated, based on a single parameter's change. For example, the timing of the nourishment in the Marsdiep case (A3) shows a limited effect compared to the A0 scenario. The large sensitivity of differently sized grains to flow velocities, shown in Figure 6.6, could make a timed nourishment with a smaller fraction a more beneficial option than suggested by A3.

Another way of increasing the robustness of the results would be the change in forcing parameters. Mainly for the shoreface nourishment, where the influence of storms is very significant, an evaluation of the sensitivity to a change in storm interval, order, and severeness would provide a more thorough view on the possible nourishment spreading. The representativity study of Section 5.3 covered this variability on a year-to-year timescale. With an eye on the changing climate, it is recommended to extensively research the influence of changing forcing conditions on the behaviour of the nourishment at a larger timescale.

8

Conclusions and recommendations

Chapter 8 concludes this study by answering the research questions in Section 8.1. Subsequently, in Section 8.2, recommendations are given for further research and for the improvement of the developed D-Flow FM model.

8.1. Conclusions

Sections 8.1.1 to 8.1.3 answer the four sub-questions that were denominated in the problem formulation in Section 1.2. Finally, the main research question is answered in Section 8.1.4.

8.1.1. Sandwindmill in relation to current methods

> SQ1: How does the Sandwindmill relate to the current nourishment methods?

For decades, nourishments in the Netherlands have been executed chiefly with trailing suction hopper dredgers. Within these decades, much knowledge has been gathered on the dredging and nourishing process with the use of TSHDs. This has led to a time-effective and economical operation. The manoeuvrability of the vessels allows for an accurate and flexible placement of the sediment. Rainbowing allows the dispositioning of sediment at less accessible locations. The Sandwindmill concept, on the other hand, is still in its design phase. The optimization could take time, and uncertainties can induce costs to avert risks. Being in the early design phase, the concept still has many optimization directions. In Section 3.2, some strategies are proposed which can bring the financial attractiveness of the Sandwindmill closer to the current methods.

Inherent to the financial competitiveness is the limitation of a moveable pipe outlet. The Sandwindmill does not have the flexibility in distributing the sediment, which dredging vessels do have. The Sandwindmill is more relying on natural processes in the distribution of the sediment. This comes with some benefits. Letting nature distribute the sediment would allow marine species to keep up with the pace of bed level growth at areas outside of the direct disposal location. This burial of marine species is one of the ecological drawbacks of the traditional, quick nourishment executions. Furthermore, the slower natural distribution fits in better with the aim of Rijkswaterstaat to work with nature. The most striking difference between the traditional methods and the Sandwindmill is the associated carbon emission. The current Dutch nourishment program is CO_2 intensive due to the emissions of the TSHDs. With forecasts indicating a growing need for nourishments, the need for a long-term sustainable alternative grows. As the Sandwindmill system runs fully on wind energy, it could make the Dutch nourishment program entirely carbon neutral.

8.1.2. Interdependency of Sandwindmill systems

> SQ2: What are the interdependencies of the Sandwindmill subsystems, and how do these relate to sediment dispersion?

Four subsystems of the Sandwindmill are distinguished in this research; mining, transport, nourishment and energy provision. Sub-question 2 is answered for each subsystem separately.

Mining
Some mining options can impose an operational limit on the system if these are not operable under harsher conditions. This holds mainly for the systems that operate at sea level. This has two consequences. If a certain nourishment volume must be placed annually, the discharge of the system when running would need to increase. To deliver a higher discharge, a larger pumping system is needed, requiring more energy. Secondly, the harsh wave conditions correlate with the high wind velocities. The system can thus not use the more powerful wind velocities for delivering energy: the energy provision system should not only be increased to account for the larger pumps, but the system should also be increased in size as it can only use the lower wind velocities. The choice for the mining option thus has a double aggravating effect on the required energy-system size. Next to the effect on this system, there is also an effect on the nourishment as larger volumes of sediment are deposited in shorter intervals and during calmer conditions.

Transport system
The transport system favours smaller grain sizes, as the fall velocity of smaller particles is lower. This leads to a smaller critical pumping velocity, which is beneficial in terms of required energy. Smaller grain sizes also lead to less pipe abrasion. Increasing the sediment concentration in the pumped mixture enhances both the energy efficiency and the risk of clogging. The gain in efficiency decreases with an increasing concentration. Finding a balance between a safe and economic concentration is thus essential, as it can lead to lower pump requirements for the same in-situ volume of sediment. From a transporting point of view, small grain sizes and high concentrations thus benefit the system. Nourishing 1,500,000 m^3 per year at 50% operational time with (a) 10% concentration and median grain size of 250 μm requires twice the amount of energy of nourishing with (b) 15% concentration and median grain size of 150 μm. Lastly, the increase in discharge reduces the energy requirements per unit of transported sediment.

Nourishment type
Shoreface and tidal channel nourishments have been evaluated in this thesis. It is assumed that the Sandwindmill system can distribute the sediment in a plane of approximately 15,000 m^2. This area has been chosen based on the cell size of the computational model. Due to the designed simplicity of the outlet system, no large interdependencies are present with other system elements. When the system is made more complex by nourishing with a spraying pontoon comparable to the dredging raft, the same wave climate-induced limitations will hold in wave-dominated areas as for the non-submarine mining equipment. Whereas the limit for offshore operability is expected to be around H$_s$ = 2 m, the breaking of waves could reduce this limit for working in the surf zone.

Energy provision
The energy provision appears to play a vital role in the development of the Sandwindmill. Firstly, this system contributes for a significant part to the system costs. Secondly, the size of the windmill for a given pump capacity is determining for the operational time of the system. Tailoring the windmill, pump sizes and sediment demand towards an optimal balance of discharge and operational time plays a significant role in the cost-efficiency of the system. Furthermore, it has been shown that the addition of battery capacity can allow the use of smaller wind turbines, which would be financially beneficial given the current battery and windmill prices.

8.1.3. Nourishment design

> SQ3: How well is the Dutch coast capable of dispersing a continuous nourishment?

In this research, two types of locations have been evaluated: a straight sandy coast and a tidal channel. The evaluation of both locations shows that the nourishment dispersion depends highly on the choice of a location. Tide-induced flows mainly govern the sediment dispersion in the tidal channel. These flows have a deterministic character, which favours the predictability of the nourishment dispersion. The high tidal flow velocities of up to 2 m/s have a large transporting capacity as they can keep and bring grains of many sizes in suspension. Furthermore, the large depth of the channel allows for the diffusion of the sediment particles when discharged by the system. Lastly, this depth provides more time for the particles to be transported by advection. These processes distinguish the application of a continuous nourishment from a classical channel wall nourishment and allow the gradual placement of volumes in the order of 1.5 million m^3 per year over a 15,000 m^2 area. For a longer-term application in the same area, the volume should be decreased to prevent the piling up of sediment.

For the shoreface nourishment, other processes are dominant in the sediment dispersion. Waves are the main driver of the sediment spreading. The stochastic character of waves makes the prediction of the nourishment behaviour more difficult. The seasonality of the dispersion is visible in the results, where the nourishment is spread out in the more energetic months. With tidal velocities reaching only 0.7 m/s, a continuous and deterministic dispersion is harder to effectuate. Only under the coincidence of energetic oblique waves and a tidal current in the same direction, the alongshore velocities that occur regularly in the Marsdiep can be achieved. Turbulence by the breaking of waves can significantly alter the transport capacity during these energetic conditions, however. Lastly, the small depth gives the nourishment less room to diffuse and be advected. The continuous nourishment at the shoreface thus has more the characteristics of a regular shoreface nourishment. Model results indeed show similar behaviour for the dispersion of the continuously nourished sediment as for regular shoreface nourishments.

A similarity between the tidal channel and the shoreface nourishments is the tendency towards an equilibrium. For the tidal channel, this equilibrium is triggered by the hydrodynamic response to the constriction of the channel. This narrowing triggers the contraction of the tidal flow, leading to increased velocities and thus a higher transporting capacity. For the shoreface, the accretion of the bottom triggers the depth-induced breaking of waves. Consequently, the transport capacity at the nourishment location increases with an increasing bottom level.

> SQ4: How can the continuous nourishments be designed to improve sediment dispersion?

In this research, a distinction has been made in the nourishment placement, grain size, timing and volume.

Placement
The difference in placement of the nourishment in wave- and tide-dominated systems has been treated in the answer to sub-question 3. A shift in the nourishment location at the tidal channel itself shows that both the regional and local development of the nourishment is highly dependent on the nourishment location. Due to the steepness of the channel walls and the high spatial variability of the flows, a slight placement shift can induce a different hydrodynamic and morphodynamic response. For the wave-dominated shoreface, a change of the placement towards a deeper location primarily affects the time it takes before waves start dissipating energy at the nourishment location. The larger depth allows the placement of more sediment, which is therefore recommended. A placement shift in the alongshore direction shows that the change in local wave climate (e.g. due to sheltering or a coastline orientation) influences the dispersion direction and magnitude.

Grain size
The susceptibility of differently sized grains to flows makes the variation in the nourished sediment characteristics an effective way of optimizing the dispersion. For the Marsdiep, reducing the grain sizes from 350 towards 250 and 150 μm did not result in significant local differences. A maximum reduction of the local accretion of 25% is observed. Mainly on a regional scale, the smaller grain sizes lead to a substantial bed level

increase. For the shoreface nourishments, the 150 μm grains shows to be much more susceptible to tide- and wave-induced currents than the 250 μm grains. Both locally and regionally, large morphological differences are observed compared to the use of a 250 μm fraction.

Timing

Timing the nourishment such that it takes place at moments with a high transporting capacity shows to be of some effect at a larger time scale. Nourishing in the Marsdiep during high flow velocities leads to a 350% increase in sediment import into the basin. Locally, little difference is observed. The disadvantage of only nourishing during higher tidal flow velocities, is that this limits the system's annual operational time in a 'forced' way, which can be costly. Applying a timed nourishment during high waves at Callantsoog is more feasible, as high waves and winds coincide regularly. Although the bed level increase at Callantsoog after one year is almost twice the value as in the base case, the timed nourishing reduces the occurrence of bed level peaks during calmer periods. Within the currently researched setting, the timing of the nourishment is not as effective as the change in grain size. Using both smaller grain sizes and a timed nourishment can have a more significant effect.

Volume

Increasing the nourishment volume leads to a sooner triggering of equilibrium behaviour. For the Marsdiep, the tidal contraction occurs sooner, leading to a quicker increase of the local transport capacity. However, simulation results show that by applying 3,000,000 m^3 per year, the increase in eroding capacity is not sufficient to remove the large volume of sediment locally. When such volumes are required for a sufficiently low volumetric price, an option would be to work from outside inwards: starting by nourishing the wall and placing the outlet in channel direction when the wall is sufficiently fed. In this way, a continuous increase in transporting capacity could lead to reaching an equilibrium between the large discharge and the increased transporting capacity. The consequences of altering the dynamics to such an extent should be extensively reviewed first. For Callantsoog, the larger applied volume also leads to sooner triggering the equilibrium behaviour, in this case by depth-induced breaking.

8.1.4. Main research question

> MQ: What type of nourishment strategy enables the Sandwindmill to be competitive with traditional nourishment methods?

The strength of the Sandwindmill is that it offers a carbon-neutral alternative to the traditional nourishment method through TSHDs. Furthermore, the slow spreading of the sediment fits in with the building with nature approach that Rijkswaterstaat pursues. Economically, the system can be competitive with the traditional methods if larger volumes can be nourished.

The evaluation of the nourishment dispersion in the tidal channel and at the shoreface shows that the nourishment timing does not significantly influence the local dispersion within the applied boundary conditions. The timing of the nourishment does thus not have to depend on the prevailing forcing conditions. When the system operation is unaffected by the wave and wind climate, the most economical system configuration is such that the system operates for 60-80% of the time. This operational time results from the most economical combination of installed pump capacity, wind capacity and battery capacity.

The placement of the nourishment in a tidal inlet allows for a larger dispersion than the placement at the shoreface. Whereas the dispersion at the shoreface is in the order of 400 metres, the tidal channel nourishment disperses in the order of 4 kilometres for the same grain size. Next to the chosen type of nourishment, the precise placement of the nourishment in the tidal channel influences the behaviour and the dispersion. A location that leads to a tidal contraction allows for the creation of favourable hydrodynamic changes. Lastly, the grain size shows to have a considerable influence on the dispersion. A grain size decrease from 250 μm to 150 μm can increase the dispersion range by a factor of three for both the shoreface and the tidal channel nourishment. The use of a smaller grain size is also favourable from the energy requirements and abrasion point of view.

8.2. Recommendations

In this section, some recommendations for future research are given. The recommendations are listed below.

- The executed research encompasses a one-year **timescale**. The objective of the Sandwindmill concept is the application of a long-term (e.g. 20 years) nourishment. It is therefore important to forecast the local and regional developments in the longer term. Scenario A5 already suggests that the appearing equilibrium does not necessarily hold for the longer term. This demonstrates the importance of longer-term modelling.

- The assumptions and simplifications that have been made to allow for one-year modelling impede the correct inclusion of small-scale processes. The (2DH) vertical averaging induces an inaccurate representation of the **sediment concentration** over the vertical. Therefore, it is recommended to set up a near field study that looks into the initial dispersion of the sediment. The inclusion of the vertical variability in sediment concentration is key to evaluate the initial dispersion. Both a numerical (2DV or 3D) or physical study could be carried out.

- Setting up a 2DV or 3D model is also recommended to include **hydrodynamic 3D processes**. This would allow for the more accurate modelling of cross-shore processes at the shoreface. In combination with the inclusion of baroclinic factors such as freshwater discharge, 3D modelling can enable a more accurate representation of sediment transports in the inlet (Elias, 2006; Wang et al., 2018).

- The D-Flow FM model used in this thesis has been set up in a limited time. A few **model improvements** are proposed for the future use of the model. The model can be used for a broader range of applications than looking at the dispersion of a continuous nourishment. The model is expected to generate a more realistic morphological development in the tidal inlets when the spatial variability in grain sizes is incorporated. Using the α_{bn} factor to calibrate the channel development further has proven to be effective in other research. Lastly, the hydrodynamic performance can be improved by deriving and applying spatially varying Neumann boundaries at the laterals.

- As the adaptation of the geometry of a tidal system can have a large influence on its dynamics, the response of the Marsdiep area to a channel nourishment should be researched carefully. Next to studying what the response would be, steering the response through **channel realignment** could be an effective way of reducing coastal erosion Lazar et al. (2017). Close monitoring of executed tidal channel nourishments can help in understanding the dynamics and validating computational models.

- The research shows no significant long-term change if a nourishment is executed only during energetic conditions. This **timed nourishing** has been only evaluated for the standard grain sizes. The response of smaller grain sizes to the timed nourishments could be different and should hence be studied. This would have implications for the operational times. Whereas the optimal operational time is currently solely based on the most economical set-up, the advantage of a timed nourishment could change the optimal operational time and thus the entire system set-up.

- When large concentrations of sediment are dumped within a small area, **density flows** could prevent the natural diffusion of the nourished sand. The pumped concentration could thus not only be dependent on the risk of clogging, but also on the likeliness of the occurrence of such flows. It should be noted that these density flows could be prevented by an appropriate initial dispersion with spray pontoons or multiple outlets, whereas the clogging risk is harder to solve.

- This research has provided guidelines for the initial assessment of an appropriate location. Section 4.1.1 shows that within the Netherlands, Walcheren and Ameland are **other attractive regions** to assess. As the erosion of critical coastal stretches is not a problem that is limited to the Netherlands, assessing the application of a continuous nourishment in other regions of the world is recommended. From a commercial point of view, a large market means the opportunity to sell the system with profits. This would enhance the importance of a cheap system over low R&D costs. For the mining systems discussed in Section 3.3, this implies that the proof of concept becomes a less critical parameter.

- The slow rate at which the sediment disperses could prevent the large-scale burial of marine species, which does occur with the current nourishing methods. To which extent marine species can keep up with the slower pace should be assessed. It is also advised to incorporate the effect of turbidity plumes in this **ecological analysis** (De Schipper et al., 2020).

- The placement of the outlets can be inherent to some **practical limitations**. If the outlets are to be placed as high as possible in the water column to increase the dispersion, the placement in a shipping channel is impracticable. The outlet locations researched in this thesis are just landward of the shipping channel. Another shipping-related issue could be the sedimentation of the Den Helder harbour, where the Dutch Marine Corps is located. Finally, the placement of sediment at the shoreface could induce rip currents that jeopardize swimmer safety.

- Lastly, it is advised to continue researching **other alternatives to dredging** to fossil fuel-driven hoppers. The Sandwindmill is one of the many possible steps towards a sustainable coastal policy. The results of this research can support the development of other sustainable nourishment concepts.

References

Aagaard, T., Davidson-Arnott, R., Greenwood, B., & Nielsen, J. (2004). Sediment supply from shoreface to dunes: Linking sediment transport measurements and long-term morphological evolution. *Geomorphology*, *60*(1-2), 205–224. doi: 10.1016/j.geomorph.2003.08.002

Arcement, G. J., & Schneider, V. R. (1989). *Guide for selecting Manning ' s roughness coefficients for natural channels and flood plains.* Denver, CO: United States Government Printing Office.

Ashton, A. D., & Murray, A. B. (2006). High-angle wave instability and emergent shoreline shapes: 1. Modeling of sand waves, flying spits, and capes. *Journal of Geophysical Research*, *111*, 1–19. doi: 10.1029/2005JF000422

Bagnold, R. (1937). The transport of sand by wind. *The Geographical Journal*, *89*(5), 409–438.

Bakker, M. A. J., Van Heteren, S., Vonhgen, L. M., Van der Spek, A. J. F., & Van der Valk, B. (2012). Recent coastal dune development: Effects of sand nourishments. *Journal of Coastal Research*, *28*(3), 587–601. doi: 10.2112/JCOASTRES-D-11-00097.1

Baptist, M., Tamis, J., Borsje, B., & Van der Werf, J. J. (2009). *Review of the geomorphological, benthic ecological and biogeomorphological effects of nourishments on the shoreface and surf zone of the Dutch coast.* Deltares. Retrieved from http://edepot.wur.nl/8938

Bayram, A., Larson, M., Miller, H., & Kraus, N. (2001). Cross-shore distribution of longshore sediment transport: Comparison between predictive formulas and field measurements. *Coastal Engineering*, *44*(2), 79–99. doi: 10.1016/S0378-3839(01)00023-0

Bijker, E. (1967). *Some considerations about scales for coastal models with movable bed.* PhD Thesis, Delft University of Technology.

Blue Mining. (2018). *Blue mining: Breaktrough solutions for mineral extraction and processing in extreme environments.* doi: 10.1109/ut.2015.7108296

Bonekamp, H., Ridderinkhof, H., Roelvink, D. J. A., & Luijendijk, A. P. (2002). Sediment transport in the Texel tidal inlet due to tidal asymmetries. , 2813–2823. doi: 10.1142/9789812791306{_}0235

Bosboom, J., & Stive, M. J. F. (2015). *Coastal Dynamics I.* Delft: Delft Academic Press. 0.5 Edition.

Boskalis. (2010). Equipment sheet: Shoalway.

Boswood, P., Voisey, C., Victory, S., Robinson, D., Dyson, A., & Lawson, S. (2005). Beach response to Tweed River entrance sand bypassing operations. *17th Australasian Coastal and Ocean Engineering Conference 2005 and the 10th Australasian Port and Harbour Conference 2005*, 119–124.

Briene, M., De Gier, T., De Ronde, J., De Swart, L., & Van den Bossche, M. (2011). *Strategie planmatige zandwinning: Belangenafweging en instrumentarium.*

Brière, C., Giardino, A., & Van der Werf, J. J. (2011). Morphological modeling of bar dynamics with Delft3D: The quest for optimal free parameter settings using an automatic calibration technique. *Coastal Engineering Proceedings*, *1*(32). doi: 10.9753/icce.v32.sediment.60

Bruun, P. (1954). *Coast erosion and the development of beach profiles.* Washington: Tech. Mem. No. 44, Beach Erosion Board, U.S. Army Corps of Engineers.

Bruun, P. (1962). Sea-Level Rise as a Cause of Shore Erosion. *Journal of the Waterways and Harbors Division*, *88*(1), 117–132.

Buijsman, M., & Ridderinkhof, H. (2007). Long-term ferry-ADCP observations of tidal currents in the Marsdiep inlet. *Journal of Sea Research, 57*(4), 237–256. doi: 10.1016/j.seares.2006.11.004

Buijsman, M., & Ridderinkhof, H. (2008). Variability of secondary currents in a weakly stratified tidal inlet with low curvature. *Continental Shelf Research, 28*(14), 1711–1723. doi: 10.1016/j.csr.2008.04.001

Bultema, S., van den Boom, H., & Krekel, M. (2000). FPSO integrity: JIP on FPSO fatigue loads. *Proceedings of the Annual Offshore Technology Conference, 2*, 695–704. doi: 10.4043/12142-ms

Butt, T., Russell, P., Puleo, J. A., Miles, J., & Masselink, G. (2004). The influence of bore turbulence on sediment transport in the swash and inner surf zones. *Continental Shelf Research, 24*(7-8), 757–771. doi: 10.1016/j.csr.2004.02.002

CERC. (1984). *Shore protection manual* (4th ed.). Vicksburg: Dept. of the Army, Waterways Experiment Station, Corps of Engineers.

Cheng, C. H., Soetaert, K., & Borsje, B. (2020). Sediment characteristics over asymmetrical tidal sand waves in the Dutch north sea. *Journal of Marine Science and Engineering, 8*(6). doi: 10.3390/JMSE8060409

CIRIA. (2009). *A guide to cost standards for dredging equipment 2009.*

Cole, W., & Frazier, A. W. (2019). *Cost projections for utility- scale battery storage* (No. June). Golden, CO. doi: NationalRenewableEnergyLaboratory

Coon, W. (1998). *Estimation of roughness coefficients for natural stream channels with vegetated banks.* U.S. Geological Survey water-supply paper 2441. Retrieved from https://pubs.er.usgs.gov/publication/wsp2441%0Ahttps://pubs.usgs.gov/wsp/2441/report.pdf

Cooper, J. A. G. (2005). Microtidal coasts. *Encyclopedia of Earth Sciences Series, 14*, 638. doi: 10.1007/1-4020-3880-1{_}212

Cooper, J. A. G., & Pilkey, O. H. (2004). Sea-level rise and shoreline retreat: Time to abandon the Bruun Rule. *Global and Planetary Change, 43*(3-4), 157–171. doi: 10.1016/j.gloplacha.2004.07.001

Davies, A. (1985). On determining the profile of steady wind-induced currents. *Applied Mathematical Modelling, 9*(6), 409–418. doi: 10.1016/0307-904X(85)90106-4

Davis, R. A., & Hayes, M. O. (1984). What is a wave-dominated coast? *Marine Geology, 60*, 313–329. doi: 10.1016/S0070-4571(08)70152-3

Dean, R. (1991). Equilibrium beach profiles : Characteristics and applications. *Journal of Coastal Research, 7*(1), 53–84.

Dean, R. (2019). *Encyclopedia of Coastal Science* (C. W. Finkl & C. Makowski, Eds.). Cham: Springer International Publishing. doi: https://doi-org.tudelft.idm.oclc.org/10.1007/978-3-319-93806-6

Defeo, O., McLachlan, A., Schoeman, D. S., Schlacher, T. A., Dugan, J., Jones, A., . . . Scapini, F. (2009). Threats to sandy beach ecosystems: A review. *Estuarine, Coastal and Shelf Science, 81*(1), 1–12. doi: 10.1016/j.ecss.2008.09.022

De Lellis, M., Reginatto, R., Saraiva, R., & Trofino, A. (2018). The Betz limit applied to Airborne Wind Energy. *Renewable Energy, 127*, 32–40. doi: 10.1016/j.renene.2018.04.034

Deltares. (2014). *3D/2D modelling suite for integral water solutions: Hydro-Morphodynamics.* Retrieved from https://content.oss.deltares.nl/delft3d/manuals/Delft3D-FLOW_User_Manual.pdf

Deltares. (2019). *D-Waves user manual.* Retrieved from https://content.oss.deltares.nl/delft3d/manuals/D-Waves_User_Manual.pdf

Deltares. (2021a). *D-Flow Flexible Mesh user manual.* Retrieved from https://content.oss.deltares.nl/delft3d/manuals/D-Flow_FM_User_Manual.pdf

Deltares. (2021b). *D-Morphology user manual.* Retrieved from https://content.oss.deltares.nl/delft3d/manuals/D-Morphology_User_Manual.pdf

Deme. (2018). *Bonny River - fact sheet.* Retrieved from `https://www.deme-group.com/technologies/bonny-river#`

De Schipper, M., De Vries, S., Mil-Homens, J., Reiniers, A., Ranasinghe, R., & Stive, M. J. F. (2015). Initial volume losses at nourished beaches and the effect of surfzone slope.
doi: 10.1142/9789814689977{_}0050

De Schipper, M., Ludka, B., Raubenheimer, B., Luijendijk, A. P., & Schlacher, T. (2020). Beach nourishment has complex implications for the future of sandy shores. *Nature Reviews Earth & Environment*, 1–15. doi: 10.1038/s43017-020-00109-9

De Sonneville, B., & Van der Spek, A. J. F. (2012). Sediment- and morphodynamics of shoreface nourishments along the North-Holland coast. In *Proceedings of the coastal engineering conference.* doi: 10.9753/icce.v33.sediment.44

De Vriend, H. J. (2003). On the prediction of aggregated-scale coastal evolution. *Journal of Coastal Research*, *19*(4), 757–759.

De Vriend, H. J., Van Koningsveld, M., & Aarninkhof, S. G. J. (2014). 'Building with nature': the new Dutch approach to coastal and river works. *Proceedings of the Institution of Civil Engineers: Civil Engineering*, *167*(1), 18–24. doi: 10.1680/cien.13.00003

De Vriend, H. J., van Koningsveld, M., Aarninkhof, S. G. J., De Vries, M., & Baptist, M. (2015). Sustainable hydraulic engineering through building with nature. *Journal of Hydro-Environment Research*, *9*(2), 159–171. doi: 10.1016/j.jher.2014.06.004

De Vries, J. (2015). *On the local dynamics of currents in the estuarine Marsdiep Basin.* PhD Thesis, NIOZ.

De Vries, S., Southgate, H. N., Kanning, W., & Ranasinghe, R. (2012). Dune behavior and aeolian transport on decadal timescales. *Coastal Engineering*, *67*, 41–53. doi: 10.1016/j.coastaleng.2012.04.002

Duran-Matute, M., Gerkema, T., De Boer, G., Nauw, J., & Gräwe, U. (2014). Residual circulation and freshwater transport in the Dutch Wadden Sea: A numerical modelling study. *Ocean Science*, *10*(4), 611–632. doi: 10.5194/os-10-611-2014

Eddy Pump. (n.d.). *Autonomous Dredge.* Retrieved from `https://eddypump.com/products/dredging-equipment/autonomous-dredge/`

Eisma, D. (1968). Composition, origin and distribution of Dutch coastal sands between Hoek van Holland and the island of Vlieland. *Netherlands Journal of Sea Research*, *4*(2), 123–267.

Elfrink, B., Broker, I., Deigaard, R., Hansen, E. A., & Justesen, P. (1996). Modelling of 3D sediment transport in the surf zone. In *25th international conference on coastal engineering* (Vol. 1, pp. 3805–3817). doi: https://doi.org/10.9753/icce.v25.{\%}p

Elias, E. P. L. (2006). *Morphodynamics of Texel Inlet.* PhD Thesis, Delft University of Technology.

Elias, E. P. L., Cleveringa, J., Buijsman, M., Roelvink, D. J. A., & Stive, M. J. F. (2006). Field and model data analysis of sand transport patterns in Texel Tidal inlet (the Netherlands). *Coastal Engineering*, *53*(5-6), 505–529. doi: 10.1016/j.coastaleng.2005.11.006

Elias, E. P. L., & Van der Spek, A. J. F. (2006). Long-term morphodynamic evolution of Texel inlet and its ebb-tidal delta (The Netherlands). *Marine Geology*, *225*(1-4), 5–21. doi: 10.1016/j.margeo.2005.09.008

Elias, E. P. L., & Van der Spek, A. J. F. (2017). Dynamic preservation of Texel Inlet, the Netherlands: Understanding the interaction of an ebb-tidal delta with its adjacent coast. *Geologie en Mijnbouw/Netherlands Journal of Geosciences*, *96*(4), 293–317. doi: 10.1017/njg.2017.34

Elias, E. P. L., Van der Spek, A. J. F., Pearson, S. G., & Cleveringa, J. (2019). Understanding sediment bypassing processes through analysis of high-frequency observations of Ameland Inlet, the Netherlands. *Marine Geology*, *415*(June), 105956. doi: 10.1016/j.margeo.2019.06.001

Elias, E. P. L., Van der Spek, A. J. F., Wang, Z., & De Ronde, J. (2012). Morphodynamic development and sediment budget of the Dutch Wadden Sea over the last century. *Geologie en Mijnbouw/Netherlands Journal of Geosciences*, *91*(3), 293–310. doi: 10.1017/S0016774600000457

Elias, E. P. L., & Vermaas, T. (2018). Een actuele sedimentbalans van de Westelijke Waddenzee (1933-2015). , 62.

Elias, E. P. L., Vonhögen-Peeters, L. M., & Bruens, A. (2013). *Ontwikkeling suppletie tussen Den Helder en Julianadorp 2007.* Deltares report 1206171-000.

Elias, E. P. L., & Wang, Z. (2020). *Sedimentbalans Waddenzee: Synthese ten behoeve van Technisch Advies Kustgenese 2.0.* Deltares.

Elko, N. A., & Wang, P. (2007). Immediate profile and planform evolution of a beach nourishment project with hurricane influences. *Coastal Engineering*, *54*(1), 49–66. doi: 10.1016/j.coastaleng.2006.08.001

Emanuel, K. (2005). Increasing destructiveness of tropical cyclones over the past 30 years. *Nature*, *436*(7051), 686–688. doi: 10.1038/nature03906

Escoffier, F. (1940). The stability of tidal inlets. *Shore Beach*, *8*(4), 114–115.

Eurostat. (2020). *Greenhouse gas emission statistics - emission inventories.* Retrieved from `http://ec .europa.eu/eurostat/statisticsexplained/`

Fredsøe, J., & Deigaard, R. (1992). *Mechanics of coastal sediment transport* (Vol. 3). doi: 10.1142/1546

Gerritsen, H. (2005). What happened in 1953? The Big Flood in the Netherlands in retrospect. *Philosophical Transactions of the Royal Society A: Mathematical, Physical and Engineering Sciences*, *363*(1831), 1271–1291. doi: 10.1098/rsta.2005.1568

Giardino, A., Werf, J. V. D., & Ormondt, M. V. (2010). *Simulating coastal morphodynamics with Delft3D: case study Egmond aan Zee.* Deltares report 1200635-005.

Gonçalves Castro, M. B., Mestemaker, B. T. W., & Van den Heuvel, H. (2019). Towards zero emission work vessels : the case of a dredging vessel. In *Proceedings of moses2019 conference.* Glasgow, Scotland.

Grasmeijer, B., Schrijvershof, R., & Van der Werf, J. J. (2019). *Modelling Dutch Lower Shoreface Sand Transport.* Deltares report 1220339-005.

Grontmij. (2013). *Zandwindmolen - financiële haalbaarheid.* GM-0109545.

Grunnet, N. M., Walstra, D. J. R., & Ruessink, B. G. (2004). Process-based modelling of a shoreface nourishment. *Coastal Engineering*, *51*(7), 581–607. doi: 10.1016/j.coastaleng.2004.07.016

Guo, L., van der Wegen, M., Roelvink, D. J. A., & He, Q. (2014, 11). The role of river flow and tidal asymmetry on 1-D estuarine morphodynamics. *Journal of Geophysical Research: Earth Surface*, *119*, 2315–2334. doi: 10.1002/2014JF003110

Hallin, C. (2019). *Long-term beach and dune evolution Development and application of the CS-model.* PhD Thesis, Lund University, Sweden. doi: 10.13140/RG.2.2.36390.37447

Hanson, H., Aarninkhof, S. G. J., Capobianco, M., Jiménez, J., Larson, M., Nicholls, R. J., . . . De Vriend, H. J. (2003). Modelling of Coastal Evolution on Yearly to Decadal Time Scales. *Journal of Coastal Research*, *19*(4), 790–811.

Healy, D., O'Callaghan, K., Browns, W., Den Broeder, M., Van Oord, G., McCullough, F., & Wright, J. (2013). *POC Maintenance Dredging Application.* Van Oord. Retrieved from =

Herman, P., Meijer-Holzhauer, H., Vergouwen, S., Wijsman, J., & Baptist, M. (2016). *Ecologische effecten van kustsuppleties. Systeembeschrijving, onderzoeksprioriteiten en ontwerp uitvoeringsplan.* Deltares.

Hersbach, H., Bell, B., Berrisford, P., Hirahara, S., Horányi, A., Muñoz-Sabater, J., . . . Thépaut, J. N. (2020). The ERA5 global reanalysis. *Quarterly Journal of the Royal Meteorological Society*, *146*(730), 1999–2049. doi: 10.1002/qj.3803

Hoekstra, P., Houwman, K. T., Kroon, A., Ruessink, B. G., Roelvink, D. J. A., & Spanhoff, R. (1997). Morphological development of the Terschelling shoreface nourishment in response to hydrodynamic and sediment transport processes. *Proceedings of the Coastal Engineering Conference*, *3*, 2897–2910. doi: 10.1061/9780784402429.224

Holthuijsen, L. H. (2009). *Waves in oceanic and coastal waters*. New York: Cambridge University Press.

Hoonhout, B. M., & Vries, S. d. (2016). A process-based model for aeolian sediment transport and spatiotemporal varying sediment availability. *Journal of Geophysical Research: Earth Surface*, *121*(8), 1555–1575. doi: 10.1002/2015JF003692

Huijts, K., Schuttelaars, H., De Swart, H., & Valle-Levinson, A. (2006). Lateral entrapment of sediment in tidal estuaries: An idealized model study. *Journal of Geophysical Research: Oceans*, *111*(12), 1–14. doi: 10.1029/2006JC003615

Huisman, B. (2014). *Modelling Coastline Evolution: Practices for the setup of coastline models*. Deltares report 1209381-005.

Huisman, B. (2019). *On the redistribution and sorting of sand at nourishments*. PhD Thesis, Delft University of Technology. doi: 10.4233/uuid:a2bbb49d-8642-4a32-b479-4f0091f2d206

Huisman, B., Walstra, D. J. R., Radermacher, M., De Schipper, M., & Ruessink, G. (2019). Observations and modelling of shoreface nourishment behaviour. *Journal of Marine Science and Engineering*, *7*(3). doi: 10.3390/jmse7030059

IPCC. (2014). *Climate change 2014: synthesis report. contribution of working groups I, II and III to the fifth assessment report of the intergovernmental panel on climate change*. Geneva, Switserland: IPCC. doi: 10.2307/1881805

IPCC. (2021). *Summary for policymakers. Climate change 2021: the physical science basis. Contribution of Working Group I to the Sixth Assessment Report of the Intergovernmental Panel on Climate Change* (Tech. Rep.). Cambridge: Cambridge University Press. doi: 10.1260/095830507781076194

Jones, A. R., Murray, A., Lasiak, T. A., & Marsh, R. E. (2008). The effects of beach nourishment on the sandy-beach amphipod Exoediceros fossor: Impact and recovery in Botany Bay, New South Wales, Australia. *Marine Ecology*, *29*(SUPPL. 1), 28–36. doi: 10.1111/j.1439-0485.2007.00197.x

Kaji, A., Luijendijk, A. P., Van Thiel de Vries, J., De Schipper, M., & Stive, M. J. F. (2014). Effect of different forcing processes on the longshore sediment transport at the Sand Motor, the Netherlands. *Coastal Engineering Proceedings*, *1*(34), 71. doi: 10.9753/icce.v34.sediment.71

Kamphuis, J. W. (1991). Alongshore sediment transport rate distribution. *Coastal Sediments '91*, *117*(6), 170–183.

Knodt, S., Kleinen, T., Dornieden, C., Lorscheidt, J., Bjørneklett, B., & Mitzlaff, A. (2016). Development and engineering of offshore mining systems - State of the art and future perspectives. *Proceedings of the Annual Offshore Technology Conference*, *4*, 3436–3457. doi: 10.4043/27185-ms

Laan, S. (2019). Understanding coastal dynamics at an ebb-tidal delta in the Wadden Sea.

Langelandsvik, L. I., Kunkel, G. J., & Smits, A. J. (2008). Flow in a commercial steel pipe. *Journal of Fluid Mechanics*, *595*, 323–339. doi: 10.1017/S0022112007009305

Lazar, M., Elias, E. P. L., & Van der Spek, A. J. F. (2017). Coastal maintenance and management of the "Voordelta", the contiguous ebb-tidal deltas in the SW Netherlands. *Coastal Dynamics 2017*, 1261–1272.

Lesser, G. R. (2009). *An Approach to Medium-term Coastal Morphological Modelling*. PhD Thesis, TU Delft.

Lesser, G. R., Roelvink, D. J. A., van Kester, J. A., & Stelling, G. S. (2004). Development and validation of a three-dimensional morphological model. *Coastal Engineering*, *51*(8-9), 883–915. doi: 10.1016/j.coastaleng.2004.07.014

Lian, J., Gou, W., Li, H., & Zhang, H. (2018). Effect of sediment size on damage caused by cavitation erosion and abrasive wear in sediment-water mixture. *Wear*, *398-399*, 201–208. doi: 10.1016/j.wear.2017.12.010

Lopez De San Roman Blanco, B., Woods Ballard, B., Simm, J., Brampton, A., Sutherland, J., Gouldby, B., & Rossington, K. (2019). *Coastal morphological modelling for.* Bristol: Environment Agency.

Louters, T., Van den Berg, J. H., & Mulder, J. P. M. (1998). Geomorphological changes of the oosterschelde tidal system during and after the implementation of the Delta project. *Journal of Coastal Research*, *14*(3), 1134–1151.

Luijendijk, A. P., de Schipper, M., & Ranasinghe, R. (2019). Morphodynamic acceleration techniques for multi-timescale predictions of complex sandy interventions. *Journal of Marine Science and Engineering*, *7*(3). doi: 10.3390/jmse7030078

Luijendijk, A. P., Hagenaars, G., Ranasinghe, R., Baart, F., Donchyts, G., & Aarninkhof, S. G. J. (2018). The state of the world's beaches. *Scientific Reports*, *8*(1), 1–11. doi: 10.1038/s41598-018-24630-6

Luijendijk, A. P., Ranasinghe, R., De Schipper, M., Huisman, B., Swinkels, C., Walstra, D. J. R., & Stive, M. J. F. (2017). The initial morphological response of the Sand Engine: A process-based modelling study. *Coastal Engineering*, *119*, 1–14. doi: 10.1016/j.coastaleng.2016.09.005

Management Ministry of Infrastructure and Water. (n.d.). *Innovaties in de Kustlijnzorg.* Retrieved from `https://www.rijkswaterstaat.nl/zakelijk/innovatie/waterinnovaties/innovaties-in-de-kustlijnzorg/index.aspx`

Manzanera, M., Alcoverro, T., Jiménez, J. A., & Romero, J. (2014). The large penumbra: Long-distance effects of artificial beach nourishment on Posidonia oceanica meadows. *Marine Pollution Bulletin*, *86*(1-2), 129–137. doi: 10.1016/j.marpolbul.2014.07.033

Matousek, V. (2004). *Dredge pumps and slurry transport: Operation limits of pump-pipeline system.* Delft: Delft University of Technology. Retrieved from `https://docplayer.net/21565164-0e4625-dredge-pumps-and-slurry-transport-vaclav-matousek-october-13-2004.html`

Matoušek, V. (2004). *Pump and pipeline characteristics; chapter 7 - dredge pumps and slurry transport.* Delft: Delft University of Technology.

McLaren, P., Steyaert, F., & Powys, R. (1998). Sediment transport studies in the tidal basins of the Dutch Waddenzee. *Senckenbergiana Maritima*, *29*(1-6), 53–61. doi: 10.1007/BF03043943

Mil-Homens, J. (2016). *Longshore sediment transport: Bulk formulas and process based models.* PhD Thesis, Delft University of Technology.

Min.V&W. (1991). *De basiskustlijn, een technisch/morfologische uitwerking* (Vol. in Dutch). doi: 10.19005/ssmep.10.0{_}13

Morim, J., Hemer, M., Wang, X. L., Cartwright, N., Trenham, C., Semedo, A., ... Andutta, F. (2019). Robustness and uncertainties in global multivariate wind-wave climate projections. *Nature Climate Change*, *9*(9), 711–718. doi: 10.1038/s41558-019-0542-5

Morselt, T. T., Brakel, J., & Van Zanten, M. (2010). *Economische en milieukundige effecten van de zandwinstrategie rapport.* Blueconomy.

Mrzljak, V., & Mrakovčić, T. (2016). Comparison of COGES and Diesel-Electric Ship Propulsion Systems. *Journal of Maritime & Transportation Science*, *Special ed*(1), 131–148. doi: 10.18048/2016-00.131

Mulder, J. P. M. (2000). Zandverliezen in het Nederlandse kustsysteem. Advies voor dynamisch handhaven in de 21ste eeuw.

Mulder, J. P. M., Hommes, S., & Horstman, E. (2011). Implementation of coastal erosion management in the Netherlands. *Ocean and Coastal Management*, *54*(12), 888–897. doi: 10.1016/j.ocecoaman.2011.06.009

Mulder, J. P. M., & Stive, M. J. F. (2011). Zandmotor (sand motor): building with nature. In *25th icid european regional conference, integrated water management for multiple land use in flat coastal areas, groningen, the netherlands, 16-20 may 2011* (p. Paper III-21).

Mulder, J. P. M., & Tonnon, P. K. (2011). " Sand Engine " : Background and design of a mega-nourishment pilot in the Netherlands. *Coastal Engineering Proceedings, 1*(32), 35. doi: 10.9753/icce.v32.management.35

Nauw, J. J., Merckelbach, L. M., Ridderinkhof, H., & van Aken, H. M. (2013). Long-term ferry-based observations of the suspended sediment fluxes through the Marsdiep inlet using acoustic Doppler current profilers. *Journal of Sea Research, 87*, 17–29. doi: 10.1016/j.seares.2013.11.013

Nederhoff, C., Schrijvershof, R., Tonnon, P., & Van der Werf, J. J. (2019). *The Coastal Genesis II Terschelling - Ameland inlet (CGII-TA) model.* Deltares report 1220339-008.

NHV. (1998). *Water in the Netherlands.* Netherlands Hydrological Society.

Nidzieko, N. J., & Ralston, D. K. (2012). Tidal asymmetry and velocity skew over tidal flats and shallow channels within a macrotidal river delta. *Journal of Geophysical Research: Oceans, 117*(3). doi: 10.1029/2011JC007384

Noortwijk, J. M. v., & Peerbolte, E. B. (2000). Optimal sand nourishment decisions. *Journal of Waterway, Port, Coastal, and Ocean Engineering, 126*(1), 30–38. doi: 10.1061/(asce)0733-950x(2000)126:1(30)

Oertel, G. F. (1988). Processes of sediment exchange between tidal inlets, ebb deltas and barrier islands. In *Hydrodynamics and sediment dynamics of tidal inlets* (pp. 297–318). New York, NY: Springer New York. doi: 10.1007/978-1-4757-4057-8{_}17

Olmer, N., Comer, B., Roy, B., Mao, X., & Rutherford, D. (2017). Greenhouse gas emissions from global shipping, 2013-2015. *The International Council on Clean Transportation*, 1–25.

Parkinson, R. W., & Ogurcak, D. E. (2018). Beach nourishment is not a sustainable strategy to mitigate climate change. *Estuarine, Coastal and Shelf Science, 212*, 203–209. doi: 10.1016/j.ecss.2018.07.011

Payo, A., Favis-Mortlock, D., Dickson, M., Hall, J. W., Hurst, M. D., Walkden, M. J., . . . Ellis, M. A. (2017). Coastal modelling environment version 1.0: A framework for integrating landform-specific component models in order to simulate decadal to centennial morphological changes on complex coasts. *Geoscientific Model Development, 10*(7), 2715–2740. doi: 10.5194/gmd-10-2715-2017

Petroliagkis, T. I., Voukouvalas, E., Disperati, J., & Bidlot, J. (2016). *Joint probabilities of storm surge, significant wave height and river discharge components of coastal flooding events.* Report EUR 27824. Retrieved from `https://core.ac.uk/download/pdf/38632343.pdf` doi: doi:10.2788/677778

Rakhorst, H. (1984). *Werking strandhoofden Noord-Holland, Texel, Vlieland. Nota WWKZ-84.H007.* Hoorn: Ministry of Transport and Public Works.

Rakhorst, H., Roelse, P., Van der Heide, P., & Maas, C. (2001). *De functie van strandhoofden langs de Noord-Hollandse kust.*

Ranasinghe, R., Swinkels, C., Luijendijk, A. P., Roelvink, D. J. A., Bosboom, J., Stive, M. J. F., & Walstra, D. J. R. (2011). Morphodynamic upscaling with the MORFAC approach: Dependencies and sensitivities. *Coastal Engineering, 58*(8), 806–811. doi: https://doi.org/10.1016/j.coastaleng.2011.03.010

Rijkswaterstaat. (n.d.). *Rijkswaterstaat Waterinfo.* Retrieved from `https://waterinfo.rws.nl/#!/nav/`

Rijkswaterstaat. (1988). *Handboek Zandsuppleties* (K. Pilarczyk, H. Verhagen, P. Roelse, L. Adriaanse, & J. Consemulder, Eds.). Delft: Waltman. doi: 10.1016/0378-3839(89)90017-3

Rijkswaterstaat. (1993). *Two-dimensional horizontal coastal flow model.* Den Haag.

Rijkswaterstaat. (2015). *Building with Nature.* Retrieved from `https://www.rijkswaterstaat.nl/english/water/projects/building-with-nature/index.aspx`

Rijkswaterstaat. (2019a). Derde actualisatie suppletieprogramma 2016-2019.

Rijkswaterstaat. (2019b). *Kustlijnkaarten 2020.* Rijkswaterstaat report WVL0120ZB47.

Rijkswaterstaat. (2019c). *Kustonderhoud Callantsoog vanaf 9 september 2019 van start.* Retrieved from `https://www.rijkswaterstaat.nl/nieuws/archief/2019/09/kustonderhoud-callantsoog-vanaf-9-september-2019-van-start`

Rijkswaterstaat. (2021). Kustgenese 2.0: kennis voor een veilige kust.

Roberts, T. M., Wang, P., & Puleo, J. A. (2013). Storm-driven cyclic beach morphodynamics of a mixed sand and gravel beach along the Mid-Atlantic Coast, USA. *Marine Geology, 346,* 403–421. Retrieved from `http://dx.doi.org/10.1016/j.margeo.2013.08.001` doi: 10.1016/j.margeo.2013.08.001

Roelse, P. (2002). *Water en zand in balans.* Rijksinstituut voor Kust en Zee.

Roelvink, D. J. A., Ruessink, B. G., Van der Kaaij, T., & Bos, K. J. (2001). *Inceptierapport perceel 2. Mare.* WL Delft.

Roelvink, D. J. A., & Stive, M. J. F. (1989). Bar-generating cross-shore flow mechanisms on a beach. *Journal of Geophysical Research, 94*(C4), 4785–4800. doi: 10.1029/JC094iC04p04785

Roelvink, D. J. A., Van Dongeren, A., McCall, R., Hoonhout, B. M., Van Rooijen, A., Van Geer, P., ... Quataert, E. (2015). *XBeach technical reference: Kingsday release.* Deltares.

Roelvink, D. J. A., Walstra, D. J. R., Van der Wegen, M., & Rana. (2016). Modelling of coastal morphological processes. In M. R. Dhanak & N. I. Xiros (Eds.), *Springer handbook of ocean engineering* (pp. 611–634). Springer, Cham.

Royal IHC. (2016). *World's first LNG-powered hopper dredger launched.* Retrieved from `https://www.royalihc.com/en/news/worlds-first-lng-powered-hopper-dredger-launched`

RVO. (2020). *Windenergie op Zee.* Retrieved from `https://www.rvo.nl/onderwerpen/duurzaam-ondernemen/duurzame-energie-opwekken/woz`

Schwimmer, R. (2007). *Shields diagram.* Retrieved from `https://serc.carleton.edu/NAGTWorkshops/sedimentary/activities/14100.html`

Shields, A. (1936). Anwendung der Aehnlichkeitsmechanik under der Turbulenzforschung auf die Geschiebebewegung. *Preussischen Versuchsanstalt Fur Wasserbau and Schiffbau*(26), 524–526.

Short, A., & Jackson, D. (2013). Beach morphodynamics. *Treatise on Geomorphology, 10,* 106–129.

Sistermans, P. G. (2002). Graded sediment transport by non-breaking waves and a current. *Communications on Hydraulic and Geotechnical Engineering, 2*(2), 1–140.

Smith, E. R., D'Alessandro, F., Tomasicchio, G. R., & Gailani, J. Z. (2017). Nearshore placement of a sand dredged mound. *Coastal Engineering, 126*(May), 1–10. doi: 10.1016/j.coastaleng.2017.05.002

Smits, A., Nienhuis, P., & Saeijs, H. (2006). Changing estuaries, changing views. *Hydrobiologia, 365*(1), 339–355. doi: 10.1007/1-4020-5367-3

Soulsby, R. (1997). *Dynamics of Marine Sands.* London: Thomas Telford.

Spanhoff, R., Biegel, E., Burger, M., & Dunsbergen, D. (2003). *Shoreface nourishments in the Netherlands.* Rijkswaterstaat report PUC_166832_31.

Steetzel, H. J., & De Vroeg, J. H. (1999). *Update and validation of the PonTos model.* Delft: Joint venture Alykon Hydraulic Consultancy & Research - WL, Delft Hydraulics.

Stive, M. J. F. (1989). *Voorspelling ontwikkeling kustlijn 1990-2090.* Den Haag: Rijkswaterstaat.

Stive, M. J. F., De Schipper, M. A., Luijendijk, A. P., Ranasinghe, R., Van Thiel de Vries, J., Aarninkhof, S. G. J., ... Marx, S. (2013). The Sand Engine: A Solution for Vulnerable Deltas in the 21st century? In *Coastal dynamics 2013: 7th international conference on coastal dynamics, arcachon, france, 24-28 june 2013* (pp. 1537–1546).

Stive, M. J. F., & Eysink, W. D. (1989). *Voorspelling ontwikkeling kustlijn 1990 - 2090, fase 3. Deelrapport 3.1.*

Stive, M. J. F., Nicholls, R., & De Vriend, H. J. (1991). Sea-level rise and shore nourishment: a discussion. *Coastal Engineering*, *16*(1), 147–163. doi: 10.1016/0378-3839(91)90057-N

Stronkhorst, J., Huisman, B., Giardino, A., Santinelli, G., & Santos, F. D. (2018, 4). Sand nourishment strategies to mitigate coastal erosion and sea level rise at the coasts of Holland (The Netherlands) and Aveiro (Portugal) in the 21st century. *Ocean and Coastal Management*, *156*, 266–276. doi: 10.1016/j.ocecoaman.2017.11.017

Swamee, P., & Jain, A. (1996). Explicit equations for pipe flow problems. *Journal of the Hydraulics Division*, *102*(5), 657–664.

Tomasicchio, G. R., D'Alessandro, F., Barbaro, G., & Malara, G. (2013). General longshore transport model. *Coastal Engineering*, *71*, 28–36. Retrieved from `http://dx.doi.org/10.1016/j.coastaleng.2012.07.004` doi: 10.1016/j.coastaleng.2012.07.004

Tong, W. (2010). *Wind power generation and wind turbine design.* Southampton: WIT Press.

Tonnon, P. K., Huisman, B., Stam, G. N., & van Rijn, L. C. (2018). Numerical modelling of erosion rates, life span and maintenance volumes of mega nourishments. *Coastal Engineering*, *131*, 51–69. doi: 10.1016/j.coastaleng.2017.10.001

Tonnon, P. K., Van der Werf, J. J., & Mulder, J. P. M. (2009). *Morfologische berekeningen MER zandmotor.* Deltares report 1201001-000.

Van de Graaff, J. (1984). *Leidraad voor de beoordeling van de veiligheid van duinen als waterkering* (Tech. Rep.). 's-Gravenhage: Technische Adviescommissie voor de Waterkeringen.

Van den Berg, G. P. (2004). Effects of the wind profile at night on wind turbine sound. *Journal of Sound and Vibration*, *277*(4-5), 955–970. doi: 10.1016/j.jsv.2003.09.050

Van de Rest, P. (2004). *Morfodynamica en hydrodynamica van de Hollandse kust.* MSc Thesis, TU Delft.

Van der Hout, C., Tonnon, P., & De Ronde, J. (2009). *Morphological effects of mega-nourishments: Using MOHOLK model for understanding effects of mega-nourishments in the areas around North Holland and Marsdiep.* Deltares report 1200659-000.

Van der Spek, A. J. F., Kruif, A. C., & Spanhoff, R. (2007). *Richtlijnen onderwatersuppleties.*

Van der Steen, F. (2015). *Sediment transport directions by infragravity waves in the surf zone at the Sandmotor.* MSc Thesis, Utrecht University.

Van Duin, C. F., Vrij Peerdeman, M., Jaspers, H., & Buchoic, A. (2017). *Winning suppletiezand 2018 t/m 2027.* De Bilt.

Van Duin, M. J. P., Wiersma, N., Walstra, D. J. R., Van Rijn, L. C., & Stive, M. J. F. (2004). Nourishing the shoreface: Observations and hindcasting of the Egmond case, The Netherlands. *Coastal Engineering*, *51*(8-9), 813–837. doi: 10.1016/j.coastaleng.2004.07.011

Van Hugten, M. P. (2019). *The Effects of a continuous nourishment on the physical behaviour of the Dutch coastline.* MSc Thesis, TU Delft.

Van Koningsveld, M., Mulder, J. P. M., Stive, M. J. F., Van der Valk, L., & Van der Weck, A. W. (2008). Living with sea-level rise and climate change: A case study of the Netherlands. *Journal of Coastal Research*, *24*(2), 367–379. doi: 10.2112/07A-0010.1

Van Oeveren, C., Oost, A., Nolte, A., Van der Werf, J. J., Tonnon, P. K., Grasmeijer, B., . . . Van der Spek, A. J. F. (2020). *Kustgenese 2.0 - Integrale synthese* (Tech. Rep.). Deltares. 1220339-009-ZKS-0008.

Van Onselen, E., & Vermaas, T. (2020). *Analyse geulwandsuppletie Ameland zuidwest.* Deltares report 11205236-002.

Van Rijn, L. C. (1993). *Principles of sediment transport in rivers, estuaries and coastal seas.* Amsterdam: Aqua Publications.

Van Rijn, L. C. (1995). *Sand budget and coastline changes of central coast of Holland.* WL Delft Hydraulics report H2129.

Van Rijn, L. C. (1997). Sediment transport and budget of the central coastal zone of Holland. *Coastal Engineering, 32*(1), 61–90. doi: 10.1016/S0378-3839(97)00021-5

Van Rijn, L. C. (2007). Unified view of sediment transport by currents and waves. II: suspended transport. *Journal of Hydraulic Engineering, 133*(6), 668–689. doi: 10.1061/(asce)0733-9429(2007)133:6(668)

Van Rijn, L. C. (2015). *Sediment import by tidal inlets: SEDBOX-model for tidal inlets Marsdiep and Vlie, Wadden sea, The Netherlands.*

Van Rijn, L. C., Nieuwjaar, M. W. C., van der Kaay, T., Nap, E., & van Kampen, A. (1993). Transport of Fine Sands by Currents and Waves. *Journal of Waterway, Port, Coastal, and Ocean Engineering, 119*(2), 123–143. doi: 10.1061/(asce)0733-950x(1993)119:2(123)

Van Rijn, L. C., Ruessink, B. G., & Mulder, J. P. M. (2002). *Coast3D - Egmond: the behaviour of a straight sandy coast on the time scale of storms and seasons: process knowledge and guidelines for coastal management: end document, March 2002.* Amsterdam: Aqua Publications.

Van Rijn, L. C., & Walstra, D. J. R. (2004). *Analysis and modelling of shoreface nourishments* (Vol. 148). WL Delft Hydraulics report Z3748.20.

Van Rijn, L. C., Walstra, D. J. R., & van Ormondt, M. (2007). Unified View of Sediment Transport by Currents and Waves. IV: Application of Morphodynamic Model. *Journal of Hydraulic Engineering, 133*(7), 776–793. doi: 10.1061/(asce)0733-9429(2007)133:7(776)

Van Weerdenburg, R., & Van der Werf, J. J. (2021). *Transportpaden in de Schelde-monding.* Delft.

Veerman, C., Bakker, I., Van Duijn, J., Fresco, L., Heidema, A., Kabat, P., ... Stive, M. J. F. (2008). *Working together with water.* Deltacommissie.

Verbrug, G. (2008). *Natura 2000-gebied Noordzeekustzone.* Ministry of Agriculture, Nature and Food Quality.

Verhagen, H. (1990). Coastal Protection and Dune Management in the Netherlands. *Journal of Coastal Research, 6*(1), 169–179.

Vikolainen, V. (2012). *Nature at Work: The feasibility of Building with Nature projects in the context of EU Natura 2000 implementation.* PhD Thesis, University of Twente.

Visser, P. (2014). *Short Term Morphological Impact of the Eierlandsedam.* MSc Thesis, TU Delft.

Vlasblom, W. J. (2003). *Designing Dredging Equipment.* Delft: Delft University of Technology.

Walstra, D. J. R., Ormondt, M. v., & Roelvink, D. J. A. (2004). *Shoreface nourishment scenarios: Detailed morphodynamic simulations with Delft3D for various shoreface nourishment designs.* Deltares report Z3748.21.

Wang, Z., Elias, E. P. L., Van der Spek, A. J. F., & Lodder, Q. J. (2018, 9). Sediment budget and morphological development of the Dutch Wadden Sea: Impact of accelerated sea-level rise and subsidence until 2100. *Geologie en Mijnbouw/Netherlands Journal of Geosciences, 97*(3), 183–214. doi: 10.1017/njg.2018.8

Wenneker, I., Spelt, B., Peters, H., & De Ronde, J. (2016). Overview of 20 years of field measurements in the coastal zone and at the Petten sea dike in the Netherlands. *Coastal Engineering, 109*, 96–113. doi: 10.1016/j.coastaleng.2015.12.009

Wiberg, P. L., & Sherwood, C. R. (2008). Calculating wave-generated bottom orbital velocities from surface-wave parameters. *Computers and Geosciences, 34*(10), 1243–1262. doi: 10.1016/j.cageo.2008.02.010

Winant, C. D., Inman, D. L., & Nordstrom, C. E. (1975). Description of seasonal beach changes using empirical eigenfunction. *Journal of Geophysical Research, 80*(15), 1979–1986.

Wiser, R., & Bolinger, M. (2008). *Annual report on U.S. wind power installation, cost, and performance trends: 2007* (Tech. Rep.). Washington: U.S. Department of Energy.

Wolinsky, M. A., & Brad Murray, A. (2009). A unifying framework for shoreline migration: 2. Application to wave-dominated coasts. *Journal of Geophysical Research: Earth Surface*, *114*(1), 1–13. doi: 10.1029/2007JF000856

Woodacre, J., Bauer, R., & Irani, R. (2015). A review of vertical motion heave compensation systems. *Ocean Engineering*, *104*, 140–154. doi: 10.1016/j.oceaneng.2015.05.004

Yang, S., Li, M., Dai, S., Liu, Z., Zhang, J., & Ding, P. (2006). Drastic decrease in sediment supply from the Yangtze River and its challenge to coastal wetland management. *Geophysical Research Letters*, *33*(6), 4–7. doi: 10.1029/2005GL025507

Yin, J., Hong, G., Zhou, Z., & Shu, M. (2020). Experimental study on dynamic response characteristics of trailing suction dredger under medium and long period waves. *Proceedings of the International Offshore and Polar Engineering Conference*, *2020-Octob*, 8–12.

Zijl, F., & Groenenboom, J. (2019). *Development of a sixth generation model for the NW European Shelf (DCSM-FM 0.5nm).*

Zijl, F., Sumihar, J., & Verlaan, M. (2015). Application of data assimilation for improved operational water level forecasting on the northwest European shelf and North Sea. *Ocean Dynamics*, *65*(12), 1699–1716. doi: 10.1007/s10236-015-0898-7

Zijl, F., Veenstra, J., & Groenenboom, J. (2018). *The 3D Dutch Continental Shelf Model - Flexible Mesh (3D DCSM-FM).* Deltares report 1220339-000.

Zijl, F., Verlaan, M., & Gerritsen, H. (2013). Improved water-level forecasting for the Northwest European Shelf and North Sea through direct modelling of tide, surge and non-linear interaction. *Ocean Dynamics*, *63*(7), 823–847. doi: 10.1007/s10236-013-0624-2

<div align="right">

A

</div>
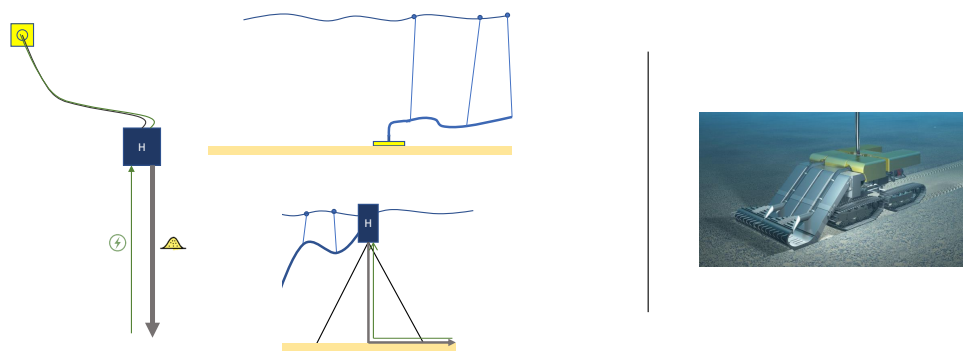
<div align="right">

Mining options

</div>

A.1. Sandcrawler

Figure A.1: Illustration of the crawler concept. The right figure is adopted from Blue Mining (2018).

The concept
The sandcrawler could be seen as a vacuum cleaner that can manoeuvre on the seafloor. Since the 1970s, companies have been busy developing deep-sea mining machines that can operate at large depths (Knodt et al., 2016). Currently, Royal IHC is developing such a machine that should be capable of mining offshore minerals at depths up to 6,000 m (Blue Mining, 2018). With a dimension of 16 x 24 m, it should be capable of mining 400 tons of nodules each hour, scraping 0.03 km^2 of sea surface per hour. As Royal IHC is one of the partners of Sweco in the development of the Sandwindmill, the technology used for the mining crawler could be used for the development of a sandcrawler. The blue mining crawler is well capable of separating the minerals from the sediment, where the minerals are being pumped towards the surface and most of the sediment is deposited behind the crawler. The sandcrawler could be significantly simplified compared to the mining crawler, as it has to operate at much smaller depths, would have to mine smaller quantities and would not need to separate substances.

The dredged material can be transported towards a hub through a flexible floating pipeline. From this hub, submerged hard pipelines can transport the mined sediment towards the coastline. This hub is also connected to the windmill through an electricity cable, which continues along the flexible pipeline towards the crawler. If it is possible to mine in the vicinity of windmills, the hub can be installed at the windmill itself, which would be operationally and financially beneficial.

The operability
The operability of the mining equipment can be highly dependent on the weather conditions. Heavy storms

can impede the workability of systems operating at the sea surface. As the sand crawler operates fully under water, it is expected that such harsh conditions will hardly influence the amount of operational hours for the mining. Orbital velocities from waves do have an effect on the bottom (Wiberg & Sherwood, 2008). Using linear wave theory, for small-amplitude and monochromatic waves, the velocity at the bottom can be found through:

$$u_b = \frac{\omega_r a}{sinh(kh)} = \frac{H\pi}{Tsinh(kh)} \tag{A.1}$$

where:
- u_b bottom orbital velocity [m/s]
- ω_r radian frequency [rad/s]
- a   wave amplitude [m]
- k   wave number [rad/m]
- T   wave period [s]
- H   wave height [m]

From this equation it can be seen that long waves induce larger velocities, and that the orbital velocity at the bottom scales linearly with the wave height. At 20 m depth, u_b for a wave of 1 m height ranges from 0.1 - 0.3 m/s for waves of T = 6 - 14 s, respectively. For high waves with H = 5 m, the maximum orbital at 20m depth would be around 1.5 m/s. It may be expected that a crawler can be weighted such, that it can withstand these velocities. There is almost no upper limit of wave heights that restrict the operability. The lower limit of the operability is determined by the availability of wind power. The capacity of the windmill can influence this lower limit. For this first mining technologies exploration, the assumption is made that the wind blows sufficiently 50% of the time during the year. This is the starting point that's being used by the Sandwindmill consortium. In sections 3.4 and 3.5, the power requirements and delivery will be analyzed more in-depth.
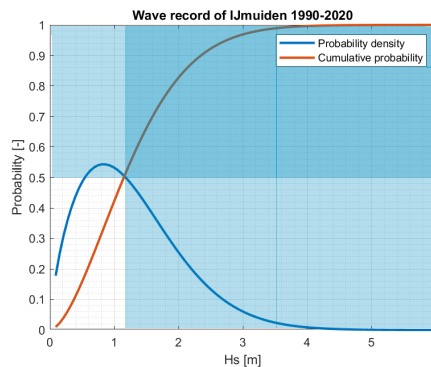
Figure A.2: The operability of the Sandcrawler is 50%, assuming a lower limit of 50% induced by the limited energy availability.

The costs

For the costs one can look at the capital expenditures (CAPEX) and the operational expeditures (OPEX). The CAPEX of the blue nodules crawler are fairly high when its purpose is not the mining of precious minerals (personal communication with Wiebe Boomsma, Royal IHC). As concluded in the explanation of the concept, simplifications to the system relative to the deep-sea crawler could be made, leading to a possible reduction of the CAPEX. These simplifications will require more RD, of which the costs could be earned back if numerous crawlers can be sold for multiple (global) nourishment applications. In order to size the market for a continuous nourishment system, an analysis of the nourishment activity around the world is needed. The CAPEX are scored to be 4/5. With regards to the OPEX, the crawler scores better. The OPEX are expected to mainly be a function of the required amount of personnel and maintenance cost. As the crawler could be operated from a distance, no full-time personnel would be needed on-site. The crawler would need a remote full-time operation as well as regular maintenance. As the equipment is rather small, the maintenance cost themselves could be on the lower side. The OPEX are thus scored at 3/5.
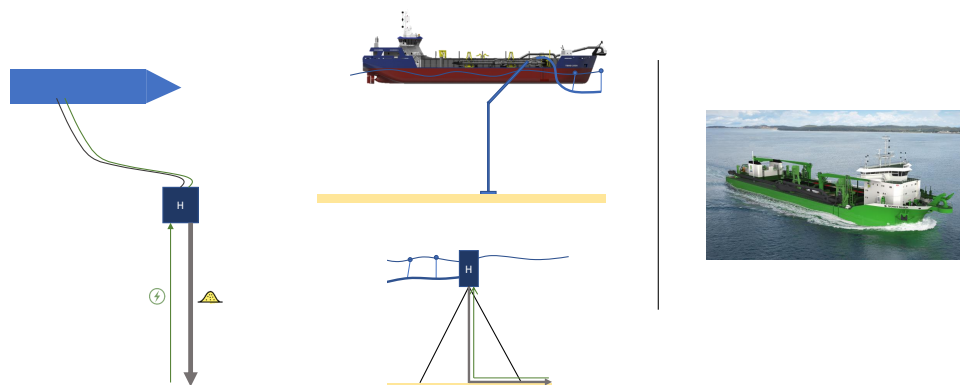
A.2. Operated winning vessel

Figure A.3: The winning vessel concept (Electrical TSHD type). Right figure adopted from Deme (2018).

The concept

The second method of mining the sediment is by the use of an existing type of winning vessel. The winning vessel could be manufactured fully electric, hybrid or diesel-powered. Types of winning vessels that are suitable for deeper, offshore dredging of sandy material are trailing suction hopper dredgers (TSHDs), cutter suction dredgers (CSD) and plain suction dredgers (PSD) (Vlasblom, 2003).

The advantage of the use of such dredgers is that they are built for the purpose of dredging on the open sea. Such vessels can withstand fairly harsh conditions and their technology has already been developed and proven for many decades. This latter is a large advantage compared to the sandcrawler. The advantage of the use of a TSHD is that the hopper could be used as a sediment buffer. In stormy conditions, there will be too high waves to dredge material. However, there will be an abundance of wind to power the system, as well as the capacity nearshore to distribute sediment due to the high waves. The hopper can also be used to increase weight and reduce the motion response to waves (Yin et al., 2020).

As the (continuous) nourishments will be executed for a large period during the year, the vessels will be out in open sea for a rather long time. This could lead to fatigue of the hull due to the harsh North Sea conditions. This is a well-known issue for floating production and storage units (FPSOs), which are often older vessels that have been transformed (Bultema et al., 2000). There are multiple reasons for this fatigue. Maintenance on regular moving vessels is easier, as they can be dry-docked or maintained in a calm harbor. Furthermore, moving vessels can avoid storms, whereas this is not always possible for a (semi-)stationary vessel. For that reason, FPSOs are often fortified drastically. It should be investigated to which extent a dredging vessel with the purpose of executing a continuous nourishment should be reinforced.

Another advantage of the use of an existing type of equipment, is that it provides the opportunity to use second-hand vessels, which would reduce the CAPEX. As the main goal of the Sandwindmill is providing a carbon-neutral alternative to traditional dredging, these vessels should be transformed to hybrid or full-electric. A pro would be if the vessel that will be used is already driven by diesel-electric propulsion systems. In such systems, diesel engines supply electric generators, which provide energy to the propulsion system and pumps (Mrzljak & Mrakovčić, 2016). As the entire Sandwindmill system should be 'carbon-neutral', the generators could be supplied by wind energy.

In order for a full-electric semi-permanent vessel to shelter during storms, battery capacity should be available to navigate the vessel to a safe harbour. In Section 3.5, battery capacity as an energy buffer is discussed. Using the installed battery capacity for both dredging support and self-sufficient sailing would be a valuable combination.

The operability

Regardless of whether a permanent or semi-permanent dredger is used, operation under the harshest conditions will be impossible. For the former, the systems will be shut down and the semi-permanent vessel could sail back to the nearest harbour to seek shelter. The ships would anchor and wait until the conditions become milder. Typical operational limits for a smaller-sized TSHD (4,500 m^3) are Hs = 2.5 m (Boskalis, 2010). High wind velocities and long waves can also impede the operational times (Healy et al., 2013). This leads to limited operational times for the vessels, see Figure A.4. Due to their smaller size, cutter suction dredgers and plain suction dredgers will have smaller operational times than the TSHDs.
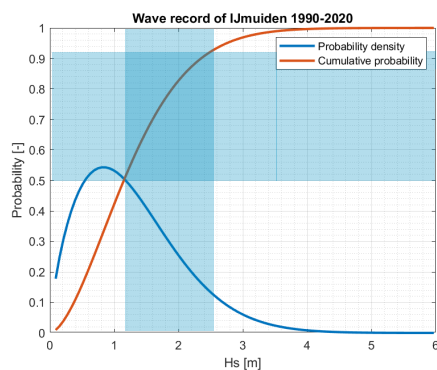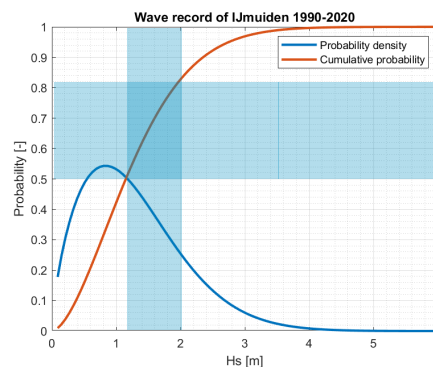

Figure A.4: The operability of an operated winning vessel will be approximately 40%, assuming a lower limit of 50% induced by the limited energy availability.

The costs

The new price of a smaller cutter dredger or a TSHD is higher than the new price of the crawler (CIRIA, 2009). Extra costs for electrification and reinforcement will apply. Buying and reinforcing used vessels might be financially more attractive, as the electrification and reinforcement should be executed on both new and used vessels. Including adaptations, the CAPEX are in the highest category (5/5). The OPEX of operated vessels will be also very significant, especially for the TSHDs which typically accommodate 14 staff members (Royal IHC, 2016). As two crews would be needed that change shifts, this would mean that the operation of the vessel may already cost 28 full time equivalents (FTE). Also the maintenance cost of the fairly large vessels could be higher than for the smaller alternatives. The OPEX are thus also scored 5/5.

A.3. Dredging raft
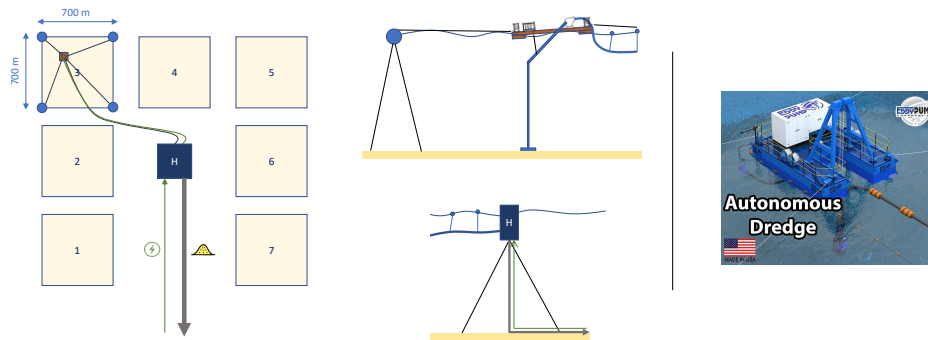
Figure A.5: Visualisation of the dredging raft concept. The right figure adopted from Eddy Pump (n.d.).

The concept
The last mining concept is the dredger raft. Compared to the other concepts, it is mechanically relatively simple. A raft is being placed between four buoys and is connected to these buoys through cables. The buoys are anchored to the seafloor. Winches aboard of the raft are connected to the cables, such that they can manoeuvre the raft between the buoys. This system allows for easy navigation of the raft. The raft carries the pumps and the suction head. The small raft will be subject to both seas and swells. Thorough active heave compensators or motion compensation systems would therefore be necessary, allowing compensation for most sea states. Optimization of the performance of such systems can be achieved by including heave prediction to the system (Woodacre et al., 2015). When dredging a 4m layer of sand and placing the buoys 700m apart, 2 Mm^3 can already be nourished. In the Netherlands, nourishing more than 2m of sediment thickness is only allowed 2km beyond the 20m depth line (Briene et al., 2011). After the dredging of the assigned area has been completed, the buoys and raft can be relocated to another designated area. An advantage of the dredging raft opposed to the crawler with regards to maintenance, is that almost all of the mechanical equipment is above the sea level.

The operability
As the dredging raft is much smaller than the operated vessels, it will be more susceptible to waves. The raft must not only be built such that it does not capsize during the harshest conditions at the location where it is applied. It must also be large enough to be able to operate sufficiently. Affordable active compensation systems can help increase the operability, operating at waves with Hs up to 2.5m (personal communication, Adriaan de Ruiter, Ampelmann). As such systems are designed for larger, more stable vessels, it is assumed here that compensation should work for waves up to 2 m.

Figure A.6: The operability of an operated winning vessel will be approximately 30%, assuming a lower limit of 50% induced by the limited energy availability.

The costs

As the raft is much smaller than the on-site-operated vessels, it is expected that the CAPEX are much lower. The CIRIA (2009) indicates the price for the largest type of a dismountable cutter dredger is approximately 30% of the price of a small TSHD. As such vessels are mainly designed for river-use, adaptations and fortifications should be made to make it seaworthy. Furthermore, the installation of a motion compensation system will cost order 50% of the initial capital costs (personal communication, Adriaan de Ruiter, Ampelmann). As these systems are currently manually (on-site) operated, a challenge to overcome is the automation of the technique. When the system can be remote controlled, the OPEX of the dredging raft could be even lower than the cost of the sandcrawler. The reason for this is that almost all moving parts will be at sea level. Due to this CAPEX thus score 1/5.

A.4. Conclusion

Each of the alternatives has been explored on their (proof of) concept, operability and costs. Based on this examination, scores have been assigned to each criterion. For the proof of concept, the winning vessels score highest as they have been operational for many decades. The sandcrawler is based on a mining crawler that is still in development, whereas the dredging raft is based on a riverine raft that should be fortified significantly. With regards to the costs, the 1-5 scale for the CAPEX and OPEX is reversed, such that the cheapest option scores 5 and the most expensive option scores 1. The same holds for the operability, where the percentage of annual operation time has been used as metric. Over the lifetime of 20 years, the OPEX could be twice as high as the CAPEX for all three technologies (e.g. for the operated vessel 30 FTE · 20 years · €75,000 salary = €45M). Therefore they are weighted double. The weight of the cost is thus three times the weight of the proof of concept and operability, which is a choice made by the writer based on the strong requirement by Rijkswaterstaat of an affordable system. The influence of the proof of concept and operability could be incorporated in the price. The former could be monetized in terms of risk. The relationship between the operability and costs is treated in Section 3.7. Based on this small exploration, it appears as if there is no dominant technology that scores best on all criteria. Based on the current scores and weights, the best option would be the dredging raft. This will be reconsidered when the operability is expressed financially in Section 3.7.

Technology	Proof of concept	Costs CAPEX	OPEX	Operability	Total
Weight	*1*	*1*	*2*	*1*	
Sandcrawler	2	2	3	5	3
Operated winning vessel	5	1	1	3	2.2
Dredging raft	3	4	5	1	3.6

Table A.1: Multi criteria analysis of the different winning options.

The executed exploration is very simplistic. It does give some insight in the drawbacks and possibilities of some mining options, which is the goal of the analysis. Specifically the operational times are of interest, as these influence the moments at which the sediment could be nourished. This timing of the nourishments can have an effect on the distribution of the sediment, which is evaluated in this thesis. The attributed scores and their underlying numbers are based on rough estimations. It is advised to execute an MCA on more winning options and on a more detailed level, supporting the scores with more precise and authentic data. Furthermore, it is advised to take into account more criteria.

B

Representativity analysis

B.1. Wave height

Figure B.1: Significant wave heights measured at IJmuiden munitiestortplaats between 1990 and 2020. The orange figure indicates the data of the year 2017, which is used in the model.

Two measurement stations for waves are being used in this analysis: IJmuiden munitiestortplaats and Eierlandsegat. To see if the wave heights in 2017 are representative for a longer period, the distribution of the heights for each month of 2017 is compared to the distribution of the significant wave height over a period from 1990 to 2020. A fit according to the Weibull distribution has been applied, which is common for the significant wave height (Holthuijsen, 2009). The result of the wave heights at IJmuiden munitiestortplaats is shown in Figure B.2. The distribution of the Eierlandsegat measurements shows the same behaviour.
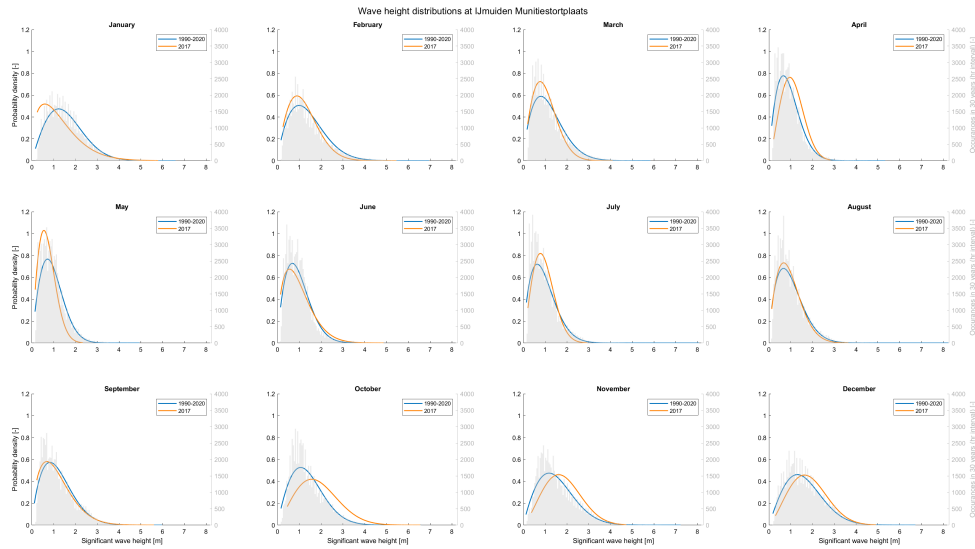
Figure B.2: Comparison of the Weibull distribution of the 2017 wave heights and the waves between 1990 and 2020, separated per month.

What can be deducted from the figure is that the overall shape of the distribution is quite similar for the year 2017 compared to the large dataset. However, 2017 has less frequent occuring large wave heights in the earlier months of the year, whereas the wave heights are more frequently higher in the last months of the year. This indicates that the spreading of the nourished sediment due to waves in January, February and March could be underpredicted by the model, and spreading in October, November and December could be slightly overpredicted by the model. As the spreading of the nourishment in the alongshore direction will also be affected by the directions of the waves, these will be taken into account as well (see equation (2.21)).

B.2. Wave direction

A simple way of comparing wave climates on the wave height, direction and their probability of occurrence is by summarizing the climates in a wave rose, see Figure B.3.

(a) Year 2017.

(b) Years 1990-2021.
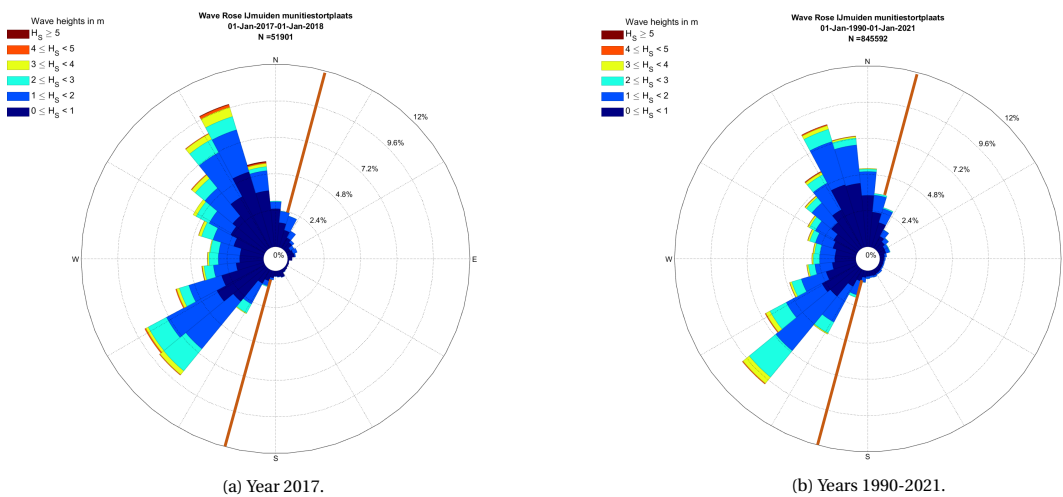
Figure B.3: Wave roses for IJmuiden munitiestortplaats. The orange line indicates the orientation of the coastline at Callantsoog

The wave rose of 2017 shows a great similarity with the wave rose of the 30 year dataset. In 2017 higher waves from the NNW are a bit more present than in the 30 years. This could lead to a larger southward component of the alongshore transport at the Callantsoog coastline. The CERC formula is applied on the data sets to check

if the sediment transports will indeed be more southward directed. Obtaining an outlook on the theoretical transports in 2017 compared to other years can contribute to a better understanding and calibration of the model results.

The wave climate in front of the coast of Callantsoog, derived with a SWAN model, shows more resemblance with the waves measured at IJmuiden than with the waves measured at Eierlandsegat. Therefore the data for this station is used for the sediment transport capacity analysis. As the measurement station is located 37 kilometers offshore at a depth of 24 meters, 50% of the waves measured at the munitiestortplaats can be characterized as deep water waves[5]. The measured waves are transformed towards the nearshore. This is done through the solving the following relations, obtained from Bosboom & Stive (2015). The subscript 'o' stands for 'offshore', the subscript 'b' stands for 'at breaking'.

$$h_b = \frac{H_b}{0.8} \tag{B.1}$$

$$c_0 = 1.56 \cdot T_0 \qquad c_b = \sqrt{g \cdot h_b} \tag{B.2}$$

$$\sin(\phi_b) = \frac{c_b \cdot \sin(\phi_0)}{c_0} \tag{B.3}$$

$$K_r = \sqrt{\frac{\cos(\phi_0)}{\cos(\phi_b)}} \qquad K_{sh} = \sqrt{\frac{1}{\tanh(k \cdot h_b)} \frac{1}{2}} \tag{B.4}$$

$$\left(\frac{2\pi}{T_0}\right)^2 = g \cdot k \cdot \tanh(k \cdot h_b) \tag{B.5}$$

$$H_b = Hs_0 \cdot K_r \cdot K_{sh} \tag{B.6}$$

where:

T_0	mean wave period	[s]
ϕ	wave angle	[-]
K_r	refraction factor	[-]
K_{sh}	shoaling factor	[-]
k	wave number	[rad/m]

The above equations are iterated until convergence of the Hs_b and ϕ_b values, leading to a set of wave heights and directions at breaking. The value of 0.8 in equation is the depth-induced breaker index, based on values from Bosboom & Stive (2015). The wave angles have been corrected for the angle of the Callantsoog coastline. Figure B.4 shows the result of these steps on the wave height and direction. Bosboom & Stive (2015) indicate that due to refraction, the angle of wave incidence around the breaker line is approximately 20°-30°. This is reflected well by the applied approach.

---

[5]When the water depth is larger than half the wave length, waves are assumed to be deep water waves. With known wave periods, through $c_0 = 1.56 T_0$ and $c_0 = \sqrt{\frac{gL_0}{2\pi}}$ the deep water wave length can be determined. Approximately 50% of the waves can be characterized as deep water waves. For simplicity, this characterization is assumed for all waves.
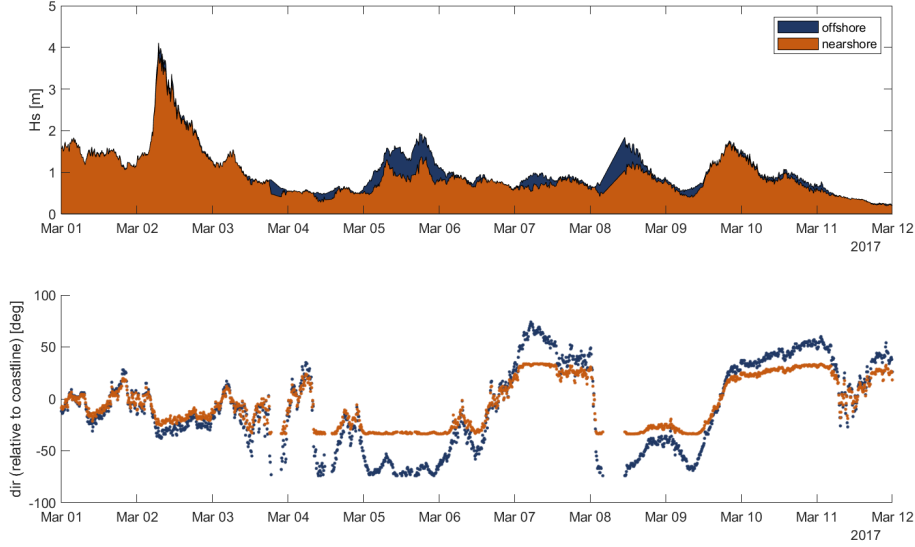
Figure B.4: Transformation of deep water wave conditions towards the point of breaking using the relations given in equations B.1 to B.6

For each month, the wave heights and directions are binned based on their probability of occurrence. For each of these bins, the sediment transport potential is determined using the CERC formula (2.21). The potential of each bin is then multiplied with the probability of occurrence. For each year the monthly transport is summed up and missing data is taken into account. Adapting the number of bins or changing the breaker parameter did not influence the results significantly. As the main interest of this CERC analysis is obtaining a view on the expected behaviour in 2017 and not to exactly calculate the transports, the coefficients are left out. The sediment transport is thus calculated with:

$$S \propto \sin 2\phi_b H_b^{2.5} \tag{B.7}$$

B.3. Limitations of approach

The applied approach has some limitations. The CERC formula does not take wind- and tide-driven currents into account, the latter having a net northward direction for the Dutch coastline due to tidal asymmetry Giardino et al. (2010). The tidal currents in this region are expected to have quite a significant effect on alongshore sediment transports of approximately 40% Van Rijn (1997). The CERC-limitation of not taking grain size into account is irrelevant as the location on which it is applied is constant, hence the grain size is constant. Another limitation of the applied approach is that offshore wave heights are transformed towards the coast, assuming undisturbed propagation towards the domain of interest. From Figure 4.4 it is clear that waves from the NW-NNW could be blocked by the features of the ebb-tidal delta. Especially high waves, responsible for high sediment transports, might break on these features. This sheltering effect is clearly visible when comparing the waves at IJmuiden and Callantsoog (model results), as shown in Figure C.3. These features could also affect the refraction, which has now been estimated with Snell's law. Although measurements of this sheltering are absent, do many researches on ebb-tidal delta and the erosion on the North Holland coast suggest that this sheltering has a significant effect on the local transport rates Elias & Van der Spek (2017); Van Rijn (1997).

C

Supporting information on model set-up

C.1. Model performance on waves

Figures C.1 and C.2 show the modelled and measured wave height and direction at the IJmuiden muni-tiestortplaats and Eierlandsegat measurement buoys.

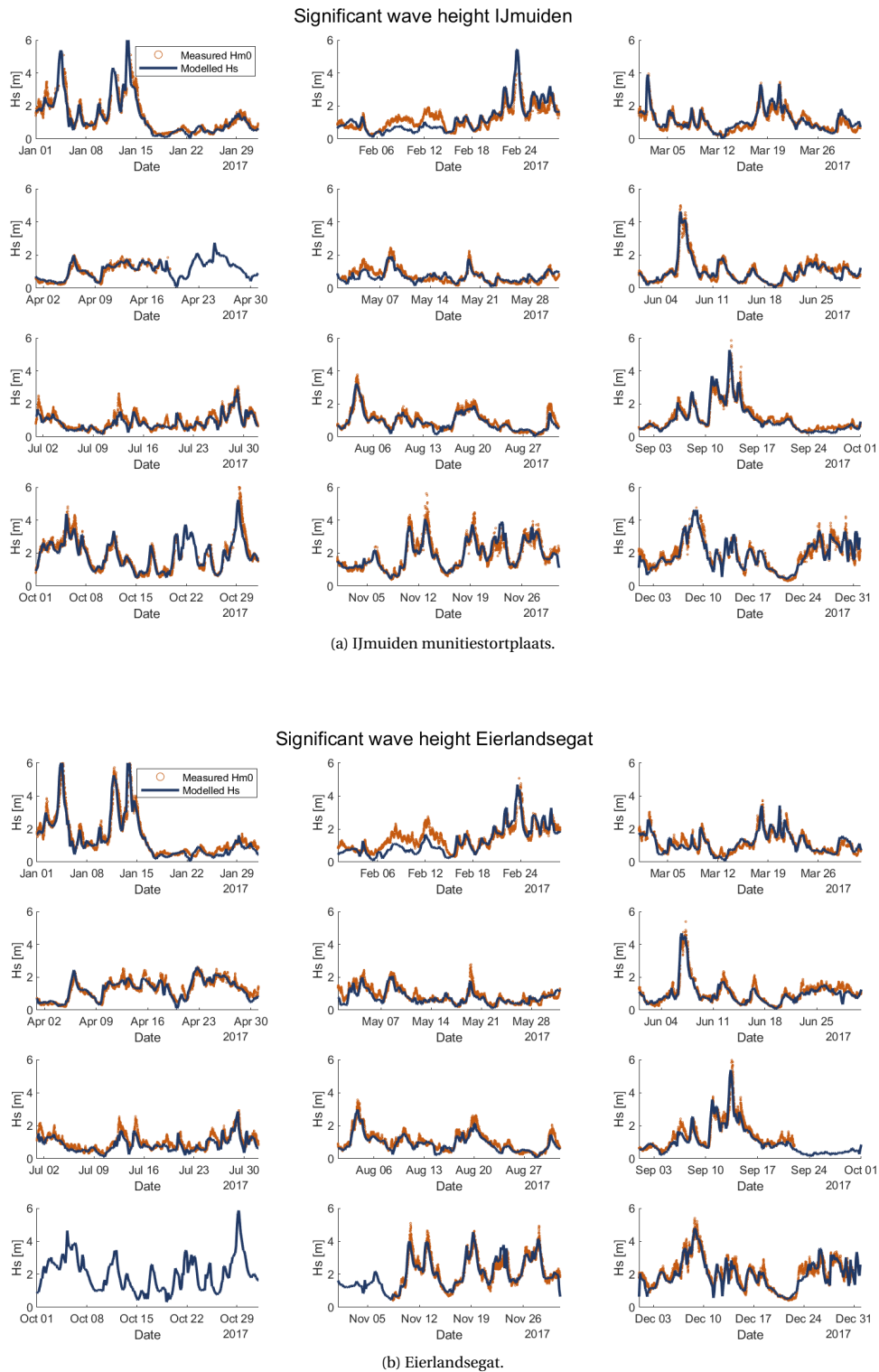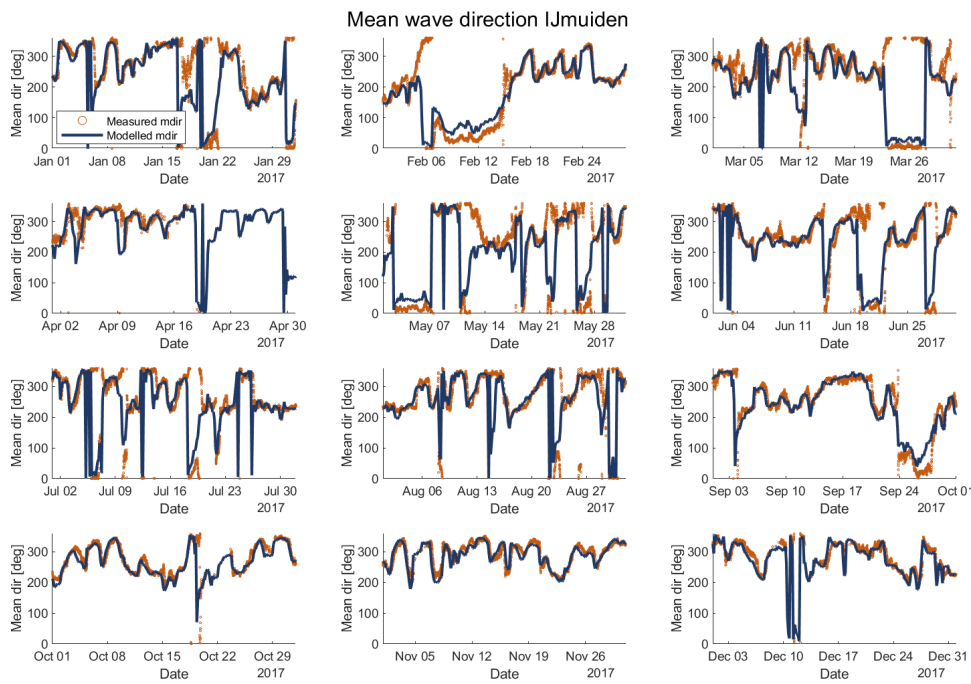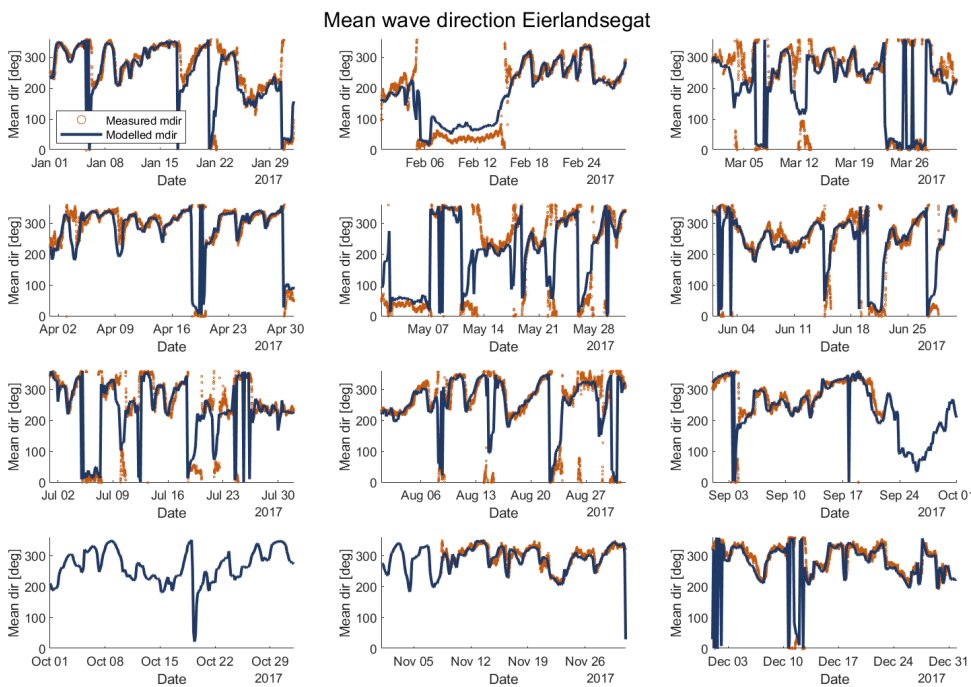(a) IJmuiden munitiestortplaats.

(b) Eierlandsegat.

Figure C.1: Model performance on the wave heights at two locations, separated for each month.

(a) IJmuiden munitiestortplaats.

(b) Eierlandsegat.

Figure C.2: Model performance on wave direction at two locations, separated for each month.

C.2. Wave sheltering

The shallow parts of the ebb-tidal delta near the Marsdiep inlet are capable of breaking the higher NW/NNW waves. This sheltering could reduce the gross southward transports at the northern part of the coast, leading to higher net transports. As there are no nearshore measurements of waves at Callantsoog, this effect cannot be described based on measurements. In Figure C.3, the modelled waves at Callantsoog are compared to measured waves at IJmuiden. The figure indeed shows the sheltering of higher NW waves.
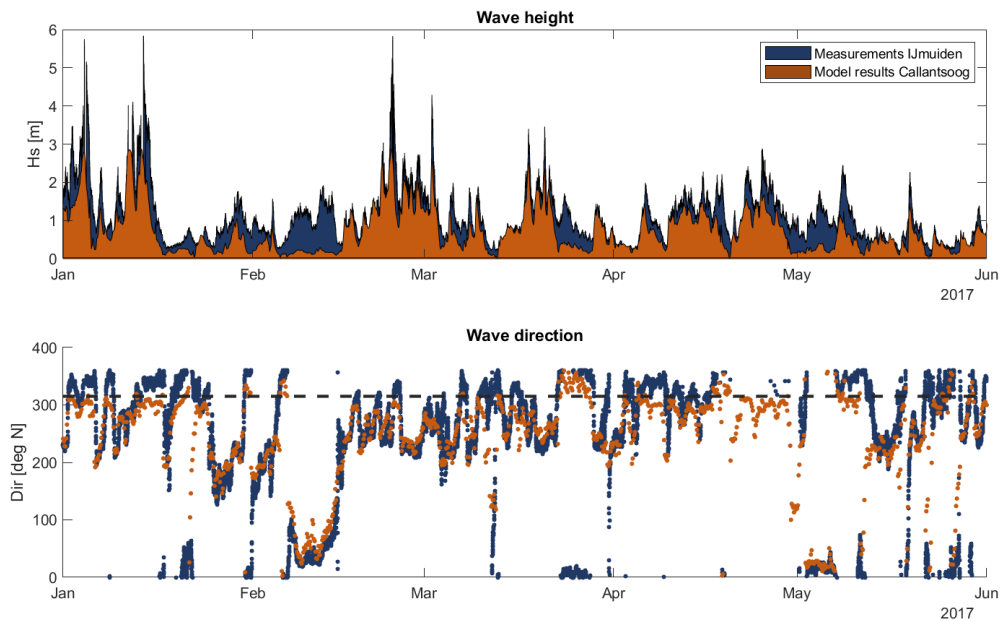
Figure C.3: Comparison of measured waves at IJmuiden munitiestortplaats and modelled waves at Callantsoog (9 m depth). The sheltering due to the Noorderhaaks is clearly visible. Lower waves pass but partly break, higher waves break and come from another direction due to refraction. The black line in the direction figure indicates the NW direction.

C.3. Influence of wind, waves and tides

In Section 5.6.1 it is discussed that the exclusion of waves is not expected to significantly alter the results of the tidal channel nourishment. Figure C.4 shows the development of the cumulative transports through the Marsdiep during NW and SW storm conditions. From this analysis, the inclusion of wind and atmospheric pressure appears to be of significant effect. The effect of waves appears to be smaller. As explained in Section 5.6.1, an increase of transports through the inlet could be due to suspension of sediments of the ebb-tidal delta. This is not expected to affect the dispersion of the channel wall nourishment.

(a) Stormy conditions with NW winds and waves.

(b) Stormy conditions with SW winds and waves.

Figure C.4: The influence of water levels, winds and waves on the sediment transport through the Marsdiep. The 'winds' include a spatiotemporal varying atmospheric pressure.

C.4. Wave roses

The wave roses presented in figure C.5 allow to compare the wave conditions of 2017 to the conditions of the period between 1990 and 2020.
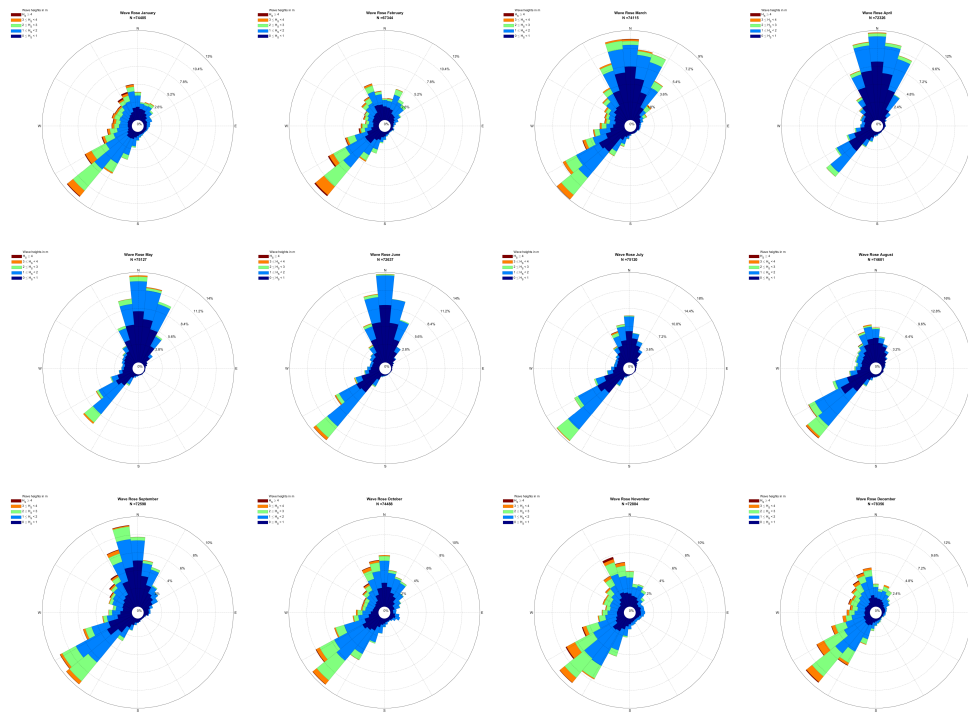
(a) Years 1990 - 2020
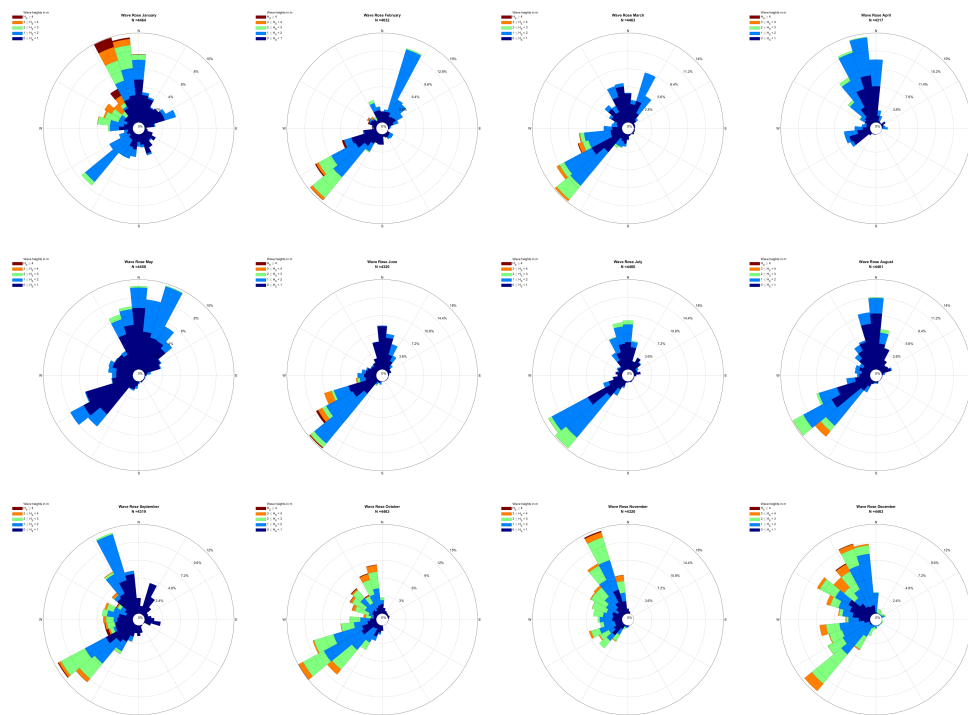
(b) Year 2017

Figure C.5: Wave roses indicating the direction and spreading of wave classes per month.

C.5. Bed slope effect

In Delft3D, the effect of the bed slope is taken into account (Deltares, 2021b). A distinction is made between a longitudinal bed slope and a transverse slope. The longitudinal bed slope is the slope in the direction of the transport that is unaffected by any slopes. The transverse slope is perpendicular to this direction. The longitudinal bed slope influences the bed-load transport as shown in equation C.1.

$$\vec{S'_b} = \alpha_s \vec{S''}$$

(C.1)

where:

$\vec{S'_b}$ vector of bedload transport adjusted for longitudinal bed slope

α_s longitudinal bed slope factor

$\vec{S''}$ vector of bedload transport adjusted

The influence of the longitudinal bed slope is calculated through a formulation by Bagnold, see equation C.2.

$$\alpha_s = 1 + \alpha_{bs} \left(\frac{\tan(\phi')}{\cos(\tan^{-1}(\frac{\partial z}{\partial s}))(\tan(\phi') + \frac{\partial z}{\partial s})} - 1 \right)$$

(C.2)

where:

α_{bs} user-defined tuning parameter [-]

ϕ' internal angle of friction (= 30°) [

$\frac{\partial z}{\partial s}$ bed slope in the direction of the unadjusted bedload vector

The magnitude of the transverse bed slope is added through a formulation based on Ikeda (1982,1988), as presented in equation C.3.

$$S_{b,n} = |S'_b| \alpha_{bn} \frac{u_{b,cr}}{|\vec{u_b}|} \frac{\partial z_b}{\partial n}$$

(C.3)

where:

Sb,n   additional bed-load transport vector, normal to unadjusted transport vector

$|S'_b|$ magnitude of bed-load vector that has been corrected for longitudinal bed slope

α_{bn} user-defined calibration coefficient

$u_{b,cr}$ critical near-bed velocity

$\vec{u_b}$ near-bed velocity vector

$\frac{\partial z_b}{\partial n}$ bed slope normal to unadjusted bedload vector

D

Simulation results

In this appendix, the executed simulations are worked out. The main findings and comparisons are treated in Chapter 5. First, the simulation results of the Marsdiep nourishments are executed. Subsequently, Section D.2 treats the scenarios of the nourishments at Callantsoog. As the base cases (A0 & B0) have been already treated in Chapter 5, they are not included in this appendix. For all analyses, the bed level change relative to a reference simulation without nourishment is indicated, unless specified otherwise. This reference simulation is also referred to as the autonomous behaviour.

D.1. Tidal channel simulations

The analysis of each A-scenario treats both the local and regional development of the bed after the one-year nourishment has been applied. Finally, the implications for the Sandwindmill system are discussed.

D.1.1. Scenario A1: Variable D_{50}

In the A1 scenario two different grain size distributions are used: one with D_{50} = 250 μm and one with D_{50} = 150 μm. As these fractions are transported more easily, a wider distribution is expected compared to A0, where a grain size of D_{50} = 350 μm has been used. This larger dispersion is considered a favourable effect, as it increases the nourishment capacity of the system.

Local morphological behaviour
The resulting cross-sectional profile is quite similar for all nourishment scenarios after one year (Figure D.1). The most pronounced difference is the slightly lower bed level at the nourishment location for the nourishment with the smaller fractions. The depth at the inner nourishment location for the A0 nourishment is 3 meters, whereas the depth for both smaller fractions is approximately 5 meters. The erosion of the deeper part of the channel is a bit smaller for these finer nourishments.
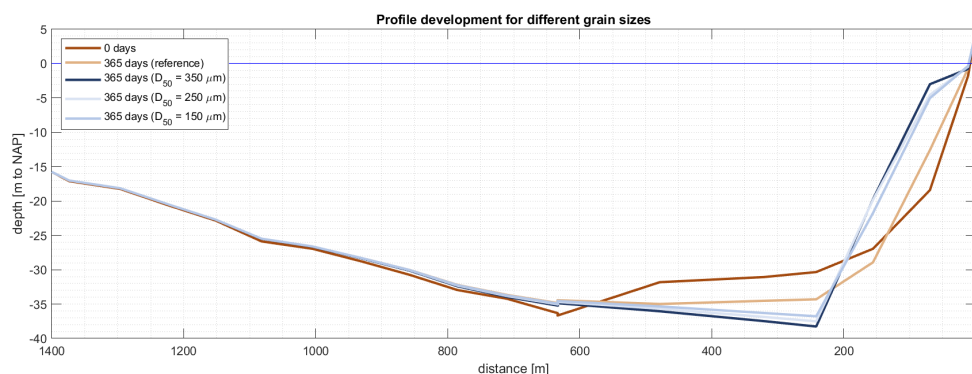
Figure D.1: Comparison of profiles after nourishing with different grain sizes for one year.

The limited difference in the cross shore development for the different grain sizes might be not as expected,

based on the behaviour on a small time scale as shown in Figure 6.6. The initial response suggests twice the bed level growth for the coarsest fraction compared to the finest fraction, whereas the profiles after one year have a an almost equal bed level growth. One explanation of the similar looking profile after one year would be that the changing local hydrodynamics affect both nourishments in a similar manner. For the coarser fractions, this adaptation of the flow evolves in a quicker manner than for the finer fractions. In other words; the coarser fractions reach the equilibrium with the flow after a shorter period, but the equilibrium of the two grain sizes with their flow fields looks approximately similar.

Regional morphological behaviour

Figure D.2 shows the bed level difference after one year between the A0 scenario and the A1 scenarios. As observed in the regional behaviour do the bed levels at the nourishment location and in flood direction increase less for finer sediment fractions. In the ebb direction is the bed level higher for the finer fractions, due to their higher susceptibility to the lower ebb velocities. Especially for the nourishment with the finest fraction it can be observed that the growth of the bed level adjacent to the the Helderse Seawall is significantly larger than for the coarser nourished fractions. As already observed in Figure D.1 is the scouring somewhat less severe for the finer fractions.
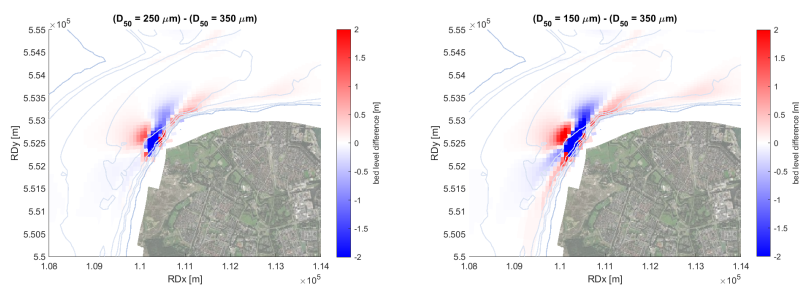
Figure D.2: Relative bed level change compared to D350 run.

The required use of the underlayer method for the finer fractions allows to trace the spreading of these nourished fractions. Figure D.3 shows the mass of sediment in the transport layer after one year, for both fractions. In these figures the larger dispersion for the 150 μm fraction can be very clearly observed. Also the higher southward transport of this fraction by the ebb currents is visible, which could be regarded as a desired effect to feed the coast and compensate for the potential effects of the lee-effect shown in Figure 6.4. Nonetheless does most of this southward transported finer sediment seem to be transported towards the Nieuwe Landsdiep channel, thereby contributing less to coastal safety than when it would have ended up more upward in the profile.
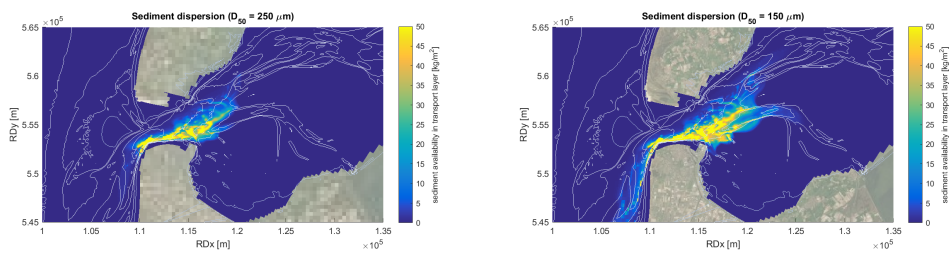

Figure D.3: Availability of nourished sediment in transport layer. Units are in kg/m^2, which converts as 50 kg/m^2 = 3 cm, assuming a porosity of 0.4. For the 250 μm 6.29% of sediment was still available at the nourishment location after a year. For the 150 μm only 5.10% was still at the initial location.

Implications for the Sandwindmill

Compared to the base case, the behaviour of finer grains is distinctive in two manners. First, the First of all, the bed level growth at the nourishment outlet is smaller, as the finer grains are more easily transported away. Secondly, the finer grains have a better ability of reaching the basin, which is one of the nourishment goals.
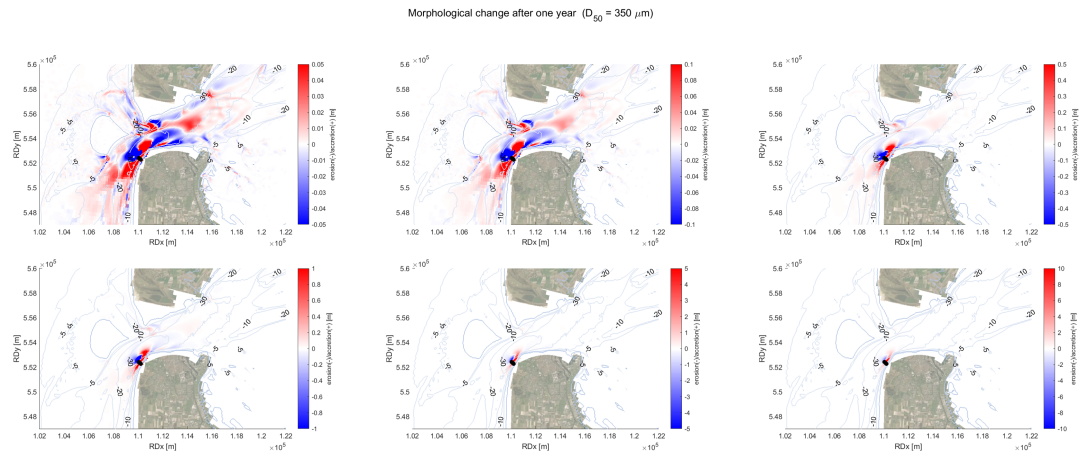
Morphological change after one year (D_{50} = 350 μm)

Figure D.4: Difference in bed development after one year between reference simulation and simulation with a nourishment of D_{50} = 350 μm for different color scales.
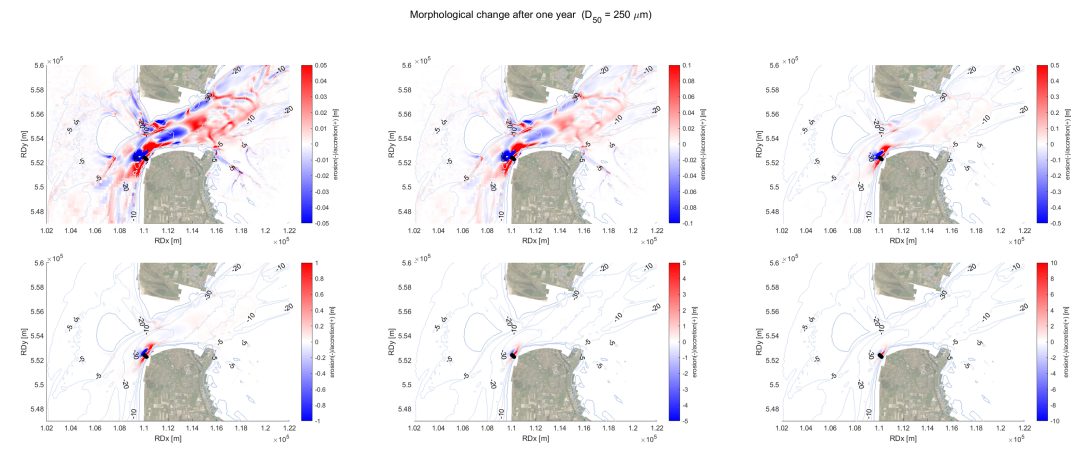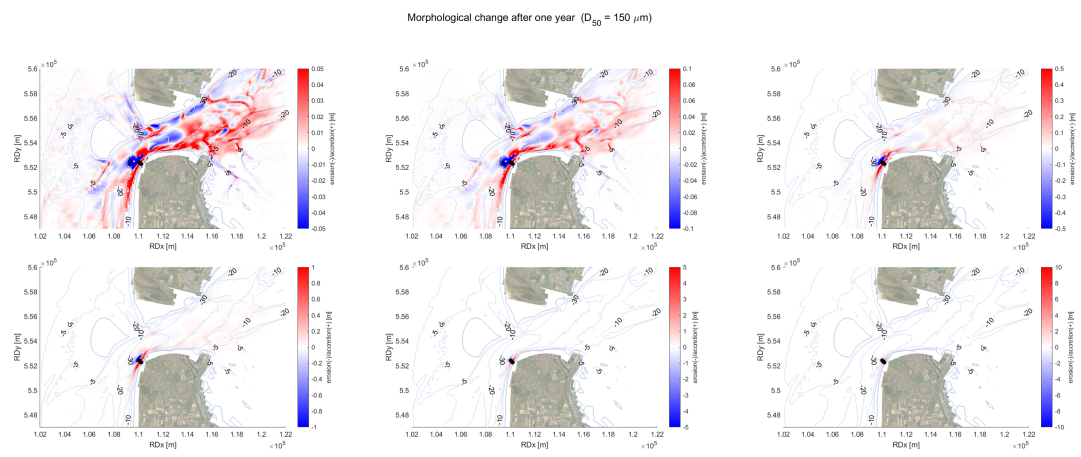
Morphological change after one year (D_{50} = 250 μm)

Figure D.5: Difference in bed development after one year between reference simulation and simulation with a nourishment of D_{50} = 250 μm for different color scales.

Morphological change after one year (D_{50} = 150 μm)

Figure D.6: Difference in bed development after one year between reference simulation and simulation with a nourishment of D_{50} = 150 μm for different color scales.

D.1.2. Scenario A2: Larger discharge

The second scenario treats the system response to a doubling in annual nourishment volume for both outlets. First, the local response is treated. Later on, the regional development and implications for the Sandwindmill system design are discussed.

Local morphological behaviour

The A0 scenario shows the bathymetry moving towards an equilibrium, which is assumed to be partly the result of the changing local hydrodynamics (Figure 6.4). A larger nourishment discharge is expected to lead to higher deposition rates. As the hydrodynamic changes are the result from the changing local bathymetry, a faster development towards an equilibrium can be expected. It is important that this hydrodynamic development is quick enough to ensure that the nourishment does not pile up too much.

From Figure D.7 it can be observed that the natural system is not capable of eroding the large quantity of sediment that is deposited at the X = 75 m location. The asymptotic behaviour appears indeed faster than in the A0 scenario, but the deposition flux is too large for the system to transport it away from the nourishment location. The nourishment at the deeper part (X = 150 m) stays well below the sea level and appears to reach an equilibrium that is well below the sea level.

The channel wall has grown significantly in thickness. Consequently, the adjacent channel erodes much more than in the reference scenario and the previous nourishment scenarios, which can be attributed to the higher flow velocities due to the enhanced constriction of the channel.
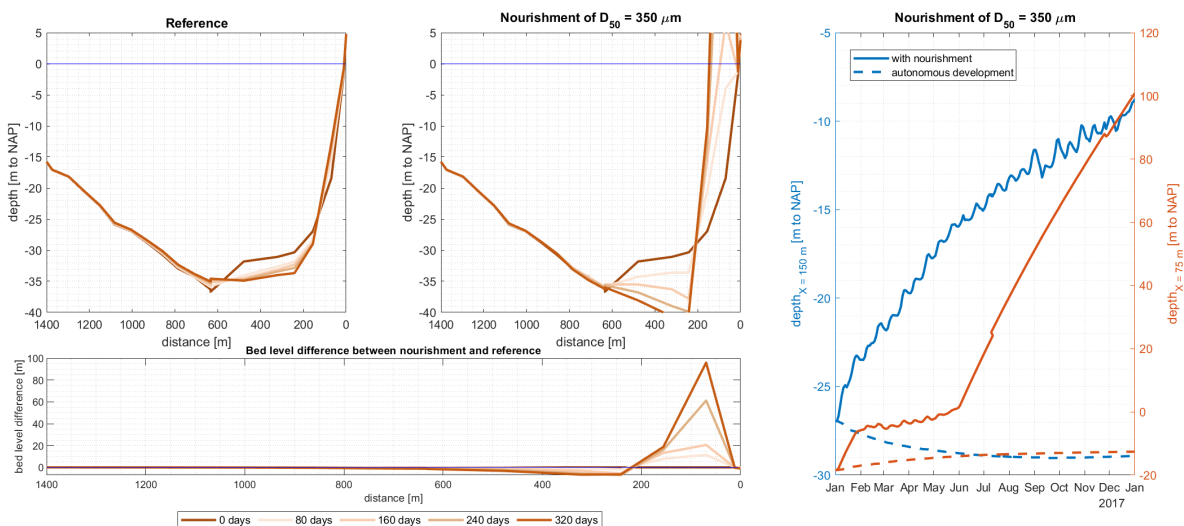
Figure D.7: Development of cross section when the nourishment discharge is doubled.

Regional morphological behaviour

As expected based on the enhanced deepening of the channel observed in Figure D.7, does the large sediment discharge influence the velocity field significantly (see Figure D.8. Local flood velocities increase from 1.5 m/s to 2 m/s at the channel side of the nourishment. In the lee of the nourishment, flood velocities decrease from 1.5 m/s to 0.4 m/s. At the lee side of the ebb a velocity decrease from 1 m/s to 0.4 m/s is observed. The ebb current at the channel side of the nourishment is increased from 1 m/s to 1.3 m/s. These highly increased velocities repress the bed level growth at the nourishment location, though they lead to more erosion in the adjacent area.
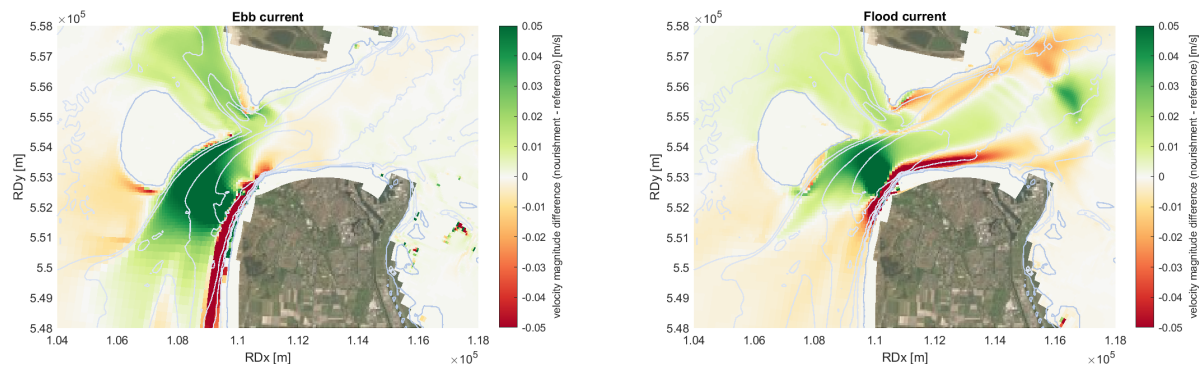
Figure D.8: Difference in current velocities during flood (left) and ebb (right) between reference and nourishment scenario after 180 days. The arrows indicate the difference of the velocity vectors between the reference and A0 scenario.

The spreading of the nourishment relative to the A0 nourishment is shown in Figure D.12. After one year, a minimum bed level increase of 5 meters is observed over a distance of 2 km. The bed has a increased with at least 2 m over a distance of 2 km. In the section just northeast of the nourishment, a relative decrease of the channel wall is observed. The channel wall does grow, but less than in the A0 case. The reasoning behind this can be the larger lee effect during flood of the larger nourishment.
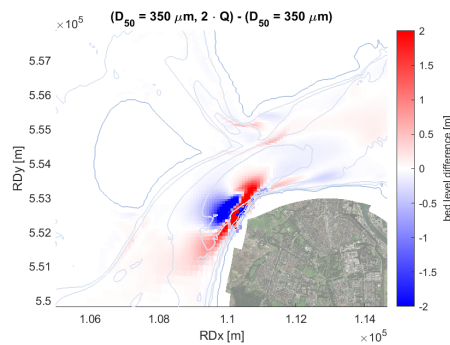
Figure D.9: Relative bed level change compared to D350 run.

Implications for the Sandwindmill

The development of the larger nourishment shows that, as expected, the system is unable to distribute too large quantities of nourished sediment. The increasing velocities due to the growing channel wall can be seen as beneficial for the long-term nourishments of the Sandwindmill. Whereas the initial sedimenation rate may seem too high for a long-term application of the Sandwindmill, does this scenario clearly show how the fast adaptation of the system to the new bathymetry can lead to a significant increase in sediment dispersion.

D.1.3. Scenario A3: High velocity

The benefit of nourishing only at high velocities could be that the sediment that is deposited could be directly transported away from the nourishment location. This would induce a larger region of influence of the nourishment and a smaller accretion rate at the nourishment location. The first development, shown in Figure D.10 shows that this enhanced spreading is visible after two days. In the sections adjacent to the nourishment, a bed level increase of approximately 30% can be observed relative to the A0 scenario. Locally a minor decrease in the bed level is observed. This decrease is difficult to observe in Figure D.10 as the absolute volume of the nourishment at the nourishment location is still much higher than in the region around the nourishment.
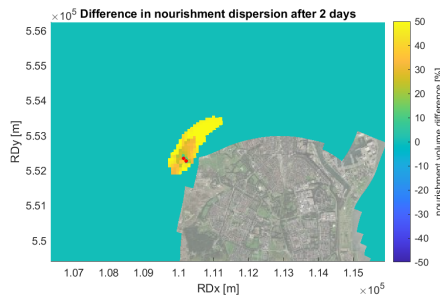
Figure D.10: Spreading of the nourished sediment after two days. Relative sediment volume of the nourished sediment of the A3 scenario to the A0 scenario is given. The figure shows the initial effectiveness of nourishing only during high velocities.

Local morphological behaviour

After one year the bed has developed in a very similar fashion as in the A0 scenario. The wiggly behaviour which is due to the spring-neap variability has decreased for the A3 scenario, but the eventual profile looks very similar (Figure D.11). The bed level at the X = 150 m location has grown slightly less than in the A0 case, despite the somewhat higher discharge (+6,000 m^3 in-situ sediment in the 6,400 m^2 cell). This shows that the execution of the nourishment at higher velocities does have some effect.
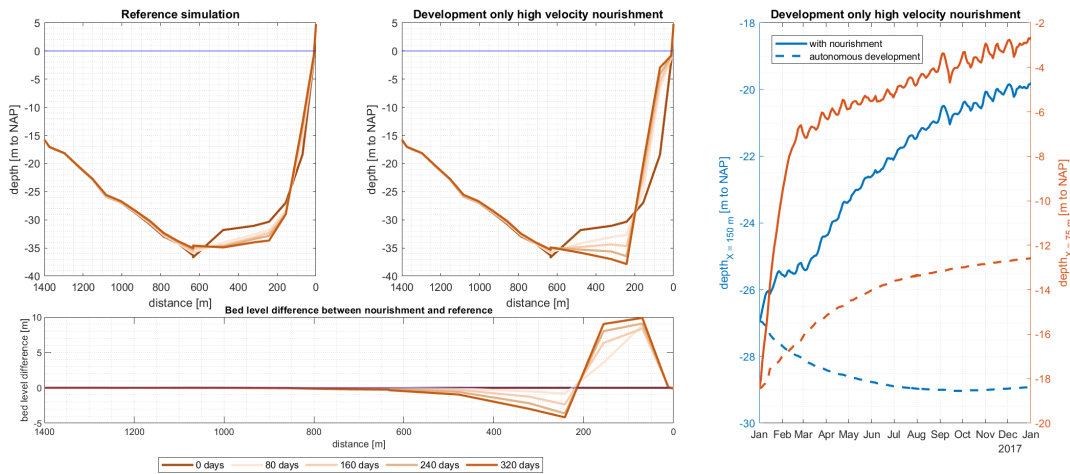
Figure D.11: Development of the bathymetry during the reference (left) and A3 (right) simulation. Nourishment locations are located at 75 and 150 m. The dashed line in the right figure indicates the autonomous bed level development.

Regional morphological behaviour

Regionally, some difference can be observed with the A0 case. The transport in the direction of the flood and ebb has increased. The increase in the flood direction is larger than the increase in ebb direction, which is expected behaviour based on the velocity asymmetry. The erosion in the channel is somewhat larger. At the nourishment location itself the bed level difference is very limited.
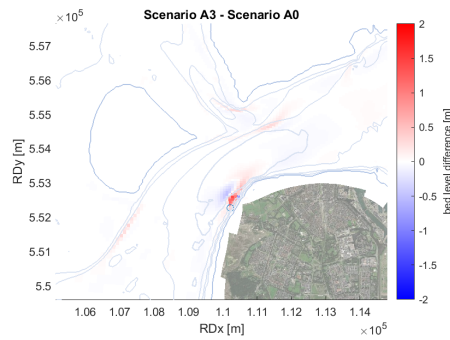
Figure D.12: Relative bed level change of high velocity simulation compared to D350 run after one year.

Implications for the Sandwindmill
The distribution of the sediment increases when the nourishments take place at higher flow velocities. On the longer term, the effect seems to be rather limited. The technical implications of applying an interval nourishment are probably too large for the benefits. As smaller grain sizes are more sensitive to the velocities, the interval nourishments possibly have a more positive influence on these.

D.1.4. Scenario A4: Displacement of outlet
Scenario A4 assesses the spreading of the nourishment when the discharge outlets are placed more towards the channel trough.

Local morphological behaviour
The cross section in Figure D.13 shows that the channel erosion is inhibited strongly in relation to the reference simulation. It becomes also apparent that the nourishment in the channel gets into an equilibrium quite fast at a depth of approximately 24 m (orange line in Figure D.13). In the later months, the bed level seems to decrease again. This development might be steered by the autonomous bed level decrease (dashed line). When looking at the absolute difference between this filled and the dashed line, a small growth can be still observed (indicating a relative bed level increase and hence no equilibrium). The growth of channel wall near the sea level is almost zero (X = 75 in figure c).
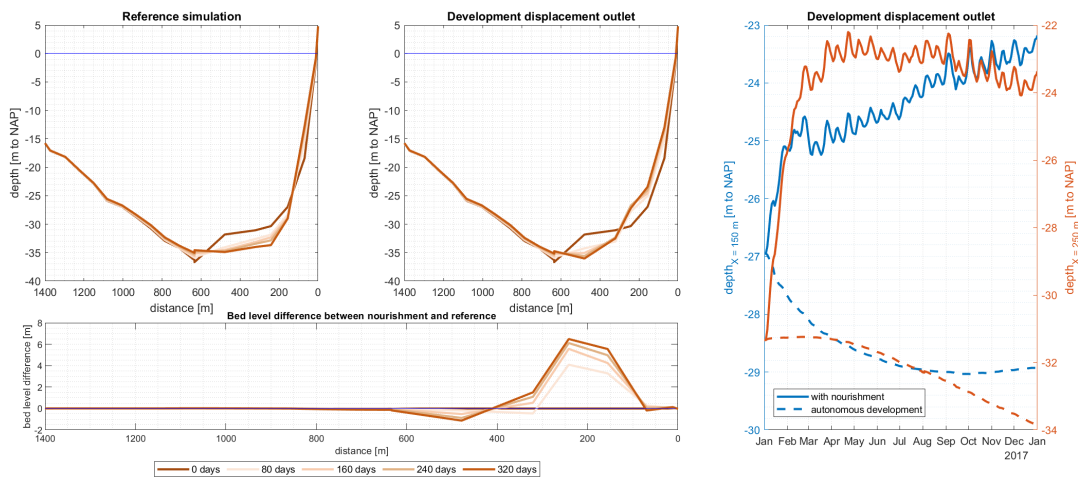

Figure D.13: Development of the bathymetry during the reference (left) and A4 (right) simulation. Nourishment locations are located at 75 and 150 m. The dashed line in the right figure indicates the autonomous bed level development.

Regional morphological behaviour

Figure D.14 shows the regional development. From the difference with the A0 scenario in Figure D.14a the smaller contribution to the steepest part of the wall can be observed. Figure D.14b shows that the growth of the channel trough that was observed in Figure D.13 spreads out over approximately 1 km in the flow direction. The figure also shows that the bed level change at the inner side of the bend is positive in comparison to the reference simulation, despite the limited growth of the channel wall at the nourishment location.

(a) Comparison with A0   (b) Comparison with reference
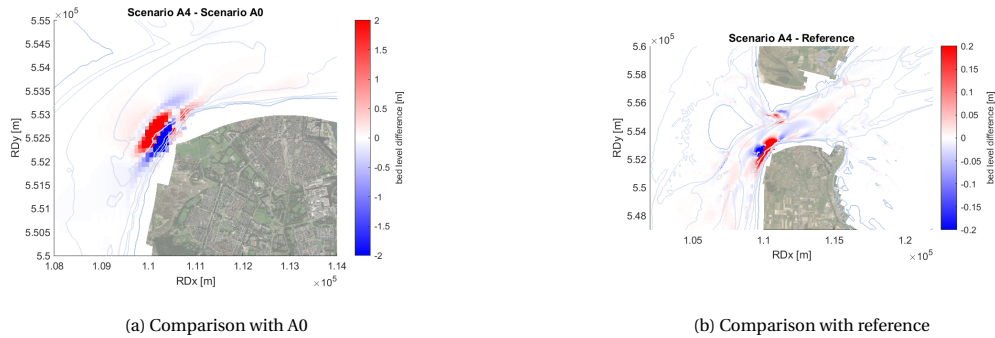
Figure D.14: Comparison of the regional behavior with a displaced outlet with A0 and the reference (autonomous/no nourishment) simulation. Figure b can be compared with upper right panel in Figure D.4.

Implications for the Sandwindmill

The simulation of scenario A4 show that the deeper placement of the nourishment could lead to an equilibrium depth at -24 m NAP. This would be very favourable for the Sandwindmill, as this would indicate that no piling up of the sediment would occur at the nourishment location. The nourished sediment would then disperse well away from the dumping spot. As the autonomous behaviour of the bed level (dotted lines) has not been fully validated, this conclusion should be treated with care. The extent of positive influence of the feeding of the deeper part of the channel on the wall stability should be evaluated.

D.1.5. Scenario A5: Morfac

The last scenario consists of a simulation of 6 morphological years, derived from simulating 6 months of water- and meteo-forcing using a morfac of 12.

Local morphological behaviour

The bathymetric changes at the nourishment location are resolved differently with the morfac of 12. After little less than a morphological year, the nourishment at X = 75 m has grown the full 18 meters, up to the mean water level. In the A0 scenario, the bed level is still 3 meters below 0 m NAP at this location after one year. The nourishment at X = 150 m reaches 0 m NAP after 1.5 years, which is sooner than anticipated on based on the asymptotic behaviour. The bed level growth after one morphological year corresponds rather well with the non-accelerated simulation (-35 to -18.9 m, compared to -19.9 for A0). After the bed level has grown to approximately 0 m NAP, it remains at this level. The locations adjacent to the original nourishment location are then nourished, as if the outlet is displaced when the bed level has grown to approximately mean sea level. The following protrusion is well visible in Figure D.15. One explanation of the slightly different behaviour with the morfac could be that the hydrodynamic forcing of the first month is not totally representative for the entire year. With a morfac of 12, a maximum bed level increase of 0.04 mm per second can be the direct result of the nourishment. It is not expected that this leads to a large change the hydrodynamics, violating the assumption of the different morphological and hydrodynamic timescales (explained in Section 5.6.2).

Regional morphological behaviour

The assessment of the regional scale of the dispersion can give insight to the longer term response of the area to the sediment abundance. It can teach something about the resuspension of the sediment. When assuming a fall velocity of 0.04 m/s for particles of 350 μm diameter (Figure 2.4), the particles will fall for approximately 12.5 minutes when deposited up in the water column with a depth of 30 meters. With maximum horizontal current velocities of approximately 1.5 m/s, this means that the maximum initial spreading of the sediment with a diameter of 350 μm is in the order of 1 km. This is under the assumption that there are no turbulent forces that alter the vertical position of sediment particles and that each sediment particle moves exactly with the velocity of the current. The other scenarios (e.g. Figure D.3) already show that the sediment is deposited further away than it could be expected to be within one tidal cycle (e.g. Figure 6.9). Looking at the longer term also gives insight in the response of the system to the different bathymetry. Next to resuspension, the influence of hydrodynamic changes on the longer term is also better visible.

Figures D.15, D.16 and D.17 show the same pattern of the longer term development as the development after one year: the deepening of the adjacent channel and the alongshore deposition of sediment seem to be also be the dominant developments on the longer term. One difference is the significant accretion at the southward side of the nourishment after 6 years (visible by comparison of figures D.17 and D.4). This development is probably forced by the increasing velocity magnitude of the ebb currents. It can be seen that no significant sedimentation occurs at the shallower part of the coastline, as it is in the lee-side of the nourishment. This implies that the bed level increase does not extend to the beaches of e.g. Julianadorp, but rather to the Schulpengat and Nieuwe Schulpengat. As the vicinity of the Nieuwe Schulpengat leads to the direct large-scale erosion of the North Holland coast, the feeding of the channel wall could still reduce coastal erosion (Elias & Van der Spek, 2017).

The calculated sediment volume change of the Marsdiep basin in six years is approximately +4 million m^3, measured from RDx = 112 km in eastward direction and compared to the reference scenario. Assuming an annual sediment import of 2 Mm^3, this increase of 33% could potentially contribute to satisfying the sand hunger of the Waddensea. On average, the 4 million m^3 in six years leads to a yearly bottom growth of 1.25 mm. This is quite significant compared to the current rate of 2 millimeter/year sea-level rise, with which the Wadden Sea wants to grow (Elias & Wang, 2020).

Implications for the Sandwindmill

Also on the longer term, the growth of the bed in proximity of the seawall is visible, which is the intended effect. Although the neighbouring pit formation could be the result of simplifications made in the modelling, its formation should be well analyzed as it could form a threat to the stability of the accumulated sediment next to it.
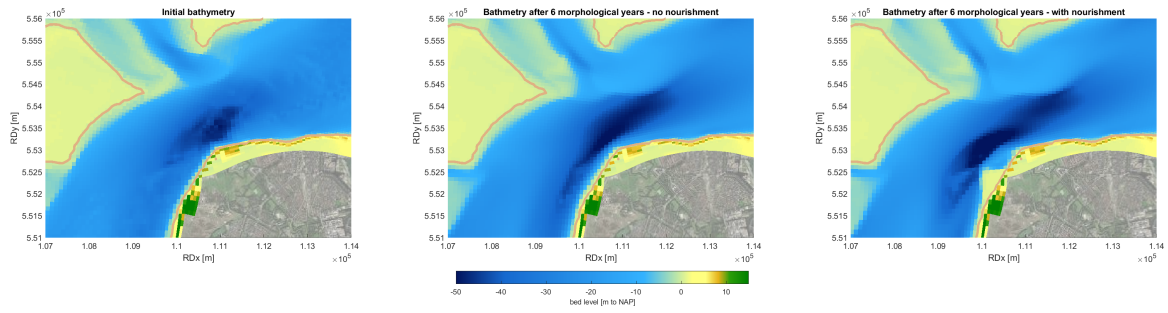
Figure D.15: Initial morphology and morphology after six years for the situation with and without nourishment.
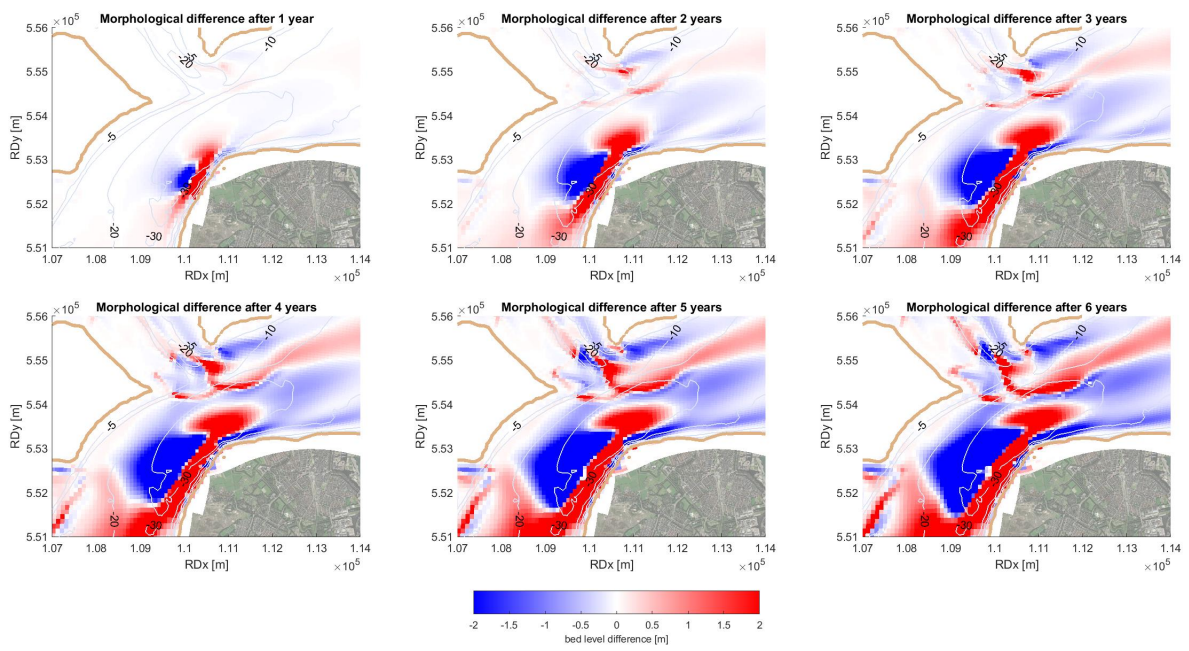

Figure D.16: Difference in morphology for the situation with and without nourishment after different morphological years.
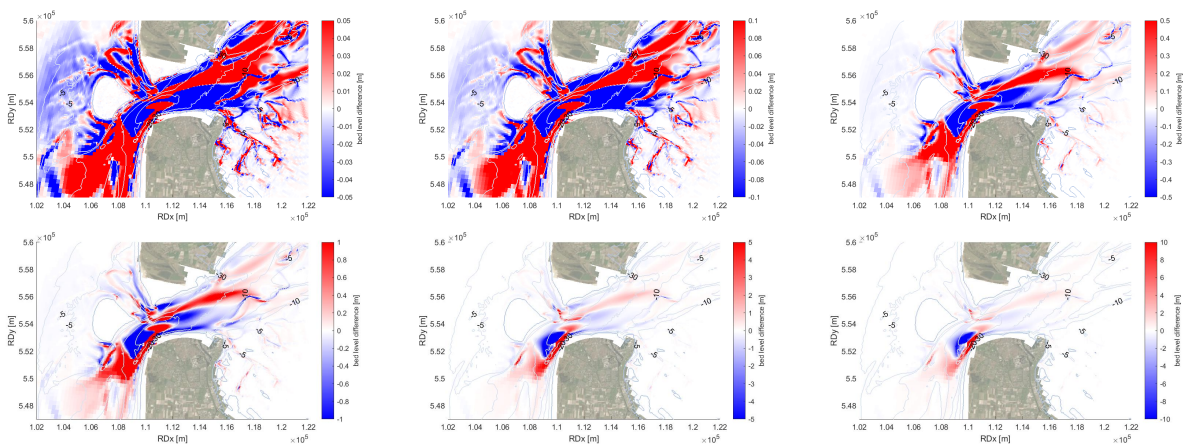

Figure D.17: Difference in morphology for the situation with and without nourishment after 6 years of morphological development, for different depth scales.

D.2. Shoreface simulations

In this section, the results of all shoreface nourishments are shown.

D.2.1. Scenario B1: Variable D_{50}

The cross-shore profile development of a nourishment with 150 μm is more limited than in the case where a grain size of 250 μm is used for the nourishment (Figure D.18). Whereas the alongshore tidal current velocity might be minimally capable of transporting the larger grains, could these currents initially redistribute the finer fractions. This leaves less sediment to be transported in cross-shore direction by the waves.

(a) Absolute difference   (b) Relative difference
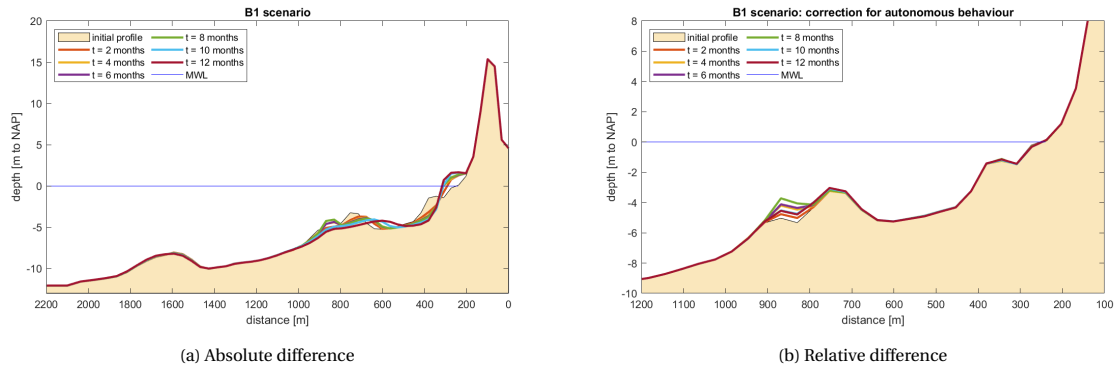
Figure D.18: The development of the cross-shore profile over a morphological year for B1.

The larger susceptibility of the finer grains to the alongshore currents becomes apparent when looking at the regional bed level changes in Figure D.19. Accretion of more than 20 cm can be observed at 4 km away from the dispersion location.
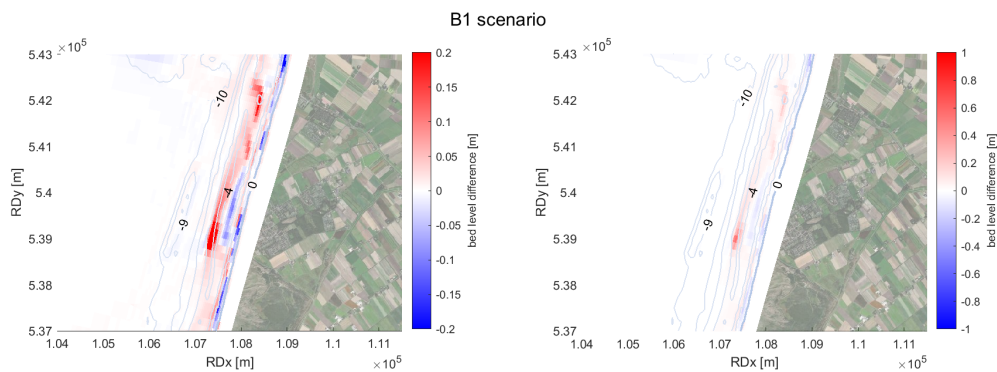
Figure D.19: The regional development of the bed level around the nourishment location for B1 after one year, with two different color scales.

The left panel of D.20 shows that the alongshore distribution in time has a gradual development. Smaller waves and the tide- and wind-driven currents are already able to pick up the sediment. The 0.1 m depth contour spreads out continuously. The largest spreading is in northward direction, which can be explained by the net northward tide-induced transport in the region.
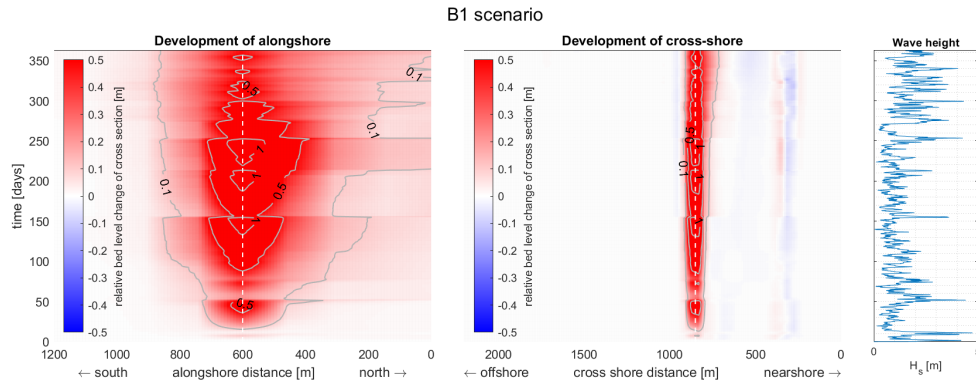
Figure D.20: Time stack of the morphological development in two sections for scenario B1. The 10 cm accretion contour extends 700 m in N direction and 260 m in S direction of the nourishment centre of gravity.

D.2.2. Scenario B2: Larger discharge

The application of an annual discharge of 200,000 m^3 has a larger influence on the cross-shore development than the 100,000 m^3 nourishment. After 8 months the bottom at the nourishment location has grown to 2 meters depth. The slowing down of the growth due to a change in depth-induced breaking enables the system not to exceed the mean water level.

(a) Absolute difference

(b) Relative
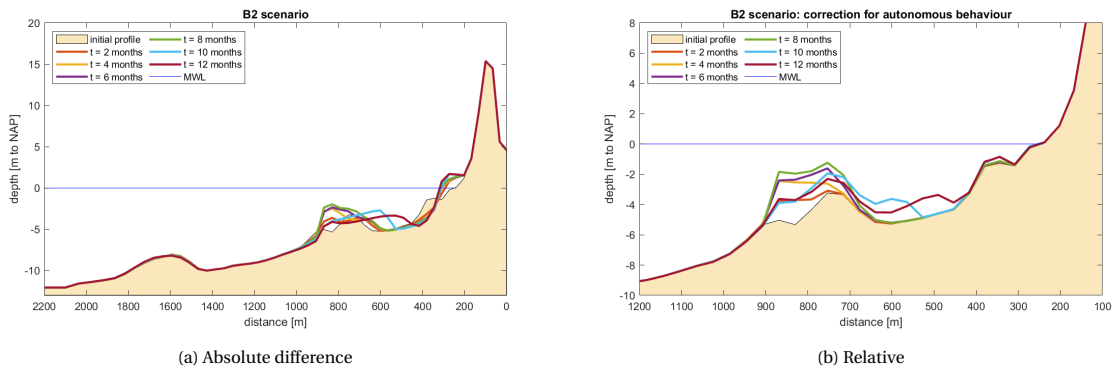
Figure D.21: The development of the cross-shore profile over a morphological year for B2.

The regional accretion/erosion pattern after one year is almost identical to the pattern of the 100,000 m^3 nourishment. Again the feeder- and lee-side effect can be distinguished.
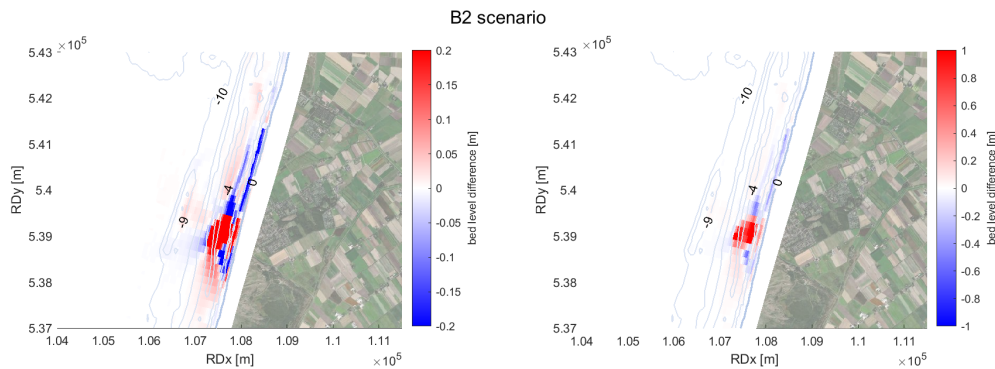

Figure D.22: The regional development of the bed level around the nourishment location for B2 after one year, with two different color scales.

The larger abundance of sediment leads to a slightly different alongshore spreading than in the standard scenario. The shape of the alongshore spreading is almost identical. This implicates that the sediment does

not come much further if more is supplied. The difference is that in the case where more sediment is supplied, the sedimentation areas accrete more. In the cross-shore direction a full net sedimentation is visible after 365 days.
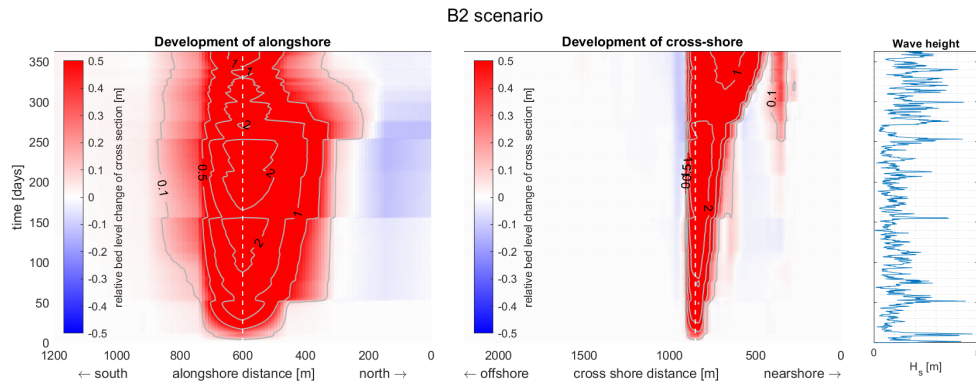

Figure D.23: Time stack of the morphological development in two sections for scenario B2. The 10 cm accretion contour extends 260 m in N direction and 230 m in S direction of the nourishment centre of gravity.

D.2.3. Scenario B3: High waves
The third scenario assesses the morphological development if the nourishments are only executed if waves with H_s > 1.5 m are present. The annual nourishment volume is the same as in scenario B0, hence the discharge is higher. From the profile development at the nourishment location, it can be seen that the bed level change is limited and that little seasonal variability is visible. The higher waves can keep the nourished material in suspension.

(a) Absolute difference
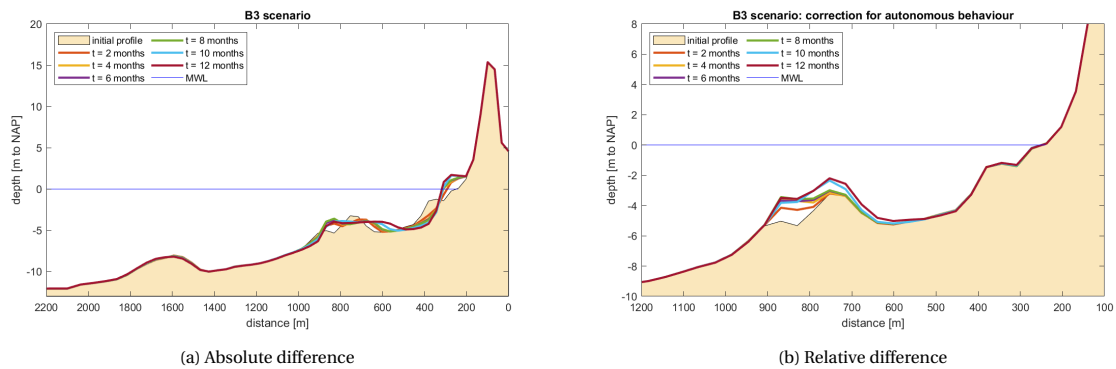
(b) Relative difference

Figure D.24: The development of the cross-shore profile over a morphological year for B3.

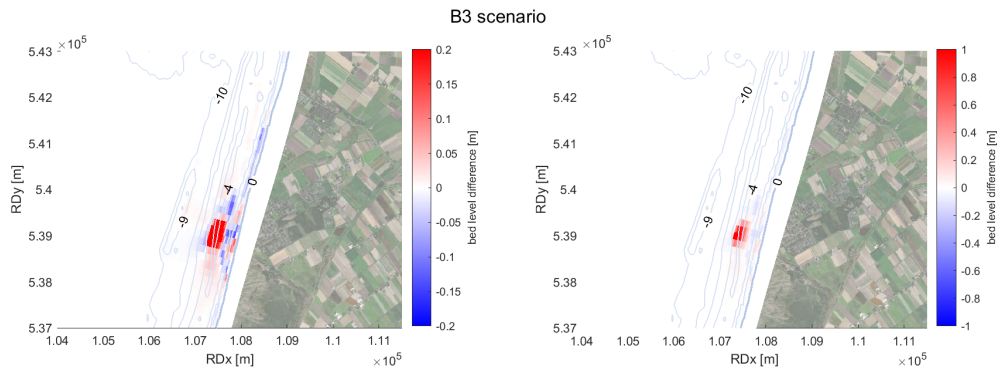On a larger scale the same behaviour as with the B0 scenario is observed.

Figure D.25: The regional development of the bed level around the nourishment location for B3 after one year, with two different color scales.

At the alongshore transect, the 0.1 m bed increase development is similar to the development of the B0 scenario. This implicates that the influence of the nourishment timing on the alongshore dispersion is small. For the nourishment location itself, the bed level does not exceed 2 meters, opposed to the B0 scenario. This could be beneficial as less sediment will pile up at the nourishment location.
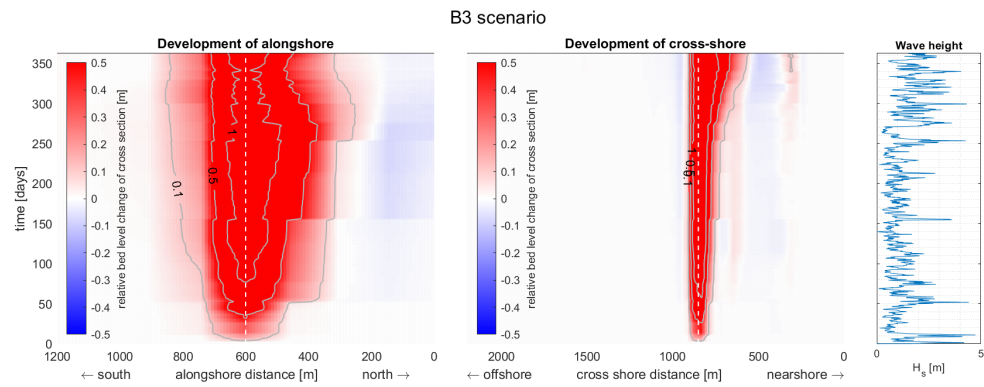

Figure D.26: Time stack of the morphological development in two sections for scenario B3. The 10 cm accretion contour extends 270 m in N direction and 250 m in S direction of the nourishment centre of gravity.

D.2.4. Scenario B4: Petten

In scenario B4 the development of a 100,000 m^2 nourishment at Petten is simulated. The slowing down of the bed level increase during the first months is smaller than in the B0 scenario, as the waves that would induce this already break on the outer breaker bank.

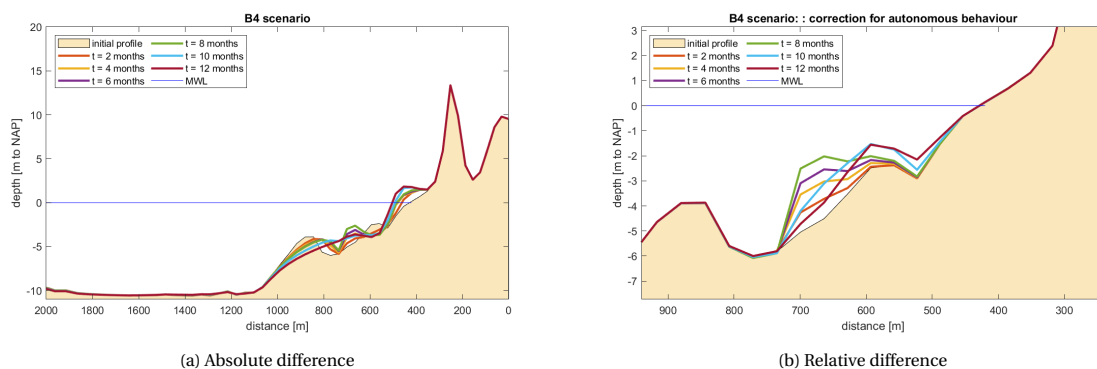(a) Absolute difference

(b) Relative difference

Figure D.27: The development of the cross-shore profile over a morphological year for B4.

The regional development at Petten is similar to the development at Callantsoog: nearshore and mainly

northward spreading and a small erosion at the adjacent coastline which can be attributed to the lee-side effect.
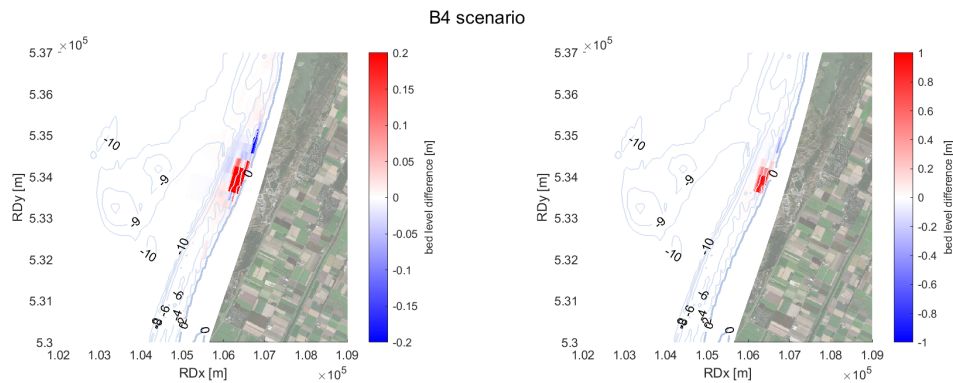

Figure D.28: The regional development of the bed level around the nourishment location for B4 after one year, with two different color scales.

The nourishment dispersion at Petten is also mainly influenced by wave events. A higher spreading in northward direction than in southward direction can be observed in the left panel of Figure D.29. Petten is less sheltered from NNW waves than Callantsoog. This northward direction shift is surprising, as the representativity study of the 2017 forcing conditions (Section 5.3) shows an equal potential in northward and southward wave-induced transports. This representativity study is conducted for the Callantsoog coastline-orientation. The different orientation of the coast at Petten makes it more susceptible to northward transports, as SW waves will approach the coast more obliquely and NW waves will approach it less obliquely.
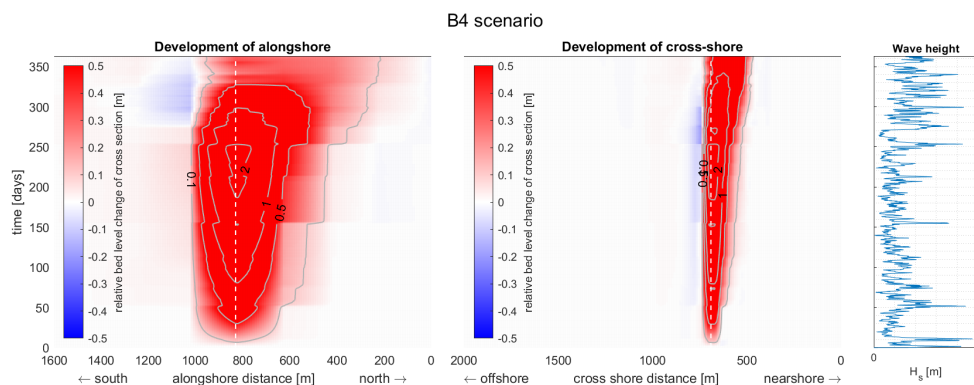

Figure D.29: Time stack of the morphological development in two sections for scenario B4. The 10 cm accretion contour extends 620 m in N direction and 130 m in S direction of the nourishment centre of gravity.

D.2.5. Scenario B5: Julianadorp
The development of the cross-section at Julianadorp (Figure D.30) shows that in cross-shore direction very little transport occurs. This limited transport can be attributed to (a) the large depth at which the nourishment has taken place, and (b) the sheltering of waves by the outer delta.

(a) Absolute difference
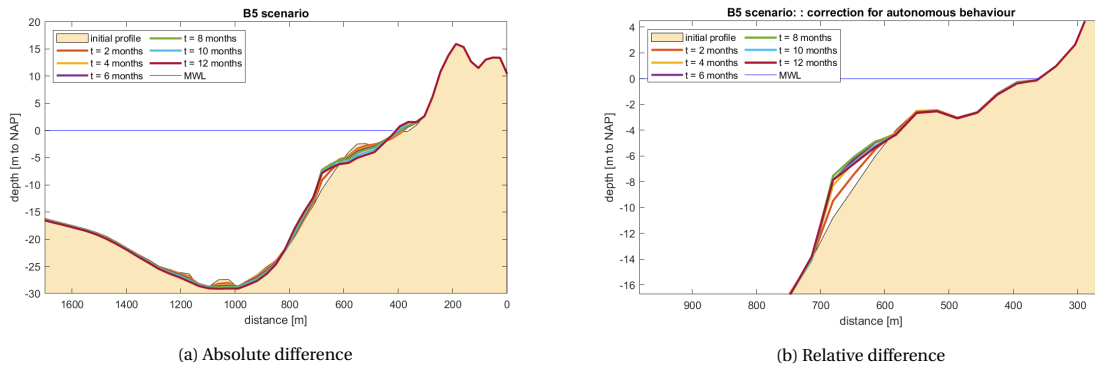
(b) Relative difference

Figure D.30: The development of the cross-shore profile over a morphological year for B5.

The regional behaviour of the nourishment has similarities with the tidal channel nourishments assessed in the A scenarios: alongshore spreading and erosion adjacent to the nourishment, due to altered flow velocities.
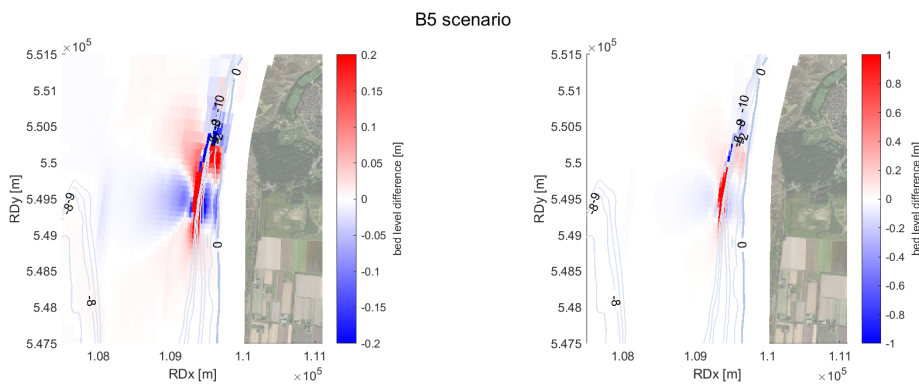

Figure D.31: The regional development of the bed level around the nourishment location for B5 after one year, with two different color scales.

The spreading of the nourishment in northern direction is larger than in southward direction, which can be attributed to the asymmetry in the flood- en ebb-tidal velocities. The smooth development of the contour lines indicates the limited influence of waves, which substantiates the choice of neglecting waves in the tidal channel nourishments of the A scenarios.
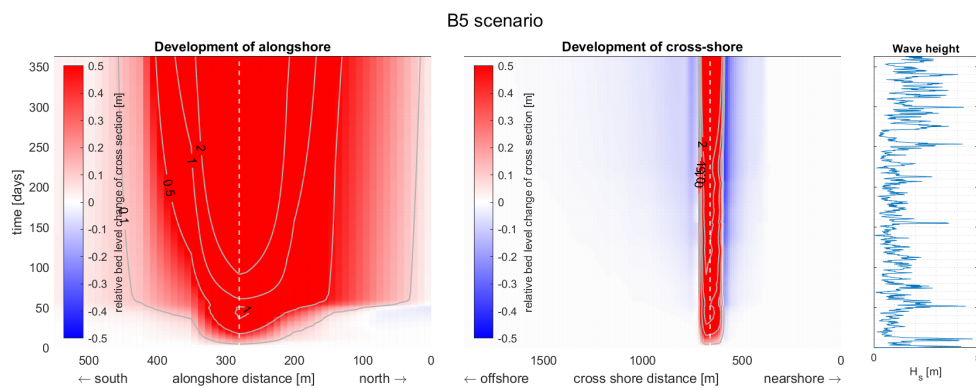

Figure D.32: Time stack of the morphological development in two sections for scenario B5. The 10 cm accretion contour extends 260 m in N direction and 180 m in S direction of the nourishment centre of gravity.

D.2.6. Scenario B6: Alongshore stretched

When comparing the cross-sectional behaviour from scenario B6 to the behaviour of B0, the most distuinguishable difference is the higher sedimentation landward of the nourishment for the B6 scenario (around

X = 500). Inspection of the resource of the sediment shows that this hump does hardly contain the nourished sediment. This hump can be attributed to the deposition of alongshore transported sediment, which is caused by the blocking of waves by the bar. This corresponds to the lee-side effect described in 6.4.1 and Van Rijn & Walstra (2004).

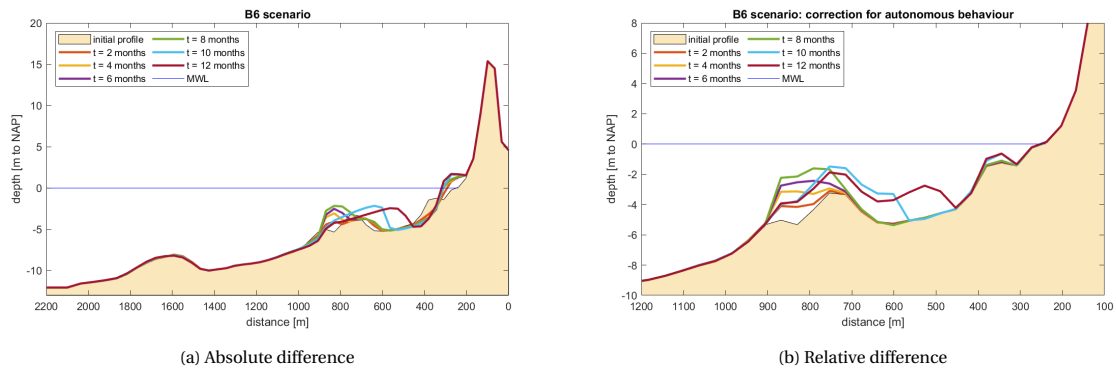(a) Absolute difference

(b) Relative difference

Figure D.33: The development of the cross-shore profile over a morphological year for B6.

Also regional response of the coast to the bar nourishment is particularly different from the behaviour during a nourishment at a smaller area. Despite the addition of more sediment to the system, does the erosive behaviour northward of the nourishment increase. Southward of the nourishment sedimentation is visible, except for a small area at the coastline. These features also correspond well with the lee-side effect.
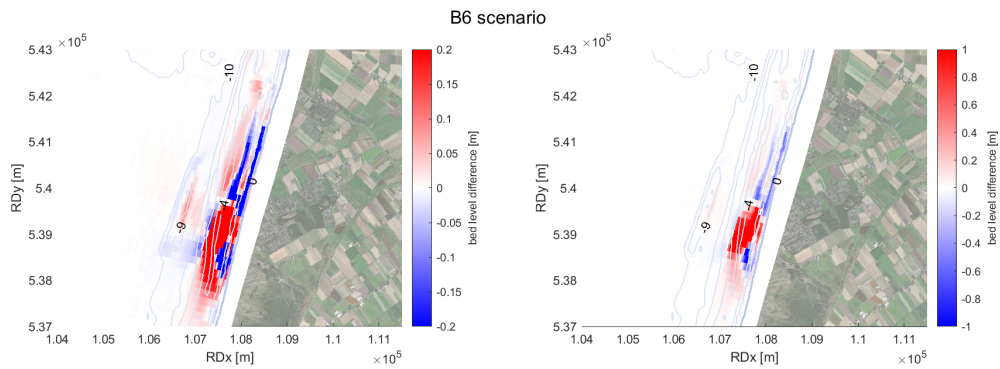

Figure D.34: The regional development of the bed level around the nourishment location for B6 after one year, with two different color scales.

The alongshore movement of the bar-shaped nourishment shows more asymmetrical behaviour than the movement of the point source nourishment. The alongshore spreading of the nourishment in northward direction is equal to the spreading in the case of a point nourishment (as executed in A0). This is in line with the hypothesis by Huisman et al. (2019), which is discussed in Section 2.3. In southward direction an expansion is visible. The examination of the resource of the material that has accreted at the south side shows that this material is not consisting of the nourished sediment.
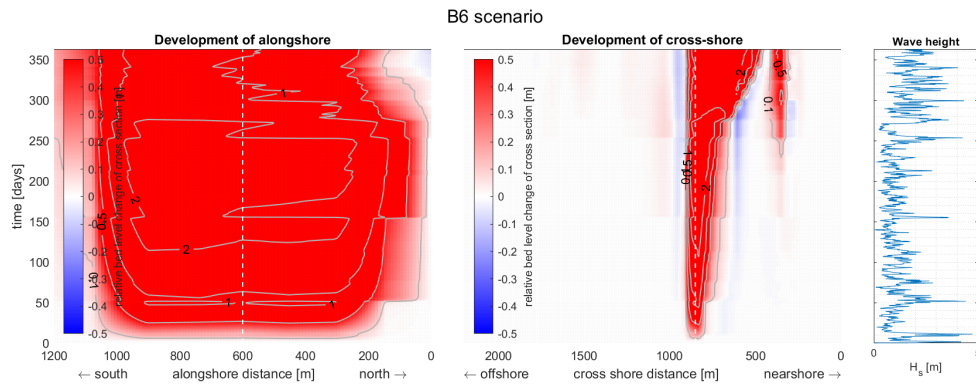
Figure D.35: Time stack of the morphological development in two sections for scenario B6. The 10 cm accretion contour extends 470 m in N direction and 870 m in S direction of the nourishment centre of gravity, indicating a dominant northward transport.

D.2.7. Scenario B7: Outer bar

From Figure D.36a it can be seen that the bed level grows almost undisturbed, up to the winter period. The increase in storminess and the increased bed level induce the breaking of waves. Figure D.36b shows that the application of the nourishment at the offshore bar has almost no effect on the nearshore zone.

(a) Absolute difference
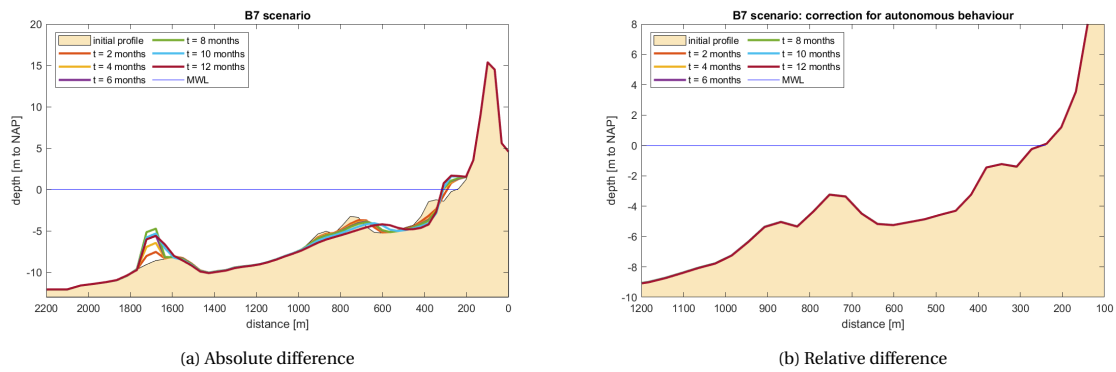
(b) Relative difference

Figure D.36: The development of the cross-shore profile over a morphological year for B7.

In the lee-side of the nourishment, some erosion is visible. The erosion might be the effect of the turbulence that is created by the wave breaking on the nourishment. Another explanation is the change in flow velocities around the nourishment, which lead to scour at the edges of the nourishment.
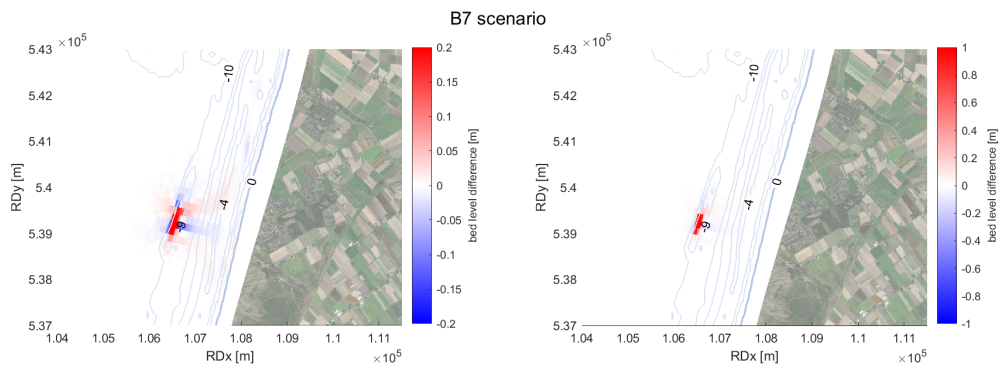

Figure D.37: The regional development of the bed level around the nourishment location for B7 after one year, with two different color scales.

The development of the scour slowly increases in time. In the more energetic winter period, it increases. This can be the result of the increased breaking of waves or the contraction of higher wave-induced velocities.
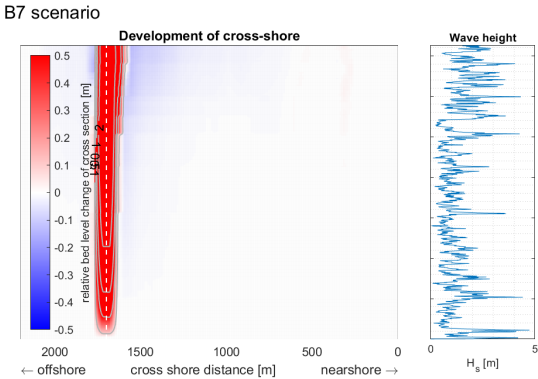
B7 scenario

Figure D.38: Time stack of the morphological development in two sections for scenario B7. No time stack on the alongshore development is available as the autonomous development has not been monitored in this section.

List of symbols

α	beach slope	°
α_b	beach slope at breaker point	°
α_{bn}	user-defined tuning parameter for transverse bed slope	-
α_{bs}	user-defined tuning parameter for longitudinal bed slope	-
α_c	constant for conversion of wind velocity to near-bed shear velocity	-
α_n	phase angle of component n	°
α_{qb}	Van Rijn's calibration factor for bed-load	-
α_s	longitudinal bed slope factor	-
γ	breaker index	-
ϵ	wall roughness height	m
$\eta(t)$	water level at time t	m
η_{qb}	Van Rijn's calibration exponent for bed-load	-
$\eta_{Xin,t}$	water level at point Xin at time t	m
$\eta_{Xout,t}$	water level at point Xout at time t	m
θ	Shields parameter	-
κ	Von Kármán constant	-
λ	friction factor	-
μ	ripple coefficient	-
ν	kinematic viscosity	m^2/s
$\nu_{t,s}$	turbulence diffusivity of sediment mass	m^2/s
ρ_a	air density	kg/m^3
ρ_m	mixture density	kg/m^3
ρ_s	sediment density	kg/m^3
ρ_w	water density	kg/m^3
τ_b	bed shear stress	N/m^2
ϕ'	internal angle of friction	°
ϕ_0	offshore wave direction	°
ϕ_b	wave angle of incidence at outer edge of breaker zone	-
ω_r	radian frequency	rad/s
ω_n	angular velocity of component n	°/h

A	shape factor	$m^{1/3}$
A_0	mean water level w.r.t. reference	-
a	thickness of bed-load layer	m
a_n	amplitude of component n	m
B	Bijker coefficient	-
C	Chézy coefficient	$m^{1/2}/s$
C_*	dimensionless Chezý coefficient	-
C_D	drag coefficient	-
C_p	power coefficient	-
C_{vd}	volumetric sediment concentration in mixture	-
C(a)	sediment concentration at reference point	-
C(z)	time-averaged sediment concentration at height z	-
c	turbulence averaged concentration	-
c_0	deep water phase velocity	m/s
c_f	dimensionless friction factor	-
D	grain size	m
D_{50}	median grain size	m
D_n	nominal grain size	m
$D_{n,r}$	reference nominal grain size	m
D_{pipe}	pipe diameter	m
F_G	gravity force	N
f_{safety}	safety factor for transport velocity	-
G_D	drag force	N
g	gravitation acceleration	m/s^2
H	wave height	m
H_b	wave height at breaking	m
$H_{s,b}$	significant wave height at breaking	m
h	water depth	m
h_b	water depth at breaking	m
h_{ref}	reference height	m
I_m	immersed mass of transported sediment	kg/s
J	number of data points	-
k	wave number	rad/m
K	empirical CERC coefficient	-
L	length of transport pipeline	m
$M_{s,real,design}$	annual nourishment mass, corrected for operational time	-
M_e	mobility parameter ($\frac{u-u_{cr}}{[(s-1)gD_{50}]^{0.5}}$)	-
N	amount of harmonic components	-
n	Manning's roughness coefficient	$s/m^{1/3}$
P	power	W
P_{wind}	power delivered by the wind	W
p	porosity	-
$Q_{m,real}$	mixture discharge	m^3/s
q	equilibrium sediment transport	kg/m/s
q_b	depth-integrated bed-load transport	$kg/(s \cdot m$
r	radius of windmill blade	m
Re	Reynolds number	-
Re_g	grain Reynolds number	-
S	deposited volume of sediment transported	m^3/s
S_b	time-averaged bed-load transport	$m^3/m/s$
$S_{b,n}$	additional bed-load transport vector, normal to unadjusted transport vector	-
S_y	net alongshore sediment transport (pores excluded)	$m^3/m/s$
s	relative density (ρ_s/ρ_w)	-

T	wave period	s
$T_{operational}$	relative annual operational time	-
T_p	peak period of the spectrum	s
t	time	h
U(z)	time-averaged fluid velocity at height z	m/s
u	depth-averaged velocity	m/s
u_*	shear velocity ($\sqrt{\frac{\tau_b}{\rho_w}}$)	m/s
$u_{b,cr}$	critical near-bed velocity	m/s
u_{cr}	critical depth-averaged velocity	m/s
u_{th}	wind velocity threshold	m/s
u_b	bottom orbital velocity	m/s
u_z	wind velocity at height z	m/s
$V_{s,situ,design}$	annual nourishment volume inlcuding pores, corrected for operational time	m^3
$V_{s,situ,year}$	annual nourishment volume inlcuding pores	m^3
v(x)	depth averaged alongshore current at location x	m/s
$v_{critical}$	critical transport velocity	m/s
v_{design}	design flow velocity	m/s
$v_{wind,h}$	wind velocity at height h	m/s
$v_{wind,ref}$	wind velocity at reference height	m/s
w_s	fall velocity	m/s
x'	distance from mean waterline, positive in offshore direction	m
x_i	observed value at time t	-
z	distance from bed	m
z_*	Rouse number ($\frac{w_s}{\kappa u_*}$)	-
z_v	height of vegetation	m

$\langle \lvert \tau_{cw} \rvert \rangle$	time-averaged shear stress magnitude of wave-current motion	N/m
$\langle c'w' \rangle$	sediment flux due to turbulence	m/s
$\overline{c(z)}$	time-averaged oscillating concentration component at height z	m^3/m^3
$\nabla_{Neumann,t}$	Neumann gradient at time t	-
Δ p	head loss	m
$\overrightarrow{S''}$	vector of bedload transport adjusted	-
$\lvert S'_b \rvert$	magnitude of bed-load vector that has been corrected for longitudinal bed slope	-
$\overline{u(z)}$	time-averaged oscillating fluid component at height z	m/s
$\overrightarrow{u_b}$	near-bed velocity vector	-
$\hat{x}_i$	modelled value at time t	-
ΔX	distance between grid points	m
$\frac{\partial z}{\partial s}$	bed slope in the direction of the unadjusted bed-load vector	-
$\frac{\partial z_b}{\partial n}$	bed slope normal to unadjusted bed-load vector	-

Acronyms

BCL   Basal coastline
BwN   Building with nature
CAPEX   Capital expenditures
CDF   Cumulative distribution function
CSD   Cutter suction dredgers
DCC   Dutch coastline challenge
FTE   Full-time equivalents
GHG   Greenhouse gas
GLT   General longshore transport
IKZ   Innovaties in kustlijn zorg
IPCC   Intergovernmental panel on climate change
KPI   Key performance indicator
LSTF   Large-scale sediment transport facility
MCL   Momentary coastline
MLW   Mean low water
MWL   Mean water level
OPEX   Operational expenditures
PSD   Plain suction dredger
RCP   Representative concentration pathway
SWAN   Simulating waves nearshore
SWM   Sandwindmill
TSHD   Trailing suction hopper dredger